VOLCANIC LAKE SYSTEMS AS TERRESTRIAL ANALOGUE FOR SULPHATE-RICH TERRAINS ON MARS

Alejandro Rodríguez

UTRECHT STUDIES IN EARTH SCIENCES

No. 112

Members of the dissertation committee:

Prof. dr. P. Agrinier
Institute de Physique du Globe de Paris (IPGP), Université Paris Diderot
Paris, France

Prof. dr. G.J. de Lange
Department of Earth Sciences, Utrecht University
Utrecht, The Netherlands

Prof. dr. J.C. Varekamp
Earth and Environmental Sciences, Wesleyan University
Middletown, CT, USA

Prof. dr. O. Vaselli
Dipartimento di Scienze della Terra (DST), Università Degli Studi Firenze
Florence, Italy

Prof. dr. W. van Westrenen
Faculty of Earth and Life Sciences, VU University
Amsterdam, The Netherlands

This PhD project was carried out at:
Petrology group, Department of Earth Sciences, Faculty of Geosciences,
Utrecht University, Utrecht, The Netherlands

ISBN/EAN: 978-90-6266-436-8

Front picture: Laguna Caliente, Poás volcano (Costa Rica). View from the southeastern rim of the main crater (April 26th, 2012).

Volcanic lake systems as terrestrial analogue for sulphate-rich terrains on Mars

De stelsels van vulkanische meren op Aarde als analogie voor sulfaatrijke gebieden op Mars

(met een samenvatting in het Nederlands)

Sistemas de lagos volcánicos como análogos terrestres a los terrenos ricos en sulfatos en Marte

(con resumen en Español)

PROEFSCHRIFT

ter verkrijging van de graad van doctor aan de Universiteit Utrecht op gezag van de rector magnificus, Prof. dr. G.J. van der Zwaan, ingevolge het besluit van het college voor promoties in het openbaar te verdedigen op vrijdag 23 september 2016 des ochtends te 10.30 uur

door

Alejandro Rodríguez Badilla
geboren op 23 juli 1977 te San José, Costa Rica

Promotor:
Prof. dr. P. Van Cappellen

Copromotor:
Dr. M.J. van Bergen

This research was funded by the User Support Programme Space Research of the Netherlands Organization for Scientific Research (NWO), project ALW-GO-PL/10-03.

To my parents: Hernán and Beatriz

CONTENTS

CHAPTER

1

Introduction

ABSTRACT

The geological history of Mars has been subdivided into the Pre-Noachian (>4.1 Ga), Noachian (4.1-3.7 Ga), Hesperian (3.7–3.1 Ga) and Amazonian (<3.1 Ga). These distinct periods are marked by major changes in style and intensity of geological processes, environmental conditions and types and rates of weathering (Hartmann and Neukum, 2001; Carr and Head, 2010; Tanaka et al., 2014). The sequence of events included periods of enhanced meteorite impacts, volcanism, erosion, sedimentation and weathering, with a prominent role of liquid water and ice, which ultimately shaped the present-day surface of the planet (Fig. 1.1). Much of the available knowledge on the Martian geological evolution has been inferred from the regolith mineralogy, as investigated by remote sensing from orbit, in-situ measurements and meteorite studies. Primary minerals are mainly crystallization products of basaltic or andesitic magmas (olivine, pyroxene and plagioclase), whereas various assemblages of secondary minerals formed near or at the surface upon interaction between igneous material and fluids during weathering/alteration, or as precipitates from aqueous solutions. Inventories of the spatial and temporal distribution of hydrous minerals demonstrate that these processes occurred under strongly different conditions, as they show a global evolution from early phyllosilicates to sulphates and finally to mainly iron (oxi)hydroxides that dominate the surface today (Bibring et al., 2005; Chevrier and Mathé, 2007; Ehlmann and Edwards, 2014) (Fig. 1.2).

This succession of secondary mineral assemblages is inferred to reflect changing weathering regimes on the Martian surface: (1) clay-type weathering in the Noachian when liquid water was abundant, (2) sulphate-type acidic weathering during the Hesperian when water became scarcer and its more sporadic presence was associated with volcanic activity and (3) very slow weathering under cold, dry and oxidizing conditions during the Amazonian, driven by acid fog and frost-thaw cycles (e.g., Chevrier and Mathé, 2007).

This thesis focuses on the origin of the wide range of sulphates that abound in vast areas on Mars but lack an encompassing hypothesis regarding their mode(s) of formation.It presents the results of an investigation into the possibility that volcanic-hydrothermal systems, similar to those currently active near the Earth's surface, were a key setting where sulphates and associated minerals could form in Hesperian times.

Front picture: hyperacid lake of Copahue volcano, Argentina. The picture was taken on March 20th, 2013. The lake was forming again from glacier melting, after it dissapeared completely due to eruptive activity.

1.1. SULPHATE-RICH TERRAINS ON MARS

On Mars, high sulphur concentrations (up to 10 wt.% SO_3) have been measured in soils of the northern plains by Viking (Baird et al., 1976; Clark et al., 1976; Toulmin et al., 1976) in Ares Vallis by Pathfinder (Rieder et al., 1997; Bell et al., 2000; Economou et al., 2001; Foley et al., 2003), in Columbia Hill outcrops (Gusev Crater) by MER Spirit and at Meridiani Planum by MER Opportunity (Gellert et al., 2004; Rieder et al., 2004; Squyres et al., 2004a; Gellert et al., 2006; Ming et al., 2006; Wang et al., 2008). Additionally, jarosite, Mg- and Ca-sulphates have been detected in situ in the aeolian and subaqueous sedimentary sequence of the Burns Formation at Meridiani Planum (Klingelhöfer et al., 2004; Squyres et al., 2004b; Clark et al., 2005; Grotzinger et al., 2005; McLennan et al., 2005; Glotch et al., 2006). The MER Spirit excavated soils that exhibit high albedo and relatively white to yellow colours at several locations south of Husband Hill (Gusev Crater) with sulphur contents up to 35 wt.% SO_3 (Johnson et al., 2007). These light-toned ("Paso Robles-class") soil deposits are dominated by Fe^{3+}-sulphates, silica and Mg-sulphates, probably associated with Ca-sulphates and phosphates (Yen et al., 2008). In Valles Marineris, sequences of polyhydrated (Mg-, Fe- and possibly Ca-rich) and monohydrated sulphates (mostly kieserite, Mg-$SO_4 \cdot H_2O$) have been detected by OMEGA and CRISM (Flahaut et al., 2010; Wendt et al., 2011; Fueten et al., 2014) (Fig. 1.1).

Fluid-rock modelling has shown that assemblages of Fe-, Mg- and Ca-sulphates, together with hematite, can be derived from low-pH, SO_4-rich fluids that interacted with basalts (Tosca et al., 2005). The sulphate-bearing assemblages at Meridiani Planum, Valles Marineris and Gusev Crater indicate that this process was once active on Mars (Clark et al., 2005; Zolotov and Shock, 2005; Ming et al., 2008). Moreover, high silica abundances associated with sulphates in soils of Meridiani Planum, Gusev Crater and in some chasmata of Valles Marineris are most likely product of intensive acid rock leaching and silica precipitation from low-pH fluids (Glotch and Bandfield, 2006; Zolotov and Mironenko, 2007; Milliken et al., 2008; Squyres et al., 2008; Weitz et al., 2010; Wendt et al., 2011).

Gypsum deposits have been identified in dune fields of Olympia Planum in the northern polar region (Langevin et al., 2005; Fishbaugh et al., 2007). Irrespective of the sedimentation mode, the gypsum could have formed by interaction of Ca-rich phases like pyroxene and plagioclase with SO_4-rich fluids (Chevrier et al., 2004; 2006; Fairén et al., 2004; Tosca et al., 2004; Tosca and McLennan, 2006).

The formation of Fe-, Mg- and Ca-sulphates on Mars' surface is often attributed to acid-sulphate alteration (Gellert et al., 2004; Morris et al., 2004; Gellert et al., 2006; Morris et al., 2006; Tosca and McLennan, 2006; Johnson et al., 2007; Bishop et al., 2009; Ehlmann et al., 2011; Gaillard et al., 2013). The presence of Fe^{3+}-sulphates implies that environmental conditions were both oxidizing and acidic (pH<4) (Nordstrom and Alpers, 1999; Bigham and Nordstrom, 2000; Nordstrom et al., 2000).

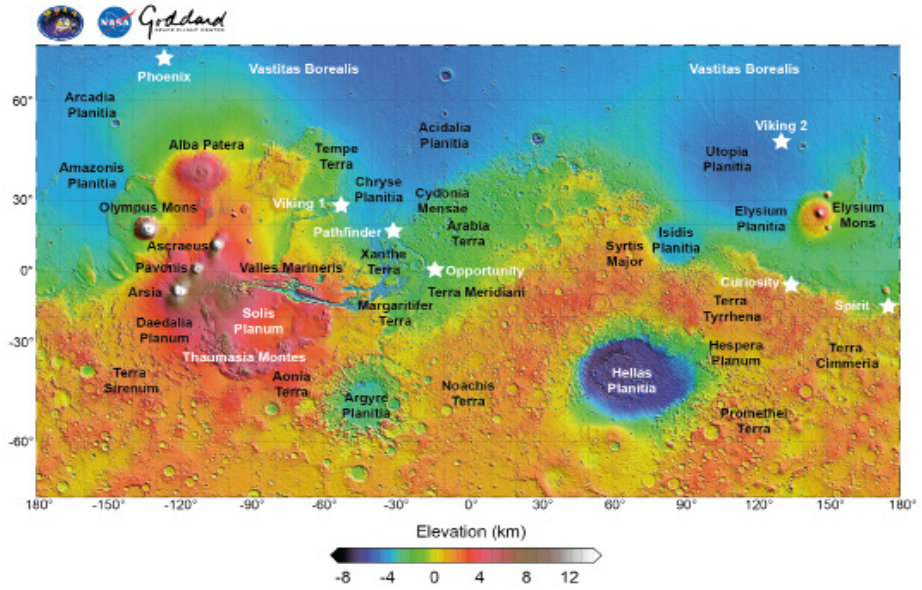

Figure 1.1. Topographic map of Mars showing main surface features and mission landing sites. The map was composed with the Mars Orbital Laser Altimeter, an instrument on board the Mars Global Surveyor spacecraft (source: NASA – MOLA Science Team).

of Fe- and Mg-sulphates are high, the abundances of these minerals point to low water/rock ratios during interaction between sulphur-rich acidic fluids and basaltic bedrock containing ferromagnesian minerals such as olivine and pyroxene.

Scenarios proposed for the formation of abundant sulphate on the Martian surface thus fall broadly into two categories (Fig. 1.3): (1) alteration of sulphide-rich rocks (Fernández-Remolar, 2005; Zolotov and Shock, 2005; Dehouck et al., 2012), followed by leaching, transfer and subsequent evaporation, and (2) *in situ* alteration in the presence of sulphur derived from acid aqueous input or acid fog, and with a strong control of the local primary rock and accompanying evaporation (Tosca et al., 2004; 2005; Chevrier and Mathé, 2007; Zolotov and Mironenko, 2007).

These models seem generally valid but are inadequate to explain the origin of all sulphate-bearing settings, in particular those where sulphates are closely associated with other products of acid alteration such as halogen-bearing phases and silica. Local enrichments of halogens are of particular interest. For example, measurements on board the Mars Odyssey spacecraft revealed a global chlorine content of 0.49 wt.% for the Martian surface (Keller et al., 2006), consistent with MER lander results of ~0.3 wt.% (Rao et al., 2002). Since these values are considerably higher than the chlorine abundances of the Martian mantle and crust (0.015 – 0.039 wt.%) (Lodders and Fegley, 1997; Rao et al., 2002; Taylor et al., 2010) and SNC meteorites (0.0014

– 0.11 wt.%) (Dreibus and Wänke, 1987; Banin et al., 1992) secondary processes are likely to be responsible for this enrichment (Keller et al., 2006). Proposed mechanisms for the formation of halogen-rich mineral assemblages include evaporite deposition (Clark et al., 2005; McLennan et al., 2005), chemical alteration through hydrothermal (Schmidt et al., 2008; Yen et al., 2008), acid-fog reactions associated with volcanic exhalations (Arvidson et al., 2004; Tosca et al., 2004), and photochemical oxidation (Marion et al., 2010; Hanley et al., 2012; Kounaves et al., 2014).

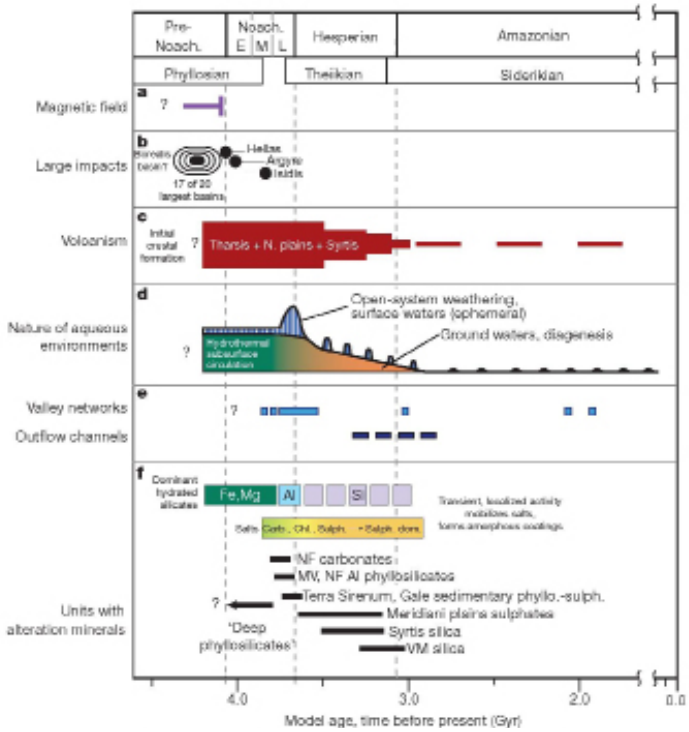

Figure 1.2. Timeline of major processes in Mars´ geological history (from Ehlman et al., 2011). Absolute ages of period boundaries have uncertainties of several hundred million years. NF: Nili Fossae, NV: Marwth Vallis; VM: Valles Marineris; Carb.: carbonates, Chl.: chlorides; Sulph.: sulphates.

The combined occurrence of minor amounts of sulphate and halogen minerals in Martian SNC (shergottite, nakhlite and chassigny) meteorites suggests the former presence of hydrothermal briny aqueous fluids (Bridges et al., 2001; Sutton et al., 2001; Greenwood, 2005; Howarth et al., 2015). The 2-3 times larger abundance of sulphides in shergottites than in terrestrial igneous rocks (Lorand et al., 2005) points to elevated sulphur concentrations in the interior of Mars. Since the sulphur content of Martian basalts is relatively high (Lodders, 1998; McSween et al., 2006; 2008), the crystallization of lavas must have released significant amounts of sulphur-rich volatiles through time (Gellert et al., 2004; Haskin et al., 2005; Gellert et al., 2006), which

would also include simultaneous emission of halogens. Reaction of volatile sulphur and chlorine compounds with water from magmatic vapours, ice or groundwater would inevitably produce acidic fluids. Likely environments for surface discharge of sulphur-rich volcanic fluids are fumaroles, solfataras, hot springs and volcanic lakes, similar to present-day active manifestations on Earth, which would imply that other halogens were emitted as well.

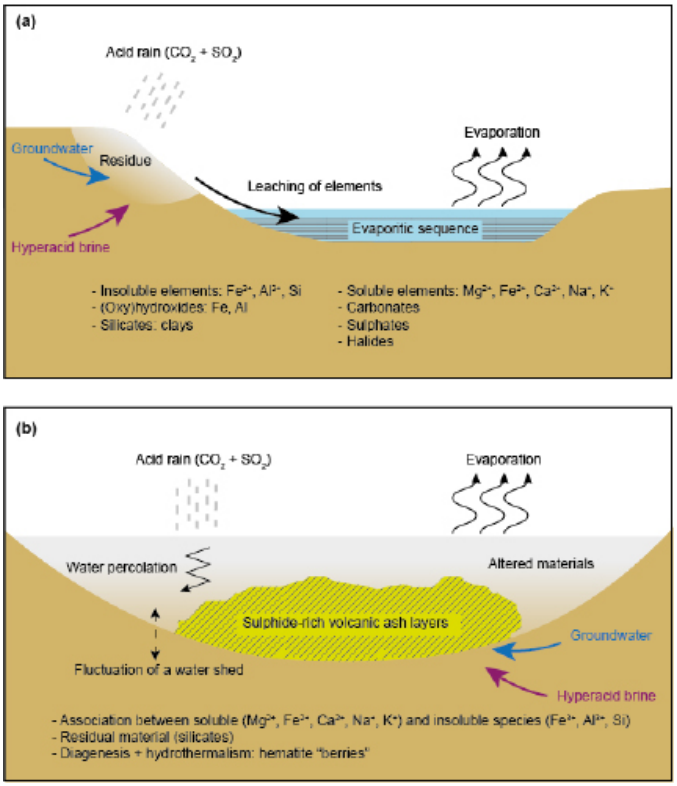

Figure 1.3. Hypothetical scenarios for the formation of sulphate deposits on Mars (modified from Chevrier and Mathé, 2007): (a) alteration, leaching, transport and subsequent deposition in a lake or a sea; (b) *in situ* alteration and transformation of minerals, driven by the input and evaporation of water.

1.2. VOLCANISM ON MARS

The crust of Mars is mostly made up of basaltic rocks carrying variable amounts of olivine, pyroxene and plagioclase (Christensen et al., 2000; Mustard et al., 2005). Global mapping using morphological (Tanaka et al., 2014) and spectral data (Christensen et al., 2001; Bibring et al., 2005) has revealed that volcanic products cover vast areas of the Martian surface, concentrated in a few large volcanic provinces located at Tharsis and Elysium Rises (Hodges and Moore, 1994), around the ancient Hellas impact basin (Williams et al., 2009) and at Syrtis Major (Grott et al., 2013). Volcanism on Mars was most likely intense during its early history and gradually

decreased over time with episodic periods of higher activity (Werner, 2009; Hauber et al., 2011; Robbins et al., 2011; Xiao et al., 2012).

Sediments analysed by the Opportunity rover at Eagle crater (Meridiani Planum), grouped under the Burns Formation (ca. 3.7-3.5 Ga), appear to be aeolian, but others exhibit textural features strongly indicative of subaqueous sediment transport (Squyres et al., 2004b; Grotzinger et al., 2005; McLennan et al., 2005), massive weathered ice deposits (Niles and Michalski, 2009) or base surges from volcanic explosions or impact events (Knauth et al., 2005; McCollom and Hynek, 2005). Textures such as cross-bedding, lamination, gradation, apparent bomb sags and probable accretionary lapilli suggest that pyroclastic and perhaps hydro-volcanic processes constructed Home Plate at Gusev crater (Squyres et al., 2007; Lewis et al., 2008). Moreover, some layered sediments examined by Mars Global Surveyor appear to thin out with increasing distance from the Tharsis region, which suggests that these post-Noachian materials could correspond to volcanic ash flows and air fall deposits from explosive eruptions (Hynek et al., 2003; Broz and Hauber, 2012).

Deposition environments proposed for the sulphate-rich interior layered deposits (ILD) terrains from Valles Marineris, include colluvial (Nedell et al., 1987), aeolian (Peterson, 1981), volcanic (Chapman and Tanaka, 2001; Komatsu et al., 2004), lacustrine (McCauley, 1978; Komatsu et al., 1993; Lucchitta et al., 1994), explosive subaerial (Lucchitta, 1987; 1990; Chapman, 2002; Hynek et al., 2013) or subglacial volcanic settings (Nedell et al., 1987; Chapman and Tanaka, 2001; Komatsu et al., 2004).

1.3. VOLCANIC-HYDROTHERMAL SYSTEMS AS TERRESTRIAL ANALOGUE

Hydrothermal systems on Earth consist of a heat source and lithologies with sufficient permeability for a fluid to circulate and transport heat and dissolved components. These requirements are often met in areas with Quaternary active volcanism where geothermal gradients are usually steep and rock permeabilities high. The heat source may be a major magma intrusion or a complex of dykes or minor intrusions. When a magma body rises towards the surface, the accompanying pressure release decreases the solubility of many of the volatiles present in the melt. Crystallization of cooling magma after its emplacement further promotes volatile saturation in the residual melt. The volatiles ultimately exsolve and escape in a gaseous mixture that mainly consist of H_2O, CO_2, SO_2, H_2S, HCl, HF and HBr (Symonds and Reed, 1993). These magma-derived gas components can react with host rocks, escape to the surface or condense in cold groundwater, creating extremely acid SO_4-Cl-type fluids (Giggenbach et al., 1988).

Hyperacid volcanic lakes are surface expressions of volcanic-hydrothermal systems and the result of the interaction of a rising magmatic gas/fluid of deep origin and a body of meteoric water derived from rain and/or snow melt. The most active lakes consist of hyperacid brine water (pH≤1) with temperatures in the range of ca. 45 to

60°C, SO_4 and Cl contents between 1000 and 100,000 ppm, and major cations (Al, Fe and Ca) up to thousands of ppm (Delmelle and Bernard, 1994; Pasternack and Varekamp, 1997; Varekamp et al., 2000; Delmelle et al., 2000; Kempter and Rowe, 2000; Gammons et al., 2005; Martínez et at., 2000; Varekamp et al., 2009; Christenson et al., 2015). Well-known examples of volcanoes hosting such lakes are Kawah Ijen in Indonesia (Delmelle and Bernard, 1994), Ruapehu in New Zealand (Christenson and Wood, 1993), Yugama in Japan (Takano et al., 1994), Santa Ana in El Salvador (Bernard et al., 2004), Poás (Martínez et al., 2000; Martínez, 2008) and Rincón de la Vieja (Tassi et al., 2005) in Costa Rica, and Copahue in Argentina (Varekamp et al., 2009) (Fig. 1.4).

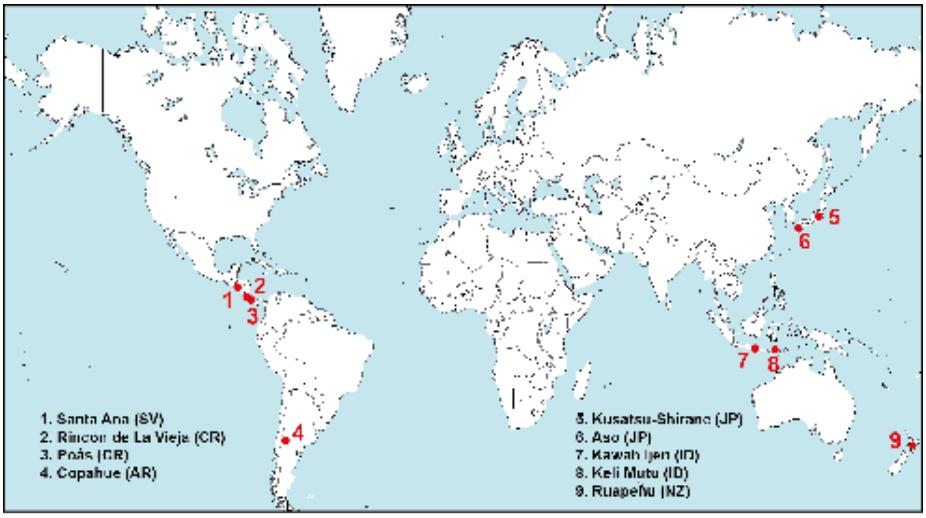

Figure 1.4. Examples of volcanoes hosting hyperacid lakes around the world. Research presented here is based on the hypothesis that metal-rich brines and gases associated with these systems could be similar to fluids involved in the formation of the sulphur- and halogen-rich mineral assemblages on the surface of Mars. This thesis discusses field and experimental data on Copahue (Argentina), Poás (Costa Rica) and Kawah Ijen (Indonesia).

Although sulphate minerals are common in terrestrial systems affected by evaporation or acid-mine drainage, there occurrence in volcanic-hydrothermal settings or acid volcanic fluids is widespread and offers opportunities to study their formation in combination with other alteration products in "Mars-like" assemblages such as amorphous silica, goethite, hematite and kaolinite. For example, the jarosite–alunite group of sulphates is known from acid-mine drainage systems (Fernández-Remolar et al., 2004) but is also is encountered in volcanic-hydrothermal settings (Delmelle et al., 2000; Van Hinsberg et al., 2010; Cousins et al., 2013; Hynek et al., 2013) and as product of fumarolic alteration in active volcanic craters (Africano and Bernard, 2000). This demonstrates that volcanic settings provide the sulphate-rich, acidic (pH<4.0) and oxidizing conditions that this group of sulphates needs for their

formation (Stoffregen, 1993; Stoffregen et al., 2000; Bishop et al., 2005; Papike et al., 2006). Studies of surface expressions of volcanic hosted hydrothermal systems thus offer opportunities to study a range of interactions between rocks and acid sulphate-chloride fluid that could explain the abundance and diversity of Martian secondary mineral assemblages.

1.4. RESEARCH APPROACH AND THESIS OUTLINE

The research described in this thesis is based on the working hypothesis that active volcanic hydrothermal systems can serve as model for studying the origin of sulphates and associated secondary minerals detected in confined terrains across the surface of Mars. Investigations were aimed at obtaining comprehensive insight into alteration processes involving acid sulphate-chloride fluids. They comprised field-based explorations, geochemical and mineralogical analysis of sampled rocks, minerals, waters and gases, modelling of fluid-solid interactions and laboratory experiments.

Field research was carried out at two active volcanoes, each with an acid crater lake and other surface expressions of a hydrothermal system in their interior. The distribution of sulphates and other secondary minerals, in conjunction with the chemical composition of associated fluids was explored to identify the nature and local controls of alteration processes. Geochemical modelling of fluid-rock interactions was performed to assess formation mechanisms and stability conditions of sulphate-bearing alteration assemblages found in the field, and to predict their possible presence at depth.

Special attention has been paid to the behaviour of halogens as tracer of processes operating in the trajectory between magma and atmosphere (Villemant et al., 2003; 2005; Wu et al., 2012; Villemant et al., 2014; Fisher et al., 2015). The rationale is that halogen compounds (HCl, HF, HBr), after H_2O, SO_2 and CO_2, are not only the most abundant volatiles in volcanic systems on Earth (Aiuppa et al., 2009), but have also been preserved as components of minerals in local associations with sulphates on Mars (Newsom et al., 1999; Schmidt et al., 2008; 2009). Chlorine stable isotope compositions of acidic volcanic waters and fumaroles, along with their Cl and Br contents, were investigated because they can be sensitive signals of interactions between deep gases and shallow water bodies within a volcanic edifice (Sharp et al., 2010; Li et al., 2015). Experiments on volcanic lake water were carried out to explore the effects of evaporation of natural hyperacid liquids on their Cl isotope compositions, Br/Cl ratios and mineral saturation states.

The selected field settings with discharges of acid sulphate-chloride fluids are the subduction-related stratovolcanoes of Poás (Costa Rica) in a hot and wet climate, and Copahue (Argentina) where cold and dry climatic conditions prevail. Poás volcano in the Central Cordillera of Costa Rica hosts an active summit crater with a hyperacid lake (Laguna Caliente), ephemeral hot springs, fumarole vents and areas

affected by acid rain and/or spray from the lake (Casertano et al., 1987; Martínez et al., 2000; Martínez, 2008). The crater area is marked by a variety of secondary mineral associations, including a range of sulphates. Copahue, a glacier-capped volcano in the eastern Andes on the border between Argentina and Chile, also hosts a highly acidic hydrothermal system at depth (Varekamp, 2004; Kading and Varekamp, 2009; 2011). This subterranean system feeds a crater lake as well as hot springs on the flank of the volcano, producing a strongly acidified watershed where a multitude of sulphates and other secondary minerals precipitate upon cooling and dilution downstream.

The possibility that geological conditions of sulphate-producing environments on Mars were similar to those of terrestrial volcanic hydrothermal systems is explored in **Chapter 2**, based on a concise literature review of representative Martian and terrestrial settings, and supported by reconnaissance geochemical modelling. It is shown that hot and acidic fluids, enriched in sulphur and halogens, issued in volcanic environments produce mineral alterations (Africano and Bernard, 2000; Van Hinsberg et al., 2010), which may well be equivalent in style and distribution to those inferred for Mars (Varekamp, 2008; Hynek et al., 2013; Marcucci et al., 2013; Marcucci and Hynek, 2014).

Chapter 3 presents the results of a field-based study into the extent to which the surroundings of Copahue volcano, with a crater lake, streams and ponds, are analogous to an ancient sulphate-forming terrain on Mars. A watershed, fed by acid seepage in the summit area, presents a variety of chemical environments in which more than 100 minerals were identified. The origin of the main sulphates and other secondary minerals is constrained from their geographic distributions, combined with chemical analyses of the associated acidic waters, saturation calculations and water-rock modelling. It is shown that the setting provides a model for an origin of sulphate mineral suites on Mars wherein waters are initially acidified by interaction with sulphur-rich volcanic gases, become enriched in cations by reaction with basaltic rocks, and subsequently evolve through evaporation or neutralization by surface fluids with higher alkalinity.

Chapter 4 is dedicated to Poás volcano. Based on the chemical compositions of fresh rocks, waters and gases, together with the secondary mineralogy observed in the field, the formation of alteration minerals was modelled by various water-rock-gas interactions. The results from local sub-environments with different fluid/rock ratios distinguish one group of minerals, with a stability that is relatively insensitive to the pH of the associated fluid, from a group of sulphur-bearing phases (including alunite-jarosite minerals and elemental sulphur) that only form under acidic conditions (pH<4). The presence of polyhydrated Mg- and Fe^{2+}-sulphates appears to be restricted to olivine-bearing rocks exposed to limited amounts of acid rain or brine spray, and requires several cycles of olivine dissolution and evaporation. It is shown that the observed mineral associations in the crater of Poás are remarkably similar

to sulphate-bearing assemblages considered to be the product of acid-sulphate alteration on Mars.

Chapter 5 explores the magnitude and causes of Cl-Br and chlorine isotope fractionation seen in fluids of the active crater of Poás volcano. Time-series data for the hyperacid lake (Laguna Caliente) cover a period of almost three decades (1985-2012) when marked changes in activity and physicochemical properties were recorded (Rowe et al., 1992a,b; Martínez et al., 2000; Martínez, 2008). Fluctuations in Br/Cl ratios of the lake water correlate with the activity status of the system and are attributable to phase separation at depth and evaporative loss of gaseous HCl at the lake surface. Condensate samples from a persistently active fumarole field on shore, collected during an interval (2010-2012) with strong changes in gas temperature (between ca. 100 and 800°C), display a large range in $\delta^{37}Cl$ values interpreted to reflect a "scrubbing" effect from the interaction between hot magma-derived gases and shallow aquifers. The results provide new insights into mechanisms responsible for Br-Cl fractionation recorded in Martian halogen-bearing minerals, and offer a complementary guide for interpretations of chlorine isotope data recently obtained on Martian materials (Farley et al., 2016; Sharp et al., 2016; Williams et al., 2016).

Chapter 6 describes evaporation experiments carried out on hyperacid brine water from the crater lake of Kawah Ijen (East Java, Indonesia). Monitoring data on the residual fluid, obtained during progressive evaporation at 60°C, provide constraints on the evolution of dissolved sulphur- and halogen-bearing species, major cations and chlorine isotopes. Observed effects of evaporative concentration such as saturation of solid and gaseous compounds were tested with thermodynamic modelling focusing on ionic strength, activity of water, pH and saturation indices for a variety of phases. Observed changes in the sign and magnitude of chlorine isotope fractionation between dissolved and gaseous Cl are attributed to a gradual change in the distribution of dissolved chlorine species, which controls the isotopic composition of the escaping HCl. The experimental findings simulate the effects of evaporation of acid sulphate-chloride brines such as may have occurred in volcanic terrains on Mars. They predict an extension of the stability of hydrous liquid to temperatures far below the freezing point of normal water.

Chapter 7 presents a synthesis of the results and a perspective on the outcome of this research.

CHAPTER

2

Volcanic hydrothermal systems as potential analogues of Martian sulphate-rich terrains

Rodríguez A. and M.J. van Bergen, 2015. Volcanic hydrothermal systems as potential analogues of Martial sulphate-rich terrains. Netherlands Journal of Geosciences, 95, 153-169, doi: 10.1017/njg.2015.12.

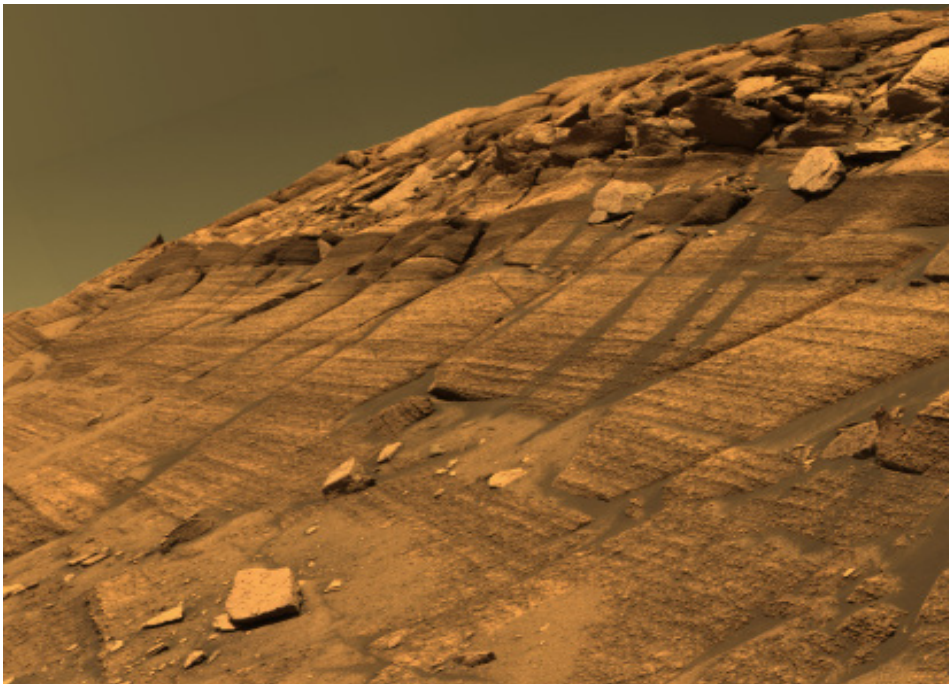

ABSTRACT

Remote sensing observations and rover missions have documented the presence of sulphate-rich mineral associations on Mars. Many of these minerals are paleo-indicators of hydrous, acidic and oxidizing environments that must have prevailed in Mars´ distant past, contrary to the present conditions. Furthermore, occurrences of silica together with high Cl and Br concentrations in Martian soils and rocks represent fingerprints of chemically atypical fluids involved in processes operating on the surface or at shallow depth. From field observations at representative active volcanoes in subduction settings, supported by geochemical modelling, we demonstrate that volcanic hydrothermal systems are capable of producing Mars-like secondary mineral assemblages near lakes, springs and fumaroles through the action of acidic fluids. Water-gas-rock interactions, together with localized flow paths of water and fumarolic gas emitted from associated subaerial vents, lead to deposition of a range of sulphates, including gypsum, jarosite, alunite, epsomite as well as silica. Evaporation, vapour separation and fluid mixing in (near-) surface environments with strong gradients in temperature and fluid chemistry further promote the diversity of secondary minerals. The mineralogical and chemical marks are highly variable in space and time, being subject to fluctuations in ambient conditions as well as to changes in the status of volcanic-hydrothermal activity. It is concluded that active processes in modern volcanic-geothermal systems may be akin to those that created several of the sulphate-rich terrains in the early history of Mars.

Front picture: NASA's Mars Exploration Rover Opportunity captured this view of Burns Cliff after driving right to the base of this southeastern portion of the inner wall of Endurance Crater. The view combines frames taken by Opportunity's panoramic camera between the rover's 287th and 294th martian days (November 13th to 20th, 2004). Source: http://photojournal.jpl.nasa.gov/catalog/PIA07110.

2.1. INTRODUCTION

High concentrations of sulphur, chlorine and bromine found by Viking, Pathfinder and MER (Mars Exploration Rovers Opportunity and Spirit) in soil and rock weathering rinds indicate that probably substantial volcanic degassing of volatile-rich magmas occurred on Mars throughout time (Gellert et al., 2004; Haskin et al., 2005; Gellert et al., 2006). The presence of sulphates at Meridiani Planum, Valles Marineris and Gusev Crater suggest that aqueous alteration by low pH sulphate-rich fluids was involved (Clark et al., 2005; Zolotov and Mironenko, 2007; Ming et al., 2008). Although none of the SNC (shergottite, nakhlite and chassigny) Martian meteorites are pervasively altered, minor amounts of sulphates and halogens like Cl and Br suggest that hydrothermal briny aqueous fluids have interacted with the host rocks and secondary phases formed afterwards upon the evaporation of these solutions (Bridges et al., 2001; Sutton et al., 2001; Greenwood, 2005). High silica abundances in soils from Meridiani Planum, Gusev Crater and in some chasmata of Valles Marineris are most likely a product of intensive acid rock leaching processes and silica precipitation from saturated thermal fluids (Glotch and Bandfield, 2006; Milliken et al., 2008; Squyres et al., 2008; Weitz et al., 2010; Wendt et al., 2011). These observations suggest that low-pH acid-sulphate weathering was a major alteration pathway at some point during Mars' geological history (Bibring et al., 2006; Ming et al., 2006; Zolotov and Mironenko, 2007). In contrast to Earth, where the carbon cycle is a major controlling factor in surface geochemistry, it seems that sulphur cycling processes dominated on Mars at least during part of its evolution (Gaillard et al., 2013). Hot and acidic fluids, enriched in sulphur and halogens, are typically encountered on terrestrial volcanoes, and the styles and distribution of mineral alteration at volcanic settings (Africano and Bernard, 2000; Van Hinsberg et al., 2010) have been compared to those inferred for Mars (Varekamp, 2008; Hynek et al., 2013; Marcucci et al., 2013; Marcucci and Hynek, 2014). Even though volcanism has been an important process in shaping Mars' surface, especially during its early geological history (Wilson et al., 2001; Neukum et al., 2004; Dohm et al., 2009; Carr and Head, 2010), its relevance to the formation of sulphate-rich mineral associations remains to be confirmed. In this paper, we explore the possibility that formation conditions of sulphate-rich assemblages, together with Cl, Br and SiO_2 enrichments on Mars were similar to those of terrestrial volcanic hydrothermal systems, based on a concise literature review of representative Martian and terrestrial occurrences, and supported by geochemical modelling. The working hypothesis is that volcanic geothermal systems can serve as potential analogues to some of the sulphate-rich terrains on Mars and that both style and extent of aqueous alteration can be assessed by comparing Martian systems with terrestrial counterparts. Although meteorite impacts could have created transient thermal anomalies in the Mars crust, leading to impact-induced hydrothermal systems that were fed by ice melting or by pre-existing subsurface fluids (Abramov and Kring, 2005; Barnhart et al., 2010), this scenario is not considered here.

2.2. MARS OBSERVATIONS

Global mapping using morphological (Tanaka et al., 1992) and spectral data (Christensen et al., 2001; Bibring et al., 2005) has revealed that volcanic products cover vast areas of Martian surface. Volcanic landforms are not uniformly distributed but are rather concentrated in a few large volcanic provinces located at Tharsis and Elysium Rises (Hodges and Moore, 1994), around the ancient Hellas impact basin (Williams et al., 2009) and at Syrtis Major (Grott et al., 2013). The oldest volcanic surfaces (ca. 4 to 3.7 Ga) are mainly present on the highland shields such as Hadriaca and Tyrrhena Montes, northeast from the Hellas impact basin (Grott et al., 2013). Volcanism in the highlands probably terminated around 1 Ga at the latest (Williams et al., 2009). More recent volcanic activity has been limited to Tharsis and Elysium. The youngest lavas in the latter volcanic province were emplaced in the Cerberus plains a few million years ago (Vaucher et al., 2009). Even though only a few Noachian volcanic terrains have been preserved, Martian volcanism was most likely intense during its early history and gradually decreased over time with episodic periods of higher activity (Werner, 2009; Hauber et al., 2011; Robbins et al., 2011; Xiao et al., 2012). Since the sulphur composition of Martian basalts is relatively high (Lodders, 1998; Mc Sween et al., 2006; 2008), the crystallization of Martian lavas must have released significant amounts of sulphur-rich volatiles. Reaction of volatile sulphur compounds with water in magmatic vapours, ice or groundwater would inevitably produce acidic fluids. Similar to Earth, likely environments for surface discharge of sulphur-rich volcanic fluids are fumaroles, solfataras, and hot springs.

2.2.1. Potential volcaniclastic facies

The sediments analysed by the Opportunity rover at Eagle crater (Meridiani Planum), that were grouped under the name of Burns Formation (ca. 3.7-3.5 Ga), appear to be aeolian, but others exhibit textural features strongly indicative of subaqueous sediment transport (Squyres et al., 2004; Grotzinger et al., 2005; Mc Lennan et al., 2005) or massive weathered ice deposits (Niles and Michalski, 2009). Some authors have also associated the sediment deposits to base surges from volcanic explosions or impact events (McCollom and Hynek, 2005; Knauth et al., 2005). The presence of textures such as cross-bedding, lamination, gradation, apparent bomb sags and probably accretionary lapilli, suggests that pyroclastic and perhaps hydro-volcanic processes constructed Home Plate, Gusev crater (Squyres et al., 2007; Lewis et al., 2008). Moreover, some layered sediments examined by Mars Global Surveyor (MGS) appear to thin out with increasing distance from the Tharsis region, which suggests that these post-Noachian materials could correspond to volcanic ash flows and air fall deposits from explosive eruptions (Hynek and Phillips, 2003; Broz and Hauber, 2012).

2.2.2. Sulphate detections

Sulphides are 2-3 times more abundant in SNC shergottites than in terrestrial igneous rocks (Lorand et al., 2005), pointing to elevated sulphur concentrations in the

interior of Mars. Moreover, surface deposits contain high levels of sulphur (SO_3 up to ~37 wt.%, average ~6 wt.%) mostly in the form of sulphates (King and McLennan, 2010). High sulphur concentrations have been detected in soils of the northern plains by Viking (up to 10 wt.% SO_3, Clark et al., 1976; Baird et al., 1976; Toulmin et al., 1976) in Ares Vallis by Pathfinder (up to 8 wt.% SO_3, Rieder et al., 1997; Bell et al., 2000; Economou, 2001; Foley et al., 2003), in Columbia Hill outcrops (Gusev Crater) by MER Spirit and at Meridiani Planum by MER Opportunity (up to 40 and 25 wt.% SO_3, respectively, Gellert et al., 2004; Rieder et al., 2004; Squyres et al., 2004; Gellert et al., 2006; Ming et al., 2006; Wang et al., 2006). The main sulphates identified by Opportunity are jarosite $(K,Na,H_3O)Fe_3(SO_4)_2(OH)_6$ (Klingelhöfer et al., 2004), gypsum and magnesium sulphates (Squyres et al., 2004; Clark et al., 2005; Wang et al., 2006).

2.2.2.1. Northern polar region

Gypsum ($CaSO_4 \cdot 2H_2O$) deposits were identified in the northern polar region dune fields of Olympia Planum using OMEGA data (Langevin et al., 2005; Fishbaugh et al., 2007). Later observations revealed that gypsum deposits are not only restricted to Olympia Planum but are present in various sediments covering the northern polar cap and the circum-polar dune field (Massé et al., 2010). The bulk of the observed gypsum consist of sand-sized grains rather than surficial crusts or fine-grained deposits, which is more consistent with percolation within aeolian deposits (Fishbaugh et al., 2007; Horgan et al., 2009; Massé et al., 2010). Gypsum crystals, either pre-existing or authigenic were probably enclosed by ice crystals during formation of the polar cap, and were then released after sublimation of the ice (Massé et al., 2010). Irrespective of the sedimentation mechanisms, gypsum could have formed by the interaction of Ca (coming from dissolution of Ca-rich phases like pyroxene and plagioclase) with SO_4-rich fluids derived either from water-condensed SO_2 produced by volcanic activity (Fairén et al., 2004; Tosca et al., 2004) or from weathering of sulphides in the presence of water under oxidative conditions (Chevrier et al., 2004; 2006). Although water, sulphur and calcium may have co-existed locally within the sand grains, mass-balance calculations suggest that sulphide oxidation and/or SO_2 coming from volcanic activity could have significantly contributed to gypsum formation (Fishbaugh et al., 2007). In view of their Late Amazonian age, the gypsum deposits from the northern polar cap do not easily fit into the global alteration history of Mars, which conveys that sulphate deposition was prominent during the Hesperian (Bibring et al., 2006)

2.2.2.2. Valles Marineris

The OMEGA spectrometer also mapped sulphates in equatorial regions like Valles Marineris (Bibring et al., 2005; Mangold et al., 2008). The interior layered deposits (ILD) terrains, containing the sulphates, represent important deposits, tens of km wide, and several km thick (Bibring et al., 2005; Gendrin et al., 2005). Deposition

environments proposed for ILD include colluvial (Nedell et al., 1987), aeolian (Peterson, 1981), spring deposits (Rossi et al., 2008), volcanic (Chapman and Tanaka, 2001; Komatsu et al., 2004) lacustrine (McCauley, 1978; Komatsu et al., 1993, Lucchitta et al., 1994), and explosive subaerial (Lucchitta, 1987, 1990; Chapman, 2002; Hynek et al., 2013) or subglacial volcanic settings (Nedell et al., 1987, Chapman and Tanaka, 2001; Komatsu et al., 2004). West Candor Chasma (Valles Marineris) is the canyon with the thickest stack of ILD and one the largest areas covered by sulphates (Mangold et al., 2008; Flahaut et al., 2010, 2012; Fuetes et al., 2014). Sequences of polyhydrated sulphates (Mg-, Fe- and possibly also Ca-rich) and monohydrated sulphates (mostly kieserite, $MgSO_4 \cdot H_2O$) have been detected by OMEGA and CRISM in Capri Chasma (Flahaut et al., 2010), Ophir Chasma and Ophir Mensa (Flahaut et al., 2010; Wendt et al., 2011), West Candor Chasma and Candor Mensa (Flahaut et al., 2014). The inferred rather monotonous distribution of these sulphates over wide areas, and intercalation of monohydrated and polyhydrated phases suggests that they may have formed via evaporation of a shallow body of standing water (Flahaut et al., 2010), rain, snow, ice (Niles and Michalsky, 2009; Weitz et al., 2010 Wendt et al., 2011) or local groundwater (Grindod and Balme, 2010). Climate change or volcanism possibly promoted the stability of liquid water on Mars' surface (Mangold et al., 2008, Kite et al., 2013). The presence of kieserite in heavily eroded scarps suggests that this phase was probably present in the original rock where it had formed either during formation and diagenesis of sediments or during hydrothermal alteration at depth (Mangold et al., 2008). Experiments have shown that kieserite is easily converted to hexahydrite $MgSO_4 \cdot 6H_2O$ and epsomite $MgSO_4 \cdot 7H_2O$ when exposed to water. In contrast, upon renewed desiccation, these minerals are not transformed back to kieserite but form amorphous phases (Vaniman et al., 2004). Also, dehydration of polyhydrated sulphates is unlikely to have occurred at any time on the surface of Mars (Roach et al., 2009). Therefore, kieserite may not have been preserved in deposits that experienced cycles of surface hydration and desiccation. Local associations of amorphous silica and jarosite in Ophir Chasma (Wendt et al., 2011), Iani Chaos (Sefton-Nash et al., 2012), Melas Chasma (Bishop et al., 2009), Juventae Chasma (Milliken et al., 2008; Bishop et al., 2009), Melas Plateau (Weitz et al., 2010) and Noctis Labyrinthus (Thollot et al., 2012) have been interpreted as products of low-temperature acid alteration of basalts.

2.2.2.3. Meridiani Planum

Jarosite, Mg- and Ca-sulphates have been detected in situ by MER Opportunity at Meridiani Planum in the aeolian and subaqueous sedimentary sequence of the Burns Formation (Klingelhöfer et al., 2004; Squyres et al., 2004; Clark et al., 2005; Grotzinger et al., 2005; McLennan et al., 2005, Glotch et al., 2006). Hematite (Fe_2O_3) nodules in this formation probably formed during early burial diagenesis of the sediments, either by replacement of pre-existing sulphates (Christensen et al., 2004) or by jarosite breakdown (Fernández-Remolar et al., 2005; Sefton-Nash and Catling, 2008). Fluid-rock modelling by Tosca et al. (2005) suggested that assemblages of

Fe-, Mg- and Ca-sulphates together with hematite can be derived from low-pH and SO_4-rich fluids that have interacted with basalts. Groundwater dissolution of jarosite may have provided Fe^{3+} for hematite precipitation, but the substantial amounts of jarosite still present would imply that the water-mediated diagenesis did not proceed long enough to convert all the iron into oxides. Hence, water/rock ratios must have been low, possibly due to water removal via freezing or evaporation (Elwood-Madden et al., 2004; Squyres and Knoll, 2005).

2.2.2.4. Gusev and Gale Craters

The MER Spirit excavated soils exhibit high albedo and relatively white to yellow colours at several locations south of Husband Hill in Gusev Crater. Alpha Particle X-ray Spectrometer (APXS) observations revealed high sulphur contents, up to 35 wt.% SO_3 (Johnson et al., 2007). Mössbauer spectrometry suggested that the soils contain Fe^{3+}-bearing sulphates in various states of hydration, such as ferricopiapite $Fe_{0.67}{}^{3+}Fe_4{}^{3+}(SO_4)_6(OH)_2{\cdot}20H_2O$, hydronium jarosite $(H_3O)Fe^{3+}{}_3(SO_4)_2(OH)_6$, fibroferrite $Fe^{3+}(SO_4)(OH){\cdot}5H_2O$, rhomboclase $HFe^{3+}(SO_4)_2{\cdot}4H_2O$ and paracoquimbite $Fe^{3+}{}_2(SO_4)_3{\cdot}9H_2O$ (Gellert et al., 2006; Morris et al., 2006; Ming et al., 2006; Wang et al., 2006; Johnson et al., 2007). Furthermore, combined Mössbauer and APXS data showed the presence of Fe-, Mg- and Ca-sulphates in Paso Robles class soils (Yen et al., 2008). Calcium sulphates in the light-toned salty soils suggest that the degree of alteration of local rocks was more severe and went beyond olivine dissolution (Wang et al., 2008). The geochemical and mineralogical observations favour ion transportation by fluids and salt deposition in an open hydrologic system as plausible scenario for the deposition of sulphates in the subsurface regolith (Wang et al., 2006). Magnesium and iron carbonates in some outcrops of volcaniclastic rocks at Columbia Hill, east of Husband Hill (Carter and Poulet, 2012) may have formed from low-temperature hydrothermal activity and limited water-rock interaction within a Noachian ephemeral lake in Gusev Crater (Ruff et al., 2014). Gale crater exposes a thick sequence of bedded deposits with an upward transition from phyllosilicate and phyllosilicate/sulphate-bearing layers to predominantly sulphate-bearing layers, possibly reflecting a global shift from near-neutral/alkaline to more acidic conditions (Milliken et al., 2010). CRISM spectra indicate the presence of mono- and polyhydrated magnesium sulphates (Milliken et al., 2010). The sedimentary deposits are probably Early Hesperian in age, and their geological characteristics could be explained by lacustrine and aeolian environments (Thomson et al., 2011; Wray, 2013). After the impact that formed Gale crater, a hydrothermal system may have been active for several hundred thousand years, and a crater lake with associated sediments is likely to have formed (Schwenzer et al., 2012).

Due to its ubiquity, acid-sulphate alteration has been a major feature on Mars' surface, having produced predominantly iron, magnesium and calcium sulphates (Gellert et at., 2004; Morris et al., 2004; Gellert et al., 2006; Morris et al., 2006; Tosca et al., 2006; Johnson et al., 2007; Bishop et al., 2009; Ehlmann et al., 2011; Gaillard et

al., 2013). The presence of Fe-sulphates implies that environmental conditions were rather oxidizing and acidic (pH<4) (Nordstrom and Alpers, 1999; Nordstrom et al., 2000; Bigham and Nordstrom, 2000). Since the aqueous solubilities of iron and magnesium sulphates are high, the abundances of these minerals point to limited interaction between sulphur-rich acidic fluids and ferromagnesian minerals such as olivine and pyroxene. Two scenarios can broadly explain the formation of abundant sulphate on the Martian surface: 1) alteration of sulphide-rich rocks (Fernández-Remolar et al., 2005, Zolotov and Shock, 2005; Dehouck et al., 2012), and 2) alteration in the presence of SO_2 (acid fog or groundwater) (Tosca et al., 2004; Tosca el al., 2005; Chevrier and Mathé, 2007; Zolotov and Mironenko, 2007).

2.2.3. Silica-rich deposits

The role of water in the formation of silica-rich deposits on Mars has been somewhat controversial. Evidence for acid leaching have been inferred for Meridiani Planum, where the Mini-TES (Miniature Thermal Emission Spectrometer) of the Opportunity rover detected as much as 25% of opaline silica (hydrated amorphous silica) and/or high-silica glass in outcrop rocks associated with sulphates (Glotch et al., 2006). This paragenesis is consistent with aqueous deposition of silica at low pH (Zolotov and Mironenko, 2007). A similar association of silica-rich phases (amorphous silica, phyllosilicates or zeolites) and (less abundant) sulphates is present in the western Hellas Basin (Bandfield, 2008). Acid hydrothermal leaching of basaltic rocks has also been proposed as formation mechanism for opaline silica deposits in the Nili Patera caldera on the Syrtis Mayor volcanic complex (Skok et al., 2010). Additionally, Alpha Particle X-ray Spectrometer (APXS) analysis of light-coloured soils by Spirit at Husband Hill (Gusev Crater) revealed the combination of elevated SiO_2 contents and the presence of Fe- and Mg-sulphates at the sites of Paso Robles (Yen et al., 2008) and Tyrone (Wang et al., 2008), indicating that these soils likely formed by the interaction between rocks and fumarolic condensates derived from degassing magma and/or by oxidative alteration of crustal Fe-sulphide deposits (Yen et al., 2008). Amorphous silica and jarosite associations have also been identified by CRISM data on plateaus above Juventae Chasma (Milliken et al., 2008, Bishop et al., 2009), Melas Chasma (Metz et al., 2009) and Ophir Chasma (Wendt et al., 2011), where they have been interpreted as the product of acid alteration of basalts. Extremely high concentrations of amorphous silica (>90% SiO_2) have been measured by MER Spirit's APXS in soils next to Home Plate, Gusev crater (Squyres et al., 2008). The silica phase is opal-A, according to thermal infrared spectra acquired by the Mini-TES (Squyres et al., 2008). From a negative correlation between the SiO_2 contents and Fe^{3+}/Fe_{tot} values in the soils, the lack of sulphur enrichments and textural evidence, Ruff et al. (2011) concluded that these silica-rich deposits probably formed by precipitation from near-neutral pH thermal springs or geysers.

2.2.4. Chlorine and bromine abundances

Both Martian basalts (meteorites and surface basalts) and the bulk Martian mantle are inferred to be 2–3 times richer in Cl than corresponding terrestrial basalts and mantle (Dreibus and Wänke, 1987; Filiberto and Treiman, 2009; Taylor et al., 2010). This could, in theory, imply that chlorine rather than water is the main volatile in Martian basaltic magmas. However, the water content in the Martian mantle is still a matter of ongoing discussion (Grott et al., 2013; Gross et al., 2013). Volatile fugacity ratios in apatites from NWA 6234, an olivine-phyric shergottite (Filiberto et al., 2012) thought to represent a crystallized primitive melt (Musselwhite et al., 2006), suggest that chlorine and water contents of the Martian mantle, parental to SNC meteorites, are higher than previously thought and similar to those of the mantle source of terrestrial mid-ocean ridge basalts (Gross et al., 2013).

Measurements on board of the Mars Odyssey Gamma Ray Spectrometer (GRS) revealed a global chlorine content of 0.49 wt.% for the Mars surface (Keller et al., 2006), consistent with MER lander measurements of ~0.3 wt.% (Rao et al., 2002). Since these values are considerably higher than the chlorine abundance of the Martian mantle and crust (0.015 – 0.039 wt.%) (Lodders and Fegley, 1997; Rao et al., 2002; Taylor et al., 2010) and SNC meteorites (0.0014 – 0.11 wt.%) (Dreibus and Wänke, 1987; Banin et al., 1992), secondary processes are likely to be responsible for this enrichment (Keller et al., 2006). The NWA 6234 shergottite has a bulk Cl content of 59 ppm and a Br/Cl molar ratio of 0.0040 (Burguess et al., 2013), comparable to the molar Br/Cl ratios of 0.0025 for Mars' bulk composition (Taylor et al., 2010). High contents of halogens (including Cl and Br) and other elements with a strong affinity for aqueous solutions in rocks found at Barnhill (north-western Home Plate, Gusev Crater) point to interaction with briny fluids (Schmidt et al., 2008). The Br/Cl molar ratios measured at Paso Robles (Gusev Crater), by MER Spirit range from 0.0025 to 0.0399 (Yen et al., 2008). At Meridiani Planum, samples measured after the rock abrasion tool (RAT), exhibited Br/Cl molar ratios of 0.025 to 0.00091 (Brückner et al., 2008). APXS analysis of sedimentary rocks at Yellowknife Bay (Gale Crater) yielded Br/Cl molar ratios between 0.097 and 0.016 (McLennan et al., 2014). Comparing all these Br/Cl ratios to both NWA 6234 and Martian bulk values, probably considerable elemental fractionation between these two halogens took place on Mars´ surface. APXS analyses on Martian rocks found on the surface, show that bromine concentrations are low in basalt samples, but enriched in samples that have probably undergone weathering, evaporation and diagenesis (Rieder et al., 2004; Clark et al., 2005). Zhao et al. (2014) concluded that the observed variability in Br/Cl ratios is largely controlled by Br abundances. From the negative correlation between Cl content of surface materials, thermal inertia and rock abundance, and the positive correlation with albedo, Keller et al. (2006) hypothesised that fine, mobile aeolian materials are enriched in Cl. Nevertheless, the uneven distribution of Cl contents, with enrichments in the equatorial regions close to Tharsis Montes, suggests that additional processes must have played a role in concentrating chlorine on Mars' sur-

face, such as evaporite deposition (Clark et al., 2005, McLennan et al., 2005), chemical alteration through hydrothermal activity (Schmidt et al., 2008; Yen et al., 2008), acid-fog reactions associated with volcanic exhalations (Arvidson et al., 2004; Tosca el al., 2004), and photochemical oxidation (Marion et al., 2010; Hanley et al., 2012; Kounaves et al., 2014).

2.3. EARTH OBSERVATIONS

2.3.1. Volcanic hydrothermal systems

Hydrothermal systems consist of a body of hot rock whose permeability is enough for a fluid to circulate and obtain heat from the rock under certain temperature and pressure conditions. This scenario can occur in various geological settings. Volcanic hydrothermal systems are found in areas with active volcanism where the geothermal gradient and rock permeability are usually high. The heat source may be a major magma intrusion or a complex of dykes or minor intrusions. When a magma body rises towards the surface, diminishing lithostatic pressures decrease the solubility of volatiles present in the melt. Also, crystallization of a cooling magma reservoir after its emplacement will promote volatile saturation in residual melt. In both cases, volatiles can ultimately exsolve, causing degassing. The volatiles mainly consist of H_2O, CO_2, SO_2, H_2S, HCl, HF and HBr (Symonds and Reed, 1993). These magmatic components can react with host rocks, escape to the surface or condense in cold groundwater, creating extremely acid fluids (SO_4-Cl-type waters) (Fig. 2.1). The acidity comes primarily from the bisulphate ion (HSO_4^-), produced by the aqueous dissolution of and its disproportionation (Kusakabe et al. 2000; Symonds et al., 2001). In addition, $HCl_{(g)}$ significantly contributes to acidity, due to its high aqueous solubility. If local boiling of deep fluids produces vapour that enters shallow aquifers, SO_4-type waters are produced. Since the pH of both SO_4-Cl- and SO_4-type waters is low (<3), their interaction with rocks promotes uptake of cations by the solution and hydrothermal alteration, which is commonly recorded by mineralogical, textural and chemical changes of the original rock. Which secondary mineral assemblages are formed is a function of many parameters such as temperature, pressure, type of primary fluids involved (e.g. meteoric, seawater), acid supply, rock composition and the water-rock ratio (which is related to permeability).

Advanced argillic alteration in internal zones of volcanoes (Fig. 2.1) is caused by rock leaching with acid waters that contain residual magmatic volatiles. A porphyritic rock can become completely silicified, with silica replacing the groundmass as well as phenocrysts. The silicification is surrounded by alunite-rich alteration and subsequently by kaolinite (Steiner, 1977; Heald et al., 1987). Deeper levels may contain phyrophyllite, diaspore and dickite; and regionally, chlorite, albite, calcite and pyrite alteration (Einaudi et al., 2003). The cation-rich acidic brine that leaves a silica-rich residue is capable of forming Mg-, Fe-, Ca- and eventually Al-sulphates, depending on water/rock ratios and temperatures (Tosca et al., 2004; 2005; Tosca and McLen-

nan, 2006). Examples of this alteration style can be observed around fumaroles and in crater settings with a hyperacid volcanic lake. At greater distances from the heat source (magma body), an adularia-sericite-type deposit can form where superficial waters mix with deeper, heated saline waters in a lateral flow system. In this case neutral to weakly acidic, alkali chloride silica-saturated waters are dominant (Heald et al., 1987).

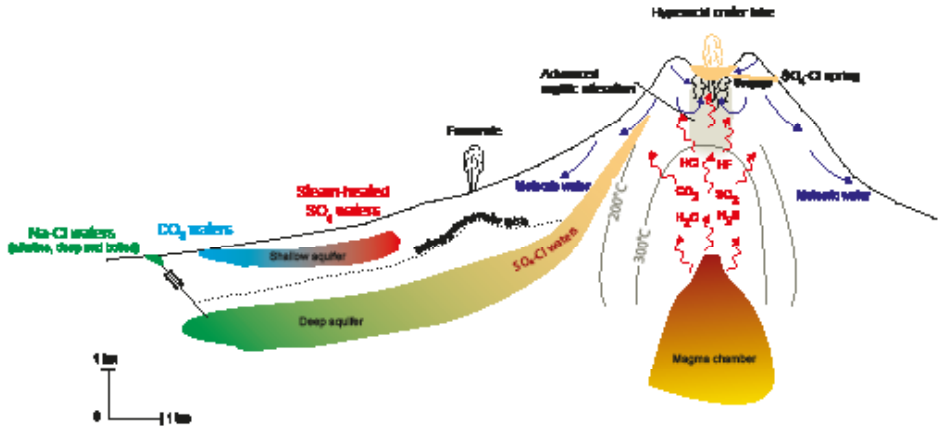

Figure 2.1. Schematic profile depicting the distribution of fluid types and alteration zones in a crater lake hosting stratovolcano setting. Modified from Henley and Ellis (1983), Heald et al. (1987) and Arnórsson et al. (2007).

2.3.2. Acid crater lakes

Hyperacid volcanic lakes are surface expressions of volcanic-hydrothermal systems and are the result of interaction of a rising magmatic gas/fluid of deep origin and a body of meteoric water derived from rain and/or snow melt. The temperatures of the SO_4-Cl-type waters of these lakes range from ca. 45 to 60°C, and pH values are commonly below 2 (Pasternack and Varekamp, 1997; Varekamp et al., 2000). The acid volcanic lakes and their associated alteration zones in host craters usually cover areas ranging from a few to tens of km^2 (Rowe et al., 1992; Africano and Bernard, 2000; Delmelle et al., 2000; Kempter and Rowe, 2000). In many cases, active fumaroles are present as well (Fig. 2.2).

The most active lakes (pH≤1) are hyperacid brines, with SO_4 and Cl contents between 1000 and 100,000 ppm, together with major cations (Al, Fe and Ca) often in the thousands of ppm (e.g., Varekamp et al., 2000; Delmelle et al., 2000; Kempter and Rowe, 2000; Gammons et al., 2005; Martínez, 2008; Varekamp et al., 2009). Volcanoes with well-known examples of such lakes are: Poás (Costa Rica, Fig. 2.2a), Kawah Ijen (Indonesia, Fig. 2.2b), Ruapehu (New Zealand), Kusatsu-Shirane (Japan), Rincón de La Vieja (Costa Rica) and Copahue (Argentina). The SO_4-Cl-type surface waters in stratovolcanoes are not always confined to crater lakes but can also be issued from springs on the flank close to the active crater, either as seepage water

from the lake or as independent outlet of the subsurface hydrothermal system.

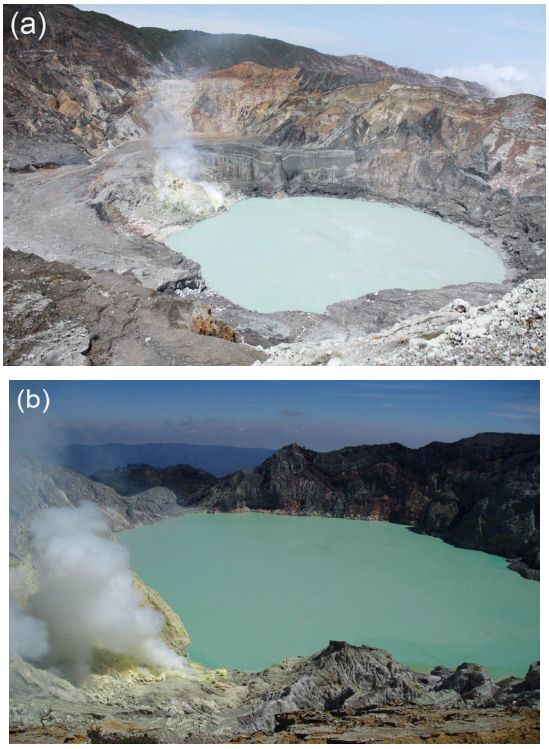

Figure 2.2. Hyperacid lakes of (a) Poás volcano (Costa Rica) and (b) Kawah Ijen (East Java, Indonesia).

2.3.3. Sulphates and silica-rich deposits

Amorphous silica, gypsum $CaSO_4 \cdot 2H_2O$, elemental sulphur S, barite $BaSO_4$ and anatase TiO_2 are saturated in many of these waters, and are commonly present as chemical precipitates in the water column and in lake-bottom sediments (e.g., Delmelle and Bernard, 1994; Varekamp et al., 2000; Martínez, 2008). In the bottom sediments of Poás, Kawah Ijen and Copahue hyper-acid lakes, where rather reducing conditions tend to prevail, pyrite FeS_2 and other sulphides are found as well. Although aggressive leaching usually leaves a bleached, silica-rich residue of volcanics in lake-hosting crater areas, silica is supplied by input of hot fluids. Cooling leads to continuous chemical sedimentation of amorphous silica, with gypsum as most abundant associated sulphate.

Furthermore, if we calculate saturation indices for hyper-acid waters of Poás and Copahue, it appears that in deeper parts of these volcanic systems, where temperatures are considerably higher, minerals such as hematite Fe_2O_3, diaspore α-AlO(OH) and alunite $(K,Na,H_3O)Al_3(SO_4)_2(OH)_6$ become oversaturated and thus prone to pre-

cipitation. We could confirm the presence of alunite, in combination with quartz and elemental sulphur, in ancient fumarole fields at Poás and in clasts ejected during the December 2012 eruption of Copahue. Jarosite $(K,Na,H_3O)Fe_3(SO_4)_2(OH)_6$, in association with amorphous silica and iron oxides has been found at Poás as an alteration product between lavas and acid rain. A closer examination of the alteration products revealed that amorphous silica is present in the outer parts of the rocks as a patina, and that the alteration proceeded to form jarosite and eventually iron oxides (Fig. 2.3). Jarosite is also abundant around Río Agrio spring (T=52°C, pH=0.49) at Copahue volcano (Fig. 2.4). Its water is saturated with jarosite and alunite since 2000 (Varekamp et al., 2009).

We found a wide range of other hydrous sulphates in the environments with hyperacid lakes, springs and streams that apparently formed as efflorescence products. Efflorescence of gypsum $CaSO_4 \cdot 2H_2O$, natrojarosite $NaFe_3(SO_4)_2(OH)_6$, khademite $Al(SO_4)F \cdot 5H_2O$, ferricopiapite $Fe^{3+}_{0.67}Fe^{3+}_4(SO_4)_6(OH)_2 \cdot 20H_2O$, magnesiocopiapite $MgFe^{3+}_4(SO_4)_6(OH)_2 \cdot 20H_2O$, and voltaite $K_2Fe^{2+}_5Fe^{3+}_3Al(SO_4)12 \cdot 18H_2O$, as well as epsomite $MgSO_4 \cdot 7H_2O$, hexahydrite $MgSO_4 \cdot 6H_2O$, pentahydrite $MgSO_4 \cdot 5H_2O$ and kieserite $MgSO_4 \cdot H_2O$ are present in the Copahue area, and epsomite at Poás. Field observations indicate that their occurrence is related to fumaroles and to rock crusts where probably limited water-rock interaction, in combination with evaporation, has taken place. Efflorescence products on the borders of a hyperacid seepage stream derived from Kawah Ijen lake include potassium alum $KAl(SO_4)_2 \cdot 2H_2O$) gypsum, alunogen $Al_2(SO_4)_3 \cdot 2H_2O$, voltaite and melanterite $FeSO_4 \cdot 7H_2O$.

2.3.4. Chlorine and bromine abundances

Halogens (Cl, F and Br) are, after H_2O, SO_2 and CO_2 the most abundant volatiles in volcanic systems on Earth (Aiuppa et al., 2009). In subareal fumarolic emissions, they are commonly present as their correspondent hydrogen compounds: $HCl_{(g)}$, $HF_{(g)}$ and $HBr_{(g)}$. These gases dissociate quite easily in water, and are therefore key contributors to the aqueous budgets of H^+, Cl^-, F^- and Br^-. In SO_4-Cl-type waters, chlorine is the most abundant halogen, followed by fluorine and bromine. The differences in abundances between the halogens are significant. In volcanic systems like Poás, Rincón de La Vieja, Copahue and Kawah Ijen (Martínez, 2008; Kempter and Rowe, 2000; Varekamp et al., 2009; Delmelle and Bernard, 1994), where Cl^- is normally present in concentrations of tens of thousands parts per million, F^- abundances are on the order of thousands of ppm and Br^- in concentrations of tens ppm. Both chlorine and bromine are hydrophile elements and behave as conservative elements in most natural systems, meaning that their abundances are only depending on dilution and concentration processes. During a very intense period of volcanic activity at Poás at the end of 1980´s, samples from the hyperacid lake revealed Br/Cl ratios up to 0.0092 (Martínez, 2008), within the values for Paso Robles soils (Gusev Crater) reported by Yen et al., (2008).

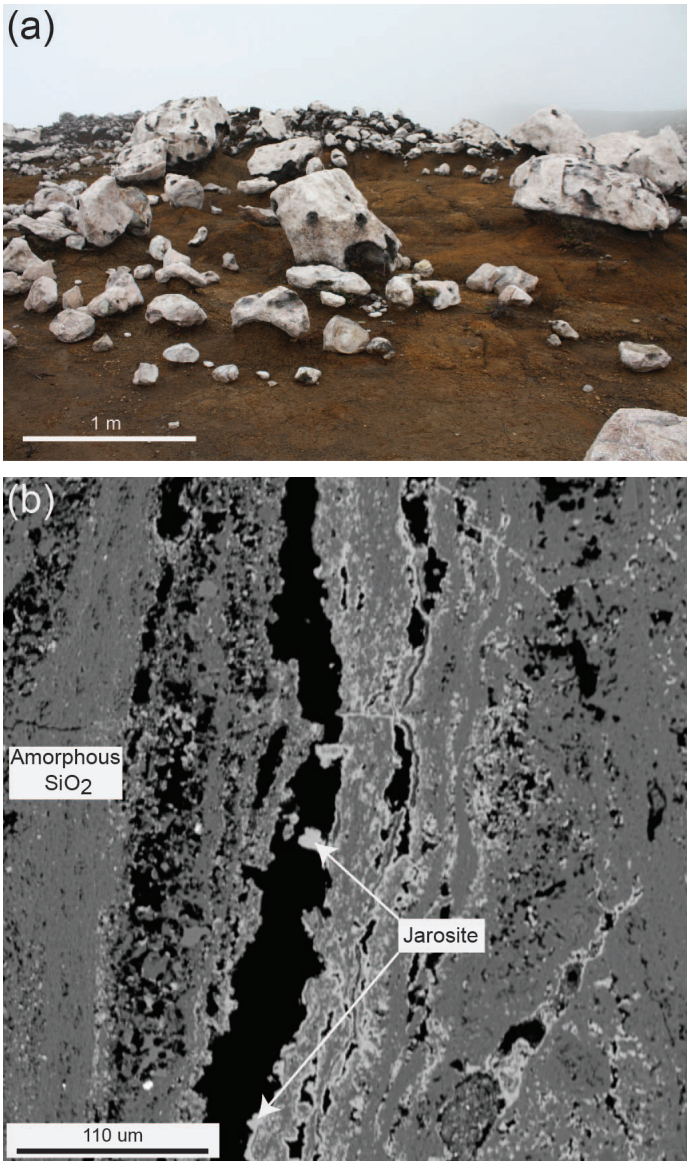

Figure 2.3. (a) Leached lava blocks at Cerro Pelón (Poás volcano, Costa Rica) showing white crusts of amorphous silica. Iron oxides are abundant in soils. (b) Electron back-scatter image of one of the blocks. Amorphous silica precipitation is probably followed by jarosite formation.

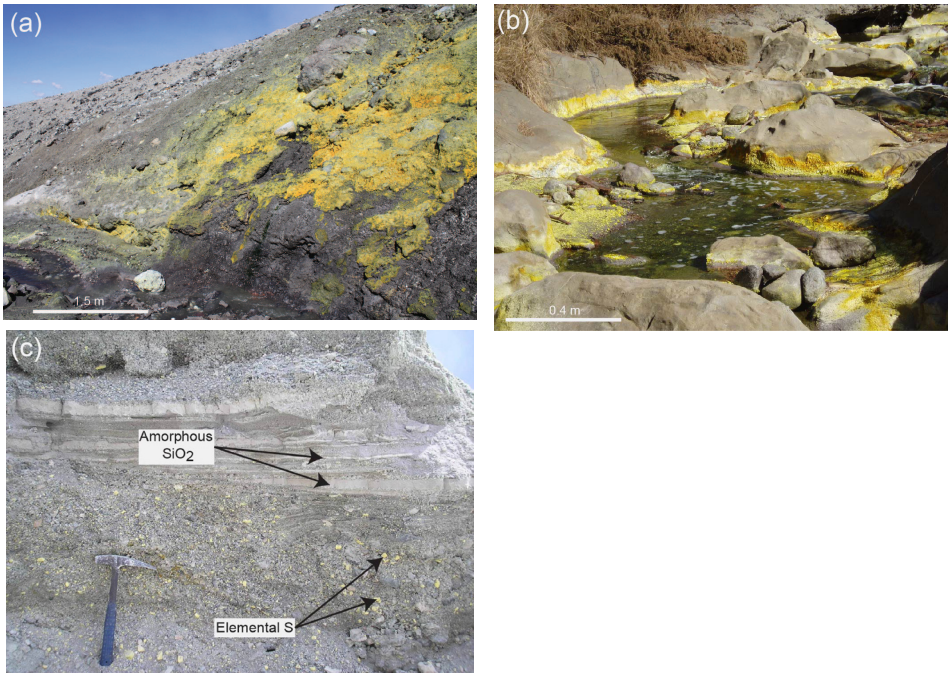

Figure 2.4. (a) Efflorescence of gypsum $CaSO_4 \cdot 2H_2O$, natrojarosite $NaFe_3(SO_4)_2(OH)_6$, khademite $Al(SO_4)F \cdot 5H_2O$, ferricopiapite $Fe^{3+}_{0.67}Fe^{3+}_4(SO_4)_6(OH)_2 \cdot 20H_2O$, magnesiocopiapite $MgFe^{3+}_4(SO_4)_6(OH)_2 \cdot 20H_2O$, epsomite $MgSO_4 \cdot 7H_2O$ and voltaite $K_2Fe^{2+}_5Fe^{3+}_3Al(SO_4)_{12} \cdot 18H_2O$ close to Río Agrio hot spring, Copahue (Argentina). (b) Efflorescence of potassium alum $KAl(SO_4)_2 \cdot 2H_2O$, gypsum, alunogen $Al_2(SO_4)_3 \cdot 17H_2O$, voltaite and melanterite $FeSO_4 \cdot 7H_2O$ at the Banyupahit stream, which is fed by seepage water of the hyperacid Kawah Ijen lake (east Java, Indonesia). (c) Amorphous silica layers and elemental sulphur chunks within exposed lake deposits of Kawah Ijen.

2.4. DISCUSSION

The vast literature on surface mineralogy of Mars, summarized above, lends support to the hypothesis that volcanic interaction with subsurface hydrologic reservoirs below and on the surface has played an important role in creating secondary mineral assemblages in the Martian geological history. Importantly, the presence of sulphate-rich deposits, silica and iron oxides together with enrichments in halogens Cl and Br suggests that the fluids involved were probably highly acidic and rich in elements like Fe, Al, Ca, Si, S, Cl and Br. These fluids are likely similar to SO_4-Cl- and SO_4-type waters in volcanic hydrothermal systems on Earth, which therefore provide opportunities to study the formation of Mars-type mineralogies *in situ*.

We have highlighted the relevance of volcanic settings with hyperacid lakes and associated acid springs, streams and fumarolic exhalations, in view of the range of secondary mineral associations that volcanic-hydrothermal systems produce. Although documented examples are mostly from settings in subduction zone, different from

the Martian context where plate tectonics probably not operate and volcanism may have been associated to mantle plumes (Grott et al., 2013), fluid-rock interaction processes on Earth can probably explain many of the sulphate-bearing mineral associations found on Mars.

2.4.1. Mineral assemblages

The acidity of SO_4-Cl-type waters in volcanic hydrothermal systems makes them highly reactive and capable of leaching cations from the phenocrysts and groundmass of surrounding volcanic rocks, so that often only a residue of amorphous silica or kaolinite $Al_2Si_2O_5(OH)_4$ is left. From these enriched waters, Ca-, Al-, Fe- and Mg-sulphates can form as product of subsequent water-rock interaction and/or evaporation. These associations are not very different from evaporite mineralogies on Mars, which seem to be dominated by Mg, Fe and Ca sulphates and silica phases, probably due the basaltic compositions of the crust, prevailing acidic regimes and relatively low water/rock ratios (Tosca et al., 2004; Tosca and McLennan, 2006). In contrast, seawater evaporites on Earth are typically dominated by halite, calcite, anhydrite and various K and Na-chlorides and sulphates (Braitsch, 1971).

Siliceous deposits on Earth are mostly formed as a residue of acid rock leaching in volcanic terrains (advanced argillic alteration) or as precipitates from hot near-neutral to alkaline aqueous solutions saturated with amorphous silica in the distal parts of volcanic hydrothermal systems or from acid volcanic lakes receiving input of hot solutions. Siliceous sinters are excellent indicators of the presence of hydrothermal reservoirs with temperatures >175°C (Fournier and Rowe, 1966). On Mars, there is evidence for silica formation both as a product of acid leaching and as precipitate from acid and alkaline hot fluids (Miliken et al., 2008; Mustard et al., 2008; Ruff et al., 2011).

As recently documented for gas-dominated settings at active volcanoes in Nicaragua (Hynek et al., 2013; Marcucci et al., 2013), environmental parameters such as temperature, pH, rock and fluid composition, and fluid-rock ratio will exert strong controls on the nature and extent of the alteration mineralogy. Local variability in secondary mineral assemblages is further promoted by steep gradients in temperature, pH and oxidation state.

2.4.2. Chlorine and bromine fractionation

Hydrobromic acid $HBr_{(aq)}$ is a stronger acid than hydrochloric acid $HCl_{(aq)}$, so that the former tends to dissociate less in aqueous solutions than the latter. Evaporation is therefore expected to fractionate Cl and Br in a solution. For example, when the acidy of a crater lake increases in response to increased input of volatiles and heat, $HCl_{(g)}$ could be expelled with the vapour phase to a greater extent than $HBr_{(g)}$, increasing the Br/Cl ratio of the water. The association of Br and Cl with S, together with textural evidence for a volcaniclastic origin of deposits in Gusev crater (Squyres et al.,

2007; Yen et al., 2008) suggest that acid fluids from a volcanic system could have had a major role in the formation of soils in this area. At Meridiani Planum, variable chloride and bromide concentrations have been attributed to low water availability (Clark et al., 2005), as it would imply that bromides (the most soluble salts) could have migrated further than chlorides. Alternative Br-Cl fractionation mechanisms involving acid solutions in an active volcanic setting should also be taken into account. In contrast, the secondary mineralogy at Gale Crater indicates that the fluids involved in water-rock interaction were probably neutral (McLennan et al., 2014).

2.4.3. Geochemical modelling

In order to illustrate a formation sequence of secondary minerals as a product of the reaction between SO_4-Cl-type waters and surrounding igneous rocks, we modelled a reaction path with PHREEQC (Parkhust and Appelo, 1999), in which a basaltic-andesite from the last eruption of Copahue volcano (December 22th, 2012) was reacted with water from Río Agrio acid hot spring (sample collected on March 19th, 2013) at 25°C. This hot spring (T=52°C, pH=0.49) is close to the active crater of Copahue and most likely represents the fluids circulating within this volcanic hydrothermal system (Varekamp et al., 2009). This reaction path model is essentially a titration model in which small amounts of rock are progressively added to a fixed mass of water. The reaction progress is a parameter employed here to describe how evolved a system is in terms of moles of rock that have reacted with the amount of water. The modelling results strongly depend on the phases (secondary minerals) that are allowed to precipitate or that are suppressed. Choices were made based on a survey of the secondary mineralogy in the field.

The sequence of minerals that are stabilized as function of the water-rock ratio or reaction progress is shown in Figure 2.5. At lower reaction progress values (≤0.01 mole rock/kg water) the mineral association consists of amorphous silica and anatase. Gypsum appears at intermediate reaction progress values (0.01 – 0.1 mole rock/kg water). Finally, at higher reaction progress values (≥ 0.1 mole rock/kg water) jarosite $KFe_3(SO_4)_2(OH)_6$, jurbanite $Al(OH)SO_4 \cdot 5H_2O$, hematite Fe_2O_3, alunite $KAl_3(SO_4)_2(OH)_6$, kaolinite $Al_2Si_2O_5(OH)_4$ and eventually smectites (Mg and K montmorillonite) are formed. In general, the initial alteration stages are dominated by sulphates (low reacted system) and the later ones by smectites (high reacted system). The mineral assemblage at low to intermediate reaction progress is in good agreement with field observation at the Río Agrio spring surroundings. In order to evaluate the temperature effect in the overall water-rock interaction, reaction path models were also carried out at 50, 75 and 100°C (not shown). The results indicate that jarosite does not form above 50°C and hematite takes over as the main Fe-bearing phase. In addition, Na-alunite $NaAl_3(SO_4)_2(OH)_6$ together with alunite form at lower reaction progress values and phillipsite (zeolite) appears at 75°C.

Experiments and models simulating alteration of basaltic rocks with sulphuric acid

solutions have shown similar alteration trends for iron and calcium sulphates, and have supported the hypothesis that Martian sulphate terrains are product of a limited water-rock interaction under extremely acid environments (Tosca et al., 2004; Golden et al., 2005; Tosca and McLennan, 2006; King et al., 2011; Hausrath et al., 2013; McCollom et al., 2013; Marcucci et al., 2014). Our model shows overall similarities with experimental results on basaltic material at lower reaction progress values but differs with respect to the appearance of aluminium sulphates (alunites and jurbanite). Alunite-group minerals were also found to be stable in thermochemical models of interaction between fumarole condensate and dacite rock (Africano and Bernard, 2000) and are probably quite common among the secondary sulphates in the summit regions of active andesitic volcanoes where magmatic fluids escape (Zimbelman et al., 2005; Scher et al., 2013). The low abundance of aluminium sulphates on Mars has been taken as indication for limited water-rock interaction (Tosca and McLennan, 2006).

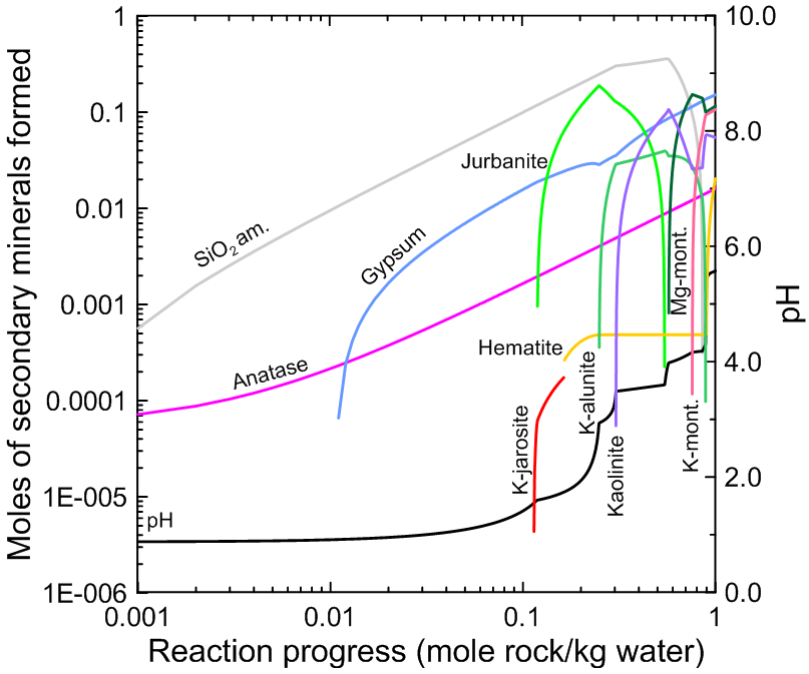

Figure 2.5. Titration model in which 1 mol (110 g) of andesite rock from the Copahue eruption of December 22th 2012 (Camfield, 2013; pers. com.) was reacted with 1 kg of water from Río Agrio spring collected on March 19th, 2013.

2.4.4. Alternative formation mechanisms for sulphate-rich assemblages

Acid mine drainage (AMD) has also been proposed as a terrestrial analogue setting for Martian sulphate-rich terrains. Río Tinto, in Spain, is probably one of the best studied examples (Fernández-Remolar et al., 2005; Fernández-Remolar and Knoll,

2008, Fernández-Remolar et al., 2011). In AMD environments, acid fluids commonly originate by means of pyrite oxidation. Since pyrite is a common secondary mineral in volcanic hydrothermal systems where reducing conditions prevail, its oxidation clearly has a potential of generating acid conditions similar to AMD systems. The source of the sulphur that lead to the formation of the massive sulphate deposits within Valles Marineris has been related to the presence of crustal sulphide deposits (i.e. pyrite) (Burns and Fisher, 1993; Chevrier et al., 2004; Chevrier et al, 2006). While metal-sulphide deposits have not been directly detected on the surface of Mars, their presence has been hinted at for a long time (Clark et al.,1982; Burns and Fisher, 1990; Baker et al., 1991; Burns and Fisher, 1993; Chevrier et al., 2006).

Permian acid-saline lake deposits in Kansas (U.S.), and their modern counterparts in south-western Australia, show many analogies to the Martian Burns Formation in terms of mineralogy and sedimentary structures (Benison and Goldstein, 2001; Benison, 2006; Benison et al., 2007; Baldridge et al., 2009; Story et al., 2010). The waters of these lakes are very shallow, inducing significant seasonal fluctuations in evaporation rates, which provide a mechanism to separate the most soluble salts (Mg-sulphates and Mg-bromide) from less soluble compounds in residual brines. There are important compositional differences with acid volcanic hydrothermal systems. While the Australian lakes typically exhibit a Na-Mg-Cl-SO_4 composition with variable but locally large amounts of Ca, K, Al, Fe, Si and Br (Benison and Bowen, 2006), the volcanic brines have an Al-Fe-Ca-SO_4-Cl composition and have a higher potential of forming Al- and Fe-sulphates. In contrast, Mg-sulphates could be more common in the Australian brines.

The extension and scale of mineral alteration and precipitation of secondary minerals from hot fluids associated with a magmatic body are not necessarily the same for Mars and Earth systems. The lower surface gravity on Mars (about 38% that of the Earth) results in a smaller lithostatic pressure gradient, implying differences in buoyancy-driven processes such as the ascent of magma diapirs (Grott et al., 2013). Since the density contrasts between magmas and host rock are considered to be similar on both planets, magma bodies should rise more slowly on Mars, and, in order to reach crustal levels before cooling and solidification, they should be larger than on Earth (Wilson and Head, 1994). Moreover, as Wilson and Head (1994) predicted, the minimum water content of Martian magmas needed to generate an explosive eruption is 0.0014 wt.%, two orders of magnitude lower than the amount in their terrestrial counterparts (0.24 wt.%). Finally, because of the thinner Martian atmosphere, particles from an explosive eruption would have travelled over greater distances on Mars than on Earth, so that geomorphologic features associated to explosive volcanism might differ between the two planets (Broz and Hauber, 2012; 2013). From these considerations, it is conceivable that volcanic-hydrothermal processes and products of acid systems on Earth have occurred at larger scales on Mars.

2.5. CONCLUDING REMARKS

Surface expressions of volcanic-hydrothermal systems on Earth share many similarities with Mars' sulphate-rich terrains in terms of alteration mineralogy and element distributions. Because volcanism has been an important process in Mars' geological history, it is likely to have produced a similar range of aggressive fluids that can be observed in the surface environment of active terrestrial volcanoes where the effects of interaction with rocks and mobilization elements are directly observable. Hence, examining secondary mineral assemblages, styles of alteration, mechanisms of fluid-solid interactions and distributions of mobile components in volcanic settings will shed light on processes that could have occurred on Mars, and will help establish for which of the many Martian sulphate-bearing sites volcanic-hydrothermal systems make good analogues.

ACKNOWLEDGEMENTS

Funding for this work was provided by NWO (Netherlands Organization for Scientific Research), project ALW-GO-PL/10-03. We thank Jessica Flahaut and an anonymous referee for their careful reviews and valuable comments that improved this manuscript considerably.

CHAPTER

3

Acid rivers and lakes at Caviahue-Copahue as potential terrestrial analogues to aqueos paleo-environments on Mars

Rodríguez A., Varekamp J.C., van Bergen M.J., Kading T.J., Oonk P.B.H., Gammons C.H. and Gilmore M., 2015. In: F. Tassi, O. Vaselli and A., Caselli, A. (eds.), Copahue volcano, pp. 141-172, doi: 10.1007/978-3-662-48005-2.

ABSTRACT

Mars carries primary rock with patchy occurrences of sulphates and sheet silicates. Both Mg- and Fe-sulphates have been documented, the former being rather uncommon on Earth. To what extent can a natural acidic river system on Earth be a terrestrial analogue for early Mars environments? Copahue volcano (Argentina) has an active acid hydrothermal system which has precipitated a suite of minerals in its hydrothermal reservoir (silica, anhydrite, alunite, jarosite). Leakage from this subterranean system through hot springs and into the crater lake have formed a strongly acidified watershed (Río Agrio), which precipitates a host of minerals during cooling and dilution downstream. A suite of more than 100 minerals has been found and conditions for precipitation of the main phases are simulated with speciation/saturation routines. The lower part of the watershed (Lake Caviahue and the Lower Río Agrio) has abundant deposits of ferricrete since 2003: hydrous ferric oxides and schwertmannite occur, their precipitation being mediated by Fe-oxidizing bacteria and photochemical processes. Further downstream, at greater degrees of dilution, hydrous aluminium oxides and sulphates form and create "alcretes" lining the river bed. The watershed carries among others jarosite, hematite, anhydrite, gypsum and silica minerals and the origin of all these minerals could be modelled through cooling/dilution of the primary hot spring fluids. Single evolution (acidification through capture of volcanic gases, water rock interaction to acquire the dissolved cations) through cooling of the primary fluids could explain most of the Fe-bearing minerals, but to precipitate Mg-sulphates, evaporation and renewed interaction with olivine-rich rocks is needed to saturate some common Mg-sulphates (e.g., epsomite). The schwertmannite beds formed through processes involving Fe-oxidizing bacteria, which may be significant if this mineral was common on Mars in the past.

Front picture: lake Caviahe and Copahue volcano in the background. Picture taken on March 12th, 2013. The volcano was strongly degassing after the eruption on December 22nd, 2012.

3.1. INTRODUCTION

The discovery of iron sulphate minerals in Martian meteorites (McSween, 1999) and on the Martian surface (e.g., Klingelhöfer et al., 2004; Ming et al., 2006; Ehlmann and Edwards, 2014) have stimulated research on the climate and hydrology of ancient environments on Mars. Was there water from which these minerals could precipitate and were these waters acid? On Earth, sulphate minerals are common in hydrothermal lakes (Delmelle and Bernard, 1994; Delmelle et al., 2000), acid-mine drainage systems, and evaporites, which must also be considered for Mars. The presence of jarosite on Mars was first measured in outcrops by the Opportunity rover (Klingelhöfer et al., 2004) and later measured regionally by spectroscopy from orbit (e.g., Farrand et al., 2009). Terrestrial jarosite has been found in volcanic-hydrothermal settings (Delmelle and Bernard, 2000; Van Hinsberg et al., 2010; Cousins et al., 2013), in alteration suites in volcanic craters (Africano and Bernard, 2000) and in acid-mine drainage systems (e.g., Fernández-Remolar et al., 2004). Martian sulphates are associated with a number of non-igneous minerals including alunite, anhydrite, goethite, hematite and kaolinite (e.g., Ehlmann and Edwards, 2014). Formation of all these minerals requires specific conditions, for example jarosite needs sulphate rich, acidic (pH<4.0) and oxidizing conditions to form (Stoffregen, 1993; Stoffregen et al., 2000) and the specific environment for each mineral is reasonably well known from theory and terrestrial occurrences (Papike et al., 2006; Bishop et al., 2005). We consider here if active acid hydrothermal systems with their crater lakes, rivers and ponds as found at Copahue volcano can be interpreted as terrestrial analogues for some of these early Mars environments that formed sulphates. Shallow hydrothermal reservoir rocks on Mars may have been exposed during cratering, so we consider mineral formation both at the surface and at shallow depth. Chemical analyses of acid waters and XRD studies of secondary minerals in and around the rivers and lakes of Copahue are combined with saturation calculations under a variety of conditions to constrain the origin of these minerals on Earth. At the end we compare the sulphate mineral suites at Mars and Copahue and point out potential reasons for observed differences.

3.2. MARS MINERALOGY

The mineralogy of the Martian surface is derived from in-situ measurements by landers and rovers, remote observations by spectrometers in orbit and by studies of the Martian meteorites (Chevrier and Mathé, 2007). The geological history of Mars has been described through a global stratigraphy, initially based on the occurrence of different rock formations and later also through crater counts and can be divided into the Noachian (>3.7 Ga), Hesperian (3.7–3.1 Ga), and Amazonian (<3.1 Ga) epochs (e.g., Hartmann and Neukum 2001; Tanaka et al., 2014). The lander and particularly orbital data have identified a plethora of igneous and aqueous minerals that can be placed in temporal context. The crust of Mars is generally basaltic with various proportions of pyroxenes, plagioclases and olivine (e.g., Christensen et al.,

2000; Mustard et al., 2005). The aqueous minerals of Mars are thus derived from the weathering of basalts in a range of environments. Global assessments of the spatial and temporal distribution of aqueous minerals shows an evolution from early phyllosilicates to sulphates and oxides that dominate the surface today (Bibring et al., 2005; Chevrier and Mathé, 2007; Ehlmann and Edwards, 2014).

3.2.1. Martian primary rocks and minerals

Compositions of unaltered Hesperian Martian rock are considered to range from basalt to andesite (Fig. 3.1; Bandfield et al., 2000; Chevrier and Mathé, 2007; McSween et al., 2009). This range is based on orbital observations, *in situ* characterisations and studies on Martian meteorites. Two end-member types of surface rock (I and II) were distinguished based on the thermal emission spectra from the Mars Global Surveyor orbiter (Bandfield et al., 2000). Type I is associated with the southern part of Mars whereas the northern part is dominated by type II. Spectral data of type I match with terrestrial basalts (42-52 wt.% SiO_2), while the type II rocks are similar to terrestrial high-SiO_2 basaltic-andesite (52-57 wt.% SiO_2) to andesitic rocks (57-63 wt.% SiO_2) (Bandfield et al., 2000). The modal mineralogy was obtained from a least-square fit using 45 mineral end-members (Bandfield et al., 2000). Type I is dominated by feldspar (50%), pyroxene (25%) and sheet silicates (15%). Orthopyroxene is more common in the Noachian terrains and clinopyroxene in the younger Hesperian terrains, while both pyroxenes coexist in other areas (Chevrier and Mathé, 2007). End-member type II is dominated by feldspar (35%), potassium-rich glass (25%), sheet silicates (15%) and pyroxene (10%). Others have interpreted the type II rock spectra as partially altered basalt (Wyatt et al., 2004). In-situ measurements by Mars rovers of rocks in its vicinity were analysed using cleaning tools like the Rock-Abrasion Tool (RAT) on the Spirit Rover to create fresh surfaces. Gusev Crater rocks are similar to primitive terrestrial basalts (Gellert et al., 2004). A compilation of rock compositions from all sources of information such as soils, in-situ rock analyses, spectral imaging and Martian meteorites is given in Figure 3.1 (McSween et al., 2009).

3.2.2. Martian aqueous minerals

Phyllosilicate minerals are widespread in the Noachian crust of Mars, indicating persistent weathering by fluids (Poulet et al., 2005; Bishop et al., 2009; Mustard et al., 2008) (Fig. 3.2). The climate was presumably warm and mild, and an atmosphere was presumably present, although a simple H_2O-CO_2-rich atmosphere would have been unlikely to keep it warm enough to maintain water liquid at this distance from the sun. During the Hesperian, phyllosilicate minerals are less abundant, and sulphate minerals are dominant. Sulphates have been found in various environments: (1) gypsum has been identified in dunes surrounding the North Pole and has been attributed to polar processes in the Amazonian (Horgan et al., 2009 and references therein), (2) Meridiani-type layered deposits of sulphates, silica and hematite;

have been interpreted to be sulphate-rich sandstones that were diagenetically altered due to rising groundwater, producing the hematite and sulphate crusts (McLennan et al., 2005; Arvidson et al., 2006). Similar deposits have been discovered in locations throughout the Valles Marineris system, where monohydrated (kieserite and szolmolnokite) and polyhydrated sulphates (epsomite, Mg-rich sulphates) occur with hematite (Glotch et al., 2006; Bishop et al, 2009, Roach et al., 2009). The correlation of many of these regions to areas inferred to be sites of groundwater upwelling (Andrews-Hanna et al., 2010) suggests that groundwater diagenesis may have been widespread.

Acid sulphates have been detected at a number of places on Mars. Jarosite was identified by the Mössbauer spectrometer onboard Opportunity as one of the sulphates at Meridiani Planum (Klingelhöfer et al., 2004). It has also been identified from orbit in association with opaline silica (Milliken et al. 2008; Weitz et al., 2011), phyllosilicates, goethite and ferrihydrite (Farrand et al., 2009), and with alunite (Wray et al, 2011). The presence of schwertmannite has been hypothesized for Mars (e.g., Bishop and Murad, 1996) but this mineral may have turned into Fe-hydroxides of Fe-oxides oxides such as goethite, ferrihydrite and magnetite over time. All of these minerals occur on Earth as well, but Ca- and Fe-sulphates are much more common on Earth than Mg-sulphates. Ferric oxides are common in many terrestrial environments as well, given the prevalence of Fe^{3+} in waters in full exchange with the O_2-rich atmosphere. Mars is a planet with no evidence for free O_2 today, but most of the iron on its surface appears to be in the Fe^{3+} form. Because surface renewal through sea floor spreading-subduction presumably has not occurred, the build-up of Fe^{3+} may have proceeded very slowly through photochemical processes.

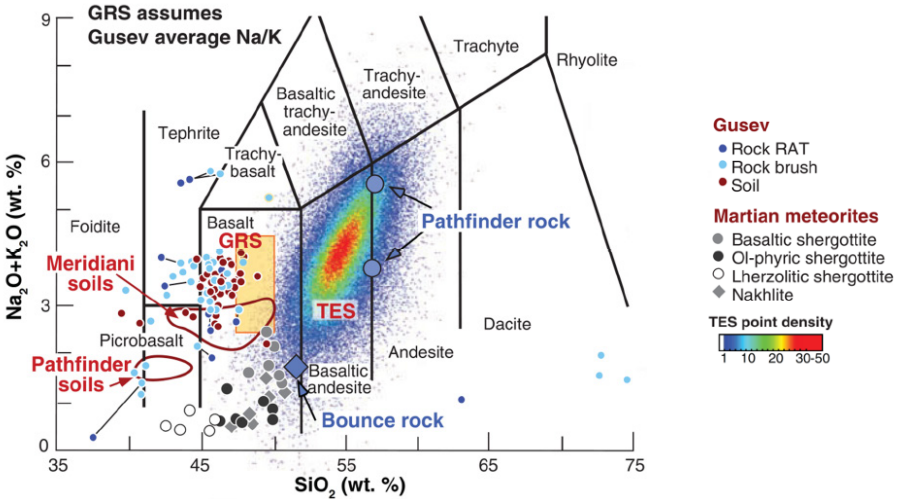

Figure 3.1. Variation of primary volcanic rocks present at some Mars locations (from McSween et al., 2009). Most rocks are relatively unevolved and range from basalt to andesite, with a notable absence of rhyolite.

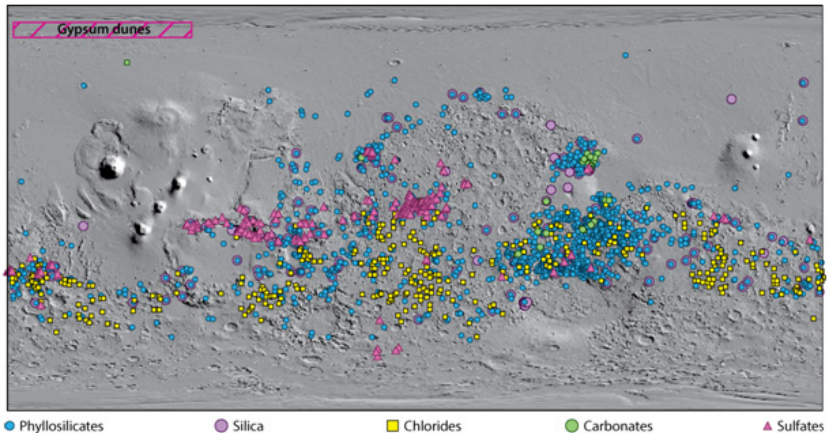

Figure 3.2. Location of aqueous minerals on the Martian surface (from Ehlmann and Edwards, 2014).

Several processes inferred from terrestrial analogues have been proposed to explain the jarosite-rich assemblages on Mars, including evaporation of saline lakes (Benison and LaClair, 2003; Baldridge et al., 2009; McHenry et al., 2011), acid fog weathering (Morris et al., 1996; McCanta et al., 2014), acid-mine type drainage (Fernández-Remolar et al., 2004), and fluid-rock interaction in hydrothermal systems (Papike et al., 2006). These mechanisms involve the weathering of rocks by H_2SO_4 generated either by dissolution of sulfides or conversion of volcanic SO_2 (e.g., Chevrier and Mathé, 2007). Perhaps the best-known sulphate occurrence on Mars is at Meridiani Planum, where jarosite, gypsum and Mg-sulphates are found within sedimentary outcrops. The sedimentary record suggests that the rocks are aeolian sandstones later cemented by sulphate-rice groundwater (e.g., Grotzinger et al., 2005; McLennan et al., 2005). There is an argument as to how much water was in the system. Some models call for open hydrological systems with long-range transport, where rivers supply soluble elements, leached from basaltic rock to a shallow lake or bay, and subsequent evaporation induces the precipitation of sulphate minerals (Chevrier and Mathé, 2007; Tosca et al., 2004) (see Fig. 1.2). Recent chemical modelling (Hurowitz and Fischer, 2014) supports such a model where S-rich fluids are produced by long-term weathering. Alternatively, sulphates are formed in cracks and fissures as a product of interaction between primary mineral phases and relatively water-limited acid fluids percolating through and/or over the surface. This model explains the presence of highly water-soluble minerals such as kieserite and chlorides next to poorly soluble Si-minerals at the Opportunity Site (Chevrier and Mathé, 2007; Morris et al., 2008; Niles and Michalski, 2009).

The hydrothermal environment of Copahue volcano in Argentina has been proposed as a terrestrial analogue to the Opportunity landing Site on Mars (Varekamp, 2004). Here, the association of volcanic lakes, acid stream water and hot springs in a dy-

namic volcanic-hydrothermal setting provides an opportunity to test evidence for fossil shallow Martian hydrothermal systems with acid fluids as a third class of models for the origin of sulphate-bearing mineral assemblages on Mars (Grotzinger et al., 2005; McLennan et al., 2005). If applicable, it would be a hybrid of the main existing models, with water/rock interaction at depth, local precipitation of sulphates, coupled with the escape and accumulation of fluids in rivers and lakes, where further water-rock interaction and evaporation may lead to the precipitation of Mars-type mineral assemblages.

In the following sections, we describe the mineralogy of surface deposits surrounding Copahue volcano that formed from leakage of the hydrothermal system (mineralized acid hot springs), dilution with glacial melt waters, or local evaporation. We subsequently model the observed fluid compositions to determine how the various minerals could have formed in the ambient environment or under shallow hydrothermal conditions.

3.3. COPAHUE MINERALS AND ROCKS

Copahue volcano is an andesitic volcanic in the eastern Andes, and much of its characteristics are described in this volume. The unusual aspect of Copahue is the presence of the highly acidic hydrothermal system at depth below the volcano (Agusto and Varekamp, 2015) from which concentrated acid brines are emitted at the surface, forming springs, acid streams and the crater lake. The direct mineral precipitates of these fluids, as well the minerals that they would precipitate upon cooling and evaporation is modelled and compared with field data of minerals. The suggestion of Copahue as a terrestrial analogue of early Mars environments was originally inspired by the presence of hematite, jarosite and gypsum in one of the local riverbeds (Varekamp, 2004). Another river bed has been covered with schwertmannite for several years (Kading and Varekamp, 2009; 2011), a mineral considered as a potential precursor mineral on Mars (Bishop and Murad, 1996). The copious quantities of sulphur emitted by Copahue during phreato-magmatic eruptions are a specific feature of this volcano (Bermúdez and Delpino, 1995).

As a first approximation, the Copahue volcanic rocks are compositional proxies for the Martian rocks. The mineralogy of recent Copahue ejecta and older lava flows is dominated by plagioclase, with two pyroxenes, olivine and one Fe-oxide. Some of the recent ashes and pumices have a glass phase with about 57wt.% SiO_2 (Varekamp et al., 2015) and the bulk composition (Varekamp et al., 2006) is similar to that of type II Martian rocks. In the following section we present and discuss the new data collected from the Copahue streams, springs and lakes, the minerals identified in the watershed, and modelling results that show under which conditions these minerals could have formed from the local fluids.

3.4. METHODS

3.4.1. Sampling methods

Samples were collected during March 11th to 22th, 2013 and other samples were collected on earlier field trips described by Gammons et al. (2005) and Varekamp et al. (2009). The geographical coordinates and altitude were taken with a handheld GPS at each sampling location (Fig. 3.3). Temperature (°C), pH, electrical conductivity (C) and redox potential (Eh) were measured using a WTW® 3430 portable multimeter. All electrodes were calibrated at least twice daily, before fieldwork and also afterwards when measurements were taken again in the cabin. Calibration of pH electrode was performed using pH 1, 4 and 7 buffers. The conductivity electrode was calibrated in a 0.01 M KCl standard. Finally, the calibration of Eh electrode was done by a 420 mV buffer solution. All redox potential measurements reported in this paper have been corrected to the Standard Hydrogen Electrode (SHE). The temperature dependence of the reference cell electrode was corrected using the conversion table provided by WTW® and according to the following equation: $Eh_{corr.} = E_{field} + 0.731T$; where $Eh_{corr.}$ is the redox potential relative to the SHE (Standard Hydrogen Electrode), E_{field} is the redox potential measured in the field and T is the measured temperature in °C. Conductivity, pH and redox potential were also measured again at room temperature in the cabin after daily fieldwork. The pH of the fluids that showed in the field values below 1 were calculated through charge balance with PHREEQC software (Parkhurst and Appelo, 1999) taking into account Pitzer and Mayorga (1973) ion interaction parameters. The reason for this approach is that linearity of the curve pH vs. potential (mV) from the electrode is strongly reduced when pH values are below zero (Nordstrom et al., 2000). Water samples were collected from rivers and hot springs for IC (ion-chromatography) and ICP-OES (inductively coupled plasma optical emission spectrometry) analyses and were filtered on site through a 0.2 μm pore size cellulose acetate membranes with the aid of a hand vacuum pump. Samples for IC analyses were collected in 250 ml HDPE bottles. For ICP-OES analyses, 60 ml HDPE bottles were used and samples were treated with 1 ml Suprapur® HNO_3 per 100 ml sample. For pH determinations at room temperature, unfiltered samples were collected in 20 ml amber glass air-tight bottles. Samples for Si analyses were diluted 10 times on site with deionised water in pre-weighted 60 ml HDPE bottles. Rocks and volcanic ejecta samples were collected in plastic bags, whereas sediments and mineral samples were collected in 50 ml Greiner® tubes.

3.4.2. Analytical methods

Conductivity, pH and redox potential were determined in the cabin at room temperature after the calibration of the respective electrodes. The concentration of Cl, F, and SO_4 in untreated, undiluted and diluted samples (5 to 25 times) where determined in a Dionex® ICS-3000 ion chromatograph (IC), equipped with a Dionex®IonPac® AS 19 column at the Department of Earth Sciences of Utrecht University. A gradient elution

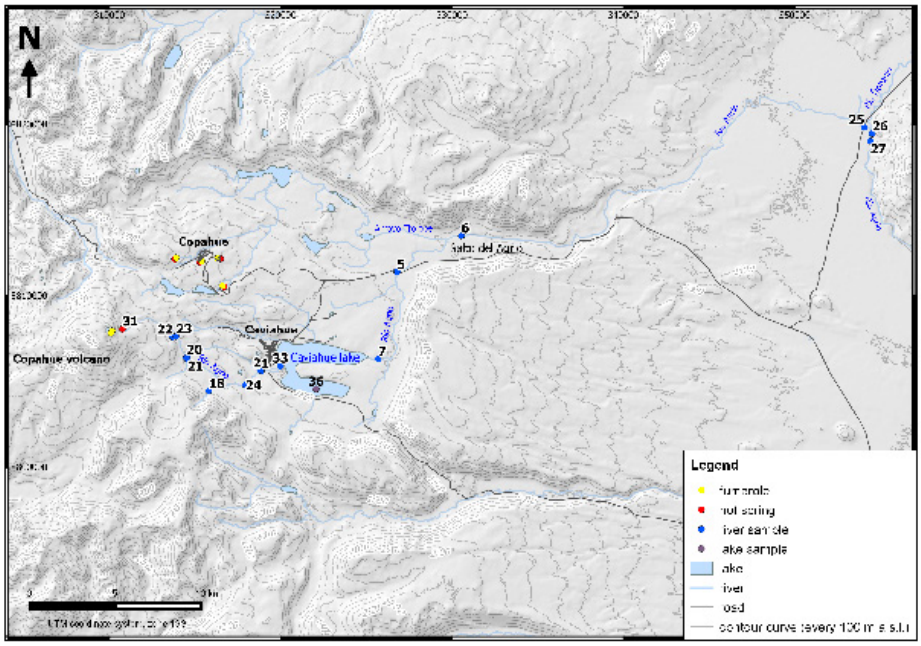

Figure 3.3. Sampling locations around Copahue-Caviahue area.

of 10 – 50 mM KOH was utilized. Concentrations of Al, B, Ca, Fe, K, Mg, Mn, Na, P, Si, Sr, Ti, V and Zn in acidified samples were determined using a Spectro® Ciros® inductively coupled plasma optical emission spectrometer (ICP-OES) at the Department of Earth Sciences of Utrecht University. The sample dilution ranged from undiluted to 25 times. Rock samples were analysed by wavelength dispersive X-ray fluorescence (XRF) at Wesleyan University.

Minerals, sediments and hydrothermally altered rocks were dried several days at low temperature (40°C) until a constant weight (<1% mass difference) was measured between two consecutive weight readings. Then the samples were ground in an agate mortar to a very fine grain size (approximately No.40 mesh). These powders were analysed by X-ray diffraction (XRD) at the Department of Inorganic Chemistry and Catalysis (Utrecht University) with a Bruker® AXS D2 Phaser powder X-ray diffractometer, in Bragg-Brentano mode, equipped a LYNXEYE® detector. The radiation used is cobalt $K_{\alpha 1,2}$ l=1.79026 Å, operated at 30kV, 10 mA. The patters from these analyses were processed and interpreted with DIFFRAC.SUITE software. Thin sections were made from rocks and volcanic ejecta and the samples were observed under the polarizing microscope. Some of these samples were selected for electron microprobe analyses. EPMA work was done on carbon coated samples on a JEOL® 8600 instrument at the Department of Earth Sciences, Utrecht University. The mi-

croprobe was equipped with an energy-dispersive spectrometer (EDS). Normal operating conditions were 15 kV accelerating voltage, 10 nA beam current and 30 s counting time. PROZA software provided by JEOL® was used to convert the raw data into elemental and oxide weight %.

3.4.3. Geochemical modelling

The geochemical modelling software PHREEQC (Parkhust and Appelo, 1999), version 3.1, was used to calculate aqueous species distributions, mineral saturation states and reaction path simulations. Lawrence Livermore National Laboratories thermodynamic database (llnl.dat) was used. This database was expanded with recent available thermodynamic data on sulphates and halides. Additionally, Pitzer and Mayorga (1973) ion interaction parameters from many ion pairs were included.

3.5. RESULTS

3.5.1. Water chemistry of Copahue fluids

The waters from Copahue crater lake and hot springs consist of SO_4-Cl hyperacid brines (pH<1). These fluids are produced by the condensation of magmatic gases (SO_2, H_2S, HCl, and HF) in meteoric waters, mainly originating through melting of the local glacier. The aqueous dissolution of $SO_{2\,(g)}$ and its disproportionation create the acidity of these waters with H^+ and the bisulphate ion (HSO_4^-) as products (Kusakabe et al., 2000; Symonds et al., 2001):

$$3SO_{2(g)} + 2H_2O \rightarrow 2HSO_4^- + 2H^+ + S_{(s)} \quad (1)$$

The species $HCl_{(g)}$ and $HF_{(g)}$ are also important contributors to the H^+ concentrations because of their almost complete dissociation in water at low temperatures (Delmelle and Bernard,1994; Delmelle et al., 2000; Symonds et al., 2001). Such hyperacid waters readily react with the surrounding rocks (e.g., Wolff-Boenisch et al., 2004), leaching cations from minerals and glasses and partially dissolve the silica matrix (Agusto and Varekamp, 2015). Samples from the Vertiente hot spring, about 100 meters below the crater lake, provide good aliquots from the hydrothermal system, because no boiling or evaporation occurs. The Upper Río Agrio waters are largely mixtures of the Vertiente spring waters with glacial melt water and/or local precipitation (rain and snow, Ouimette, 2000; Varekamp et al., 2001; 2009). A summary of water analyses of the Vertiente spring and the upper reaches of the Upper Río Agrio is given in Agusto and Varekamp (2015). The water sampling locations of the March 2013 expedition are shown in Figures 3.4 and 3.5, and the chemical composition of these samples is presented in Tables 3.1 and 3.2.

Copahue volcano erupted in December 2012 and the water samples were collected in March 2013, just three months after the eruption. At that time, the flow of the hot

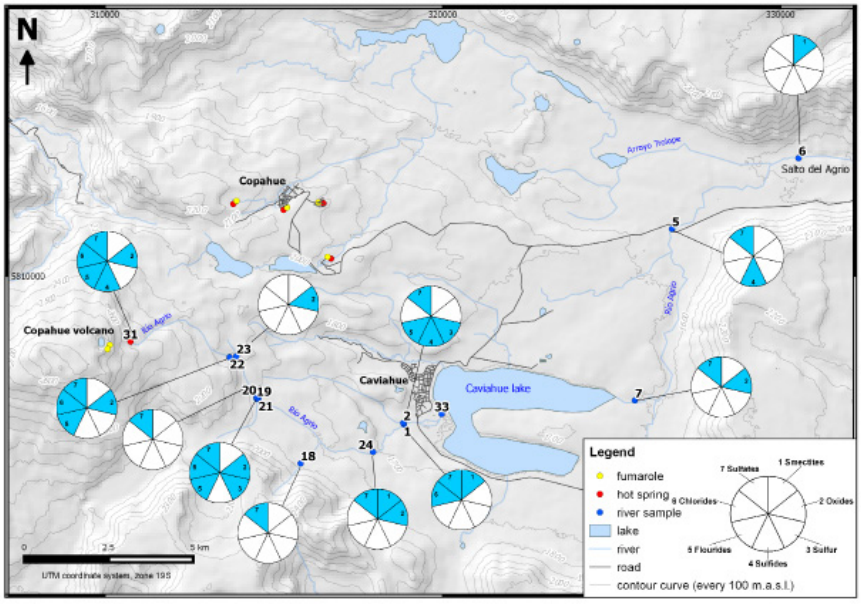

Figure 3.4. Rose diagrams of mineral ocurrences.

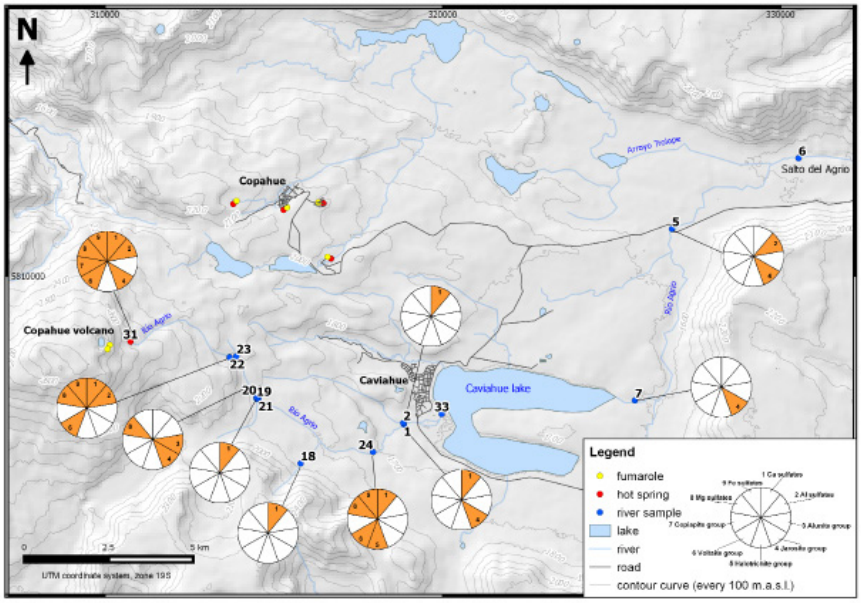

Figure 3.5. Rose diagrams of sulphate mineral ocurrences.

Table 3.1. Sampling sites and locations with pH, temperature (°C), electrical conductivity (E.C., µ/cm) and anion contents (mg/kg).

Site	Location	pH (20±1°C)	T(°C)	E.C. (µS/cm) (20±1°C)	ORP [a] (mV)[H] (20±1°C)	F	Cl	Br	SO4
1	URA (before juntion with Arroyo Jarra)	2.33	11	4100	n.m.[b]	8	350	0.6	1120
2	Arroyo Jarra	7.46	12	373	n.m.	0.3	20	b.d.l.[c]	92
5	LRA (bridge)	2.88	9	1023	n.m.	2	66	b.d.l.	230
6	LRA (before Salto del Agrio)	3.38	11	624	n.m.	1	39	b.d.l.	140
7	LRA (Lago Caviahue outlet)	2.70	9	1600	785	3	90	b.d.l.	320
18	URA (reddish tributary)	7.50	12	43	n.m.	0.2	0.9	b.d.l.	3
19	URA (Río Blanco tributary)	5.88	11	698	403	2	61	b.d.l.	220
20	URA (before Río Blanco)	1.72	17	11480	648	21	880	2	2710
21	URA (after Río Blanco junction)	1.92	14	7610	652	12	510	0.9	1580
22	URA (before Río Colorado junction)	1.57	15	14820	647	29	1230	2	3710
23	URA (Río Colorado tributary)	3.53	20	2690	594	4	280	b.d.l.	1050
24	URA (Cascadas del Agrio)	2.30	10	4190	669	7	350	b.d.l.	1120
25	LRA (before Rio Ñorquín junction)	6.99 (24.1°C)	n.m.	361 (24.1°C)	470	0.6	27	b.d.l.	93
26	LRA (after Río Ñorquín junction)	7.01 (24.6°C)	n.m.	361 (24.6°C)	470	0.8	25	b.d.l.	85
27	LRA (500 m past Río Ñorquín junction)	7.86 (24.4°C)	n.m.	338 (24.4°C)	545	0.8	22	b.d.l.	73
31	URA (Vertiente spring)	0.65 (23.9°C)	52	75500	636	200	9410	18	26900
33	URA (before Lake Caviahue)	2.43	20	3450	689	6	305	b.d.l.	1000
36	Caviahue Lake (surface)	2.82	12	n.m.	n.m.	n.a.[d]	n.a.	n.a.	n.a.

Notes: (a) Redox potential referred to the H electrode; (b) not measured; (c) below detection limit; (d) not analysed.

springs was relatively modest, the fluids were slightly less concentrated and acidic as in some earlier years, and showed some compositional differences with earlier fluid compositions of the same hot spring (Alexander, 2014). The hot spring waters (Site 31) had more than 2.5% SO_4 and close to 1% Cl, at a pH of 0.65 and a temperature of 52.4°C (Table 3.1). A large fraction of these waters is of magmatic origin, with up to 60% magmatic water in some years (Varekamp et al., 2004; Agusto and Varekamp, 2015).

The main rock-forming cations in the fluids are high in concentration (between 1000 and 3000 ppm of Fe, Al and Ca). The Al/Cl decreased after the 2012 eruption, similar to a decrease in 2001 after the 2000 eruption, which is explained with the retention of Al in alunite in the hydrothermal reservoir (Agusto and Varekamp, 2015).

The compositions of the Upper Río Agrio (Table 3.2) are largely diluted versions of the hot springs with admixtures of smaller hot springs, mineralized tributaries and

glacial melt water dilution. The pH of Río Agrio increases downstream from 0.5 to 2.5, just before entering Lake Caviahue. That lake represents a further dilution of the Upper Río Agrio waters with pH 2.2 - 3, and has a significant compositional lag time when the composition of the Upper Río Agrio changes over time because of non-steady state effects (Varekamp, 2008). The outflow of Lake Caviahue (Lower Río Agrio) is further diluted by melt water tributaries and the pH reaches values >3 near the large water fall just outside the caldera (Salto, site 6). The riverbed of the Lower Río Agrio has been covered in red ochre deposits since at least 2003, which was determined to be a mixture of schwertmannite and ferrihydrite phases (Kading and Varekamp, 2011).

Table 3.2. Major and trace element contents of the sampling sites of Table 3.1. Concentrations in mg/kg.

Site	Al	B	Ca	Fe	K	Mg	Mn	Na	P	Si	Sr	Ti	V	Zn
1	91	0.1	110	53	53	99	7	56	0.8	31	0.6	0.1	0.1	0.1
2	0.2	b.d.l.[a]	20	0.1	4	17	0.2	18	0.0	17	0.1	b.d.l.	b.d.l.	b.d.l.
5	23	b.d.l.	20	14	5	15	0.8	13	0.1	15	0.2	0.0	0.0	0.0
6	13	b.d.l.	16	6	4	12	0.5	10	0.0	13	0.1	0.0	0.0	0.0
7	32	b.d.l.	25	20	6	20	1.1	15	0.3	15	0.2	0.0	0.0	0.0
18	b.d.l.	b.d.l.	3	0.6	b.d.l.	2	b.d.l.	3	b.d.l.	13	0.0	b.d.l.	b.d.l.	b.d.l.
19	2	b.d.l.	45	0.3	6	43	2	19	b.d.l.	19	0.1	b.d.l.	b.d.l.	b.d.l.
20	240	0.3	220	130	50	190	15	120	3	36	1.4	0.4	0.4	0.3
21	140	0.2	150	72	31	130	10	77	1	29	0.9	0.2	0.2	0.2
22	380	0.4	240	190	72	190	12	140	4	39	1.8	0.6	0.6	0.5
23	14	0.2	180	12	18	180	19	74	b.d.l.	25	0.6	b.d.l.	b.d.l.	0.1
24	89	b.d.l.	110	47	21	100	7	57	0.8	29	0.6	0.1	0.1	0.1
25	b.d.l.	b.d.l.	26	b.d.l.	4	13	0.1	9	b.d.l.	20	0.2	b.d.l.	b.d.l.	b.d.l.
26	b.d.l.	b.d.l.	26	b.d.l.	4	13	0.1	9	0.0	20	0.2	b.d.l.	b.d.l.	b.d.l.
27	b.d.l.	b.d.l.	28	b.d.l.	4	13	0.1	10	b.d.l.	20	0.2	b.d.l.	b.d.l.	b.d.l.
31	2900	3.2	1100	1300	600	580	23	800	40	76	13.5	2.6	4.4	2.9
33	80	0.1	100	52	19	94	7	52	0.7	33	0.6	0.1	0.1	0.1
36	28	n.a.[b]	26	20	6	20	n.a.	16	0.2	15	n.a.	n.a.	n.a.	n.a.

Notes: (a) below detection limit; (b) not analysed.

3.5.2. Alteration mineralogy in the field

More than 140 secondary minerals were found in the field based on powder XRD determinations. The sampling sites covered the Río Agrio course from its origin at the hot spring (site 31) to just before Salto del Agrio (site 6). Some small tributaries were also included in the sampling campaign. The minerals have been grouped in families as an aid to visualize their distributions in a qualitative way (Figs 3.4 and 3.5). The radial graphs only depict the presence of mineral groups, not their abundance.

Sulphates, silica minerals (tridymite, cristobalite-α, quartz), and oxides of Fe, Ti, Mn and Al are the most common minerals identified along Río Agrio. Hematite and ferrohexahydrite were only found at sites 7 and 24, respectively. Some iron oxides were poorly crystalline and could not be determined by the XRD technique. Chlorides (Fe and Mg-rich) and Fe-fluorides were observed at the Vertiente hot spring (site 31), just before Río Colorado (site 22) and near the junction with Río Blanco (site 19). Smectites were only found near site 1 and site 6. Sulphates occurred in the stretch between the Vertiente spring (site 31) and site 5, behind Lake Caviahue. The most common sulphates were gypsum, K-jarosite, Na-jarosite, voltaite, pertlikite and the Mg-sulphates epsomite and hexahydrite. In most sites, the Na and K jarosites were found together. No obvious geographic abundance trends could be derived from the data (Table 3.3). The 2012 ashes carried abundant hydrothermal debris, in which we found the following minerals: cristobalite, quartz, tridymite, pyrite, elemental sulphur, K- and Na-alunite, hematite, anhydrite, gypsum, kaolinite and montmorillonite, among others.

3.5.3. Schwertmannite in the Copahue volcano watershed

The Upper and Lower Río Agrio had no macroscopic mineral deposits in the riverbeds or suspended in the water column prior to 2000. This all changed after the 2000 eruption, when intrusion of new magma into the hydrothermal system led to highly mineralized fluid emissions into the ambient environment (Varekamp et al., 2001). The Lower Río Agrio riverbed was covered with a yellow ochre just after the confluence of the Arroyo Trolope and Lower Río Agrio for the first time in 2003 (Fig. 3.6). The pH of the mixed fluids was close to or exceeded 3 and the riverbed of the Salto waterfall turned from bare rock to a cover of fluffy brown-yellow precipitate. The Lower Río Agrio turned brown downstream from the Salto for many kilometres, until further dilution by the Río Ñorquín waters led to pH values increase up to 4-5 (Gammons et al., 2005a).

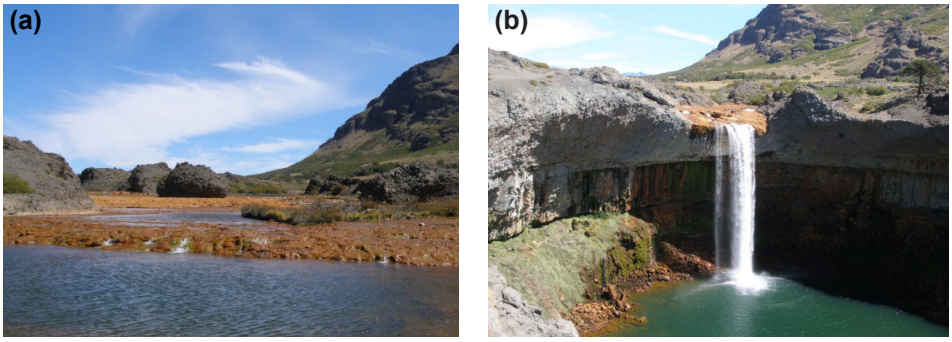

Figure 3.6. Post-2003 hydrous ferric oxide-sulphate mineral phases in: (a) river bed of the Lower Río Agrio; (b) at the Salto del Agrio waterfall.

Chemical analyses of the brown ochre (Table 3.4) revealed it to be a mixture of bacterial organic matter, with small flakes of the mineral schwertmannite and several Fe-oxides, presumably ferrihydrite or goethite (Kading and Varekamp, 2009). The identification of schwertmannite is not easy because it tends to be a poorly crystallized mineral: XRD patterns corresponded to schwertmannite; the stoichiometry of the Fe/S was obtained from SEM-EDAX analyses and was largely compatible with the pure mineral or mixed with ferrihydrite (Fig. 3.7a). In addition, the reflectance spectrum of the ochres strongly resemble that of schwertmannite (Figure 3.7b), and as Schwertman himself argued after discussing the many techniques to detect schwertmannite, its colour is actually quite characteristic (Schwertman and Cornell, 2000). Definite evidence was provided by TEM studies, showing the characteristic spacings in an electron diffractogram (Fig. 3.8a). The bright field images show the crystallinity of the sample (fine spacings) but also small domains of 50-100 nm that may reflect the fine-grained nature of the mineral or maybe related to its mode of precipitation (Fig. 3.8b).

Table 3.3. Common mineral phases used in the modelling and observed in the field.

Rhomboclase	$HFe^{3+}(SO_4)_2 \cdot 4H_2O$	Alunite	$KAl_3(SO_4)_2(OH)_6$
Kieserite	$MgSO_4 \cdot H_2O$	Na-alunite	$NaAl_3(SO_4)_2(OH)_6$
Hexahydrite	$MgSO_4 \cdot 6H_2O$	Jarosite	$KFe_3(SO_4)_2(OH)_6$
Epsomite	$MgSO_4 \cdot 7H_2O$	Na-jarosite	$NaFe_3(SO_4)_2(OH)_6$
Halite	NaCl	H-jarosite	$(H_3O)Fe_3(SO_4)_2(OH)_6$
Sylvite	KCl	Anhydrite	$CaSO_4$
Ferrohexahydrite	$FeSO_4 \cdot 6H_2O$	Gypsum	$CaSO_4 \cdot 2H_2O$
Siderotile	$FeSO_4 \cdot H_2O$	Jurbanite	$AlSO_4(OH) \cdot 2H_2O$
Diaspore	AlO(OH)	Sulfur	S
Rozenite	$FeSO_4 \cdot 4H_2O$	Pyrite	FeS_2
Hematite	Fe_2O_3	Szolmolnokite	$FeSO_4 \cdot H_2O$
Schwertmannite	$Fe_8O_8(OH)_6SO_4 \cdot nH_2O$	Melanterite	$FeSO_4 \cdot 7H_2O$

Chemical analyses of the ochres show strong enrichments in the oxyanion forming elements V, P and As (Table 3.4). The arsenic may be adsorbed on the surface of the mineral or may be part of its structure, substituting the SO_4 group (Acero et al., 2006; Regensburg and Peiffer, 2005; Schrot and Parnell, 2005; Webster et al., 1998). The Lower Río Agrio waters that precipitated these ochres became depleted in dissolved As, V and P (Kading, 2010). Since 2003, the precipitation front of ochres in the Lower Río Agrio moved from the Salto gradually upstream to almost reach the exit of Lake Caviahue. In 2010, yellow precipitates started to form at the lake exit and some lake water filters had a yellowish precipitate (Kading and Varekamp, 2011).

The P enrichment on the schwertmannite led to a secondary ecosystem in the Lower

Río Agrio: extensive fields of green algae grew on the brown schwertmannite oozes, using both the decaying bacterial matter and phosphorus as a fertile substrate. The isotopic composition of the organic matter in one of the Lower Río Agrio ochre samples has a $\delta^{13}C$ of -21.1 ‰ (C=31.3 %) and $\delta^{15}N$ of +7.7‰ (N=2.63 %) with C/N (wt.) = 11.9. These samples were mixtures of the fresh yellow flocculate with bacterial matter and some debris of the green algae. The source of the nitrogen may be related to effluents of local waste water into the lake, but the $\delta^{13}C$ and C/N values suggest that the sample contains abundant bacterial organic matter (Cowie et al., 2009).

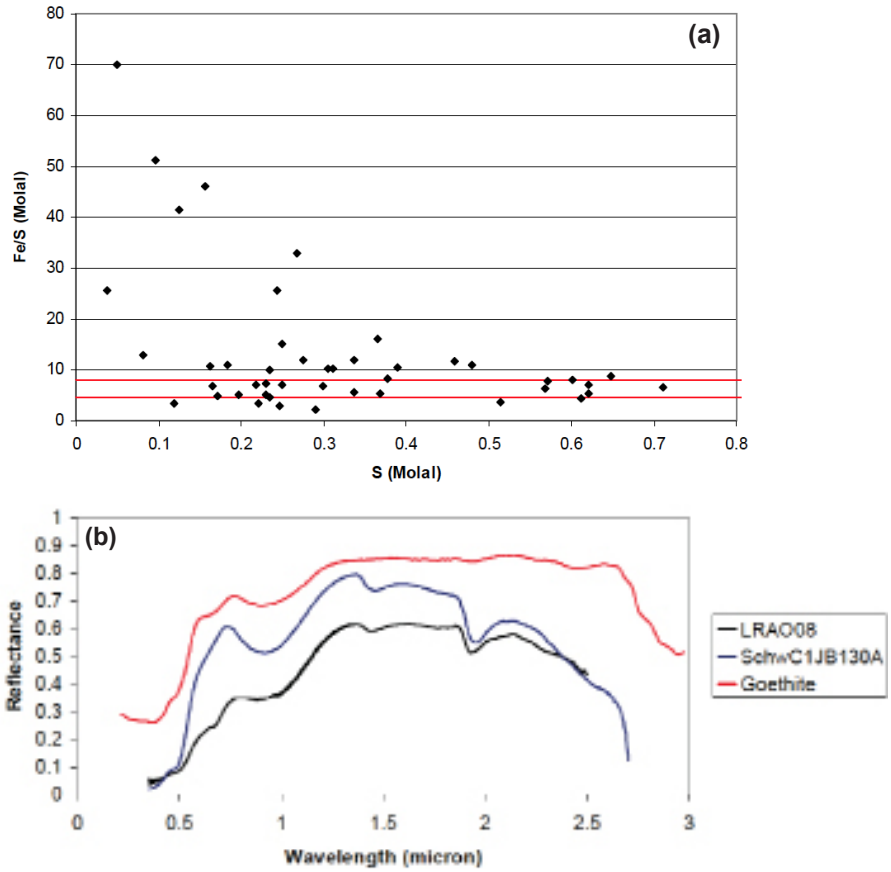

Figure 3.7. (a) Fe/S versus S in the ochres from the Lower Río Agrio as determined by SEM-EDX; the red lines delineate the zone with schwertmannite stoichiometry; many samples have Fe excess, presumably ferrihydrite. (b) The reflectance spectra show the pattern for the ochre (LRA008) and literature reference spectra for schwertmannite and goethite.

The total amount of schwertmannite that precipitated along the Lower Río Agrio is on the order of 60 tonnes/month, leading to the retention of large quantities of Fe, As, P and V in the water shed (Kading and Varekamp, 2009). The fluid emissions from Copahue became more acidic prior to the 2012 eruption and the waters in the lake and Lower Río Agrio were no longer saturated with schwertmannite. The river bed ochres have started to redissolve since 2012 or even earlier, which also released their toxic load of arsenic to areas downstream, while leaving behind a matte brown Fe-oxide coating on the rocks. In conclusion, the schwertmannite deposits at Caviahue occur in a natural setting instead of in an acid mine drainage field where the mineral is commonly encountered (Yu et al., 1999; Kumoulainen et al., 2007; Jonsson et al., 2005; Gagliano et al., 2004; Brady et al., 1986; Blodau and Knorr, 2006), and are ephemeral because of changing water composition trends.

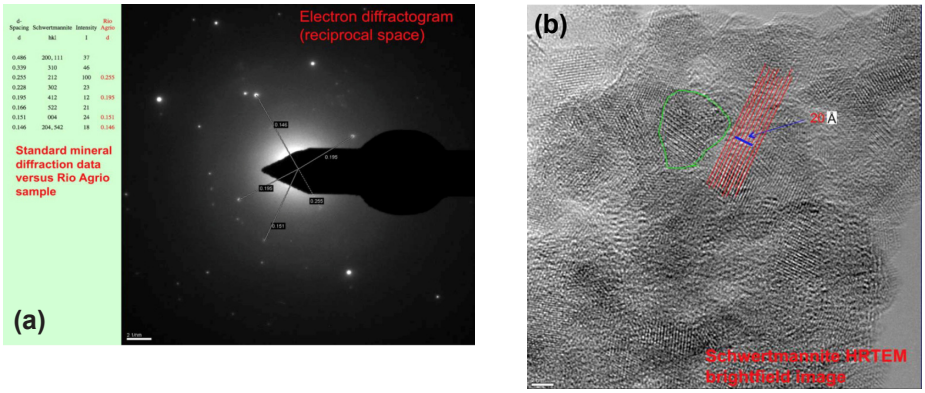

Figure 3.8. Transmission Electron micrographs of schwertmannite samples from the Lower Río Agrio. (a) Electron diffractogram with some of the characteristic spacings labeled. (b) Bright field image, showing small patches (green outline, 50-100 nm) of crystalline mineral with some of the spacings indicated.

Table 3.4. Chemical composition of ochres in the Lower Río Agrio.

Sample	Al (%)	Ca (%)	Mg (%)	K (%)	Mn (%)	Ti (%)	Fe (%)	P (ppm)	As (ppm)	V (ppm)	C (%)	N (%)
SPZO09	7.4	3.68	1.67	1.22	0.083	0.61	8	4500	890	480	8	0.58
SPZO08	4.85	2.05	1.04	0.7	0.063	0.53	20.2	6000	620	970	6.4	0.64
SALTOA08	0.38	0.13	0.07	0.34	0.005	0.05	21.3	2300	70	210	20.4	1.93
LRA08	1.35	0.19	0.12	0.03	0.022	0.13	30	5800	1040	1130	-	-
SALTO08	2.24	0.62	0.25	0.26	0.029	0.21	26.5	5400	820	1100	8.9	1.07

3.5.4. Saturation states of fluids collected before 2012

We used the compositions of local Copahue rocks (Varekamp et al., 2006) and the composition of products from the 2012 eruption for the numerical water-rock equilibration experiments (Varekamp et al., 2015). Water analyses from samples taken at the Vertiente spring between 1997 and 2009 (Gammons et al, 2005; Varekamp et al., 2009; Kading, 2010) were used in a first set of models that predict the saturation state of relevant minerals (following Stefansson et al., 2001) at the exit temperature and higher temperatures (Fig. 3.9). The spring waters were always close to saturated with gypsum and anhydrite, and slightly undersaturated with jurbanite. Jarosite minerals were generally far below saturation; except in 2003 when the spring water was also oversaturated in the H-jarosite.

Saturation indices for alunites vary strongly, although they never reach saturation at spring exit temperatures. Increasing saturation levels with temperature (up to ca. 200˚C) predict that alunite occurs in the hotter and deeper parts of the volcanic-hydrothermal system where temperatures up to 280°C have been estimated (Varekamp et al., 2004). In 2000, 2001 and 2004, however, the waters could have been saturated with alunite at temperatures as low as 75-100°C. Hydrothermally altered andesites expelled during the 2012 eruption contained H-rich alunite inside vesicles, testifying that this mineral is potentially stable at depth. Likewise, fluids are expected to be saturated in diaspore, kaolinite, and hematite (not shown) at temperatures higher than measured at the spring. As an exception, hematite was also saturated below the spring-water temperature in 2003, which was confirmed by its presence along the streambed in the vicinity of the spring (Varekamp, 2004). In the same year, jarosite was close to saturation in the spring fluid as well. The hydrous Fe and Mg-sulphate minerals szolmolnokite, melanterite, rhomboclase, rozenite, kieserite, hexahydrite, epsomite, ferrohexahydrite, and siderotile were undersaturated in the spring fluids during the entire period, as were the chlorides halite and sylvite. Elemental sulphur and pyrite (not shown) were occasionally close to equilibrium.

3.5.5. Mineral saturation trends along the Río Agrio

In a second set of geochemical models, we explored changes in saturation indices downstream along the Río Agrio, based on the compositions of stream water samples taken in 2013 at 14 locations. These changes are largely controlled by cooling, and mixing with near-neutral and more diluted tributary waters which induces pH shifts. The pH values of the Upper Río Agrio waters increase steadily from 0.49 at the Vertiente spring (site 31), to ca. 1 at the entrance of Lake Caviahue, and to pH=3.38 just before Salto del Agrio at the rim of the Caviahue caldera (Table 3.1 and Fig. 3.10). Further downstream, after the junction between the Lower Río Agrio and the Río Ñorquín, there is a step increase to values close to pH 6. The 2013 spring waters (52.4°C) were oversaturated in quartz, in equilibrium with gypsum and anhydrite, and slightly undersaturated in K-jarosite, amorphous silica, goethite, hematite, and

Mg-nontronite. While the saturation state of quartz and amorphous silica remained fairly constant along the river, the indices for gypsum and anhydrite decreased because of dilution and cooling.

K-jarosite was oversaturated from Cascadas del Agrio area (site 24) on down to site 5, after which the entrance of near-neutral water from the Arroyo Trolope tributary induces dilution and a pH increase, leading to undersaturation of this mineral. The Na- and H-jarosite end-members followed the same tendencies. Goethite, hematite, ferrihydrite and Mg-nontronite reached saturation higher up in the URA watershed, and their indices further increased after dilution with near-neutral waters below Salto del Agrio. The pH increase after Salto del Agrio was also associated with oversaturation of new phases such as gibbsite, kaolinite, Mg-montmorillonite, leonhardite and stilbite. In summary, from the Río Agrio spring (Vertiente, site 31) to the point where the stream mixes with Arroyo Trolope (just before Salto del Agrio), the modelled secondary mineralogy was dominated by jarosite, goethite, hematite, ferrihydrite and Mg-nontronite. Downstream from Salto del Agrio, goethite, hematite ferrihydrite, gibbsite, kaolinite, Mg-montmorillonite and eventually stilbite and leonhardite were oversaturated.

3.5.6. Modelling schwertmannite stability

The iron and sulphate concentrations in the Lake Caviahue and the Lower Río Agrio waters lead to conditions suitable for hydrous ferrous iron precipitates (Bigham et al., 1990; 1996a; 1996b; Bigham and Nordstrom, 2000). We ran speciation models for the Lake Caviahue and Lower Río Agrio water analyses between 1997 and 2009 and entered the ion activities into the equilibrium expression for schwertmannite saturation (e.g. Fig. 3.11; Kading, 2010). The lake was undersaturated in schwertmannite for the first decade but started to enter the stability field of this mineral in 2008 and 2009 (Fig. 3.11). The Lower Río Agrio was also schwertmannite saturated at that time, as documented by the precipitates in the river. We expected the whole lake to turn bright yellow-brown in 2010, but the onset of new volcanic activity led to a depression of the pH values in the Upper Río Agrio and then in Lake Caviahue, and first the lake and then the Lower Río Agrio became undersaturated in schwertmannite again.

Schwertmannite is a common but ephemeral mineral at Copahue and its stability is strongly influenced by pH variations ($[H^+]^{22}$, equations 2, 3). Relative minor dilutions or mixing with fluids with a higher alkalinity will push the fluids out of the schwertmannite stability field. Much of this increase in pH is caused by the influx of tributary streams, in particular the Trolope and Ñorquín rivers (Gammons et al. 2005a; Parker et al., 2008). Alkalinity is also added by groundwater influx, especially below Salto del Agrio where irrigation water applied to fields in the river valley returns to the stream as diffuse seepage with neutral pH and elevated HCO_3^- alkalinity (Parker et al., 2008).

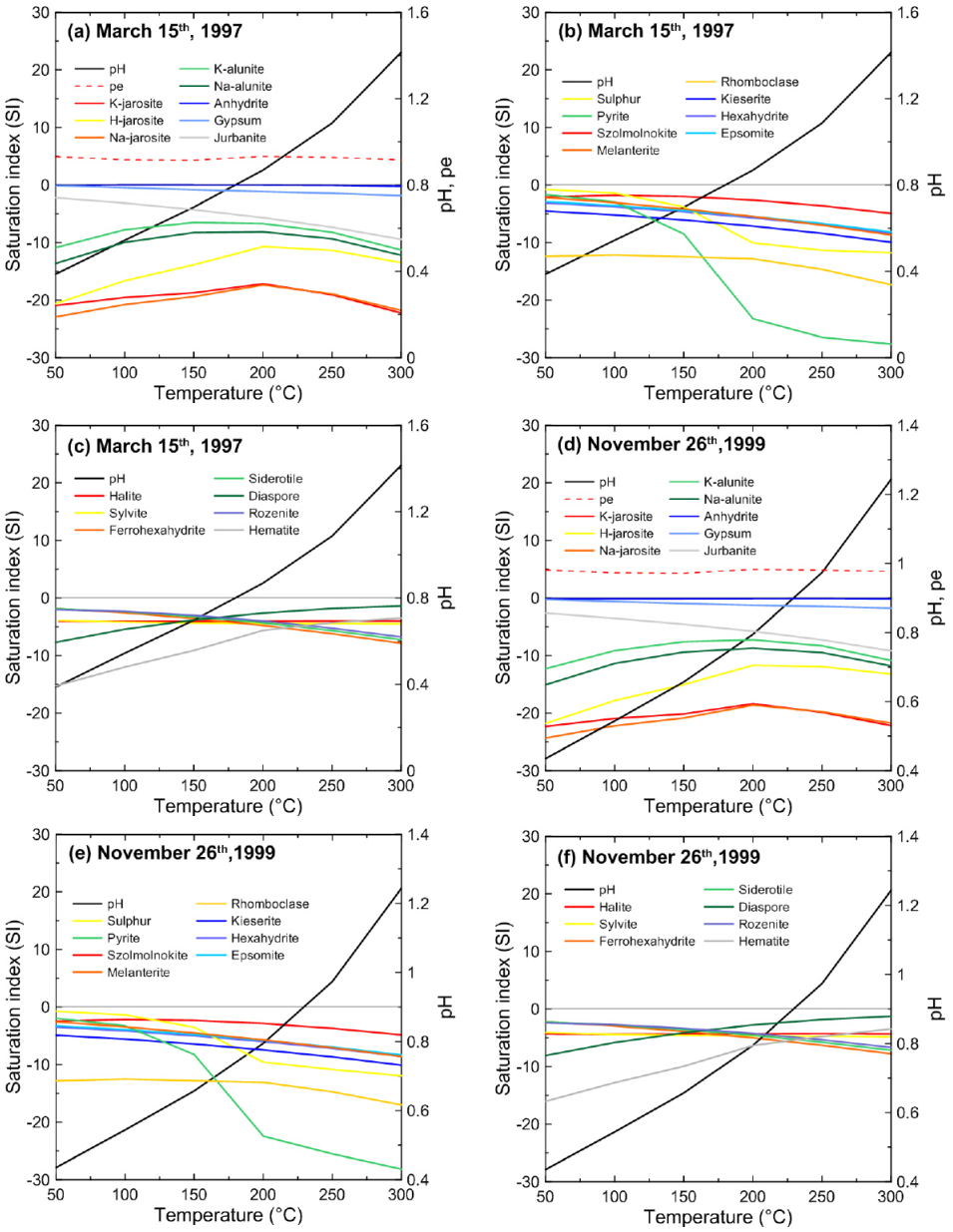

Figure 3.9. Summary of two runs modelling the saturation states for selected minerals as a function of temperature for Vertiente spring-water compositions between 1997 and 1999.

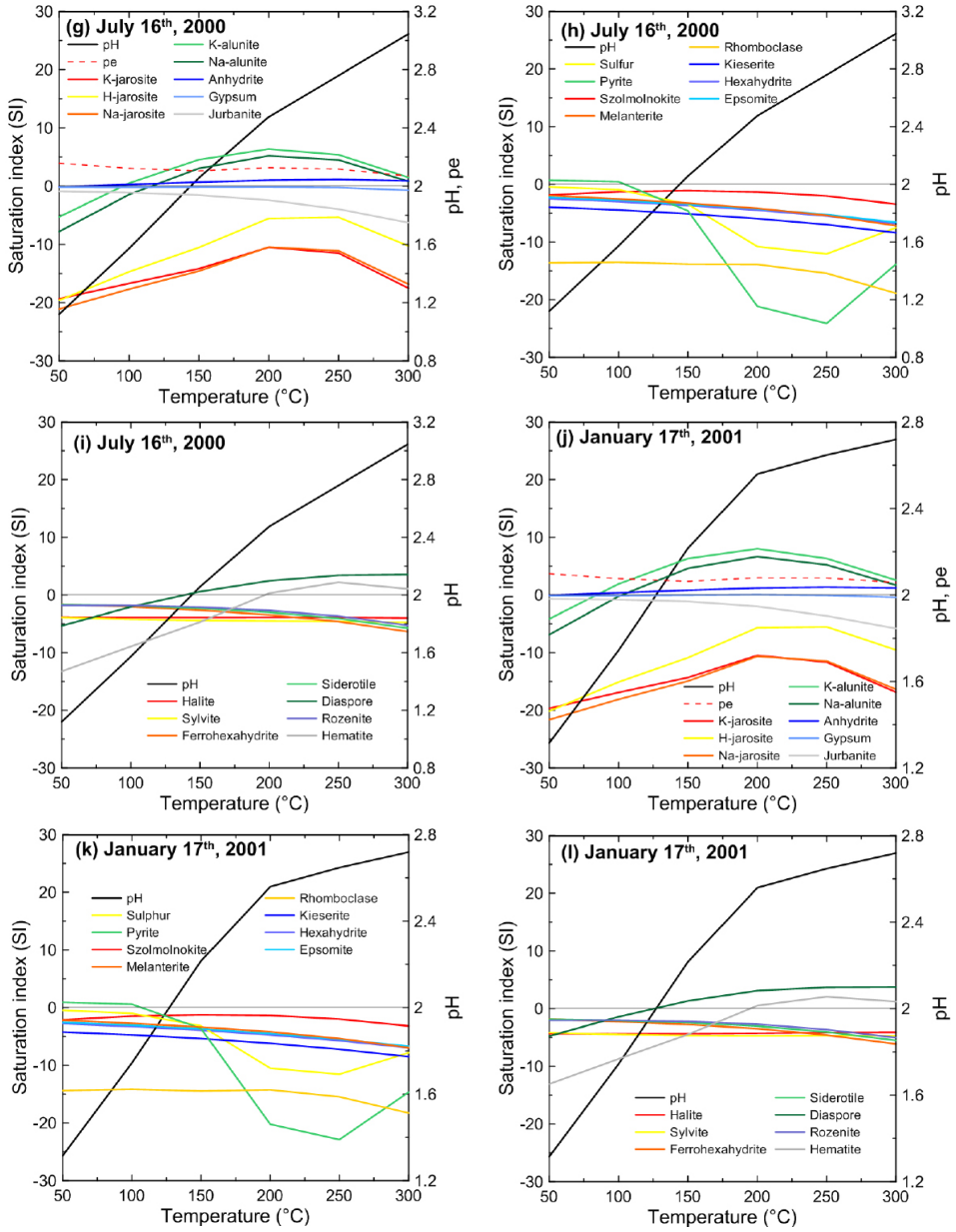

Figure 3.9 (continued). Summary of two runs modelling the saturation states for selected minerals as a function of temperature for Vertiente spring-water compositions between 2000 and 2001.

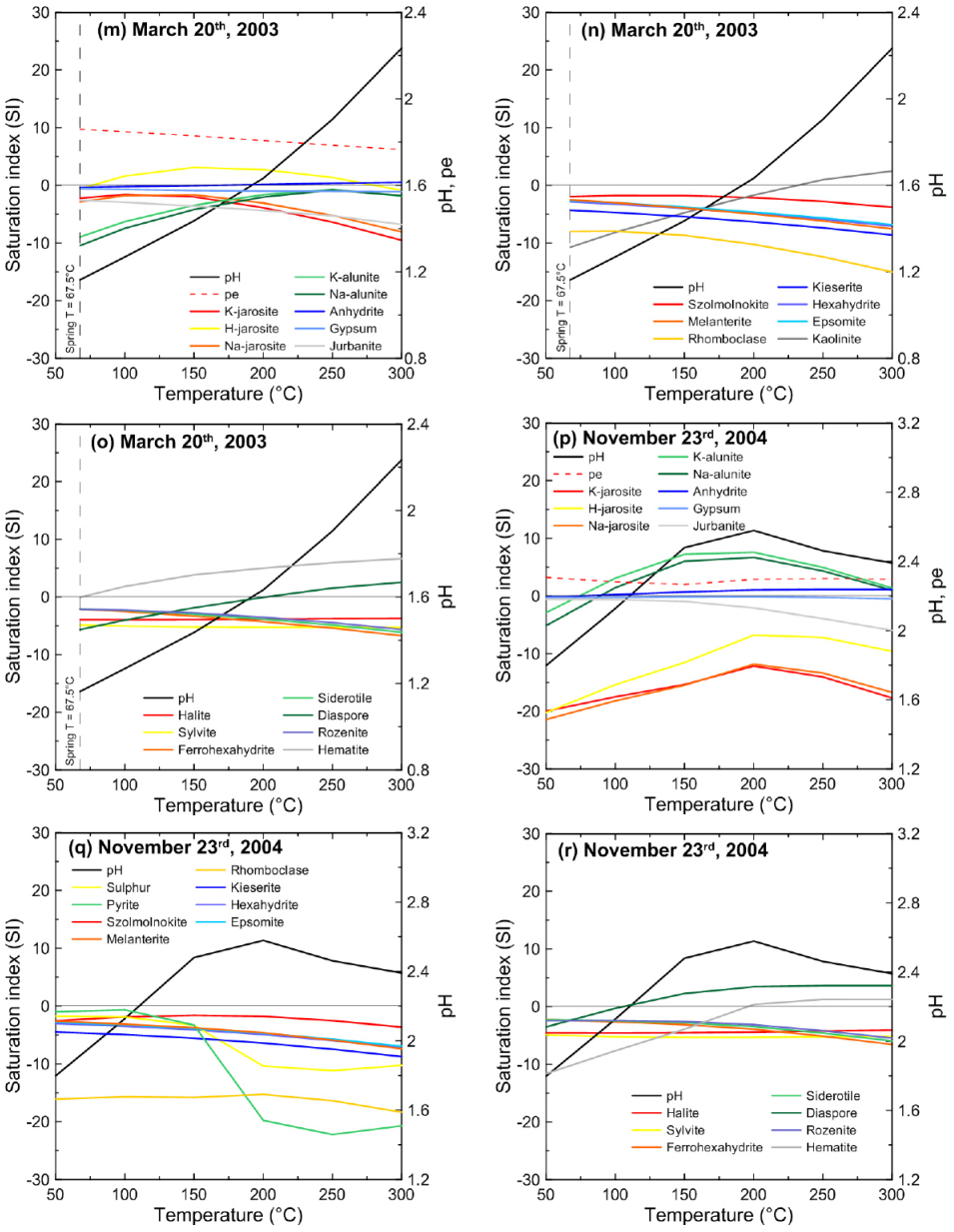

Figure 3.9 (continued). Summary of two runs modelling the saturation states for selected minerals as a function of temperature for Vertiente spring-water compositions between 2003 and 2004.

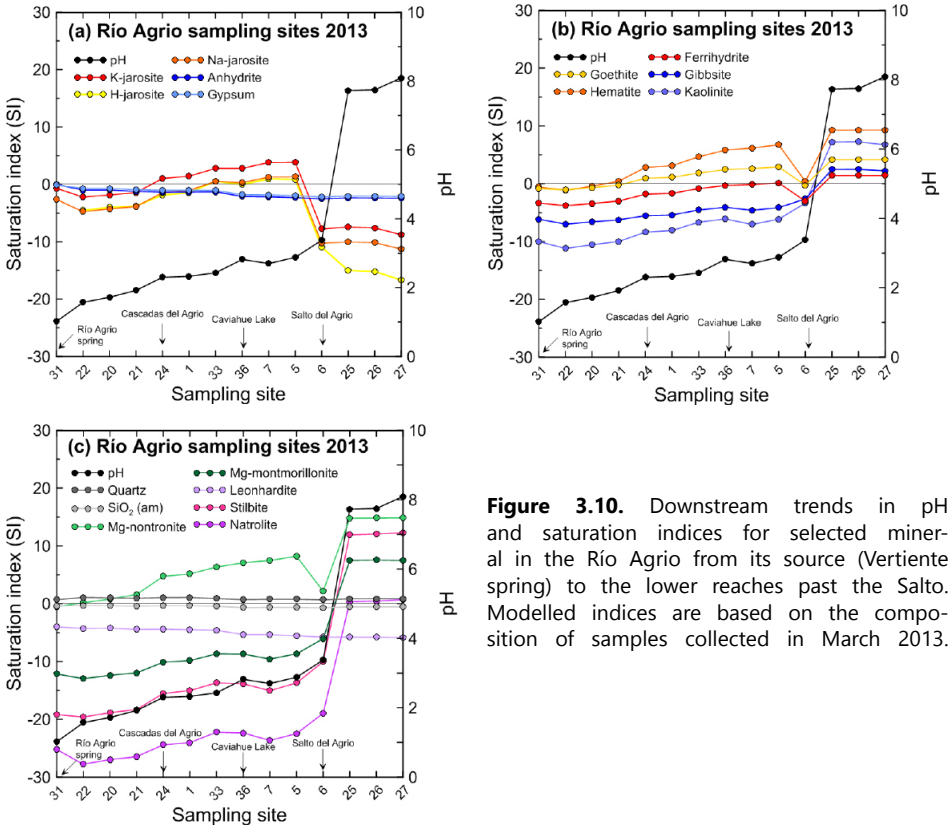

Figure 3.10. Downstream trends in pH and saturation indices for selected mineral in the Río Agrio from its source (Vertiente spring) to the lower reaches past the Salto. Modelled indices are based on the composition of samples collected in March 2013.

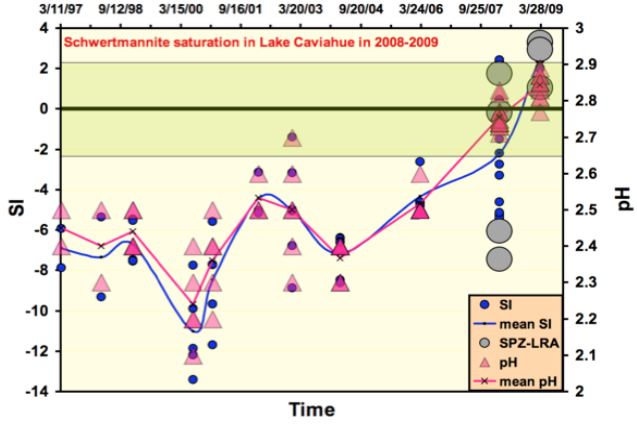

Figure 3.11. Schwertmannite saturation state of Lake Caviahue and the Lower Río Agrio (sample SPZ-LRA); saturation occurred in 2008-2009.

$$8Fe^{3+} + SO_4^{2-} + 14H_2O = \underbrace{Fe_8O_8(OH)_6SO_4}_{schwertmannite} + 22H^+ \quad (2)$$

$$K_{schwertmannite} = \frac{[Fe^{3+}]^8[SO_4^{2-}]}{[H^+]^{22}} \quad (3)$$

The spatial gradients in pH cause precipitation of these hydrous ferric oxides (HFO, including amorphous ferric hydroxide, ferrihydrite, and schwertmannite) and hydrous aluminium oxide (HAO, including amorphous $Al(OH)_3$, as well as hydrous Al-sulphates, such as basaluminite).

Precipitation of HFO is most pronounced where pH transitions from <2.5 to >3. In summer low-flow periods, this pH transition is often located immediately below the confluence of Arroyo Trolope, where abundant, freshly-formed HFO stains the river and its banks a bright orange-red colour (compare photographs in Figs. 3.12a,b). Because of photo-redox cycling (discussed below), HFO may dissolve and re-precipitate over the entire length of the Río Agrio below this point. Extensive outcrops of ferricrete (goethite-cemented alluvium) exist along the stream banks as far as 10 km below the Trolope confluence (Figs. 3.12c,d), and show that Fe precipitation must have been a dominant characteristic of the Río Agrio well into pre-historic times. Because of the higher solubility of Al relative to Fe, HAO precipitation does not occur until the pH>4.5.

Evidence of this reaction is seen below Salto del Agrio by the localized accumulation of white HAO precipitates along the edges of Río Agrio where irrigation return water enters the stream. Precipitation of HAO proceeds to completion after the confluence of Río Ñorquín, a large tributary with high alkalinity, where a prominent white ledge of Al-cemented boulders ("alcrete") exists in the mixing zone between the two rivers (Fig. 3.12d).

Previous workers (McKnight and Bencala, 1988; McKnight et al., 1988, 2001; Kimball et al., 1992; Voelker et al., 1997; Sullivan et al., 1998; Emmenegger et al., 2001; McKnight and Duren, 2004; Gammons et al., 2005b; Sherman, 2005; Parker et al., 2008, Gammons et al., 2008; Nimick et al., 2011) have documented (24 h) cycles in the concentration and redox speciation of dissolved iron in streams that are acidic due to pyrite oxidation. These cycles are caused by day-time photo-reduction of dissolved or colloidal Fe (III) to dissolved Fe (II) (reactions 4 and 5) and re-oxidation of Fe (II) to dissolved or colloidal Fe (III) compounds at night (reactions 6 and 7), as follows:

Day:

$$Fe(OH)^{2+} + h\nu = Fe^{2+} + OH \cdot \quad (4)$$

$$Fe(OH)_{3(s)} + h\nu + 2H^+ = Fe^{2+} + OH \cdot + 2H_2O \quad (5)$$

Right: $$Fe^{2+} + 1/4O_2 + 1/2H_2O = Fe(OH)^{2+} \quad (6)$$

$$Fe^{2+} + 1/4O_2 + 5/2H_2O = Fe(OH)_{3(s)} + 2H^+ \quad)$$

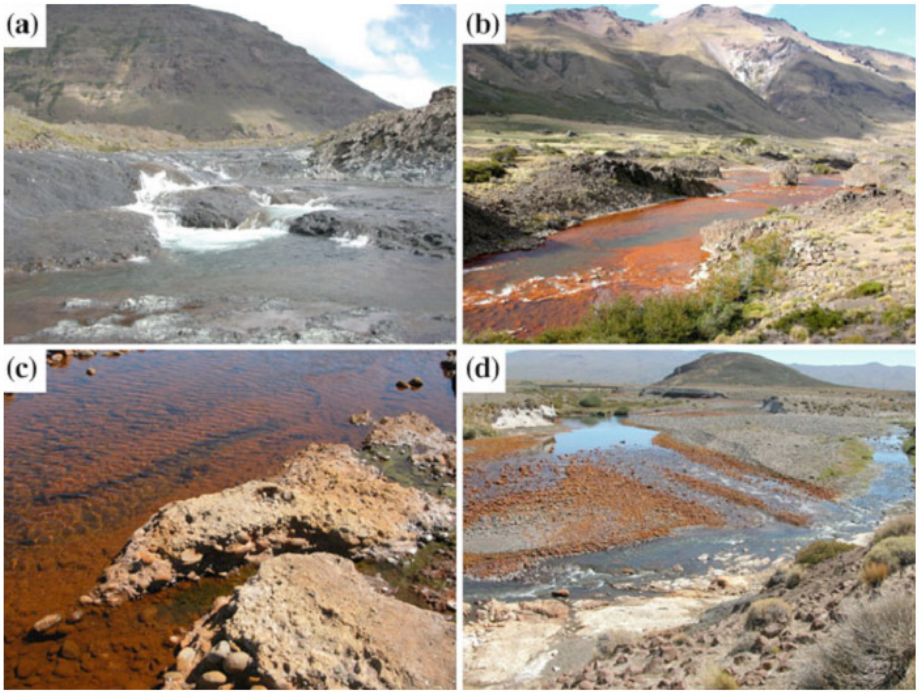

Figure 3.12. Photographs (taken in February, 2009) of the lower Río Agrio in low-flow conditions. (a) R. Agrio above confluence with Arroyo. Trolope. (b) R. Agrio below confluence with A. Trolope. (c) Ferricrete deposits (centre, bottom) along the bank of the river. (d) Confluence of R. Agrio (left) and R. Ñorquín (right), with large, cream-colored ledge of Al-cemented boulders (alcrete).

David and David (1976) showed that photo-reduction of Fe (III) occurs in the ultraviolet (UV) to near-UV region of 200 to 450 nm, with a local maximum near 300 nm, and is sensitive to changes in pH, temperature, light intensity, major solute chemistry, and Fe(II) concentration. Collienne (1983) found that maximum Fe (III) photo-reduction rates take place in the pH range 2 to 4 where $Fe(OH)^{2+}$ is the dominant dissolved ferric species. This is also the pH range of Río Agrio for many kilometres below the outlet of Lake Caviahue, usually extending well below the confluence of Arroyo Trollope. Parker et al. (2008) conducted diel sampling along the Río Agrio just upstream of Salto del Agrio, as well as at two sites with higher pH further downstream. Results for dissolved Fe (II), Fe (III) and total dissolved Fe are summarized in Figure 3.13a, along with data for photosynthetically-active radiation (PAR). The results show the predicted photo-reduction trends, i.e., a decline in dissolved Fe (III)

concentration during the day (high PAR) coincident with an increase in dissolved Fe (II), and reverse trends at night. Because the rate of abiotic oxidation of Fe (II) is very slow at low pH (Singer and Stumm, 1970), Parker et al. (2008) attributed the night time increase in Fe (III) to iron-oxidizing bacteria (IOB). The IOB oxidize Fe (II) during the daytime hours as well, but at a rate that is slower than the production of Fe (II) by photo-reduction. The amount of energy potentially gained by a micro-organism that catalyzes the oxidation of Fe (II) using O_2 is ~10 times greater than the amount of energy gained by precipitation of HFO. Fe(III) photo-reduction via reactions (5) or (6) creates a short-lived OH· radical which is destroyed by reaction with other redox-sensitive species (Collienne, 1983; Kimball et al., 1992; Voelker et al., 1997), such as dissolved organic carbon (DOC).

Gammons et al. (2008) quantified the amount of free energy made available to iron-oxidizing bacteria by daytime photo-reduction in the Tinto and Odiel rivers of southern Spain. The same approach is used here to investigate the bioenergetics of Fe (II) oxidation in Río Agrio, using data collected by Parker et al. (2008). The amount of free energy consumed or released during Fe (II) oxidation via reaction (6) is dependent on the concentrations of reactants and products and can be determined as follows:

$$\Delta G_r = \Delta G_r^0 + RT \ln Q \qquad (8)$$

$$Q = \frac{[Fe(OH)^{2+}]}{[Fe^{2+}][O_2]^{1/4}[H_2O]^{1/2}}$$

Where ΔG_r^0 is the standard state free energy change (-32.0 kJ/mol) for reaction (6) (based on data in Faure, 1997), R is the gas constant, T is the absolute temperature, Q is the ion-activity quotient and the squared brackets refer to species activities (Faure, 1997). To calculate the activities of $Fe(OH)^{2+}$ and Fe^{2+} (and therefore Q),the chemical composition of each hourly river water sample at Salto del Agrio site (Parker et al., 2008) was entered into the program Visual Minteq (Vers. 3.0, a recent version of the original MINTEQA2 program of Allison et al., 1991). The activity of water was taken as unity, and the activity of O_2 was assumed to reflect saturation with atmospheric O_2. In the study of Parker et al. (2008), Río Agrio remained well-oxygenated above Salto del Agrio throughout day and night. The results (Fig. 3.13b) indicate in a ΔG_r range from -28.8 to -31.7 kJ per mole of Fe^{2+} oxidized, with a 24 h average of -30.3 kJ/mol. These values are strongly exergonic (thermodynamically favourable), and overlap with the reported free energy changes of -25 to -37 kJ/mol for Fe (II) oxidation in Río Tinto and Río Odiel, Spain (Gammons et al., 2008). As discussed by Gammons et al. (2008) and Lees et al. (1969), the disequilibrium created by sunlight and Fe (III) photo-reduction is sufficient to support a thriving population of IOBs in Río Tinto, as is also evidently the case in Río Agrio.

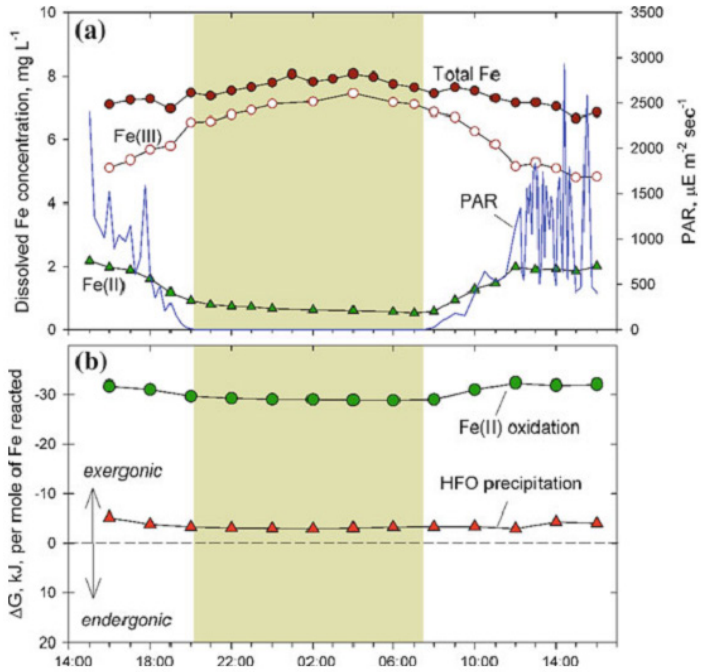

Figure 3.13. Diel change in iron chemistry on lower Río Agrio at Salto del Agrio in February, 2009. (a) Changes in concentration of dissolved Fe(II), Fe(III), total dissolved Fe, and photosynthetically active radiation. (b) Changes in the "exergonicity" of Fe^{2+} oxidation (eq. 6) and precipitation of hydrous ferric oxide (eq. 7) (from Parker et al., 2008).

3.5.7. Scenarios involving evaporation and water-rock interaction

Evaporation of splash water or standing pools, as well as interaction with rocks in the streambed or on the borders are ubiquitous features along Río Agrio, so we ran a set of models to investigate the relevance of these processes to the formation of a suite of secondary minerals. In evaporation models, waters from the Vertiente hot spring (site 31), collected in 2003 (Gammons et al., 2005) and 2013, were first titrated with O_2 to create equilibrium with local atmospheric conditions (10°C, pressure corresponding to 2483 m amsl), and were then evaporated at the same conditions. The results for 1 kg of water with compositions equal to the 2003 and 2013 samples (Fig. 3.14) show that evaporation has the most obvious effects on the formation of gypsum and iron (III) fluoride. Gypsum was already saturated in the 2013 sample at 10°C before evaporation was imposed, whereas it only reaches saturation in the 2003 sample after ca. 60% water loss. Iron (III) fluoride (FeF_3) becomes stable in the 2003 sample when most of the water is evaporated, whereas saturation is not reached in the 2013 sample. We have detected the presence of FeF_3 in solid samples collected at the Vertiente (site 31) and at site 23 (before the junction with Río Colorado) during our 2013 campaign. In view of the strong undersaturation of the

mineral in the 2013 waters, we speculate that the solid product is a residue from an earlier period when dissolved Fe and F concentrations were much higher and the mineral could form during evaporation of splash or standing pool water.

In our water-rock interaction models, 1 mole (110 g) of andesite from the 2012 eruption of Copahue (Varekamp, 2015) was reacted with 1 kg of the 2013 sample of the Vertiente spring. Where necessary, the number of theoretically stable phases was restricted in model outcomes by allowing the formation of only those phases that are most consistent with our field observations. Figure 3.15 illustrates the results for a run at 24°C, 1 atm and an initial water/rock (W/R) ratio of 0.1. Amorphous silica and anatase, saturated from the start, were the only phases precipitating at low reaction progress, followed first by gypsum and then by jarosite and jurbanite. Goethite, K-alunite and kaolinite appeared afterwards. Finally, at the highest reaction-progress values, montmorillonites (Mg and K end-members) and magnetite formed. We also tested interaction models (not shown) for lower water/rock ratios or higher temperatures. A run for a 10-fold lower W/R ratio (0.01) yielded a similar mineral sequence as in Figure 3.15, but more clays and eventually zeolites appeared at high reaction progress values. The main outcome of the temperature evaluation is that, above ca. 50°C, neither jarosite nor jurbanite are formed, and Na-alunite becomes dominant over K-alunite.

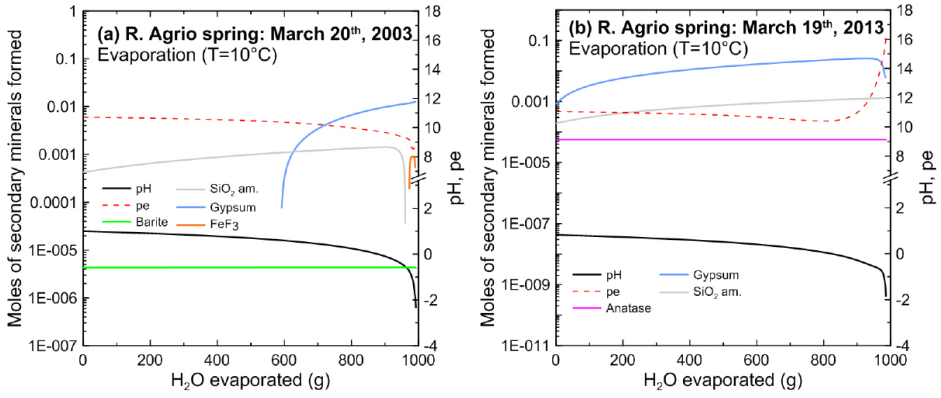

Figure 3.14. Simulations predicting the formation of minerals during progressive evaporation of Vertiente spring (Río Agrio spring) water for (a) 2003 and (b) 2013 samples. Associated changes in pH and pe are also shown. Note that Ba was not analysed in the 2013 sample and Ti not in the 2003 sample, precluding the calculation for barite and anatase saturation in these cases.

3.5.8. Modelled scenarios for the formation of Mg-sulphates

Since Mg-sulphates did not form in any of the above experiments, we explored additional interaction models for hypothetical Mg-enriched systems, based on the assumption that the Vertiente spring water and Copahue's andesitic rocks contain insufficient magnesium to create these minerals via simple pathways. In a first scenario, we modelled the interaction between acid fluid and olivine as the only reactive

solid material available. It has been proposed that olivine dissolution was possibly an important process on Mars (Bandfield and Rogers, 2008). An olivine composition of $Fa_{34}Fo_{66}$ was adopted, based on EPMA analysis of phenocrysts in a fresh sample collected after the Copahue 2012 eruption. One mole of olivine (160.7 g) was reacted with the 2013 Vertiente spring water at 24°C. The resulting secondary mineral assemblage (Fig. 3.16a) was largely similar to that found in the water-andesite model (Fig. 3.15), except that K-montmorillonite did not form and higher pH values (>10) were ultimately reached. The saturation indices for Mg-sulphates show maxima (highest for epsomite) but without reaching saturation levels (Fig. 16b). A decrease in the saturation indices near the end of the reaction is presumably due to Mg^{2+} consumption by Mg-montmorillonite at the highest pH conditions.

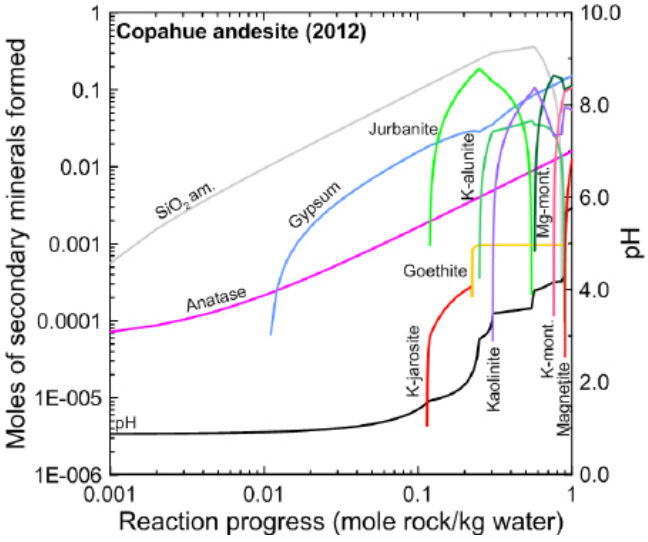

Figure 3.15. Water-rock interaction model simulating the reaction between andesite rock (composition similar to the products of the Copahue 2012 eruption) and water from the Vertiente hot spring (site 31) at 24°C.

In a more complex scenario, we simulated a multiple-step process involving both solid-fluid interaction and evaporation to create sufficiently magnesium-rich conditions for the formation of Mg-sulphates. We envisaged an open system in which a fluid, after reaction with an Mg-rich solid, evaporates to some extent, after which the more concentrated residue reacts again with a fresh aliquot of the same solid. As input for the evaporation step, we used a fluid with a composition simulated in the previous water-olivine reaction model just before K-jarosite started to precipitate (i.e. at a reaction progress value of ca. 0.05; Fig. 3.16a), when much of the cation budget needed to form sulphates (other than gypsum) in the ultimate products was still in solution. With progressive evaporation, the saturation indices for Mg-sulphates increased only slowly until the final stages when most of the fluid was

evaporated and epsomite reached saturation (Fig. 3.17). In a subsequent step, we let the liquid from the last stage of this evaporation experiment react again with Fo_{66} olivine, which produced epsomite ($MgSO_4 \cdot 2H_2O$) and ferrohexahydrite ($FeSO_4 \cdot 6H_2O$) together with anatase, gypsum and amorphous silica (Fig. 3.18). Even though both the evaporation and the second interaction model could not be completed because of convergence problems with PHREEQC (due to the high ionic strengths of the solutions), our findings suggest that the formation of Mg-sulphates in the Copahue environment requires interaction between relatively small volumes of acid fluid and Mg-rich solid in combination with evaporation.

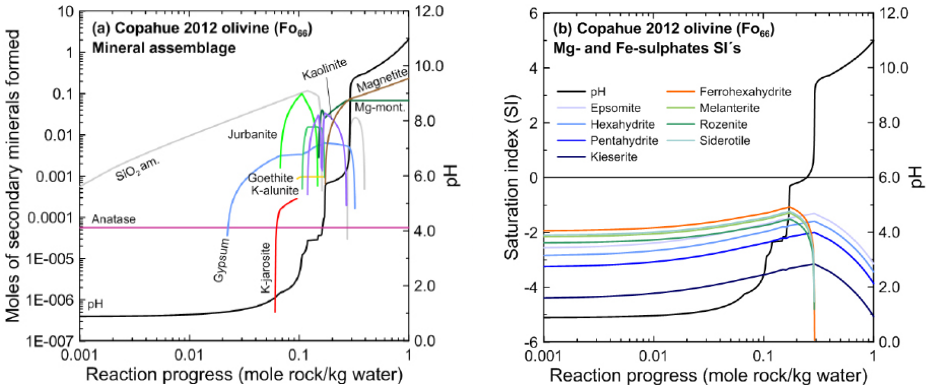

Figure 3.16. Water-rock interaction model simulating the reaction between (a) andesite rock (composition similar to the products of the Copahue 2012 eruption) and (b) water from the Vertiente hot spring (site 31) at 24°C.

3.6. DISCUSSION

Firstly, we reviewed the occurrences of sulphate-bearing mineral assemblages on Mars and evaluate here in how far the mineralogy at Copahue-Caviahue shows similarities with the documented and inferred Mars minerals. Secondly, through modelling we investigate under which conditions these Copahue fluids could crystallize minerals that occur on Mars but are currently rare or absent at Copahue. The absorption of hot volcanic gases by shallow ground waters, in this case glacial melt waters, leads to hot and acid hydrothermal fluids inside Copahue volcano. These aggressive fluids dissolve and react with the surrounding rock matrix producing fluids that are saturated in anhydrite, some sulphides and hydrothermal silica. When the fluids react with newly intruded chilled magma, alunite starts to crystallize, and in some cases the various end-members of jarosite become stable. The main minerals in the hydrothermal reservoir rock thus are silica, anhydrite, alunites and possibly jarosites, as also shown by lithics ejected during Copahue eruptions. When the fluids escape from the hydrothermal system into the ambient environment (hot springs, crater lake), cooling, dilution, evaporation and oxidation through atmospheric oxygen may occur, leading to another suite of minerals becoming saturated as detailed

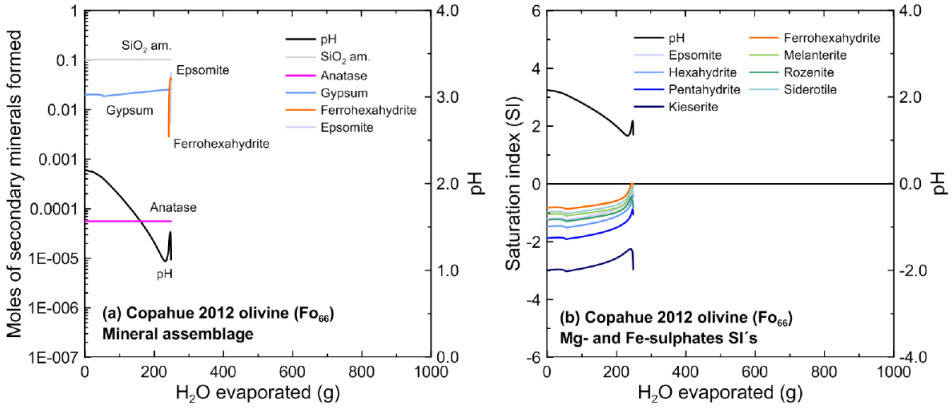

Figure 3.17. Evaporation model for Vertiente hot spring water previously modified by interaction with olivine (fluid composition before formation of jarosite, cf. Fig. 3.16). (a) Secondary minerals represented by amorphous silica, anatase and gypsum. (b) Saturation indices for Mg- and Fe- sulphates. Note that both ferrohexahydrite and epsomite reached equilibrium near the end of this run. See text for details.

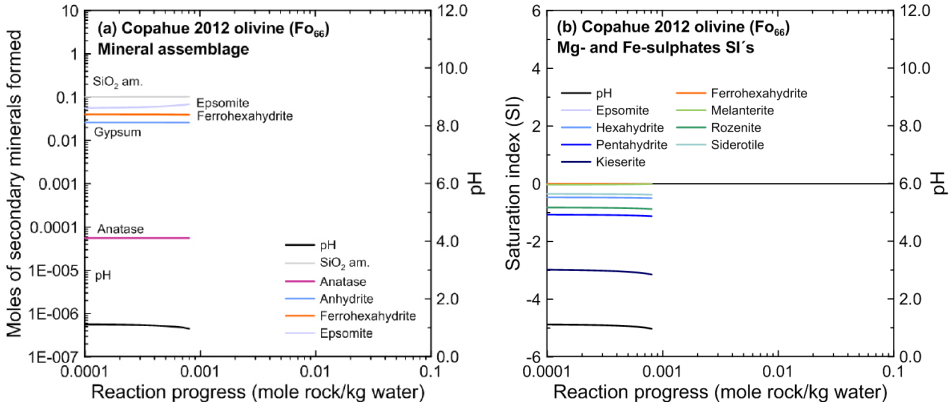

Figure 3.18. Final step in a hypothetical model showing the formation of ferrohexahydrite and epsomite as products of interaction between the fluid residues of evaporation (as modelled in Fig. 3.17) and olivine.

above. Further downstream, after substantial dilution to pH values around 3, microbiotic reactions as well as photo-reduction processes, may occur, cycling some dissolved components through various aqueous species and creating conditions for the saturation with schwertmannite. The crystallization of those HFO-sulphates then leads to adsorption and incorporation of the trace elements arsenic, phosphorus and vanadium. Ultimately, schwertmannite may convert to hydrous ferric oxides such as ferrihydrite and goethite which may over time turn into hematite. We note that at Copahue it appears that schwertmannite crystallization is conditioned or at least modulated by Fe-oxidizing acidophilic bacteria, as found in the Lower Río Agrio. The

Copahue hydrothermal fluids are rich in Mg^{2+} and Fe^{2+}, especially directly following intrusive events, and these cations are probably largely derived from dissolution of mafic phases such as olivine and pyroxenes. Oxidation of Fe^{2+} leads to the precipitation of ferric oxides and sulphates, whereas Mg sulphates are rare. Combination of acid water-rock interaction with evaporation and subsequent reaction with olivine may lead to Mg-sulphates crystallization.

Weathering experiments of basaltic rocks (Gíslasson and Arnórsson, 1993; Nesbith and Young, 1984; Nesbith and Wilson, 1992; Tosca et al., 2004; Golden et al, 2005 and Hausrath et al., 2013) and olivine (King et al., 2011) suggest that the bulk composition of the starting material, low water/rock ratios and incongruent rock or glass dissolution may lead to the formation of magnesium sulphates. Mars is largely a basaltic planet (Baratoux et al., 2009; Carr and Head, 2010; Grott et al., 2013) whereas silicic and intermediate rocks predominate on the continents of the earth. Some of these major differences in surface rocks between the two planets are reflected in their secondary minerals. While on Earth secondary mineral assemblages are dominated by clay minerals, aluminium hydroxides, and iron oxi/hydroxides, on Mars the secondary mineralogy is primarily represented by magnesium, iron and calcium sulphates and iron oxides (Hurowitz and McLennan, 2007). Nevertheless, the rivers and lakes at Caviahue-Copahue formed secondary mineral associations that resemble some Mars terrains and their mechanisms of formation were documented by our analytical studies and constrained by the modelling above.

With regards to the search for Mars analogues at Copahue, several features of Lower Río Agrio are significant. The acidity of Río Agrio watershed has a volcanic source, unlike other putative Mars analogues, such as the Río Tinto, Spain, which owe their acidity to mining and accelerated weathering of sulphide bedrock minerals. The spatial distribution of active HFO-sulphate precipitates and ancient ferricrete deposits along lower Río Agrio may be examples of the types of mineral deposits that could conceivably exist on Mars in paleo-fluvial environments. The thickest accumulations of ferricrete along the Río Agrio exist along the margins of the stream where alkaline groundwater mixes with acidic river water, not within the main channel of the river. Most of the HFO that precipitates in the main channel is swept downstream during periods of high flow, leaving a thin (<1 cm), transient coating of orange-red "muck" on boulders and outcrops when the river levels recede. Thirdly, the existence of HAO flocks and Al-cemented gravel in the lower reaches of Río Agrio suggest that similar geologic deposits could exist on Mars. In the absence of active volcanic-hydrothermal systems, groundwater under the Martian regolith would most likely have a neutral to alkaline pH through interaction with basalt, just as it does on Earth. By mixing with this groundwater, or mixing with non-acidic tributary streams, the "pH endpoint" of titration of an acidic Martian river with distance away from its volcanic-hydrothermal source could have been > 5, resulting in precipitation of dissolved Al as HAO. Such precipitates could be preserved as alcrete deposits along paleo-river banks, as sediment in a terminal playa lake, or as coatings on mineral surfaces be-

neath the paleo-river channel in an event on which surface water soaked into the ground before it evaporated or froze.

It has been postulated that schwertmannite was an important mineral on Mars (Bishop and Murad, 1996), either in its far past or even still occurring today. If the analogy with Caviahue holds, the mineral formation on Mars may also have been facilitated by Fe-oxidizing bacteria and photo-reduction and/or photo-oxidation processes. The disequilibrium created by sunlight and Fe (III) photo-reduction is sufficient to support a thriving population of IOBs in Río Tinto (Gammons et al. 2008), and similar processes occur in the Río Agrio. The effectiveness of the IOBs to oxidize Fe (II) to Fe (III) is a function of O_2 concentrations in the water and thus in air (reaction 6). For early Mars, the partial pressure of O_2 is poorly constrained, but reaction (6) is thermodynamically favourable for water with the same chemistry as Salto del Agrio samples as long as is greater than 10^{-22} to 10^{-24} bars. The question then becomes: could O_2 partial pressures have been this high in an early Martian atmosphere?

Astrobiologists have speculated that a significant amount of organic carbon could have been deposited on Mars by comets, and yet empirical data that have been returned from orbital and land-based probes show only few traces of organic compounds on Mars (Benner et al., 2000; Ming et al., 2013). Iron photo-reduction may have provided a means to break down DOC or solid organic carbon molecules. Following the Río Agrio analogy, organic carbon delivered to the surface of Mars could have been largely oxidized by free radicals such as $OH\cdot$ that formed via the Fe (III) photo-reduction reactions (4) and (5) presented earlier. This assumes that: 1) water existed on the Martian surface; and 2) the water was acidic enough to mobilize ferric iron. The importance of Fe (III) photo-reduction on Mars is rarely discussed in the astrobiology literature. Most researchers discuss Fe (II) photo-oxidation (Cairns-Smith, 1978, and the later work of Braterman et al., 1983; Borowska and Mauzerall, 1986; Lundgreen et al., 1989; Kim et al., 2013). Short wave-length UV-C light (maximum at 267 nm, Kim et al., 2013) in controlled laboratory experiments created Fe(II) photo-oxidation, as opposed to Fe (III) photo-reduction, which is induced by light over a wider range of wavelengths (200 to 450 nm, maximum at 300 nm, David and David, 1976). In the absence of a protective ozone layer in the upper atmosphere, UV-C radiation could have easily penetrated Mars' thin atmosphere, as it presumably did the atmosphere of early Earth. It is unknown if Fe (II) photo-oxidation occurs simultaneously with Fe (III) photo-reduction in full spectrum sunlight, and what the relative rates of these two opposing reactions are over a wide range of pH, and in the presence of other solutes, such as possibly dissolved organic carbon.

Obviously, if firmer evidence of schwertmannite presence from the Mars surface can be supplied, this may lead to many inferences regarding the presence of bacteria as well the atmospheric composition at the time. Our modelling and observations make it likely that schwertmannite may have formed on Mars in analogy to the processes documented in Río Agrio watershed. The key parameters here are that the waters

are both acidic and sulphate-rich because of absorption of volcanic gases, and Fe-rich because of high temperature water-rock interaction at depth. The schwertmannite stability zone at Copahue is distal from the hot springs and caused both by an increase in pH through dilution and the Fe-cycling discussed above. If schwertmannite was common at the surface of early Mars, we would also expect adsorption of As, V and P, which would probably create an overall surface enrichment in these elements. Greenwood and Blake (2006) suggested that Mars surface rocks are indeed enriched in phosphorus.

Hurowitz et al. (2012) designed an inverse schwertmannite precipitation scheme, where neutral groundwaters became enriched in Fe (II) through interaction with basaltic basement. Once at the surface, photo-oxidation processes reduced the pH which then led to schwertmannite saturation while coming from the higher pH values (the sulphate source is not obvious in this model). The precipitation of schwertmannite would then lead to even lower pH values, creating conditions of acid surface waters on Mars. Our observations and modelling shows that in Río Agrio the opposite occurs: strongly acid fluids become neutralized and once the pH=3 limit is exceeded; schwertmannite starts to crystallize as discussed above.

3.7. CONCLUSIONS

Many minerals observed on the surface in the Copahue-Caviahue watershed are also thought to occur on Mars: silica, jarosite, gypsum, hematite, various hydrous Fe-oxides and hydrous Fe-sulphates and schwertmannite. Alunite is uncommon at the surface at Copahue but is an important mineral that formed in the hydrothermal reservoir at elevated temperatures. In analogy, alunite on Mars may be found at the surface near impact craters that de-roofed former volcanic hydrothermal systems. The abundance of many Mg-sulphates on Mars is in contrast with their limited occurrence in the Río Agrio watershed, where Mg is an almost conservative element. Modelling suggests that more extensive interaction between acid fluids and olivine-rich basement rocks, possibly coupled with evaporation could easily lead to Mg-sulphate formation. Mars is largely a basaltic planet, rich in olivine, whereas Copahue is an andesitic volcano where the most mafic rocks were the 2012 scoria with some olivine and a bulk rock magnesium content of 4.5 % MgO (Varekamp et al., 2015). The potential presence of schwertmannite on Mars leads to many speculations regarding presence of bacteria, composition of the atmosphere as well as surface enrichments in the oxyanions of V, As and P. At first sight, Copahue appears to be a good terrestrial analogue for some Martian environments that carry sulphate minerals (Varekamp, 2004).

ACKNOWLEDGEMENTS

Funding for this study to J.C. Varekamp was provided by grants NSF EAR-0949376 and NSF RAPID-1331167, the National Geographic Society (grant # 7409-03), a Franklin Research Grant of the American Philosophical Society (2004), and the Wes-

leyan University Harold Stearns Endowed Chair fund. J.C. Varekamp appreciated the hospitality of the School of Earth Sciences at Bristol University, UK, where he was a resident Fellow during the spring of 2013. Tristan Kading acknowledges a Space Grant Fellowship in 2009, and Alejandro Rodríguez was funded by NWO (Netherlands Organization for Scientific Research), project ALW-GO-PL/10-03. The TEM studies were done at the CAMCOR facility at the University of Oregon (Eugene, OR).

CHAPTER

4

Surface alteration mineralogy in active volcanic systems: an example of Poás volcano, Costa Rica

ABSTRACT

The alteration mineralogy in the crater area of Poás volcano (Costa Rica) has been studied to constrain acid fluid-rock interaction processes and conditions relevant for the formation of sulphate-bearing mineral assemblages found on the surface of Mars. Individual sub-environments, which include the hyper-acid lake (Laguna Caliente), ephemeral hot springs, fumarole vents and areas affected by acid rain and/or spray from the lake, are marked by distinct secondary mineral associations, with sulphates commonly as prevailing component. The sulphates occur in a wide mineralogical diversity comprising gypsum/anhydrite, various polyhydrated Al-sulphates, alunite-jarosite group minerals, halotrichite-, voltaite- and copiapite-group minerals, epsomite and römerite. Depending on the sub-environment, they are variably associated with clay minerals (kaolinite-group and smectite-group), zeolites, SiO_2-polymorphs, Fe-(hydro)oxides, Ti-oxides, native sulphur, sulphides, chlorides, fluorides, phosphates and carbonates. Geochemical modelling was performed to identify mechanisms responsible for the formation of the secondary minerals found in the field, and to predict their possible stability under conditions not seen at the surface. The results indicate that the appearance of amorphous silica, hematite, anhydrite/gypsum, pyrite, anatase and kaolinite is relatively insensitive to the degree of acidity of the local aqueous system. On the other hand, alunite-jarosite group minerals, elemental sulphur and $Al(OH)SO_4$ only form under acidic conditions (pH<4). The presence of polyhydrated Mg- and Fe^{2+}-sulphates is restricted to olivine-bearing rocks exposed to acid rain or brine spray. Modelling suggests that their formation required a repetitive sequence of olivine dissolution and evaporation in an open system involving limited amounts of fluid. The mineral variety in the crater of Poás is remarkably similar to sulphate-bearing assemblages considered to be the product of acid-sulphate alteration on Mars. The analogy suggests that comparable fluid-rock interaction controls operated in Martian volcanic environments.

Front picture: Laguna Caliente, Poás volcano (Costa Rica). Picture taken on May 8th, 2012.

4.1. INTRODUCTION

The distribution of hydrous alteration minerals on Mars indicates that the oldest terrains (Noachian) are typically dominated by phyllosilicates, middle-aged terrains (Hesperian) by various sulphates, and the youngest (Amazonian) by ferric oxides (e.g., Bibring et al., 2006). Apart from these apparent global mineralogical changes in the history of the planet, there is increasing evidence that large varieties of alteration phases also formed in close spatial associations in single environments. For example, Thollot et al. (2012) described the occurrence of numerous hydrated minerals including halloysite/kaolinite, Fe-smectite, Si-OH bearing phases and polyhydrated, monohydrated, and hydroxylated Fe-sulfates (including jarosite) in a closed depression in the Noctis Labyrinthus region. The authors attributed the mineral variability to local variations in the pH of altering acid sulfate fluids, which possibly formed from groundwater and magmatic sulfur in a site under the influence of volcanic activity and associated hydrothermalism. Similar examples of mineral diversities at a local scale include depressions elsewhere in the Noctis Labyrinthus region (Weitz et al., 2011), in Valles Marineris (Weitz and Bishop, 2016), and the Columbus crater in the Terra Sirenum region, the latter arguably being a groundwater-fed paleolake (Wray et al., 2011). Evidence for acid fluids as major agents in water-rock interaction processes on Mars also comes from Meridiani Planum and Gusev crater where soils and rocks are not only enriched in sulphur but also in halogens (Klingelhöfer et al., 2004; Squyres et al., 2004; McLennan et al., 2005; Grotzinger et al., 2005; Tosca and McLennan, 2006; Chevrier and Mathé, 2007; Squyres et al., 2007).

Terrestrial volcanoes hosting hyperacid lakes are settings where fluid-rock interaction occurs in strong chemical, temperature and redox gradients, leading to a diversity of alteration products on small spatial scales. Also, these systems are commonly fed by input fluids, derived from magmatic sources, with a typical acid sulphate-chloride composition (e.g., Varekamp et al., 2000; Christenson et al., 2015; Rouwet et al., 2016). For these reasons, the surface expressions of volcanic-hydrothermal systems on Earth are potentially powerful analogues for interpreting specific Martian settings where a variety of acid alteration products formed in close proximity.

This chapter documents the distribution of alteration products in the active crater area of Poás volcano (Costa Rica), where a hyperacid lake, subaerial fumaroles, hotsprings and deposition of acid rain/spray provide a range of conditions potentially suitable for the formation of sulphur- and chlorine-bearing secondary minerals through interaction with solid volcanic materials. Geochemical modelling is applied to test mechanisms and circumstances required for the formation of the mineral assemblages observed at the surface, and to assess conditions under which secondary minerals are stable in the hydrothermal system at depth.

4.2. GEOLOGICAL SETTING

Poás volcano, located in the Central Cordillera of Costa Rica, is a broad basaltic-an-

desitic stratovolcano with a maximum elevation of 2708 m amsl (Fig. 4.1a). The volcanic products mainly consist of calc-alkaline basaltic and andesitic lavas and pyroclastics (Prosser and Carr, 1987; Cigolini et al., 1991; Malavassi, 1991) but the rock composition spans the range from basalts to dacites (Ruiz et al., 2010). The 1.3 km wide active crater, located between Von Frantzius and Botos craters, hosts an acidic lake known as Laguna Caliente in a 300 m-diameter pit and a ~30 m high composite pyroclastic cone (CPC, Casertano et al., 1987; Martínez et al., 2000; Martínez, 2008) (Fig. 4.1b). The CPC was constructed from tephra during the 1953-55 eruption. Lava flows emitted from the base of the CPC flowed towards the lake and formed a terrace (Casertano et al., 1987; Rowe et al., 1992a). Although fumarolic activity has been continously migrating over the last 20 years around the main crater (Vaselli et al., 2003), the main fumarolic activity nowadays occurs on the northern flank of the CPC. During the last 700 k.a. Poás volcano has been rising over the Proto-Central-Cordillera in different episodes of effusive, explosive and erosive activity (Ruiz et al., 2010). In the last 200 years, the activity of Poás has been characterized by frequent phreatic explosions and continuous fumarolic activity (Alvarado, 2009). More details about the petrology, geochemistry, age and geographic distribution of the units and formations around Poás volcano can be found in Prosser (1983), Prosser and Carr (1987), Kussmaul (1988), Cigolini et al. (1991), Malavassi (1991), Campos et al. (2004), Gazel and Ruiz (2005), Carr et al. (2007) and Ruiz et al. (2010).

Over the last decades, Laguna Caliente has shown temperatures between 22 and 94°C (Martínez, 2008). As a product of the dissolution of magmatic volatiles (SO_2, H_2S, HCl) in meteoric waters, sulphate (3300–285,000 mg/kg) and chloride (2500–15,000 mg/kg) are the major anions in this lake. The resulting acidity (pH= -0.87-1.75) make these waters very reactive and prone to dissolvr surrounding rocks and incorporate rock-forming elements in solution (Rowe et al.,1992a; 1992b; Rowe and Brantley, 1993; Martínez et al., 2000; Martínez, 2008). Martínez (2008) subdivided the activity of Poás since the early 1970s into five stages. During Stage I (1972 - August 1980), fumarolic discharges were strong within the lake and were accompanied with occasional phreatic explosions. Stage II (September 1980 – April 1986) was characterized by a relative quiescence in the lake and absence of phreatic activity despite a strong discharge of high-temperature fumaroles through the CPC. In the following Stage III (May 1986 - August 1995), a vigorous subaqueous fumarolic discharge and intense phreatic activity accompanied a strong volume decrease, ultimately leading to a dry-out of the lake. Stage IV (September 1995 – February 2005) was a calm period, when the lake re-established and subaerial fumaroles and hot springs appeared in the surrounding crater area (Vaselli et al., 2003). This stage was followed by an intense fumarolic discharge into the lake, together with frequent phreatic eruptions and a steady decrease of the lake volume during Stage V (March 2005 – October 2014). Fumarolic activity concentrated at the CPC, occasionally showing incandescence as gas temperatures rose above 600°C (OVSICORI-UNA, intern. reps.).

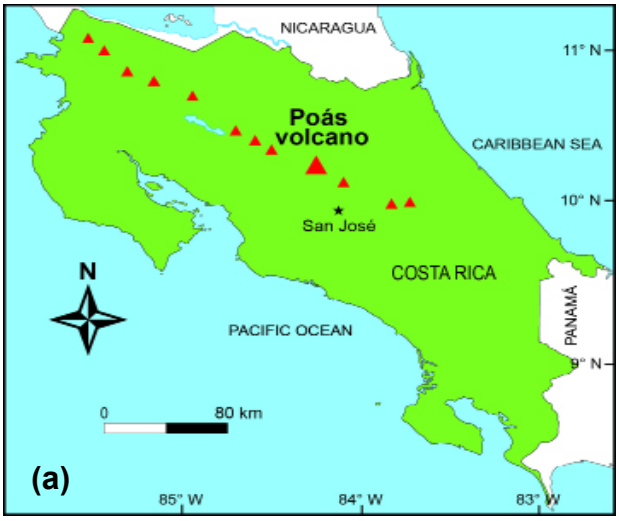

Figure 4.1. (a) Location of Poás volcano (Costa Rica). (b) Photograph of Laguna Caliente and the composite pyroclastic cone (CPC), taken from the NE rim of the main crater on May 11th, 2012.

4.3. SAMPLING AND ANALYTICAL METHODS

4.3.1. Sampling techniques

Field work was carried out in April-May 2012. Geographic coordinates and altitude were registered with a handheld GPS at each sampling location. Mineral and rock samples were collected from several sites (Fig. 4.2) within the crater area and in the "dead zone", an area SW of the lake that is occasionally affected by acid rain. Minerals were gathered with a non-metal spatula and put into 25 ml plastic Greiner® tubes. Fresh and altered rocks were stored in plastic bags.

A considerable number of samples from Laguna Caliente, hot springs around the lake, fumarole condensates and gases used in this study were collected by OVSICORI-UNA (Observatorio Vulcanológico y Sismológico de Costa Rica, Universidad Nacional). Data for some of these samples were documented by Martínez et al. (2000) and Martínez (2008). Temperature (°C), pH, electrical conductivity (C) and redox potential (Eh) were measured *in situ*, using an OMEGA® HH2001A K-type thermocouple and a WTW® 3430 portable multimeter. All electrodes were calibrated daily before fieldwork. Calibration of the pH electrode was performed using pH 1, 4 and 7 buffers. The conductivity and Eh electrode were calibrated in a 0.01 M KCl standard and a 420 mV buffer solution, respectively. Water samples for IC (ion-chromatography) and ICP-OES (inductively coupled plasma optical emission spectrometry) analysis were filtered on site through 0.2 µm pore size cellulose acetate membranes with the aid of a hand pump. Samples for IC analyses were collected in 250 ml HDPE bottles. For ICP-OES analyses, 60 ml HDPE bottles were used and samples were treated with 1 ml Suprapur® HNO3 per 100 ml of sample. For pH determinations at room temperature, unfiltered samples were collected in 20 ml amberglass air-tight bottles.

4.3.2. Analytical techniques

Minerals, sediments and hydrothermally altered rocks were dried at low temperature (40°C) during several days until a constant weight (<1% mass difference) was measured between two consecutive readings. Then the samples were ground in an agate mortar to a very fine grain size (approximately No.40 mesh). The powders were analysed by X-ray diffraction (XRD) at the Department of Inorganic Chemistry and Catalysis (Utrecht University) with a Bruker® AXS D2 Phaser powder X-ray diffractometer, in Bragg-Brentano mode, equipped with a LYNXEYE® detector. The radiation used was cobalt $K_{\alpha 1,2}$ l = 1.79026 Å, operated at 30 kV, 10 mA. The diffraction patterns were processed and interpreted with DIFFRAC.SUITE software. Thin sections of fresh and altered rocks were investigated under a polarizing optical microscope. Some of the samples were selected for electron microprobe analysis (EPMA), which was done on carbon coated samples with a JEOL® 8600 instrument, equipped with an energy-dispersive spectrometer (EDS), at the Department of Earth Sciences, Utrecht University. Operating conditions were 15 kV accelerating voltage, 10 nA bean current and 30 s counting time. PROZA software provided by JEOL® was used for matrix correction.

Conductivity, pH and redox potential of water samples were determined in the laboratory at room temperature (19±1°C) using a WTW® 3430 portable multimeter. Calibration of the pH electrode was performed using pH 1, 4 and 7 buffers. The conductivity and Eh electrode were calibrated in a 0.01 M KCl standard and a 420 mV buffer solution, respectively. The concentrations of F^-, Cl^-, Br^- and SO_4^{2-} in untreated and diluted samples (25 to 500 times with deionised water) were determined in a Dionex® ICS-3000 ion chromatograph (IC), equipped with a Dionex®IonPac® AS 19

column at the Department of Earth Sciences of Utrecht University. A gradient elution of 10 – 50 mM KOH was utilized. Concentrations of total sulphur (S_T), Al, B, Ca, Fe, K, Mg, Mn, Na, P, Si, Sr, Ti, V and Zn in diluted samples (10 to 100 times with 2% v/v Suprapur® HNO_3) were determined using a Spectro® Ciros® ICP-OES at the Department of Earth Sciences of Utrecht University.

4.3.3. Geochemical modelling

The PHREEQC software, version 3.1 (Parkhust and Appelo, 1999), was used to calculate aqueous species distributions, mineral saturation states and simulations of reaction path, heating and evaporation processes. The Lawrence Livermore National Laboratories thermodynamic database (llnl.dat), expanded with recently available thermodynamic data on sulphates and halides was used for this purpose. In addition, ion interaction parameters from Pitzer and Mayorga (1973) were included for many relevant ion pairs. The pH values of extreme acid fluids (pH<1) were recalculated from charge balance with PHREEQC because of the strongly reduced linearity of the pH vs. potential (mV) curve for the electrode when pH values are below zero (Nordstrom et al., 2000). Thermodynamic calculations involving equilibria between fumarolic gases, solids and liquids were performed using the SOLVGAS and GASWORKS codes of M.H. Reed (University of Oregon). It must be emphasized that the modelling work presented here assumes thermodynamic equilibrium and ignores any effects of reaction kinetics. Hence, it predicts direct precipitation of a mineral from the solution as soon as it becomes saturated. Obviously, mineral precipitation can be considerably delayed or can completely fail to appear in natural systems if crystal nucleation or growth are the limiting processes (Stumm and Morgan, 1996). Furthermore, the thermodynamic models used are most suitable for closed-system behaviour without mass or energy exchange with the surroundings, which is a simplification of the crater lake settings studied.

4.4. RESULTS

For convenience, the results will be grouped around different scenarios, arbitrarily based on the relative amounts of solid and fluid (water or gas) involved in reactions at each of the investigated sites within the crater area (Fig. 4.2): a low rock/water scenario in the crater lake itself, a medium rock/water scenario represented by hot springs, and a high rock/water scenario for areas affected by acid rain or acid brine spray from the lake. We also ranked the active and fossil fumaroles at Poás as a high rock/fluid setting. For each case, the chemical composition of fluids and associated primary and secondary minerals will be described. The geochemical models explore the reaction between primary phases (i.e., rock or mineral) and fluids (liquid or gas), with the secondary phases as a reaction products. The models are used to constrain the formation of secondary minerals and to gain insight into the operating transformation processes and elemental mobility for a specific system. In order to facilitate the interpretation of XRD results, the secondary minerals were grouped into 11

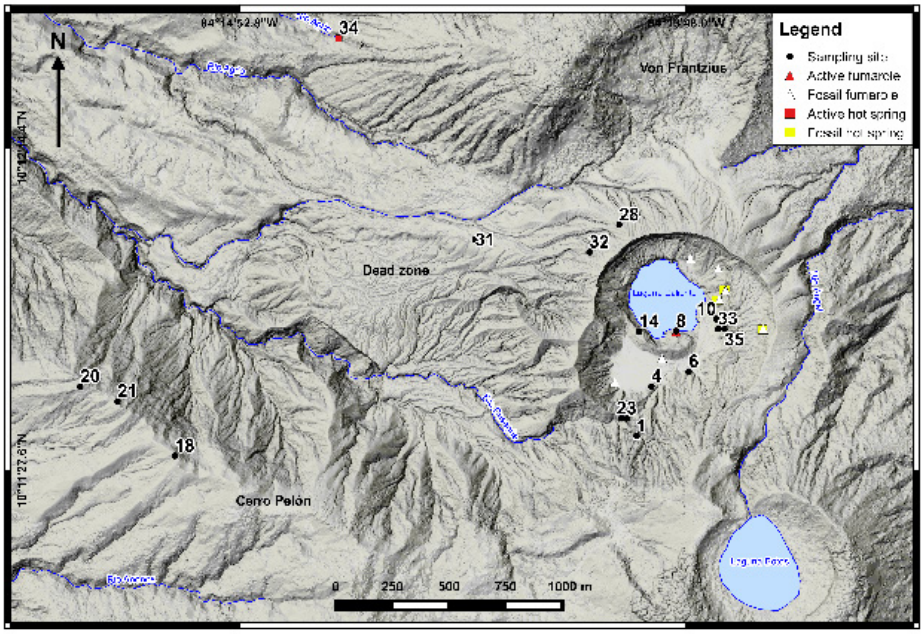

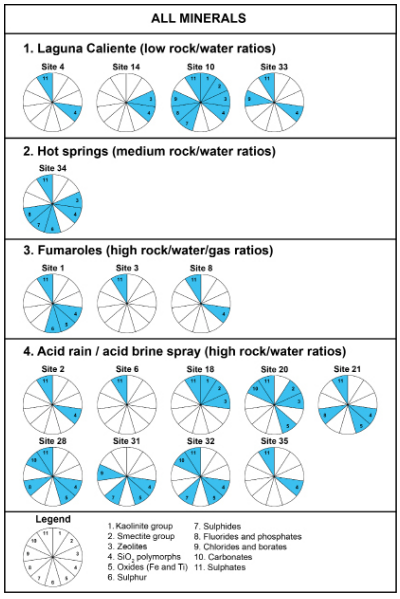

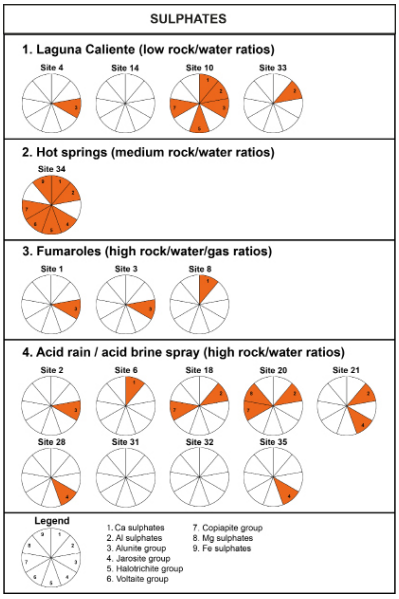

Figure 4.2. Secondary mineralogy at Poás volcano in different settings according to their rock/water/gas ratios. Minerals were identified by powder XRD, except for site 35, for which EMPA was used.

categories: 1) kaolinite group, 2) smectite group, 3) zeolites, 4) SiO_2 polymorphs, 5) oxides (Fe and Ti), 6) elemental sulphur, 7) sulphides, 8) fluorides and phosphates, 9) chlorides and borates, 10) carbonates and 11) sulphates. In view of their large diversity of interest for this study, the sulphate minerals were further divided into 9 subcategories: 1) calcium sulphates, 2) aluminium sulphates, 3) alunite group, 4) jarosite group, 5) halotrichite group, 6) voltaite group, 7) copiapite group, 8) magnesium sulphates, and 9) iron sulphates.

4.4.1. Scenario 1: Laguna Caliente (low rock/water ratios)

4.4.1.1. Water chemistry

The hyperacid water of Laguna Caliente (pH<2) has a SO_4-Cl composition and can be regarded as mixture between so-called volcanic water (Giggenbach, 1991) and meteoric water (Fig. 4.3). Volcanic waters are particularly associated with andesitic rocks around the world (Truesdell, 1991; Giggenbach and Corrales, 1992). The high acidity is mainly caused by HSO_4^- and $HCl_{(aq)}$, products of the input of magma-derived gases HCl and SO_2. The pH is mainly buffered by the HSO_4^--SO_4^{-2} pair, and an acidy increase is to be expected with a temperature decrease because the dissociation constant of HSO_4^- decreases with temperature. Other gases such as HF and HBr are minor contributors to the acidy through their aqueous dissociation. The chemical composition of Laguna Caliente water is variable and strongly dependent on the balance between heat and volatile input and dilution with meteoric or groundwater. From the early 1980s till April 2014, average contents of SO_4, Cl, F were 50000, 21000 and 1800 mg/kg, respectively (Fig. 4.3), and those of Al, Fe, Ca and Mg were 1400, 1200, 1000 and 600 mg/kg, respectively. Highest concentrations of all of these elements were recorded during periods of intense activity, as was the case in Stages III and V (Rowe et al., 1992b; Martínez et al., 2000; Martínez, 2008). The extreme acidity of the water (pH<2) makes it aggressive and capable of dissolving important amounts of rock, so that it carries large quantities of rock-forming elements (Varekamp et al., 2000; Delmelle et al., 2000; Varekamp et al., 2001). The high concentrations of Al, Fe, Ca and Mg in Laguna Caliente water are mainly derived from the dissolution of silicate minerals and glass.

Because direct redox potential measurements of the water of Laguna Caliente are scarce, the redox state of the system must be estimated for modelling purposes. Since $H_2S_{(g)}$ and $SO_{2(g)}$ are the most abundant gaseous S species that enter the aqueous system of Laguna Caliente, the S^{2-}/S^{6+} couple probably plays an important role in regulating the redox state. Based on occasional determinations of dissolved $H_2S_{(g)}$ and $SO_{2(g)}$ in the lake waters (see Martínez, 2008), a maximum concentration of 0.2 ppm $H_2S_{(g)}$ was adopted. Speciation models in PHREEQC that assume a redox potential control by the S^{2-}/S^{6+} couple yielded results consistent with the field occurrence of secondary minerals, as well as with the fact that most of the dissolved Fe must be in its Fe^{2+} form, given the high acidity of the waters. Similar observations apply to

acid mine drainage (AMD) environments (Nordstrom et al., 2000; Fernández-Remolar et al., 2005; Hubbard et al., 2009).

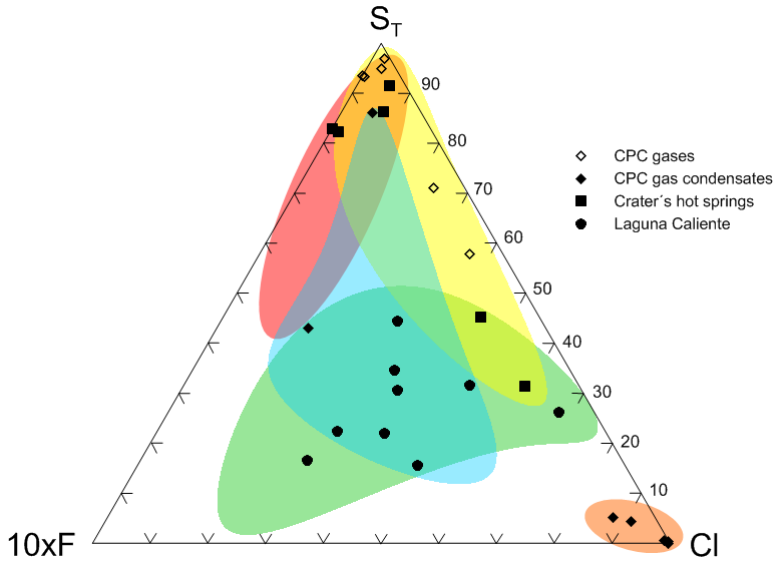

Figure 4.3. S_T-10xF-Cl molar (%) composition of fluids from Poás volcano. The composition range is illustrated for: Laguna Caliente (green), main crater´s hot springs (yellow), CPC gases (red), CPC gas condensates (orange) and acid rain from Cerro Pelón (2003-2006; OVSICORI, unpublished data) (light blue). The points, except for the acid rain, correspond to the samples from Tables 4.2-4.5.

Representative samples for each of the activity stages (see section 4.2) were selected, based on the completeness of chemical data and the availability of sufficient material for re-analysis if needed. Two samples representing Stage V, labelled Substage VA and Substage VB, were included to distinguish between different levels of activity during this interval (the former less active than the latter). The labels only indicate a difference in chemical composition (Table 4.2) and are not intended to introduce new substages in the volcanic history of Poás. For geochemical modelling, two compositions were selected from the complete data set available of Laguna Caliente. They were labelled LoALW (Low Activity Lake Water), sampled during Substage IVC (January 31th, 2002) and HiALW (High Activity Lake Water), sampled during Stage VB (May 27th, 2011). These LoALW and HiALW compositions represent periods of low and high activity in the history of the lake, respectively, and thus represent compositional extremes.

4.4.1.2. Primary and secondary mineralogy in the field

According to XRD analysis of ancient lake sediments exposed in the southern and eastern sectors of the crater (sites 4, 10; Figs. 4.2, 4.4; Table 4.1) and in recent sediments deposited on the western shore of the lake (site 14; Fig. 4.2; Table 4.1) include

Table 4.1. Mineral determinations by XRD and EMP analysis (see Fig. 4.2).

1. KAOLINITE		Kaolinite $Al_2Si_2O_5(OH)_4$ Halloysite $Al_2Si_2O_5(OH)_4$
2. SMECTITES		Montmorillonite $(Na,Ca)_{0.3}(Al,Mg)_2Si_4O_{10}(OH)_2 \cdot nH_2O$ Saponite $Na_{0.3}Mg_3(Si,Al)_4O_{10}(OH)_2 \cdot 4H_2O$
3. ZEOLITES		Cowlesite $CaAl_2Si_3O_{10} \cdot 5\text{-}6(H_2O)$ Phillipsite $(K,Na)_2(Si,Al)_8O_{16} \cdot 4H_2O$ Mordenite $(Ca,Na_2,K_2)Al_2Si_{10}O_{24} \cdot 7H_2O$ Chabazite $(Ca,Na_2,K_2,Mg)Al_2Si_4O_{12} \cdot 6H_2O$ Ca-chabazite $(Ca_{0.5},Na,K)_4Al_4Si_8O_{24} \cdot 12H_2O$ K-chabazite $(K_2,Ca,Na_2,Mg)Al_2Si_4O_{12} \cdot 6H_2O$ Sr-brewsterite $(Sr,Ba)Al_2Si_6O_{16} \cdot 5(H_2O)$
4. SiO_2 POLYMORPHS		Trydimite SiO_2 Cristobalite α SiO_2 Quartz SiO_2
5. Fe AND Ti OXIDES		Goethite FeO(OH) Hematite Fe_2O_3 Magnetite $Fe^{2+}Fe^{3+}_2O_4$ Magnesioferrite $MgFe_2O_4$ Rutile TiO_2 Titanomagnetite $Fe^{2+}(Fe^{3+},Ti)_2O_4$ Anatase TiO_2
6. SULPHUR		S
7. SULPHIDES		Greigite $Fe^{2+}Fe^{3+}_2S_4$ Wurtzite (Zn,Fe)S Tennantite $Cu_{12}As_4S_{13}$
8. FLUORIDES AND PHOSPHATES		Carobbiite KF $MgNaF_3$ Woodhouseite $CaAl_3(PO_4)(SO_4)(OH)_6$ [illegible] Na_3PO_4 Ralstonite $Na_xMg_xAl_{2-x}(F,OH)_6 \cdot H_2O$
9. CHLORIDES		Potassium halite $K_xNa_{1-x}Cl$ Sophiite $Zn_2(SeO_3)Cl_2$
10. CARBONATES		Tychite $Mg_2Na_6(CO_3)_4SO_4$ Ankerite $Ca(Fe^{2+},Mg)(CO_3)_2$
11. SULPHATES	**11.1 CALCIUM**	Gypsum $CaSO_4 \cdot 2H_2O$ Anhydrite $CaSO_4$
	11.2 ALUMINIUM	Alunogen $Al_2(SO_4)_3 \cdot 17H_2O$ Meta-alunogen $Al_2(SO_4)_3 \cdot 27H_2O$ Khademite $Al(SO_4)F \cdot 5H_2O$ Rostite $Al(SO_4)(OH,F) \cdot 5H_2O$
	11.3 ALUNITE	K-alunite $KAl_3(SO_4)_2(OH)_6$ Na-alunite $KAl_3(SO_4)_2(OH)_6$ Minamiite $(Na_{[illegible]}K_{[illegible]}Ca_{[illegible]})Al_3(SO_4)_2(OH)_6$ Huangite $Ca_{0.5}Al_3(SO_4)_2(OH)_6$
	11.4 JAROSITE	K-jarosite $KFe_3(SO_4)_2(OH)_6$ H-jarosite $(H_3O)Fe_3(SO_4)_2(OH)_6$
	11.5 HALOTRICHITE	Halotrichite $FeAl_2(SO_4)_4 \cdot 22H_2O$ Pickeringite $MgAl_2(SO_4)_4 \cdot 22H_2O$ Apjohnite $MnAl_2(SO_4)_4 \cdot 22H_2O$
	11.6 VOLTAITE	Voltaite $K_2Fe^{2+}_5Fe^{3+}_3Al(SO_4)_{12} \cdot 18H_2O$ Pertlikite $K_2(Fe^{2+},Mg)_2(Mg,Fe^{3+})_4Fe^{3+}_2Al(SO_4)_{12} \cdot 18H_2O$
	11.7 COPIAPITE	Copiapite $Fe^{2+}Fe^{3+}_4(SO_4)_6(OH)_2 \cdot 20H_2O$ Magnesiocopiapite $MgFe^{3+}_4(SO_4)_6(OH)_2 \cdot 20H_2O$
	11.8 MAGNESIUM	Epsomite $MgSO_4 \cdot 7H_2O$
	11.9 IRON	[illegible] $Fe^{2+}_{x}Fe^{3+}_{y}(SO_4)_{z} \cdot 13.5H_2O$

Table 4.2. Chemical analysis of waters from Laguna Caliente, Poás volcano. Concentrations in mg/kg. Conductivity (mS/cm) and pH were measured in the laboratory at T = 19 ± 1°C.

Stage/ sub-stage	Date	$T_{sampling}$ (°C)	pH	Cond.	SO_4	S_T[a]	F	Cl	Br	Al	B	Fe	Ca	Mg	Na	K	Si	Mn	Sr	Ti	V	Zn	TDS	Data source
II	29-Nov-85	45	0.3	390	63000	21000	1090	23400	57	2380	20	1260	880	650	610	240	35	31	18	5.6	6.2	2.6	82800	(1)
III	10-Jan-87	58	-0.01	n.d.[b]	64400	n.d.	1590	30400	61	2070	n.d.	1020	2340	550	520	250	88	25	n.d.	n.d.	n.d.	n.d.	107000	(2,3)
III	30-Aug-94	60	0.54	n.d.	19200	5200	1019	10100	305	1830	n.d.	1570	1020	570	470	145	35	30	n.d.	n.d.	n.d.	n.d.	36000	(2,4)
IVA	20-Oct-95	30	1.21	41	6230	3100	190	4200	19	470	5	540	710	530	410	66	72	28	5	n.d.	b.d.l.[c]	1.1	13000	(1)
IVB	17-Apr-98	37	0.68	87	10900	4430	460	8870	17	1000	n.d.	950	1300	630	560	83	77	31	n.d.	n.d.	n.d.	n.d.	24900	(5)
IVC	31-Jan-02	30	1.51	22	3590	1470	52	2540	5	360	n.d.	330	620	230	190	39	110	11	3	n.d.	n.d.	0.9	12600	(1,5)
IVD	12-Aug-03	33	0.61	142	8860	5290	720	18200	n.d.	1410	n.d.	780	1340	490	400	110	32	21	n.d.	n.d.	n.d.	n.d.	35000	(5)
IVE	25-May-04	28	1.31	30	3940	1880	30	5380	8	680	n.d.	420	750	340	280	48	120	14	n.d.	n.d.	n.d.	n.d.	12000	(1,5)
VA	30-Nov-05	54	0.64	134	13600	7530	920	11600	n.d.	1630	n.d.	670	1440	360	450	130	119	15	n.d.	n.d.	n.d.	n.d.	34000	(5)
VB	27-May-11	62	-0.25	571	101500	34900	1170	26700	68	2030	16	1030	660	400	430	240	52	19	13	12.9	5.6	2.4	n.d.	(1)

Notes: (a) total sulphur (ICP-OES); (b) n.d. = not determined; (c) b.l.d = below detection limit. Sources: (1) this study; (2) OVSICORI-UNA; (3) Rowe et al., (1992b); (4) Martinez et al. (2000); (5) Martinez (2008).

tridymite, cristobalite, quartz, kaolinite, sauconite, cowlesite, phillipsite, greigite, woodhouseite and ralstonite. In addition, sulphates are represented by gypsum, K-alunite, Na-alunite, minamiite, meta-alunogen, halotrichite and magnesiocopiapite.

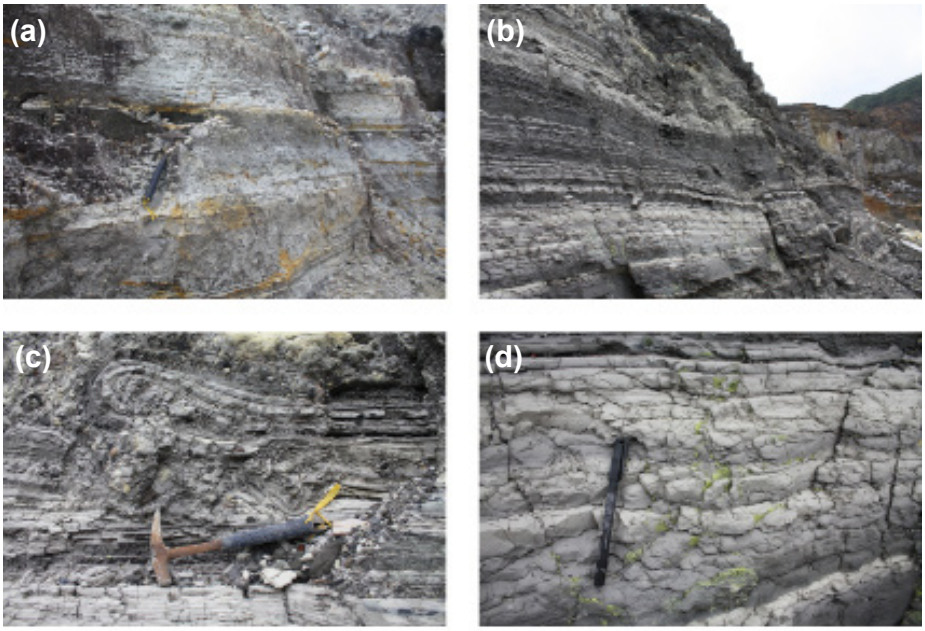

Figure 4.4. Ancient Laguna Caliente sediments on site 4 (a) and site 10 (b) to (d); see Figure 4.2. Tabular (a,b) and convolute bedding (c). Within the sediments, elemental sulphur is commonly present (d).

Two andesitic lava samples, collected within lake sediments exposed on the eastern shore of Laguna Caliente (site 10; Figs. 4.2, 4.4; Table 4.1), were investigated for the effect of alteration by Laguna Caliente water. Fresh sections of these lavas show a vesicular texture, with phenocrysts of plagioclase, pyroxenes and opaques. The plagioclase composition is close to An_{58}, whereas pyroxenes consist of two groups: augite $Wo_{38.8}En_{41.6}Fs_{19.6}$ and enstatite $Wo_{3.9}En_{62.2}Fs_{33.9}$, and opaques range between magnetite $Fe^{2+}Fe^{3+}{}_2O_4$ and ulvöspinel $TiFe^{2+}{}_2O_4$. In the altered parts of the lavas, both plagioclase and pyroxene phenocrysts are intensely silicified. Frequently, the entire crystal structure has been replaced by a SiO_2-rich phase which corresponds to amorphous silica. In general, silicification is less pervasive in the pyroxenes than in the plagioclase. Within the lava vesicles, the most common alteration mineral is an Al_2O_3-SO_3-rich phase, which corresponds to alunite with a composition close to the H-alunite end-member (Figs. 4.5, 4.6). There is also an Al_2O_3-SiO_2-rich phase with a composition close to kaolinite. Pyrite and elemental sulphur globules are present within the vesicles as well. Textures indicate that pyrite and sulphur formed before

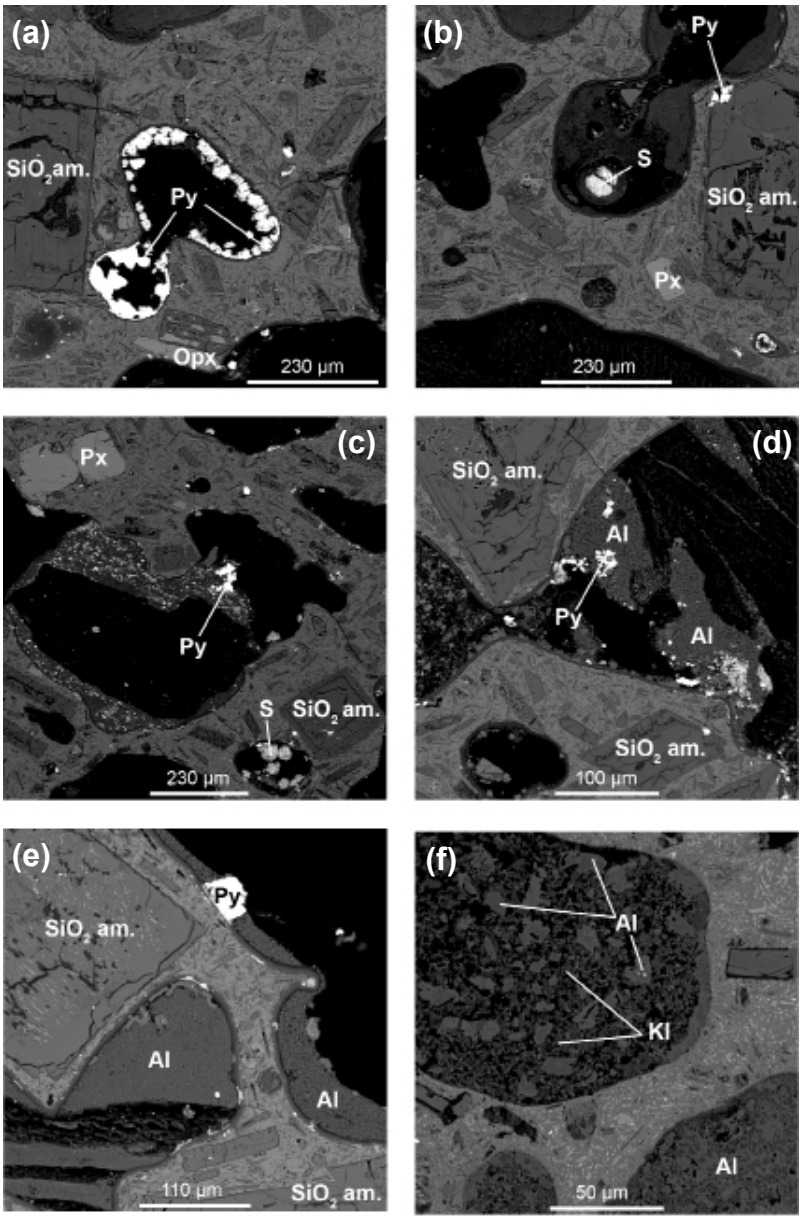

Figure 4.5. EMP images of a lava within ancient Laguna Caliente sediments (site 10; Figs. 4.2, 4.4). Primary minerals: pyroxene (Px) and orthopyroxene (Opx). Secondary minerals: amorphous silica (SiO_2 am.), elemental sulphur (S), pyrite (Py), alunite (Al) and kaolinite (Kl).

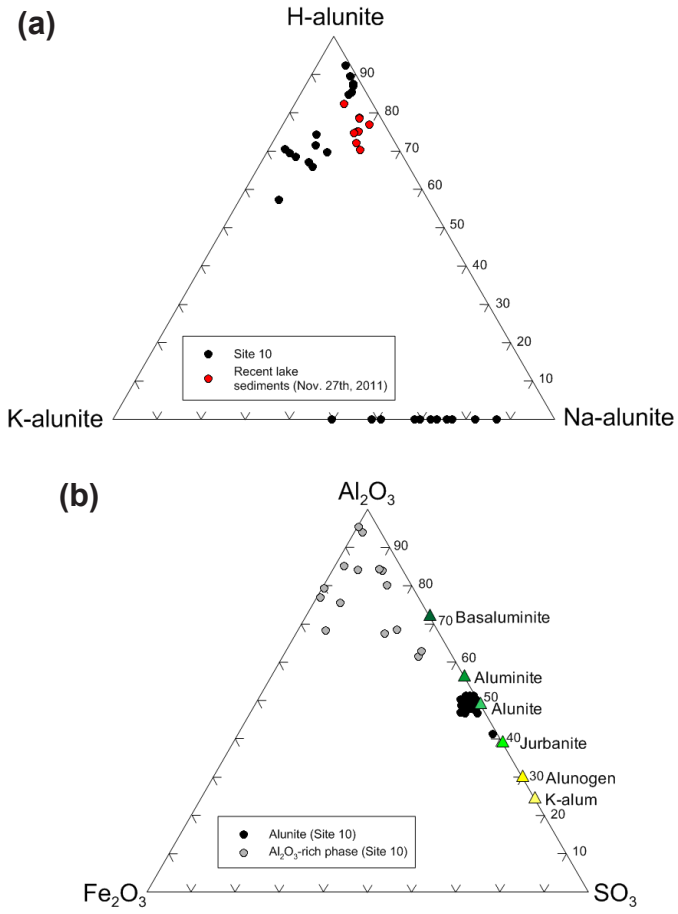

Figure 4.6. (a) EMP analyses (Fe_2O_3-Al_2O_3-SO_3; wt.%) of some of the secondary minerals present in a lava within the ancient Laguna Caliente´s sediments (site 10; Figs. 4.2, 4.4, 4.5). Alunite and an Al_2O_3-rich phase are the most abundant secondary minerals in the vesicules. The following minerals are also shown: basaluminite $Al_4(OH)_{10}SO_4{\cdot}5H_2O$, aluminite $Al_2(OH)_4SO_4{\cdot}7H_2O$, jurbanite $Al(OH)SO_4{\cdot}5H_2O$, alunogen $Al_2(SO_4)_3{\cdot}17H_2O$ and K-alum $KAl(SO_4)_2{\cdot}12H_2O$. (b) Compositionally, the alunites from site 10 are close to the alunite H-end member $HAl_3(SO_4)_2(OH)_6$ and between the K- and Na-end members ($KAl_3(SO_4)_2(OH)_6$ and $NaAl_3(SO_4)_2(OH)_6$, respectively). For comparison, a sample of recent bottom sediments from Laguna Caliente, collected on November 27th, 2011 by OVSICORI personnel, was included.

H-alunite and kaolinite. Temporal relationships between amorphous silica and the other alteration minerals are unclear, but silica probably formed early, considering that it is a residue after the mobile cations (Ca^{2+}, Al^{3+}, Fe^{2+}, Mg^{2+}, Na^{+} and K^{+}) were incorporated into solution (Oelkers, 2001).

4.4.1.3. Heating model

Heating models (Fig. 4.7) were ran in PHREEQC to explore changes in the saturation state of representative minerals when temperature increases from those measured in the lake (30° and 62°C) up to 300°C. The heating models only consider a temperature increase, ignore any reaction with surrounding rock, and thus predict changes in the chemical composition of the lake water solely in response to mineral precipitation or dissolution.

The heating models provide insight into the saturation state of acid brine water at depth, e.g. in the hydrothermal system below the lake, envisage changes in response to an increased input of heat due to increased volcanic activity, and simulates chemical effects on lake water that circulatback into the deeper parts within volcanic edifice. Conversely, the runs can also be interpreted in a reverse way as cooling models for deep hot brine water travelling upward and ultimately feeding the lake.

Under surface conditions, Laguna Caliente waters were saturated with elemental sulphur and pyrite, and close to saturation with amorphous silica, anhydrite and gypsum (Fig. 4.7). A temperature rise will increase the solubility of amorphous silica, pyrite and elemental sulphur, and will decrease the solubility of gypsum, anhydrite, diaspore, kaolinite, K-alunite, Na-alunite, and AlF_3. In aqueous systems, the solubility curves of gypsum and anhydrite intersect at 42°C, with gypsum being the stable phase below and anhydrite the stable phase above this temperature (Braitsch, 1971).

The LoALW composition (T=28°C) formed pyrite up to 100°C, followed by anhydrite, diaspore and AlF_3. While K-alunite was only stable between 100 and 200°C, anhydrite, diaspore and eventually AlF_3 persisted up to 300°C. The pH increased until K-alunite or diaspore appeared, remained more or less constant, then decreased and finally increased at temperatures higher than 250°C. On the other hand, the HiALW composition (T=60°C) only precipitated elemental sulphur when the temperature increased.

4.4.1.4. Water-rock reaction model

Results of PHREEQC water-rock reaction path models, with the same set of water samples and a basaltic-andesite analysed by Cigolini et al. (1991) as reactants, are presented in Figure 4.8. In every run, 1 mole of rock (110 g) was reacted with 1 kg of crater lake water. The water-rock reaction path can be visualised as a titration model in which the water sample (acid) is incrementally titrated with small amounts of rock (base). As a rule, the pH of the system will increase due to H^+ consumption by the rock, and at the same time cations will be liberated into solution. It must be noted that the crater lake water used in the interaction models is not a "pristine" liquid end-member, since the samples collected at the surface represent liquids that had previously reacted with surrounding rocks at depth before reaching the crater area.

Also, as discussed in the previous section, the fluids that reach Laguna Caliente were probably chemically modified by mineral precipitation due to cooling and boiling. Nevertheless, due to their extreme acidy, the waters are still capable of dissolving large amounts of rock. As the reaction progress proceeds, secondary phases or minerals will be formed and, in some cases, their presence will be transient. Each model was run at a constant temperature, corresponding to the lake water temperature when the sample was taken. Minerals allowed to precipitate were selected according to the assemblages found by XRD and EMP analysis. Finally, for practical purposes, it is assumed that dissolution of primary phases in the rock occurs congruently. This implies that the basaltic andesite is considered to behave as a homogenous phase, similar to a glass, and that all of its components dissolve instantaneously.

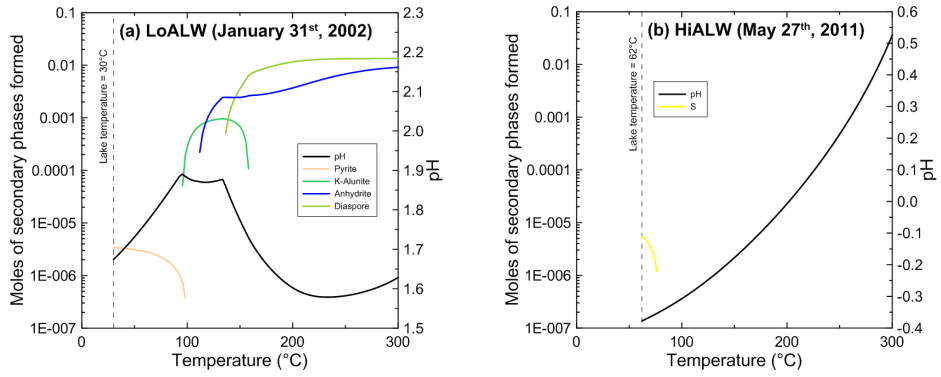

Figure 4.7. Heating models of Laguna Caliente´s waters from lake temperature till 300°C. (a) LoALW: Low-activity lake water (T=30°C). (b) HiALW: High-activity lake water (T=62°C). These high- and low-activity labels refer to the volcanic activity of Laguna Caliente in terms of input of heat and magmatic volatiles.

The water-rock reaction path models for the LoALW composition showed amorphous silica, hematite and anatase at low reaction-progress values (<0.001 mole rock/kg water). At intermediate values (0.01 - 0.1 mole rock/kg water) K-alunite, $Al(OH)SO_4$, kaolinite, pyrite and fluorite appear. Finally, at high values (>0.1 mole rock/kg water), illite is added to the mineral assemblage. The HiALW composition produced fewer secondary minerals and probably represents the scenario of the most unreacted system due to the low pH values reached at the end of the run. This system is characterized by the formation of anatase and amorphous silica followed by anhydrite and H-alunite $HFe_3(SO_4)_2(OH)_6$.

In summary, the water-rock interaction models for Laguna Caliente, representing a low rock/water system, demonstrate that during low volcanic activity periods, the secondary mineral assemblage is marked by the presence of amorphous silica, anatase, hematite, $Al(OH)SO_4$, K-alunite, kaolinite, pyrite, fluorite, gypsum and illite. In

contrast, during periods of high activity, the mineral assemblage with be constituted only by amorphous silica, anatase, anhydrite and eventually H-jarosite.

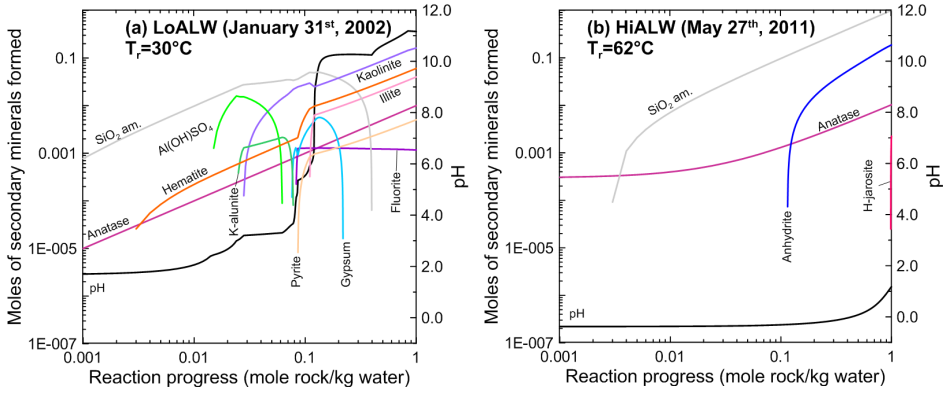

Figure 4.8. Water-rock reaction path models between Laguna Caliente´s waters and the basaltic-andesite analysed by Cigollini et al. (1991). T_r refers to the temperature of the run, which corresponds to the temperature of Laguna Caliente. In every run 1 mole of rock (110 g) was reacted with 1 kg of crater lake water. (a) LoALW: Low-activity lake water (T=30°C). (b) HiALW: High-activity lake water (T=62°C). These high- and low-activity labels refer to the volcanic activity of Laguna Caliente in terms of input of heat and magmatic volatiles.

4.4.1.5. Evaporation model

Water evaporation is a major process in crater lakes (Pasternak and Varekamp, 1997) and induces changes in the chemical composition of the waters such as increasing concentrations of dissolved species until saturation is reached and phases precipitate or evaporate along with the water (Varekamp et al., 2000; Rouwet and Ohba, 2015). The rate of evaporation usually fluctuates as it is a function of different parameters that vary with time, of which heat input from magma at depth is an important factor. The evaporation process for Laguna Caliente water was simulated by removing small amounts of H_2O from a 1 kg of sample; at a constant temperature corresponding to the one of the lake when the sample was taken (Fig. 4.9). The run reached 98% of water loss. Beyond this point there were convergence problems with PHREEQC due to the high ionic strength of the solutions that, in the case of the HiALW composition, went up to 37.9 mol/kg H_2O from a starting value of 2.39 mol/kg H_2O. Phases precipitating in the HiALW model are anatase, anhydrite and elemental sulphur. As a consequence of water removal, the pH drops and reaches values below -8. This extreme acidity promotes the formation of gaseous hydrogen chloride ($HCl_{(g)}$). This gas often forms in Laguna Caliente and as well as in other acidic volcanic lakes (Martínez et al., 2000; Rouwet and Ohba, 2015). The saturation indices of amorphous silica, halite NaCl, and iron and magnesium sulphates such as szolmolnokite $FeSO_4 \cdot H_2O$, rozenite $FeSO_4 \cdot 4H_2O$, siderotile $FeSO_4 \cdot 5H_2O$, melanterite $FeSO_4 \cdot 7H_2O$, kieserite $MgSO_4 \cdot H_2O$, and epsomite $MgSO_4 \cdot 7H_2O$ steadily increased until

80% of the water was evaporated and then abruptly decreased. Similar evaporation runs were performed on the LoALW composition at 30°C in order to explore possible temperature effects. In this case, gypsum formed instead of anhydrite, and amorphous silica was present. Anatase could not form because Ti was not analysed in the LoALW sample. The temperature effect was particularly reflected in the type of calcium sulphate present (gypsum or anhydrite) and in the saturation of amorphous silica (Fig. 4.9).

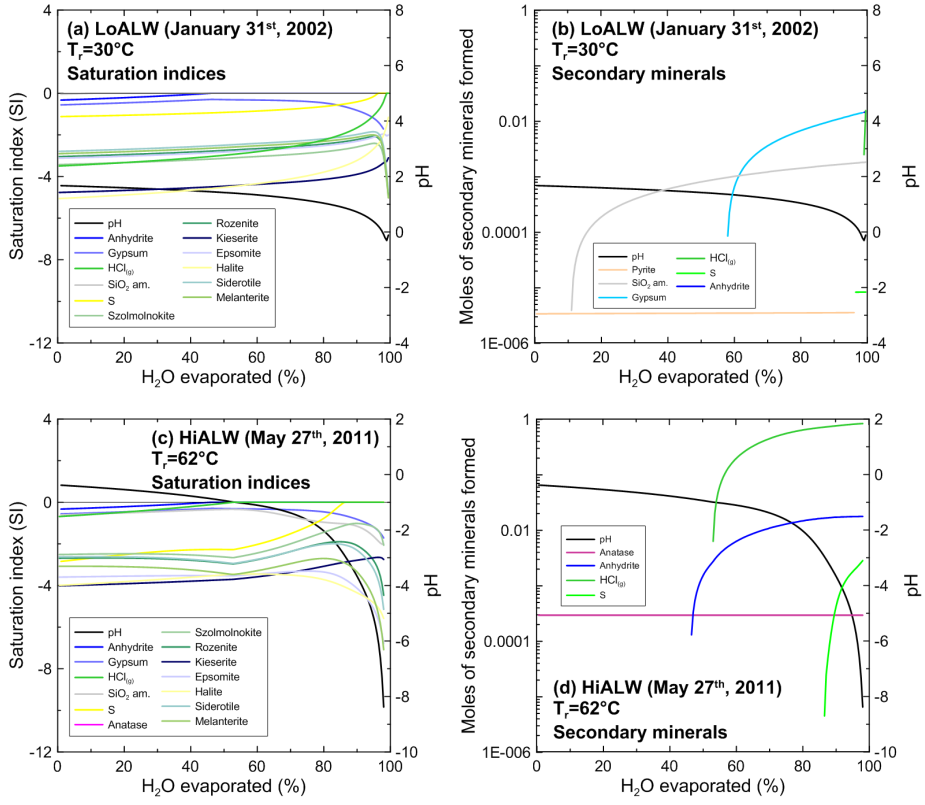

Figure 4.9. Evaporation models of Laguna Caliente´s waters showing both the saturation indices of some minerals and the moles of secondary minerals formed upon evaporation. In every model the starting amount of crater lake water is 1 kg. T_r refers to the temperature of the run, which corresponds to the lake temperature. (a), (b) LoALW: Low-activity lake water (T=30°C). (c), (d) HiALW: High-activity lake water (T=62°C). These high- and low-activity labels refer to the volcanic activity of Laguna Caliente in terms of input of heat and magmatic volatiles.

In summary, the results of models for the low rock/water scenario, applied to the Laguna Caliente waters, demonstrate that the observed secondary mineralogy can be generated by a combination of the simulated processes. Elemental sulphur, pyrite, anatase, anhydrite, gypsum, diaspore, K-alunite and AlF_3 can form

solely by heating/cooling of brine water at depth or evaporation at the surface, without any concomitant rock interaction. On the other hand, the formation of H-jarosite, hematite, $Al(OH)SO_4$, kaolinite, illite and fluorite required rock dissolution.

4.4.2. Scenario 2: hot springs (medium rock/water ratios).

4.4.2.1. Water chemistry

Hot springs issuing acidic waters existed at various locations on the eastern terrace of Laguna Caliente from March 1999 till January 2007. Samples from the years 2000, 2001, 2003 and 2006, documented by Martínez (2008) and Vaselli et al. (2003) were included in this study. The hot spring waters were sub-boiling SO_4-rich steam heated waters with temperatures between 42 and 92°C and pH values between 0.99 and 2.47 (at 20-24°C) (Fig. 4.3; Table 4.3). Presumably, hot vapours coming from degassing magma interacted with meteoric waters that may have been derived through subsurface flow from Botos Lake, since it is located topographically higher than the active crater (Sanford et al., 1995). No samples of alteration minerals were collected from sites were the hot springs existed since most were covered by landslide deposits produced by an earthquake on January 8th, 2009.

4.4.2.2. Water-rock reaction model

Water-rock reaction models follow the same approach as the ones described in section 4.4.1.4, including use of the basaltic andesite described by Cigolini et al. (1991). Each run was carried out at the temperature of the spring (Fig. 4.10). Two spring samples were selected as end-member examples in terms of initial temperature and pH: White Algae (August 23rd, 2000; T=42°C) and Norte-Este (February 14th, 2003; T=87°C). At low reaction progress values (<0.001 mole rock/kg water), the modelled secondary mineral association for the White Algae composition is represented by anatase, amorphous silica, hematite, K-alunite and kaolinite. At intermediate reaction progress (0.01 – 0.1 mole rock/kg water), pyrite and illite appear. Diaspore formed at high reaction progress (>0.1 mole rock/kg water). The runs with the Norte-Este spring composition show a dominance of amorphous silica, anatase and hematite at low reaction progress (<0.001 mole rock/kg water), followed by K-alunite, kaolinite, anhydrite, pyrite and illite. Diaspore and magnetite become stable at high reaction progress values (>0.1 mole rock/kg water).

4.4.3. Scenario 3: fumaroles (high rock/fluid ratios).

This scenario is represented by the active fumarole field on the northern flank of the CPC (site 8; Fig. 4.2) and fossil fumarole fields on the south-western (sites 1, 3; Figs. 4.2, 4.11), eastern and north-eastern walls of the crater. The fumaroles of the last two groups were particularly active from mid-1999 till 2007 (Martínez, 2008; Vaselli et al., 2003; Fischer et al., 2015). Variable rock/water/gas proportions mark the

interactions within fumarole conduits and vents, whereby the liquid water phase corresponds to the gas condensate. Following the description of the alteration mineralogy, modelling results for rock-gas and rock-gas condensate interaction will be treated. For this study, only samples from the CPC were taken into account.

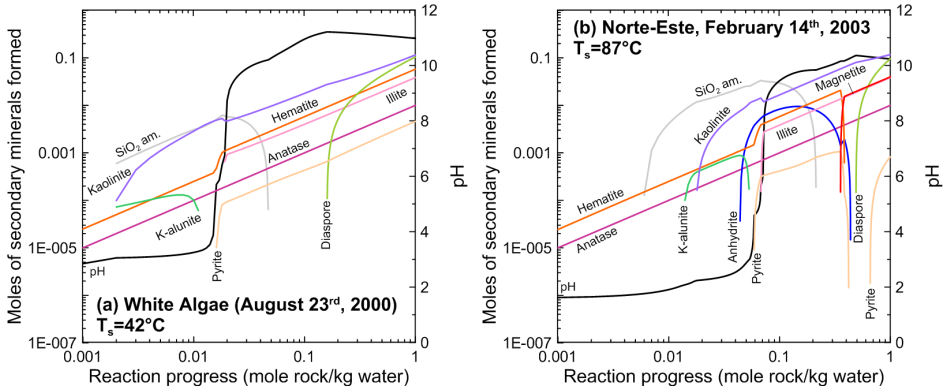

Figure 4.10. Water-rock reaction path models between the waters from the hot springs, active during the years 2003-2006, located inside the main crater and the basaltic-andesite reported by Cigollini et al. (1991). T_s is the temperature of the hot spring. In every run 1 mole of rock (110 g) was reacted with 1 kg of hot spring water.

4.4.3.1. Gas and gas condensate chemistry

The gases of the CPC fumaroles consist mainly of H_2O (up to 95 mol %), followed by CO_2, SO_2, H_2, HCl, HF and H_2S (Vaselli et al., 2003; OVSICORI, 2012, unpublished data; F. Tassi, pers. comm., 2012; Fischer et al., 2015). Since the aqueous solubilities of these gas components are very different, the fumarole composition is extremely variable and dependent on the degree of interaction of deeply derived gas with shallow aquifers. This interaction has been referred to as "scrubbing" by Symonds et al. (2001). These authors demonstrated that low-temperature (<250°C) gas is likely to have experienced "scrubbing" by aquifers in which a considerable amount of the components dissolved in the water (specially HCl, HF and, to a minor extent, SO_2), leaving the gas relatively enriched in the less soluble components such as CO_2. In any case, magma gases commonly experience processes such as cooling, oxidation and condensation before reaching the atmosphere (Africano and Bernard, 2000).

In order to assess changes in the chemical composition of the Poás fumarolic gases due to cooling, the SOLVGAS software (Symonds and Reed, 1993) was used. SOLVGAS is well suited for restoring volcanic gas compositions, modelling the speciation of gas mixtures and computing the saturation indices of potential sublimates. For this modelling, gas samples taken by OVSICORI on June 25th, 2010 (T=763°C), August 16th, 2010 (T=650°C) and March 18th, 2011 (T=250°C) were used (Fig. 4.3;

Table 4.4). Gas cooling models ran in SOLVGAS from the sampling temperature down to 25°C demonstrated that, at T≤100°C, these gases experience an important total sulphur loss in the form of (1) droplets of the following sulphuric acid hydrates: $H_2SO_4 \cdot 2H_2O$, $H_2SO_4 \cdot 3H_2O$, $H_2SO_4 \cdot 4H_2O$, $H_2SO_4 \cdot 6H_2O$, and (2) elemental sulphur. Between 100 and 25°C liquid H_2O and $H_2SO_4 \cdot H_2O$ form.

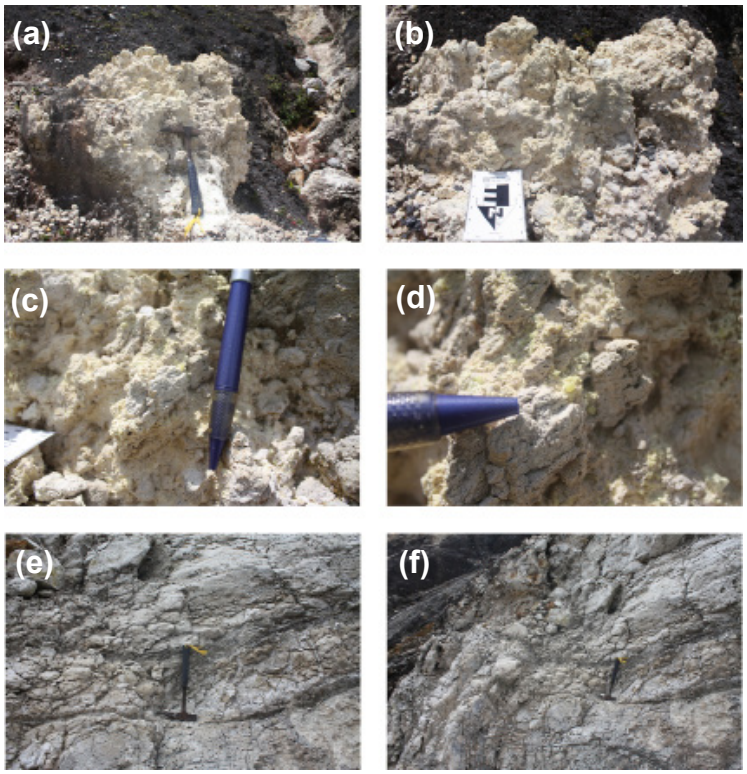

Figure 4.11. Fossil fumaroles on site 1: note the pervasive acid alteration that has leached the rock and left a residue of cristobalite α, quartz, tridymite, anatase and K-alunite (a), (b); accompanied with elemental sulphur deposition (c), (d). A similar alteration style was observed at site 3 (e), (f), where K- and Na-alunite together with minamiite where present.

When high-temperature gases cool during their rise through the fumarole conduit, atmospheric O_2 ultimately enters the system leading to the oxidation of the gas phase. At low temperatures (<350°C), elemental sulphur can be produced by the reaction (Mizutani and Sugiura, 1996):

$$SO_2 + 2H_2S \Leftrightarrow 3S^0 + 2H_2O \quad (1)$$

Below 330°C (H_2SO_4 boiling temperature), acidic droplets can form by H_2S oxidation

Table 4.3. Chemical analysis of waters from the hot springs in the main crater. Concentrations in mg/kg.

Hot spring	Date	$T_{sampling}$ (°C)	pH 20-24±2°C	SO_4	F	Cl	Al	Fe	Ca	Mg	Na	K	Si	Mn	TDS	Source
Este	Feb-00	89	0.12	12200	16	25	520	1000	550	350	180	13	n.d.[a]	13	14900	(6)
	21-Nov-00	91	2.1	2800	1.4	29	42	350	380	33	170	b.l.d.[b]	n.d.	4.3	3800	(4)
	16-Jun-05	92	0.99	16780	33	3885	n.d.	n.d.	n.d.	n.d.	n.d.	n.d.	n.d.	n.d.	n.d.	(4)
White Algae	23-Aug-00	42	2.47	2220	3.0	0.40	82	55	570	19	45	3.7	93	0.90	3090	(6)
	21-Sep-01	52	1.55	6680	10	813	480	570	310	81	130	19	220	3.5	9300	(4)
Norte-Este	23-Aug-00	89	1.51	2890	0.6	22	2.0	470	330	180	260	24	220	8.1	5887	(4)
	14-Feb-03	87	1.95	2530	b.d.l	33	n.d.	n.d.	n.d.	n.d.	n.d.	n.d.	n.d.	n.d.	n.d.	(4)

Notes: (a) n.d. = not determined; (b) b.l.d = below detection limit. Sources: (4) Martínez et al. (2000); (6) Vaselli et al. (2003).

Table 4.4. Chemical analysis of gases from the CPC. Concentrations in molar percentages.

Date	$T_{sampling}$ (°C)	CO_2	HCl	HF	SO_2	H_2S	S	H_2O	N_2	CH_4	Ar	O_2	H_2	CO	Total	Source
25-Jun-10	763	15.84	0.78	0.35	9.17	0.08	0.00	72.45	0.06	0.00	0.00	0.00	1.08	0.10	99.92	(2,6)
16-Aug-10	650	14.84	0.71	0.30	8.76	0.14	0.00	74.10	0.06	0.00	0.00	0.00	0.94	0.09	99.94	(2,6)
18-Mar-11	250	15.84	0.65	0.21	7.60	0.12	0.00	74.57	0.07	0.00	0.00	0.00	0.85	0.07	99.98	(2,6)

Sources: (2) OVSICORI-UNA; (6) Tassi (2012; pers. comm.).

upon increasing $f\,O_2$(Symonds, 1990):

$$H_2S_{(g/l)} + 2O_{2\,(g/l)} \Leftrightarrow H_2SO_{4\,(g/l)}$$

In addition, sulphuric acid can also form by SO_2 disproportionation (Africano and Bernard, 2000):

$$4SO_{2\,(g/l)} + 4H_2O_{(g/l)} \Leftrightarrow 4H_2SO_{3\,(l)} \Leftrightarrow 3H_2SO_{4\,(l)} + H_2S_{(g/l)}$$

The stability of H_2SO_4 together with its hydrated forms mentioned above also depends on the total amount of S in the gases and increases with decreasing temperature. Moreover, $HCl_{(g)}$ and $HF_{(g)}$ could dissolve in these H_2SO_4 droplets and decrease the pH of the gas condensate (Symonds 1990; Symonds et al., 1992). At low temperatures (<200°C) elemental sulphur can be produced as follows (Kusakabe and Komoda, 1992):

$$3SO_{2\,(g/l)} + 3H_2O_{(g/l)} \Leftrightarrow 3H_2SO_{3\,(l)} \Leftrightarrow 2H_2SO_{4\,(l)} + S^0_{(l/s)} + H_2O_{(g/l)} \qquad 4)$$

Reactions 2-4 can explain the low pH of volcanic condensates.

4.4.3.2. Secondary mineralogy in the field

Minerals detected by XRD include SiO_2 polymorphs (cristoballite, quartz and trydimite), anatase, elemental sulphur, calcium sulphates (anhydrite and gypsum) and sulphates of the alunite group, represented by K-alunite, Na-alunite and minamiite (Fig. 4.2; Table 4.1). Pervasive alteration observed at sites 1, 3 and 8 (Figs. 4.2, 4.11) completely erased primary minerals and textures, leaving a silicified rock residue of attack by acid fluids. Hence, these sites present good examples of acid alteration.

4.3.3.3. Gas-rock reaction model

The reaction between the CPC gases and surrounding rocks was modelled using GASWORKS (Reed, 1982), which is a complementary program to SOLVGAS and computes both gas-solid-liquid equilibria and reaction progress. For the simulations, the gas samples (Table 4.4) of June 25th, 2010 (T=763°C), August 16th, 2010 (T=650°C) and March 18th, 2011 (T=250°C) were reacted with a basaltic andesite (Cigolini et al., 1991). In each model, one mole of gas sample (~26 g) was cooled and reacted with one mole of basaltic andesite (~110 g) from the corresponding sampling temperature down to 114°C. Below this temperature convergence problems occurred. Nevertheless, it is well representative for the lowest temperatures recorded for the CPC fumaroles. The modelling results in terms of saturation indices and amounts of secondary minerals formed are shown in Figure 4.12. The predicted secondary mineral assemblages for the samples of June 25th, 2010 (T=763°C) and August 16th, 2010

(T=650°C) are the same and consist of liquid sulphur as the most abundant phase, followed by $MnSO_4 \cdot H_2O$, $Na_2SO_4 \cdot 5H_2O$, K_2SO_4, and finally MgF_2 and anhydrite. Magnesium fluoride was the only phase formed in the model with the sample of March 18th, 2010 (T=250°C). According to the cooling models explained above, the total sulphur content of this sample was probably already considerably depleted. Therefore, sulphur availability for the formation of sulphates or elemental sulphur was limited.

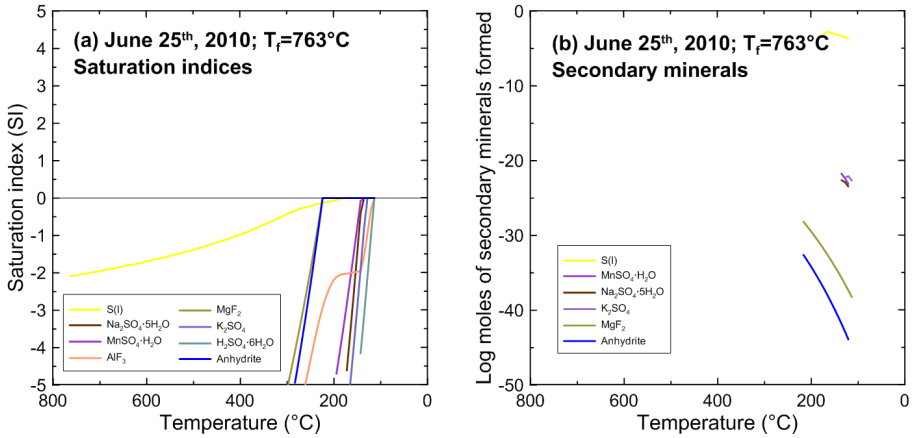

Figure 4.12. Gas-rock reaction path model. One mole of a gas sample (26 g) collected from the CPC was cooled from T_f=763°C to 114°C and reacted with 1 mole (110 g) of the basaltic-andesite reported by Cigollini et al. (1991). T_f refers to the fumarole temperature. During the reaction path the solids formed were successively excluded (fractionated) from the residual fluid. From (a) and (b) it can be observed that the secondary minerals start forming at T<250°C.

4.4.3.4. Gas condensate-rock reaction model

The reaction between gas condensates of the CPC fumaroles collected on September 8th, 2010 (T=760°C) and February 10th, 2012 (T=107°C) (Fig. 4.3; Table 4.5) and the basaltic-andesite (Cigolini et al., 1991) were simulated in PHREEQC. In all runs, 1 kg of the gas condensate was titrated with 1 mole of the basaltic-andesite (~110 g) at 95°C (Fig. 4.13). The high temperature sample (T=760°C) only produced amorphous silica and anatase during low (<0.01 mole rock/kg water) and medium (0.01-0.1 mole rock/kg water) reaction progress values. Hematite, kaolinite and K-alunite, followed by pyrite, illite, fluorite and magnetite became stable at high reaction progress (>0.1 mole rock/kg water). The low temperature composition (T=107°C) resulted in a more complex secondary mineralogy along the reaction path. Amorphous silica, anatase and hematite formed during low reaction progress (<0.01 mole rock/kg water), then K- and Na-alunite, anhydrite and kaolinite at medium reaction progress (0.01-0.1 mole rock/kg water), and finally pyrite, illite, magnetite and diaspore appeared at high reaction progress (>0.1 rock/kg water).

Table 4.5. Chemical analysis of gas condensates from the fumaroles of the CPC. Concentrations in mg/kg.

Date	$T_{sampling}$ (°C)	$pH_{19\pm1°C}$	$Cond._{19\pm1°C}$ (mS/cm)	SO_4	F	Cl	Br	Data source
19-Jan-10	650	0.09	231	1180	72	21900	51	(1,2)
07-Apr-10	566	2.02	2.5	2770	104	5440	6	(1,2)
08-Sep-10	760	0.09	231	654	14	21400	14	(1,2)
22-Oct-10	590	0.58	73.8	2910	130	4220	8	(1,2)
18-Mar-11	250	-0.27	465	68	86	47000	78	(1,2)
10-Feb-12	107	0.46	103	5480	4	39	n.d.	(1,2)
20-Jul-12	301	0.84	n.d.	4000	30	103	n.d.	(1,2)

Sources: (1) This study; (2) OVSICORI-UNA.

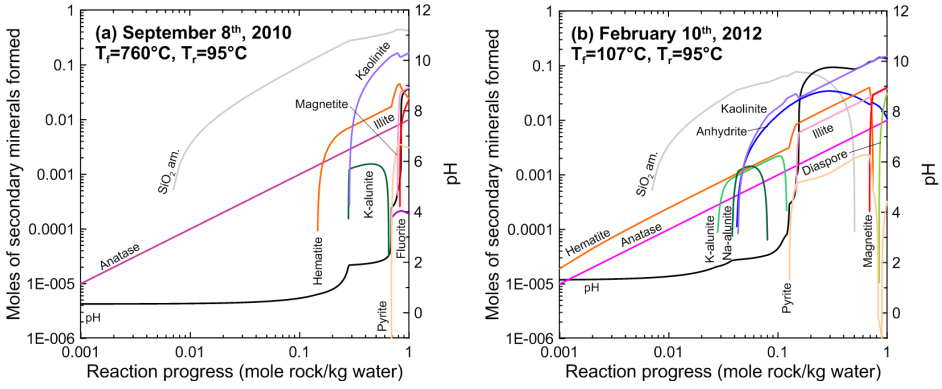

Figure 4.13. Water-rock reaction path models between fumarole gas condensates from the CPC and the basaltic-andesite reported by Cigollini et al. (1991). T_f and T_s refer to the temperature of the fumarole and the one at which the reaction path was ran, respectively. In every run 1 mole of rock (110 g) was reacted with 1 kg of gas condensate.

4.4.4. Scenario 4: acid rain / acid brine spray (high rock/water ratios).

This scenario supposes high rock/water ratios similar to the gas condensate-rock interaction case, but is treated separately because of the spatial extension of the impact of airborne acid deposition and the specific secondary mineralogy produced. Areas around Laguna Caliente receive input from acid rain and brine spray, either continuously or during phreatic eruptions. Due to the prevailing north-easterly wind direction at the summit of Poás volcano, the impact of acid fluids transported as aerosols particularly affect an area SW of Laguna Caliente, known as the "dead

zone", which is approximately 2 km^2 large and is characterized by intense rock alteration and absence of vegetation (Figs. 4.2, 4.3 and 4.14).

4.4.4.1. Secondary mineralogy in the field

XRD analysis of deposits from the 1910 eruption, SW of Laguna Caliente (site 2; Fig. 4.2; Table 4.1), revealed the presence of tridymite, cristobalite, quartz and K-alunite. Gypsum and anhydrite were found on the ceiling of a cave at site 6 (Figs. 4.2, 4.14; Table 4.1), and probably formed from infiltrated acid brine from Laguna Caliente that was expulsed during a phreatic eruption. Material collected from the NE rim of the main crater (sites 28, 31,32; Fig. 4.2; Table 4.1) contained cristobalite, goethite, hematite, magnetite, tennantite, ralstonite, potassium halite, tychite, ankerite, H-jarosite and polyhalite. Lake sediments ejected by a phreatic eruption on April 13th (2012) and collected on the southern plain of the main crater (site 33; Fig. 4.2; Table 4.1) contained cristobalite, polyhalite and meta-alunogen.

Basaltic-andesitic lava blocks in the "dead zone" close to Cerro Pelón (sites 18, 20, 21; Figs. 4.2, 4.15; Table 4.1), which contain clinopyroxene, orthopyroxene and olivine (up to 5%) as phenocrysts, exhibit a complex secondary mineralogy consisting of halloysite, nontronite, sauconite, montmorillonite, mordenite, phillipsite, chabazite, goethite, hematite, magnetite, carobbiite, kogarkoite, ralstonite, alunogen, meta-alunogen, rostite, K-jarosite, copiapite, magnesiocopiapite, epsomite, tamarugite and sodium alum. A close observation of the alteration pattern of the the blocks revealed that their crusts are primarily composed of massive amorphous silica and jarosite void fillings (Figs. 4.15a, 4.15b). Smectites and kaolinite were identified in inner parts of the blocks (Fig. 4.15c). The most altered primary mineral is olivine, which commonly appears as "ghosts" (Figs. 4.15c, 4.15d), whereas fresh olivine is rare (Fig. 4.15e). Amorphous silica has replaced various primary minerals (Fig. 4.15f). A lava flow near the east shore of Laguna Caliente with the same composition as these lava blocks shows a similar alteration pattern. Most of the clinopyroxene, orthopyroxene and plagioclase phenocrysts are relatively fresh (Fig. 4.16a) but olivine is considerably altered or shows a "ghost" texture (Figs. 4.16b, 4,16c). Jarosite precipitated in veins that dissected the matrix and some phenocrysts (Figs. 4.16d – 4.16e, 4.17a – 4.17f). EMP analysis revealed a K-jarosite composition $(K_{0.68}Na_{0.12}H_{0.21})(Fe_{2.98}Al_{0.13})(SO_4)_{2.10}(OH)_6$ with H^+ and Na^+ substitution up to 50% and 25%, respectively (Fig. 4.18).

In summary, the alteration mineralogy in samples representing this scenario shows the following systematics: (1) silica polymorphs and tennantite probably formed at relatively high temperatures; (2) this probably also applies to the fluorides, since modelling showed that MgF_2 is stable in the CPC fumaroles; moreover, ralstonite is a common alteration product of cryolite (AlF_3), which is often found in fumarolic vents, as is carobbiite; (3) zeolites could be alteration products formed at higher temperatures as it is common in many hydrothermal systems; these minerals can also be products of advanced water/rock interaction at relatively high pH values

(>8); (4) carbonates are probably products of interaction with meteoric water at ambient temperature and near neutral pH conditions; (5) sulphates such as alunogen, meta-alunogen, rostite and especially copiapite, magnesiocopiapite, jarosite and epsomite reveal water-poor conditions, given the large solubility of these salts; (6) samples from lava blocks in the "dead zone" and from a lava flow near Laguna Caliente exhibit an alteration mineralogy dominated by amorphous silica, jarosite, kaolinite and smectite; (7) the intense alteration of olivine and its association with jarosite and epsomite, suggest that Fe- and Mg-rich fluids capable of forming Fe- and Mg-sulphates are mainly derived from olivine. In the following section, this evidence will be used in the modelling strategy.

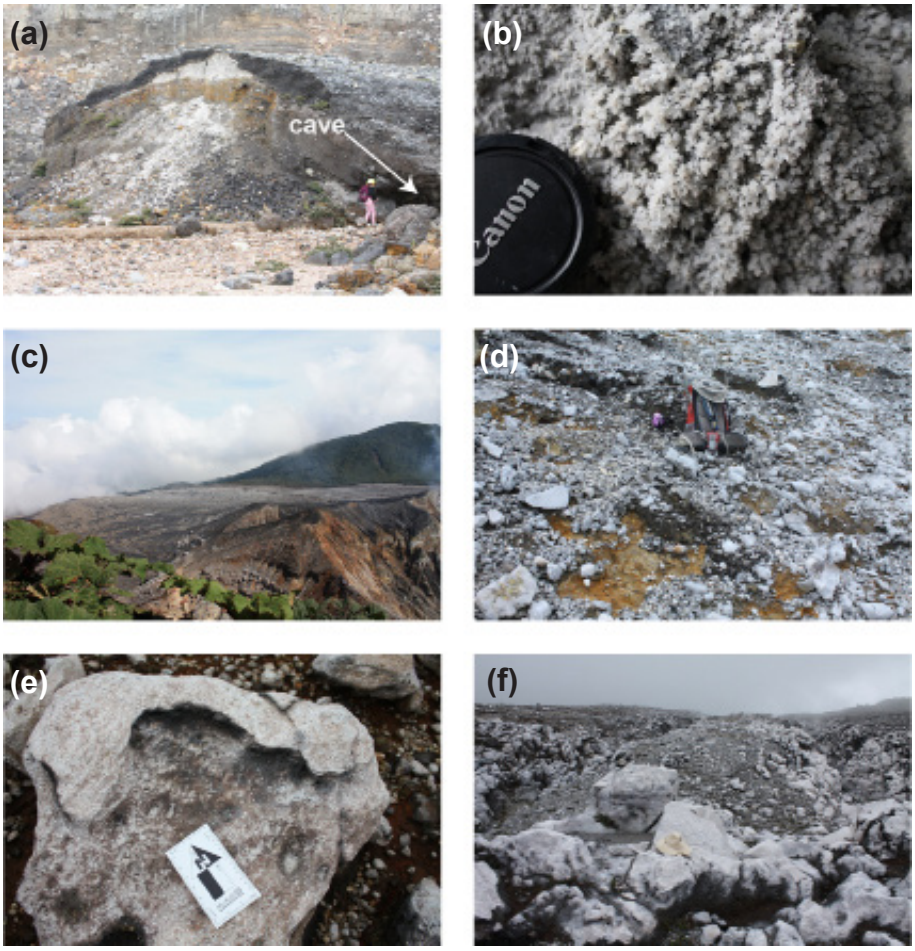

Figure 4.14. Examples where rocks have been exposed to the action of acid rain/acid brine spray (high rock/fluid ratios). (a), (b) site 6, acid brine expelled from Laguna Caliente, due to phreatic eruptions, produced gypsum and anhydrite efflorescences observed on the ceiling of a cave. (c) View from the "dead zone" from the southern rim of the main crater. (d), (e), (f) The lavas in this zone show white patinas mainly composed of amorphous silica, followed a few centimetres deeper by Al- and Mg-sulphates together with minerals from the jarosite and copiapite group (see Fig. 4.2).

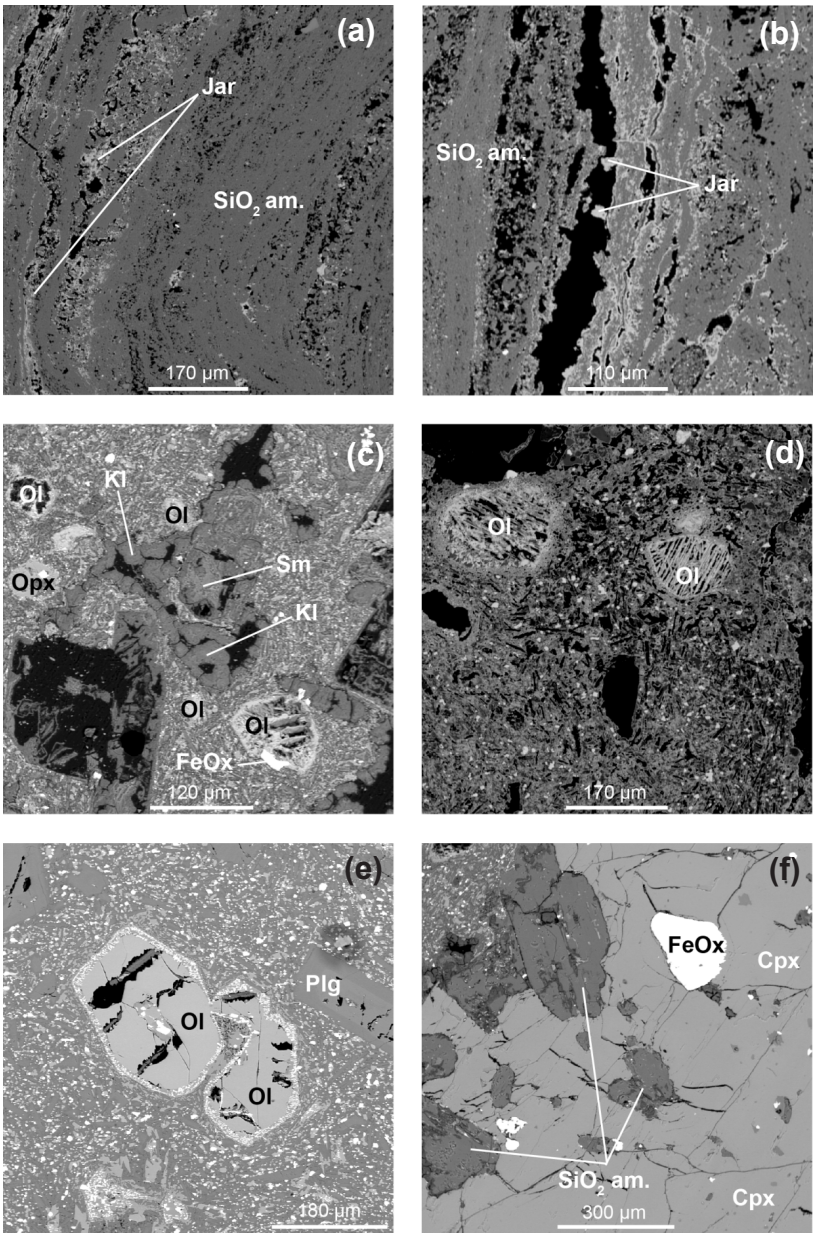

Figure 4.15. EMP images of a basaltic andesite from site 21, close to Cerro Pelón (see Fig. 2). (a), (b) amorphous silica (SiO_2 am.) crusts and jarosite (Jar) fillings in the patinas of the lavas. (c), (d) olivie (Ol) ghost textures, iron oxides (FeOx), kaolinite (Kl), smectites (Sm) and orthopiroxene (Opx). (e), (f) less altered sections containing plagioclase (Plg), olivine, clinopyroxene (Cpx), iron oxides and silicified phases.

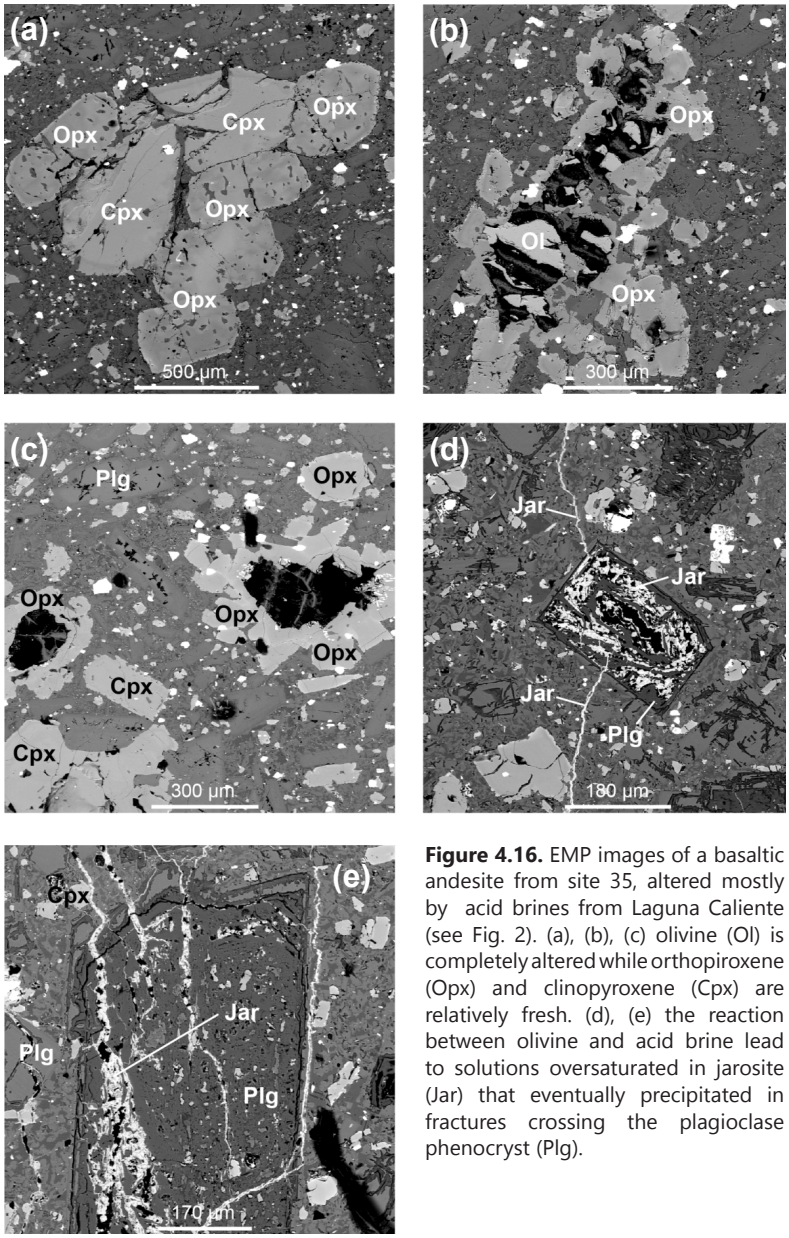

Figure 4.16. EMP images of a basaltic andesite from site 35, altered mostly by acid brines from Laguna Caliente (see Fig. 2). (a), (b), (c) olivine (Ol) is completely altered while orthopiroxene (Opx) and clinopyroxene (Cpx) are relatively fresh. (d), (e) the reaction between olivine and acid brine lead to solutions oversaturated in jarosite (Jar) that eventually precipitated in fractures crossing the plagioclase phenocryst (Plg).

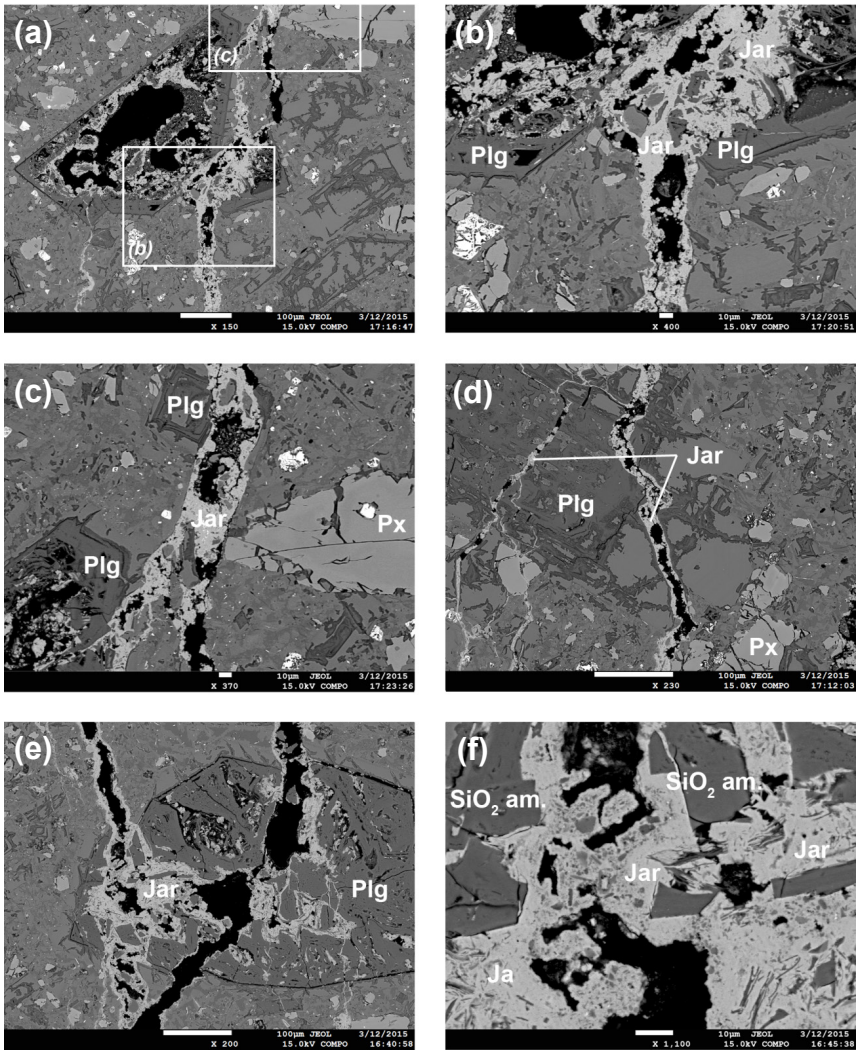

Figure 4.17. (a) to (f) EMP images of a basaltic andesite from site 35, altered mostly by acid brines from Laguna Caliente (see Figs. 2.16) and showing textural relations between jarosite (Jar) and primary minerals such as plagioclase (Plg) and pyroxene (Px). Plagioclase shows commonly an advance degree of silicification (SiO_2 am.) and jarosite precipitates afterwards within fractures or voids.

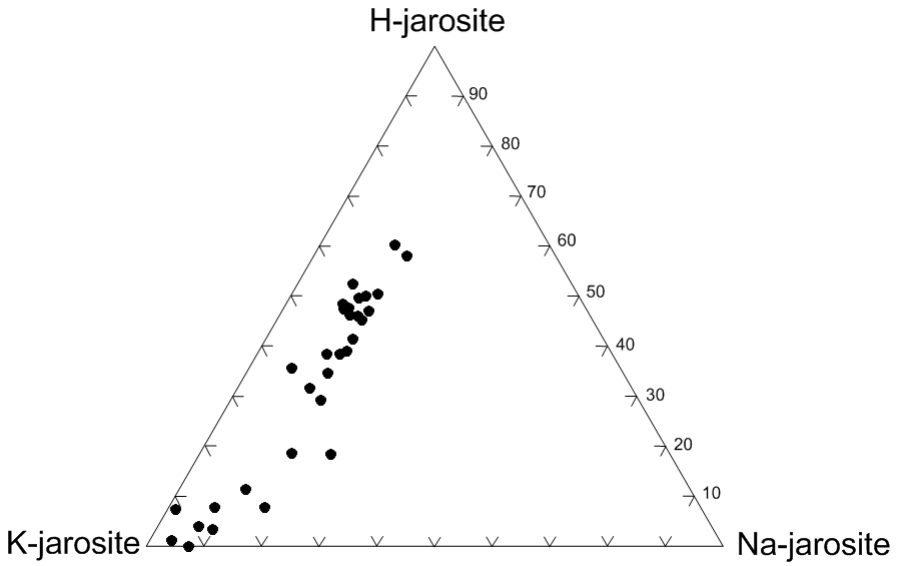

Figure 4.18. Compositions of the jarosites found on the basaltic andesite from site 35 (see Figs. 4.2, 4.16 and 4.17) from EMP analyses (n=30). On average, they present the following composition: $(K_{0.68}Na_{0.12}H_{0.21})(Fe_{2.98}Al_{0.13})(SO_4)_{2.10}(OH)_6$.

4.5.4.2. Water-rock reaction model

A sample from Laguna Caliente collected on August 30th, 1994 (Stage III) (Martínez et al., 2000) was titrated by the addition of small amounts of olivine in PHREEQC. A composition of Fo_{75} was adopted, based on an average of EPM analyses of olivines in the basaltic-andesitic blocks of Cerro Pelón. Up to 1 mole of this olivine (156.01 g) was reacted in 1000 steps with 1 kg of Laguna Caliente sample at T=24°C. At low reaction progress (<0.01 mole rock/kg water) only amorphous silica formed, which was followed by K-jarosite, goethite and jurbanite $Al(SO_4)(OH)\cdot 5H_2O$ at medium reaction progress (0.01-0.1 mole rock/kg water), and finally by K-alunite, kaolinite Mg-montmorillonite and laumontite at high reaction progress (>0.1 mole rock/kg water) (Fig. 4.19a). From this run, an aliquot of the solution obtained during step 40, before the formation of K-jarosite, was evaporated in 1000 steps at T=24°C until 97.6% of the initial water was removed. Beyond this point, the run did not converge, mainly due to the high ionic strength of the solution (2.24 mol/kg H_2O). The cecondary phases formed where only amorphous silica and gypsum (Fig. 4.19b). The solution from the last step of the evaporation run was reacted again with 1 mole of Cerro Pelón olivine in 1000 steps. However, the run did not go further than step 320, after 0.320 moles or 49.9 grams of the olivine had reacted with the solution. The secondary phases formed were gypsum and amorphous silica (<0.01 mole rock/kg water), followed by anhydrite, goethite and K-montmorillonite (0.01-0.1 mole rock/kg water), and ultimately elemental sulphur and magnetite (>0.1 mole rock/kg wa-

ter) (Fig. 4.19c). Since the concentrations of Fe^{2+} and Mg^{2+} remained high, another evaporation model was run in which a solution from step 56 of the previous model (after the reaction of 0.052 moles or 8.74 g of olivine) was evaporated at T=24°C. In this second evaporation step, the run did not converge after removal of 41.7% of the initial 24.34 g of water, because of the extremely high ionic strength (43.91 mol/kg H_2O). Nevertheless, amorphous silica and gypsum were present (Fig. 4.19d). In order to add more Mg^{2+} and Fe^{2+} to the system, a final reaction run was performed in which the solution from step 327 of the previous evaporation run was reacted again with 1 mol of olivine at T=24°C. This time the run was subdivided into 10,000 steps in order to track small changes in mineral saturation states. The secondary minerals formed were amorphous silica, gypsum and elemental sulphur (<0.001 mole rock/kg water), and epsomite and ferrohexahydrite (0.001-0.001 mole rock/kg water) (Fig. 4.19e). This combined sequence of previous runs modelled a hyperacid water-olivine reaction scenario for an open system, in which subsequent cycles of reaction and evaporation were envisaged.

4.4.5. Summary of geochemical models

The geochemical modelling results presented above are a representative selection of water-rock reaction path and heating models from a more comprehensive set of runs that were performed for each setting. Here, the stability of secondary minerals as a function of pH or temperature is summarized taking all the results into account. As will be discussed below, the initial pH of water is an important variable, even more than temperature, which signals the degree of previous water-rock interaction in the system, or the extent of dilution with near-neutral meteoric water. Low-pH compositions can be regarded as a low-reacted system since more rock needs to react with these fluids in order to increase the pH and/or deliver more cations into solution and consequently form secondary minerals. In contrast, high-reacted systems, represented by high-pH samples, may reflect a considerable degree of neutralization due to rock interaction.

A compilation of six heating models for Laguna Caliente water is presented in Figure 4.20. As explained in section 4.4.1.3., the heating models simulate a scenario for the properties and behaviour of a fluid circulating in the deeper parts of the hydrothermal system of Poás volcano. Up to 98°C, the only minerals predicted to precipitate from the solutions are elemental sulphur and pyrite. Anhydrite appears at 98°C, followed by diaspore (136°C) and AlF_3 (173°C), and these phases continue to be stable until 300°C, which was the end-temperature in the models. Potassium alunite only forms between 95° and 164°C.

Water-rock models of Laguna Caliente, as described in 4.4.1.4., are summarized in Figure 4.21. Nine runs cover different stages and substages of activity of the lake. Anatase and amorphous silica are the most persistent minerals, present from pH -0.4 to 11.2. In addition, anhydrite (pH -0.3 to 9.6), hematite (pH 1.1 to 11.2) and

gypsum (pH 1.3 to 10.3) are also stable over a large range. Hydronium jarosite (pH 1.1 to 1.2) and potassium jarosite (pH 1.2 to 1.3) are present in a narrow pH interval under acidic conditions at the beginning of the water-rock reaction path models, followed by K-alunite (pH 1.7 to 3.8), $Al(OH)SO_4$ (pH 1.7 to 3.7) and Na-alunite (pH 2.6 to 3.0). Finally, at pH >2 the mineral assemblage consists of kaolinite (pH 2.6 to 11.2), fluorite (pH 3.9 to 11.2) pyrite (pH 4.6 to 11.2) and illite (pH 5.9 to 11.2).

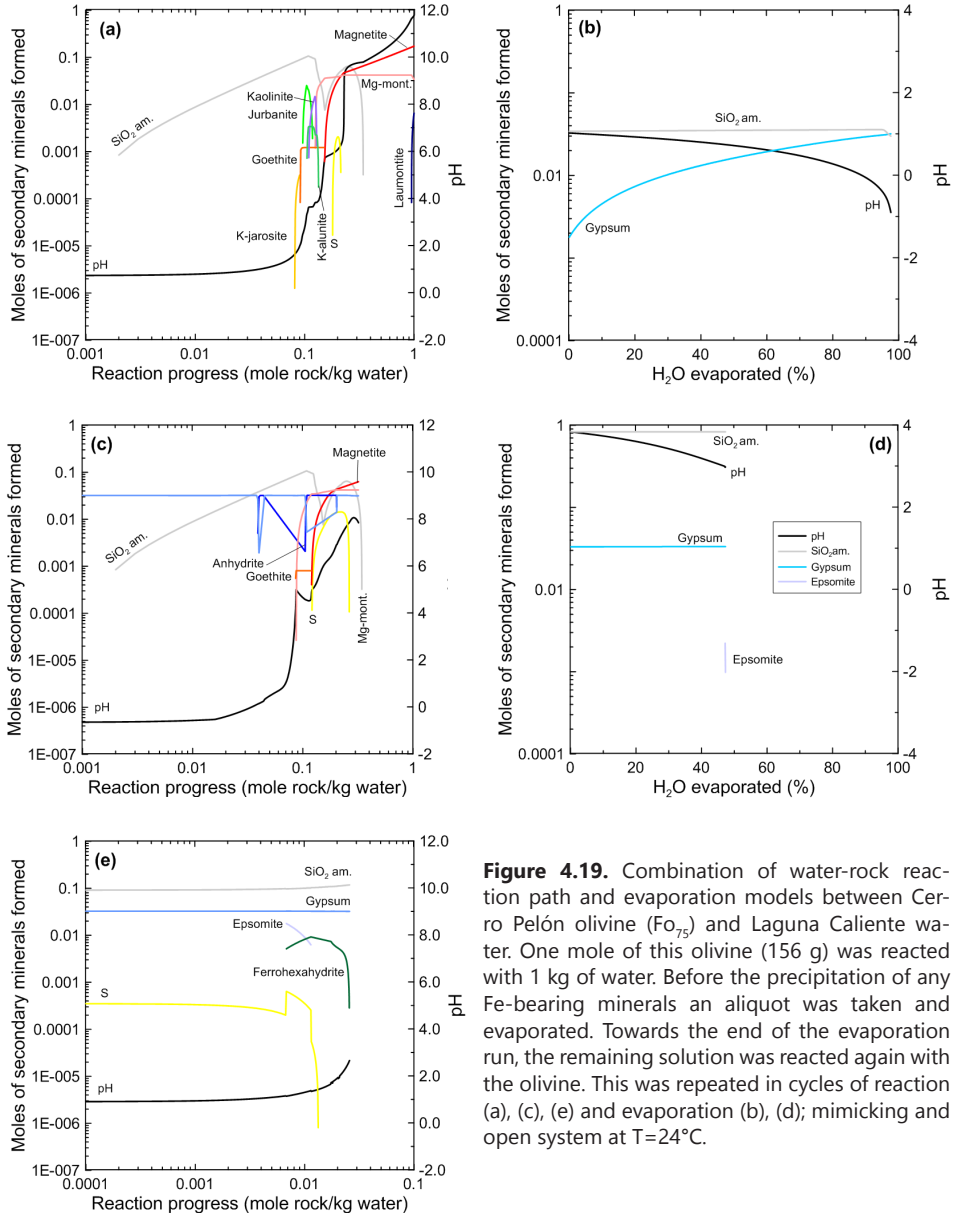

Figure 4.19. Combination of water-rock reaction path and evaporation models between Cerro Pelón olivine (Fo_{75}) and Laguna Caliente water. One mole of this olivine (156 g) was reacted with 1 kg of water. Before the precipitation of any Fe-bearing minerals an aliquot was taken and evaporated. Towards the end of the evaporation run, the remaining solution was reacted again with the olivine. This was repeated in cycles of reaction (a), (c), (e) and evaporation (b), (d); mimicking and open system at T=24°C.

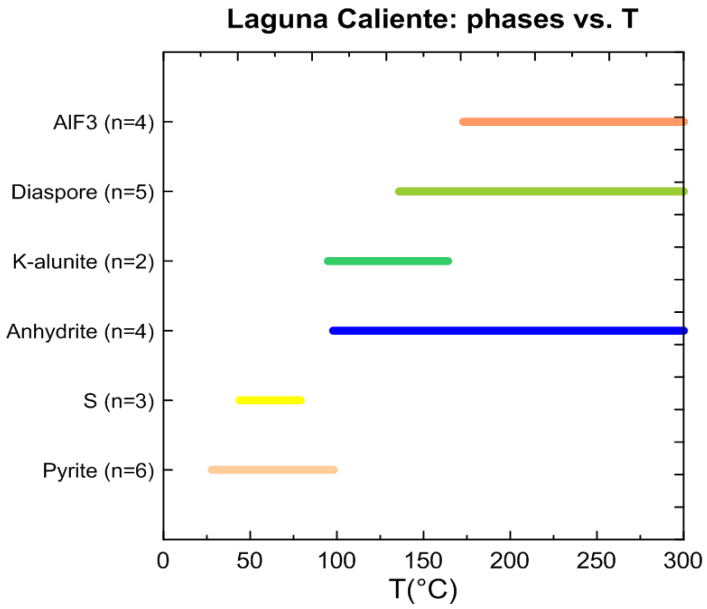

Figure 4.20. Laguna Caliente: secondary minerals vs. temperature. Compilation of six heating models. The runs went from lake temperature (28-62°C) to 300°C and included representative lake samples from both active and quiet periods of Laguna Caliente in terms of volcanic activity. The secondary minerals are oversaturated at the following temperature ranges: pyrite (28-98°C), S (44-79°C), anhydrite (98-300°C), K-alunite (95-164°C), diaspore (136-300°C) and AlF_3 (173-300°C).

Figure 4.22 presents a compilation of seven water-rock interaction models for the hot spring compositions (section 4.4.2.2.), similar to the complete versions shown in Figure 4.10. These waters have considerably higher pH values than the lake water suggesting that they may have interacted more extensively with rocks. Also, the $HCl_{(aq)}$ contribution to acidity is much less important. In the water-rock interaction models the hot spring waters are always saturated in anatase (pH 0.7 to 11.0), amorphous silica (pH 0.7 to 10.2), hematite (pH 0.9 to 11.0) and anhydrite (pH 1.2 to 10.3). Hydronium jarosite (pH 0.8 to 0.9) followed by K-alunite (pH 1.6 to 3.6), Na-Alunite (pH 1.9 to 2.7) and $Al(OH)SO_4$ (pH 2.3 to 2.9) are only stable where low pH conditions still prevail. Kaolinite also appears early, but continues to be saturated over an extended pH range (pH 2.1 to 11.0). Pyrite (pH 4.1 to 11.0) and fluorite (pH 4.3 to 10.7) start to form at higher pH values. The most advanced stages of rock interaction are characterized by the presence of illite (pH 5 to 11.0), magnetite (pH 9.9 to 10.2) and finally diaspore (pH 10.2 to 11.2).

The gas condensate-rock reaction models for the CPC fumaroles, described in section 4.4.3.4., are summarized in Figure 4.23. Anatase (pH 1.3 to 9.7), amorphous silica (pH 1.3 to 9.7), anhydrite (pH 2.0 to 9.7) and kaolinite (pH 2.1 to 9.7) are stable

throughout the runs. Only at low pH, elemental sulphur (pH 1.3 to 2.3), K-alunite (pH 1.9 to 3.2) and Na-alunite (pH 2.1 to 2.3) are part of the mineral assemblage. Pyrite also forms under acid conditions (pH 1.3) but continues to be stable until pH 7.3. Fluorite (pH 4.1 to 9.7) and hematite (pH 4.4 to 9.7) precipitate at higher pH conditions, followed by illite (pH 5.3 to 9.7) and brucite (pH 7.5 to 9.7).

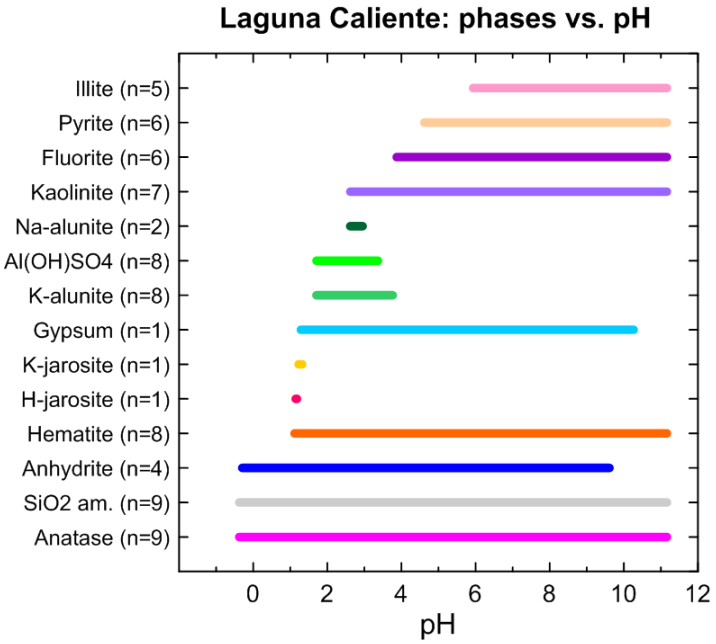

Figure 4.21. Laguna Caliente: secondary minerals vs. pH. Compilation of nine water-rock reaction path models, in which 1 mole (110 g) of the basaltic-andesite reported by Cigollini et al. (1991) was reacted with 1 kg of water from Laguna Caliente at constant temperature. The water samples represent both active and quiet periods of Laguna Caliente in terms of volcanic activity, with temperatures between 28 and 62°C. The secondary minerals are oversaturated at the following pH ranges: anatase (-0.4 to 11.2), SiO_2 am. (-0.4 to 11.2), anhydrite (-0.3 to 9.6), hematite (1.1 to 11.2), H-jarosite (1.1 to 1.2), K-jarosite (1.2 to 1.3), gypsum (1.3 to 10.3), K-alunite (1.7 to 3.8), $Al(OH)SO_4$ (1.7 to 3.7), Na-alunite (2.6 to 3.0), kaolinite (2.6 to 11.2), fluorite (3.9 to 11.2), pyrite (4.6 to 11.2) and illite (5.9 to 11.2).

4.5. DISCUSSION

4.5.1. Field observation vs. geochemical modelling

In general, there is a good agreement between the secondary minerals predicted in the models and the ones observed in the field. Differences can be attributed to incomplete sampling, analytical issues, assumptions and limitations in modelling as a consequence of the often extreme acidity and salinity of the fluids, and missing phases in the thermodynamic database. Analytical restrictions include the sensitivity of powder XRD analysis, which will usually not detect crystalline phases with a

concentration less than 5 volume % (Poppe et al., 2002), and grain sizes that are too small for microprobe analysis of phases that are not stable under the electron beam.

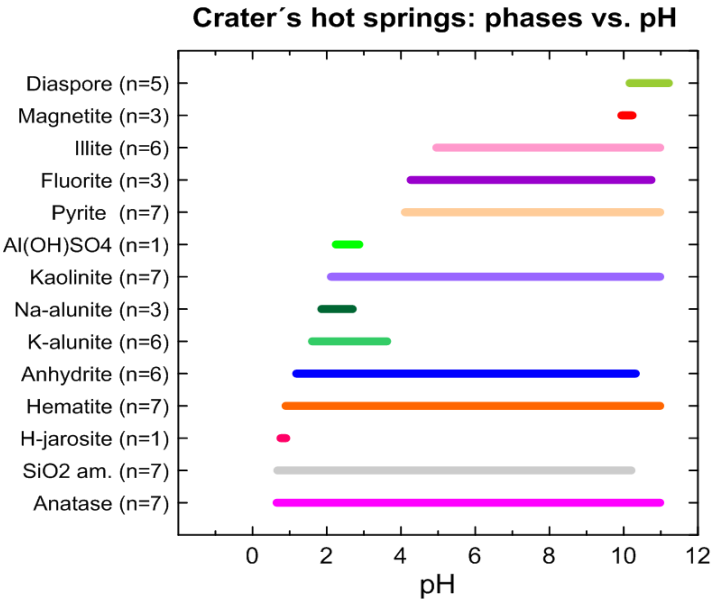

Figure 4.22. Crater´s hot springs: secondary minerals vs. pH. Compilation of seven water-rock reaction path models, in which 1 mole (110 g) of the basaltic-andesite reported by Cigollini et al. (1991) was reacted with 1 kg of water from the hot springs located in the main crater that were active during the years 2003-2006 (T=42-92°C). The secondary minerals are oversaturated at the following pH ranges: anatase (0.7 to 11.0), SiO_2 am. (0.7 to 10.2), H-jarosite (0.8 to 0.9), hematite (0.9 to 11.0), anhydrite (1.2 to 10.3), K-alunite (1.6 to 3.6), Na-alunite (1.9 to 2.7), kaolinite (2.1 to 11.0), Al(OH) SO_4 (2.3 to 2.9), pyrite (4.1 to 11.0), fluorite (4.3 to 10.7), illite (5.9 to 11.2), magnetite (9.9 to 10.2) and diaspore (10.2 to 11.2).

Modelling results suffer from the limitation that the thermodynamic database (llnl.dat) used in PHREEQC only includes pure end-members for solid solutions. Similar to what analysed alunites and jarosites of Poás show, many other sulphates form solid solutions. For example, the halotrichite group consists of monoclinic hydrated sulphates with the general formula $XY_2(SO_4)_4 \cdot 22H_2O$, where X is a divalent (Co^{2+}, Fe^{2+}, Mg^{2+}, Mn^{2+}, Ni^{2+}, Zn^{2+}) cation and Y a trivalent (Al^{3+}, Cr^{3+}, Fe^{3+}) cation. Complete solid solutions between the various end members are expected to exist (Ballirano, 2006). Another example is magnesiocopiapite $MgFe^{3+}{}_4(SO_4)_6(OH)_2 \cdot 20H_2O$ of the copiapite group with general formula $A^{2+}R^{3+}{}_4(SO_4)_6(OH)_6(OH)_2 \cdot 20H_2O$, where R is dominated by Fe^{3+} in all members,which shows a complete substitution by divalent (Mg^{2+}, Fe^{2+}) and trivalent (Fe^{3+}, Al^{3+}) cations on the A-site (Bayliss and Atencio, 1985; Robinson, 1999).

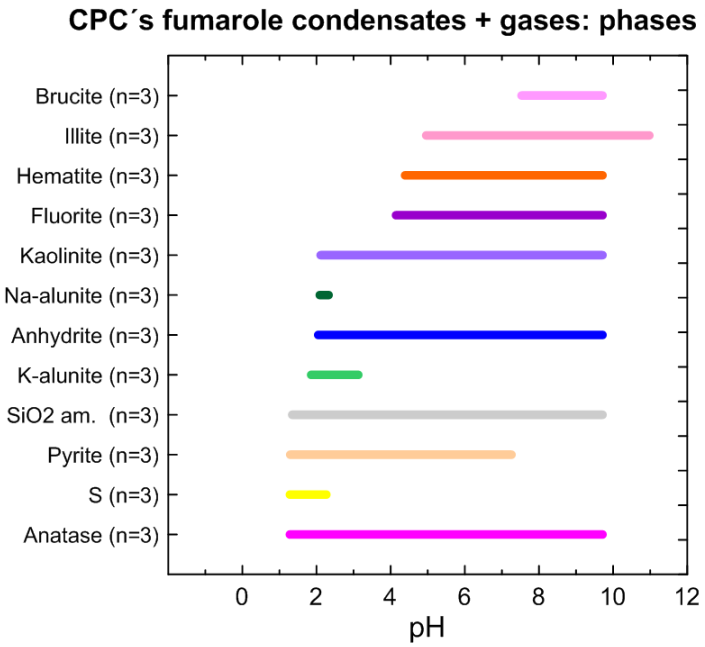

Figure 4.23. CPC´s fumarole gas condensates: secondary minerals vs. pH. Compilation of three gas condensate-rock reaction path models, in which 1 mole (110 g) of the basaltic-andesite reported by Cigollini et al. (1991) was reacted with 1 kg of gas condensate from the fumaroles located on the CPC (T=250, 650 and 763°C). The runs were carried out at constant temperature (T=95°C). The secondary minerals are oversaturated at the following pH ranges: anatase (1.3 to 9.7), S (1.3 to 2.3), pyrite (1.3 to 7.3), SiO_2 am. (1.3 to 9.7), K-alunite (1.9 to 3.2), anhydrite (2.0 to 9.7), Na-alunite (2.1 to 2.3), kaolinite (2.1 to 9.7), fluorite (4.1 to 9.7), hematite (4.4 to 9.7), illite (5.3 to 9.7) and brucite (7.5 to 9.7).

Silica polymorphs (tridymite, cristobalite and quartz), detected by XRD, may have formed at temperatures higher than those considered in the water-rock interaction models (T≤300°C). The only stable SiO_2-phase at the lake-water temperatures (T≤70°C) is amorphous silica. The zeolites are products of water-rock interaction at higher pH values than covered by the models, suggesting a local reduction of acidity of the aqueous system, either by addition of more rock or by dilution with near-neutral meteoric water. Zinc and phosphorous were not analyzed in the lake waters, which explains why neither sauconite nor woodhouseite appeared as secondary phases in the models.

The absence of greigite ($Fe^{2+}Fe^{3+}{}_2S_4$) in the models despite its inclusion in the thermodynamic database (llnl.dat), is possibly attributable to an inadequate estimation of the redox state. Hence, the S^{2-}/S^{6+} and Fe^{2+}/Fe^{3+} ratios in Laguna Caliente waters must be better constrained since the models assume that all S^{2-} is consumed by Fe^{2+} to form FeS_2 and there should probably be more Fe^{3+} in the system to produce greigite. Other minerals such as ralstonite, H-alunite, minamiite, meta-alunogen,

halotrichite and magnesiocopiapite that were detected in the field did not appear in the models since they are not included in the database.

According to the speciation results, Al tends to form complexes with F such as AlF^{2+}, AlF_2^+ and AlF_3^0, increasing the Al solubility in Laguna Caliente waters and ultimately promoting the formation of solid AlF_3. Moreover, SO_4^{2-} has also a strong affinity to Al^{3+} and forms complexes such as $AlSO_4^+$ and $Al(SO_4)_2^-$ that eventually lead to the formation of aluminium-hydroxysulphate minerals. For instance, alunogen $Al_2(SO_4)_3 \cdot 17H_2O$ is the most stable aluminium sulphate under extremely low pH conditions (<0) and probably only forms by efflorescence in capillary films (Nordstrom, 1982). Subsequent dehydration of alunogen can yield meta-alunogen (Zhou and Wang, 2013). hydration of alunogen can yield meta-alunogen (Zhou and Wang, 2013). Both meta-alunogen and alunogen have been also reported at Te Kopia geothermal field (Taupo volcanic zone, New Zealand) where they are confined to sheltered and humid microenvironments associated with warm (T=25-50°C) and acid (pH=2.5-3.0) ponds (Martin et al.,1999).

Previous XRD analyses of sediments collected from the lake bottom on September 14th (2011) identified rhomboclase $HFe^{3+}(SO_4)_2 \cdot 4H_2O$ and bilinite $Fe^{2+}Fe^{3+}{}_2(SO_4)_4 \cdot 22H_2O$ (Rodríguez and van Bergen, 2015). Their origin is unclear. Both bilinite and rhomboclase have been described in AMD systems related to oxidized sulphide deposits (Jambor et al., 2000; Hammarstrom et al., 2005). Nordstrom and Alpers (1999) described the formation of rhomboclase stalagmites at Iron Mountain in association with extremely acid water (pH=-3.6). The origin of meta-alunogen, halotrichite and magnesiocopiapite is possibly related to their occurrence in lake sediments, ejected during phreatic eruptions that subsequently dried and were protected from rain.

4.5.2. Buffers and chemical changes as a product of water-rock interaction in the waters of Poás volcano

Water-rock interaction promotes neutralization in acid SO_4-Cl waters and causes liberation of cations from solid rocks and minerals. Following the principle of electric charge balance, any lack of cations in acid waters is thought to be compensated by H^+. Varekamp et al. (2000) defined the "degree of neutralization" (DON) as an indication of the amount of acid consumption through rock dissolution, estimated by the residual acidy (%). If effects from dilution with near-neutral meteoric waters can be ignored, a system could be dominated by rock dissolution (low residual acidity) or magmatic volatiles (high residual acidity). In such cases, pH would be a good indicator of how evolved a fluid is by reaction with surrounding rocks. From the water-rock reaction models it can be inferred that, of all the secondary phases, jarosites, followed by alunites are typically indicative for low pH conditions that are mostly associated with intermediate reaction progress values (<0.1 mole/kg water). Nevertheless, if the initial pH is extremely low (e.g., pH~0), both jarosites and alunites remain stable until high reaction progress values (>0.1 mole rock/kg

water) are reached. The obvious reason is that aqueous systems with higher H^+ concentration need more rock to become neutralized. Hence, a meaningful comparison between modelling results for different compositions concerning the stability of secondary mineral should be based on pH rather than reaction progress.

According to Marini et al. (2003), several buffers operate in acidic volcanic waters at different pH intervals (pH 0.5-1.5 and pH 3.5-5). The pH curves in the water-rock models of Laguna Caliente, hot springs and fumarole condensates suggest that a number of buffers were active (cf., Marini et al., 2003).

The first operates at pH -0.8 to 2.0 and is controlled by the HCl/Cl^- and/or the HSO_4^-/SO_4^{2-} couple. The second buffer (pH 1.5) is not always active and involves either K-jarosite or H-jarosite consumption to produce $Al(OH)SO_4$ and hematite:

$$KFe_3(SO_4)_2(OH)_6 + Al^{3+} = \quad (5)$$
$$K^+ + Fe^{3+} + SO_4^{2-} + Fe_2O_3 + Al(OH)SO_4 + 2H_2O + H^+$$

$$HFe_3(SO_4)_2(OH)_6 + Al^{3+} = \quad (6)$$
$$Fe^{3+} + SO_4^{2-} + Fe_2O_3 + Al(OH)SO_4 + 2H_2O + 2H^+$$

The third buffer is transient, occurs at pH values slightly lower than 3, and is controlled by $Al(OH)SO_4$ and K-alunite:

$$Al(OH)SO_4 + K^+ + 3H_2O = KAl_3(SO_4)_2(OH)_6 + SO_4^{2-} + 3H^+ \quad (7)$$

A fourth and more stable buffer (pH 2.5 to 3.5) involves $Al(OH)SO_4$ and kaolinite:

$$2Al(OH)SO_4 + 2SiO_{2am} + 3H_2O = Al_2Si_2O_5(OH)_4 + 2SO_4^{2-} + 4H^+ \quad (8)$$

If $Al(OH)SO_4$ is absent as secondary phase, particularly in the hot springs and fumaroles condensates, K-alunite or Na-alunite can also buffer the solutions:

$$KAl_3(SO_4)_2(OH)_6 + 3SiO_{2am} + {}^3/_2 H_2O = \quad (9)$$
$${}^3/_2 Al_2Si_2O_5(OH)_4 + 2SO_4^{2-} + K^+ + 3H^+$$

$$NaAl_3(SO_4)_2(OH)_6 + 3SiO_{2am} + {}^3/_2 H_2O = \quad (10)$$
$${}^3/_2 Al_2Si_2O_5(OH)_4 + 2SO_4^{2-} + Na^+ + 3H^+$$

Finally, a fifth buffer (pH 9.8 to 10.3) is controlled by illite formation:

$$Al_2Si_2O_5(OH)_4 + 0.3Al^{3+} + 0.6K^+ + 0.25Mg^{2+} + 1.55SiO_{2(aq)} = K_{0.6}Mg_{0.25}Al_{1.8}Al_{0.5}Si_{3.5}O_{10}(OH)_2 + 2SO_4^{2-} + 2H^+ \quad (11)$$

However, since kaolinite is still being formed rather than consumed at these high pH values, the following reaction is probably more important:

$$2.3Al^{3+} + 0.6K^+ + 0.25Mg^{2+} + 3.5SiO_{2(aq)} + 5H_2O = K_{0.6}Mg_{0.25}Al_{1.8}Al_{0.5}Si_{3.5}O_{10}(OH)_2 + 8H^+ \quad (12)$$

In the CPC gas condensates, pyrite oxidation brings extra acidy in the solution, preventing a rapid pH increase as a result of rock dissolution; this is reflected by a flattening of the curve around pH 7:

$$2FeS_2 + {}^{15}/_2 O_{2(g)} + 4H_2O = Fe_2O_3 + 4SO_4^{2-} + 8H^+$$

The role of CO_2 as buffer in the aqueous systems in the summit area of Poás volcano is insignificant. Even though CO_2 is the second most abundant gas after H_2O in the CPC fumaroles (Table 4.4), its contribution to acidity when fumarole gas interact with water is minimal, due to its presence as $CO_{2(g)}$ and eventually also in the undissociated form. Moreover, with exception of tychite and ankerite at site 28 (Fig. 4.2, Table 4.1), carbonates are absent in the crater area, indicating that CO_2 is unimportant in the formation of secondary minerals.

In summary, the mineral alteration assemblages in Laguna Caliente, hot springs and CPC fumaroles predicted by the water-rock interaction models is characterized by the stability of H- and K-jarosite under highly acidic conditions (pH 0.7 to 1.3) conditions, followed by K-Na-alunite, $Al(OH)SO_4$ and elemental sulphur (pH 1.3 to 3.8). Secondary phases associated with relatively high pH conditions (5.0 to 11.2) include illite, brucite, magnetite and diaspore. The acid conditions required for the formation of aluminium and iron sulphates are associated with poorly reacted systems. In these cases fluids interacted with much less rock than in neutral or high-pH aqueous systems, where phyllosilicates, iron and aluminium oxides usually prevail.

4.5.3. Presence of Fe-, Mg- and Al-sulphates and formation conditions

Evidence from the geochemical models indicates that the presence of jarosite is transient and requires extremely low pH conditions. Nevertheless, the mineral was not found in samples of the Laguna Caliente sediments. The only locations XRD and EPM analysis confirmed the occurrence of jarosites are: (1) a lava flow on the eastern margin of Laguna Caliente (site 35; Figs. 4,2; 4.16 to 4.18; Table 4.1), and (2) the "dead zone" (sites 21, 28; Figs. 4.2, 4.15; Table 4.1). Previously, jarosite together with alunite were also identified by powder XRD in the hot springs that were active from March 1999 to January 2007 (Martínez, 2008). It is conceivable that some of the he-

matite occurrences in the field indicate the former presence of jarosite, since olivine dissolution experiments with H_2SO_4 solutions suggest that H- and Na-jarosites can be precursors of hematite (King et al., 2011). Iron sulphates, together with minerals from the copiapite, voltaite and halotrichite groups were also identified in the Río Agrio hot spring (site 34, Fig. 4.2, Table 4.1) by XRD. Epsomite was found at site 20 (Fig. 4.2, Table 4.1).

Furthermore, the formation of Fe- and Mg-sulphates at Poás seems associated with the presence of olivine in lavas such as those outcropping around Cerro Pelón (Fo_{75}) and on the eastern margin of Laguna Caliente (Fo_{65}). At both locations, commonly only olivine ghosts were observed, indicating complete dissolution of this mineral, while other primary phases such as clinopyroxene, orthopyroxene and plagioclase are considerably less altered or, in many cases, completely intact (Figs. 4.15 to 4.17). This observation is in agreement with the almost congruent dissolution of olivine when in contact with highly acidic solutions (Tosca et al., 2004), which is kinetically favoured over glass, pyroxene or plagioclase dissolution (Hausrath et al., 2008). An overall order of mineral dissolution under acidic conditions is phosphates > olivine > pyroxene ≥ Fe-Ti oxides ≥ mafic silicate glass ≥ felsic silicate glass (Nesbitt and Young, 1984; Nesbitt and Wilson, 1992; Wolff-Boenisch et al., 2004).

The Poás sites where Fe- and Mg-sulphates were found have medium to high rock/water ratios in common. In the high rock/water locations, the chemical alteration of rock occurs mainly via acid rain and/or brine spray. The models of Figure 4.19 predict that K-jarosite, jurbanite, K-alunite, followed by epsomite and ferrohexahydrite could form here in a repetitive sequence of olivine dissolution and evaporation in an open system involving limited water amounts. Although römerite was the only simple (iron) sulphate identified by XRD in the "dead zone" (Fig. 4.2), these models for combined water-rock interaction and evaporation illustrate that conditions and processes would be favourable for the formation of other sulphates as well. Their absence in the materials studied might be attributable to their transient stability under changing conditions (e.g., following heavy rainfall), since re-dissolution is expected to be a function of pH, temperature and solution chemistry (Miller et al., 2016 and references therein).

Experimental constraints on the formation of Fe- and Mg-sulphates have been discussed by Tosca et al. (2004), Golden et al. (2005) and Hausrath et al. (2013). In the acid weathering experiments of Tosca et al., (2004), involving reaction and evaporation steps, hexahydrite $MgSO_4 \cdot 6H_2O$ did not form upon pyroxene dissolution, apparently because this mineral did to release enough Mg^{2+} to produce appreciable amounts of Mg-sulphate. Through geochemical modelling of acid dissolution of synthetic basalts and evaporation of the resulting weathering solutions, Tosca et al. (2005) confirmed that the presence of olivine is required instead. Aluminium sulphates such as alunogen and tamarugite $NaAl(SO_4)_2 \cdot 6H_2O$ form as a result of glass dissolution (Tosca et al., 2004). As the authors pointed out, the glass releases more

Al^{3+} than plagioclase because of its faster dissolution rate.

Golden et al. (2005) performed laboratory experiments at 145°C to simulate weathering of volcanic rock by acid fog and acid leaching. Interaction of H_2SO_4 with basaltic sand and tephra from Hawaii resulted in the formation of hexahydrite, $MgSO_4 \cdot nH_2O$, K- and H-jarosite, voltaite, $Fe_2(SO_4)_3$, anhydrite, gypsum and amorphous silica. The Mg-sulphates where more abundant in experiments with the basalt, which had a 6 times higher MgO content than the tephra. Jarosites only formed in open-system leaching experiments.

Experimental interaction between H_2SO_4 vapour and basaltic glass and San Carlos olivine at T=150-155°C (Hausrath et al., 2013) resulted in the formation of Mg-sulphates (hexahydrite and kieserite) as the most common alteration product in the case of olivine, and Ca- and Al- sulphates in the case of basaltic glass.

4.5.4. Implications for Mars

4.5.4.1. Fe-, Mg- and Ca-sulphate abundances on Mars

Volcanic products cover vast areas of Martian surface (Tanaka et al., 1992; Christensen et al., 2001; Bibring et al., 2005). Even though only a few Noachian volcanic terrains have been preserved, Martian volcanism was most likely intense during the early history of the planet and it gradually decreased over time with episodic periods of higher activity (Werner, 2009; Hauber et al., 2011; Robbins et al., 2011; Xiao et al.,2012). Since the sulphur composition of Martian basalts is relatively high compared to their terrestrial counterparts (Lodders, 1998; McSween et al., 2006; 2008) the emplacement of Martian intrusives and lavas must have released significant amounts of sulphur-rich volatiles. Reaction of volatile sulphur compounds with water in magmatic vapours, ice or groundwater will then inevitably have produced acidic fluids. Due to its ubiquity, acid-sulphate alteration has been a major feature on Mars´ surface (Ehlmann et al., 2011; Gaillard et al., 2013). Moreover, surface deposits contain high levels of sulphur (SO_3 up to ~37 wt.%, average ~6 wt.%) mostly in the form of sulphates (King and McLennan, 2010).

Jarosite, Mg- and Ca-sulphates have been detected in situ by MER Opportunity within sedimentary sequences of the Burns Formation at Meridiani Planum (Klingelhöfer et al., 2004). Fluid-rock modelling by Tosca et al. (2005) suggested that assemblages of Fe-, Mg- and Ca-sulphates, together with hematite, can be derived from low-pH and SO_4-rich fluids that have interacted with basalts. Jarosite could have been a precursor for hematite since its dissolutions may have provided Fe^{3+}. However, substantial amounts of jarosite still present would imply that water-mediated diagenesis did not convert all the iron into oxides. Therefore, rock/water ratios may have been high, possibly due to a water-limited environment as a result of freezing or evaporation (Squyres and Knoll, 2005; Elwood-Madden et al., 2009).

Sequences of polyhydrated sulphates (Mg-, Fe- and possibly also Ca-rich) and monohydrated sulphates (mostly kieserite) have been detected by OMEGA and CRISM in Valles Marineris (Fueten et al., 2010; Wendt et al., 2011; Fueten et al., 2014). The monotonous distribution of these sulphates over wide areas and the intercalation of monohydrated and polyhydrated phases suggest that they may have formed via evaporation of a shallow body of standing water, rain, snow, ice or local groundwater (Niles and Michalski, 2009; Flahaut et al., 2010; Grindrod and Balme, 2010; Weitz et al., 2010; Niles and Michalski, 2011). Local associations of amorphous silica and jarosite have been interpreted as products of low-temperature acid alteration of basalts (Milliken et al., 2008; Bishop et al., 2009; Weitz et al., 2011; Wendt et al., 2011; Sefton-Nash et al., 2012; Thollot et al., 2012).

Gypsum deposits have been identified using OMEGA data various sediments covering the northern polar cap and the circum-polar dune field on Mars (Langevin et al., 2005; Fishbaugh et al., 2007; Massé et al., 2010). Irrespective of the sedimentation mechanisms, gypsum could have formed by the interaction of Ca-rich phases like pyroxene and plagioclase with SO_4-rich fluids derived either from water-condensed SO_2 produced by volcanic activity (Fairén et al., 2004; Tosca et al., 2004) or from aqueous weathering of sulphides under oxidative conditions (Chevrier et al., 2004; 2006).

4.5.4.2. Alteration processes - Poás volcano vs. Mars

An environment with high rock/water ratios and limited water availability (rocks exposed to acid rain and/or hyperacid brine spray) that is essential for the formation of Fe- and Mg-sulphates at Poás volcano is consistent with the required conditions inferred for the origin of these minerals on Mars. Similarly, the water-rock interaction models for Poás also revealed that: (1) olivine is the primary mineral that preferentially gives rise to Fe- and Mg-rich solutions, and (2) the most effective way to form both Fe- and Mg- sulphates is through cycles of reaction and evaporation in an open system. In particular, Fe-sulphates point to rather oxidizing and acidic (pH<4) environmental conditions (Nordstrom and Alpers, 1999; Bigham and Nordstrom, 2000; Nordstrom et al., 2000). In the geochemical models presented here, oxidation of Fe^{2+} to Fe^{3+} by atmospheric O_2 was ignored. This does not seriously affect the comparison since the current Martian atmosphere is extremely oxygen-depleted compared to its terrestrial counterpart; = $7.9x10^{-6}$ bar vs. = 0.21 bar, respectively (Owen, 1992). Moreover, during active volcanism on early Mars, its atmosphere may have been even more anoxic than today, so that the kinetics of Fe-oxidation by $O_{2(g)}$ were probably orders of magnitude slower than in currently active acidic environments at the Earth´s surface (Burns, 1993; Catling and Moore, 2003).

A direct consequence of high rock/water ratios is that mineral phases with slow dissolution rates such as pyroxene and plagioclase do not contribute substantially to secondary mineral assemblages. Hence, under low H_2O-availability conditions

Al-mobilization into alteration phases will be limited (Hurowitz and McLennan, 2007). The larger availability of water at Poás and the fact that its rocks are less mafic (mainly andesites and basaltic andesites) compared to their Martian counterparts (mainly basalts), explain to some extent why at Poás Ca- and Al-sulphates are more common than Fe- and Mg-sulphates. On Mars, Mg-, Fe- and Ca-sulphates and accompanying phases such as amorphous silica seem to dominate the mineralogy of evaporites (Tosca and McLennan, 2006), whereas Ca-sulphates usually prevail and are associated with carbonates and chlorides in terrestrial evaporate deposits. Exceptions are the vast gypsum deposits in the Martian northern polar regions. It is conceivable that they precipitated from acidic fluids comparable to Laguna Caliente, given that gypsum abundantly forms in the lake as the only sulphate.

The presence of alunite and jarosite in the crater area of Poás confirms that the occurrence of these minerals on Mars is an indicator of past aqueous systems. In addition, the Poás setting attests to the acidic, oxidizing, sulphur and aluminum-rich conditions that are also required for their stability. Finally, since on Mars the rise of extensive volcanism during the Hesperian may have been responsible for the acidic environments, following alkaline conditions that prevailed earlier during the Noachian (Bibring et al., 2006; Milliken et al., 2010), the use of the magmatic-hydrothermal system of Poás as analogue for Martian alunite and jarosite-forming processes seems well justified. From dissolution experiments Miller et al. (2016) proposed that alunite is better preserved in less acidic and warmer aqueous conditions than jarosite, and that alunite is expected to be preserved longer when solutions are dilute, especially under alkaline and high-temperatures conditions. The authors further noted that in high salinity brine environments both minerals would dissolve slower are expected to be equally preserved. The field observations and models for Poás are consistent since the geochemical models suggest that K-alunite should be present in deeper and hotter sections at Poás (95 to 164°C) and that both K- and Na-alunite are present at higher pH values (1.6 to 3.8) than H- and K-jarosite (0.8 to 1.2).

4.6. CONCLUSIONS

Field evidence and geochemical modelling have been used to demonstrate that acid fluids of Poás volcano are capable of producing complex mineral assemblages, including Ca-, Al-, Fe- and Mg-sulphates, and to investigate the role of temperature changes, interactions with rocks and minerals, and evaporation. At a macroscopic scale, the models indicate that the formation of amorphous silica, hematite, anhydrite/gypsum, pyrite, anatase and kaolinite is fairly insensitive to the degree of acidity of the aqueous system studied. On the other hand, Fe-sulphates (H- and K-jarosite) followed by elemental sulphur and Al-sulphates (K-, Na-alunite and Al(OH) SO_4) only form in this setting under acidic conditions (pH<4). Finally, the modelling evidence shows that minerals such as fluorite, illite, brucite, magnetite and diaspore require relatively high pH values (pH>4) and/or temperatures to form, which ex-

plains their absence at the surface of the crater area.

To a significant extent, local variations in secondary mineralogy within the crater area reflect differences in the relative proportions of rock and acidic fluid during interaction, which is particularly relevant for Mg-, Fe- and Al-sulphates. In general, the Fe- and Mg-sulphates require the highest rock-water ratios to form. A further key factor for their occurrence is probably the presence of olivine as a source of Mg and Fe. For these reasons, the presence of Fe- and Mg-sulphates was found to be restricted to surfaces of olivine-bearing rocks affected by acid rain or acid brine spray. The modelling results rule out a simple interaction mechanism but suggest an open-system scenario where fluid evolved in a repetitive sequence of interaction with olivine and evaporation. Conversely, the Al-sulphates can also stabilise where brine water is more abundant, and pH and/or temperature are higher.

The secondary mineral assemblages at Poás are strongly reminiscent of sulphate-bearing mineral associations detected on the surface of Mars. The conditions and mechanisms inferred for their formation in the crater area of Poás can therefore be considered to approximate Martian geological environments wherein these minerals formed, particularly in settings with a large mineralogical diversity at small spatial scales. Volcanic activity, acid alteration and low water availability are required to produce Fe- and Mg-sulphates at Poás, conditions that presumably also marked Hesperian times on Mars when similar assemblages could originate. Differences in rock compositions and atmospheric chemistry poses limits to this comparison, in particular when considering the less mafic rock types and oxidizing environment of the crater lake setting studied here. Nevertheless, the results of this work demonstrate that active volcanic-hydrothermal systems on Earth can be regarded as excellent analogues to study processes responsible for the formation of sulphates and associated alteration in the early history of Mars.

ACKNOWLEDGEMENTS

We would like to thank Gino González, Yemerith Alpízar and Raúl Mora (RSN-ICE), Erick Fernández, Jorge Brenes and Geoffroy Avard (OVSICORI-UNA) for their support during fieldwork. Mark Reed and Jim Palandri (Oregon University) kindly provided a copy of SOLVGAS and GASWORKS software and helped with using it on our samples. We are grateful to Franco Tassi (Università degli Studi di Firenze) for allowing us to perform chemical analysis of fumarolic gases at his laboratory. This work was funded by NWO (Netherlands Organization for Scientific Research), project ALW-GO-PL/10-03.

CHAPTER

5

Chlorine isotope and Cl-Br frationation in fluids of Poás volcano (Costa Rica): insight into an active volcanic-hydrothermal system

Rodríguez A., Eggenkamp H.G.M., Martínez-Cruz M. and van Bergen M.J., 2016. Chlorine isotope and Cl–Br fractionation in fluids of Poás volcano (Costa Rica): insight into an active volcanic–hydrothermal system. J. Volcanol. Geotherm. Res. 325, 70-85, doi:10.1016/j.jvolgeores.2016.05.020.

ABSTRACT

Halogen-rich volcanic fluids issued at the surface carry information on properties and processes operating in shallow hydrothermal systems. This paper reports a long-term record of Cl-Br concentrations and $\delta^{37}Cl$ signatures of lake water and fumaroles from the active crater of Poás volcano (Costa Rica), where surface expressions of magmatic-hydrothermal activity have shown substantial periodic changes over the last decades. Both the hyperacid water of its crater lake (Laguna Caliente) and subaerial fumaroles show significant temporal variability in Cl-Br concentrations, Br/Cl ratios and $\delta^{37}Cl$ values, reflecting variations in the mode and magnitude of volatile transfer. The $\delta^{37}Cl$ signatures of the lake, covering the period 1985-2012, show fluctuations between +0.02±0.06‰ and +1.15±0.09‰. Condensate samples from adjacent fumaroles on the southern shore, collected during an interval (2010-2012) with strong changes in gas temperature (107-763°C), display a much larger range from -0.43±0.09‰ to +14.09±0.08‰. Most of the variations in Cl isotope, Br/Cl and concentration signals can be attributed to interaction between magma-derived gas and liquid water in the volcanic-hydrothermal system below the crater. The $\delta^{37}Cl$ were lowest and closest to magmatic values in (1) fumarolic gas that experienced little or no interaction with subsurface water and followed a relatively dry pathway, and (2) water that captured the bulk of magmatic halogen output so that no phase separation could induce fractionation. In contrast, elevated $\delta^{37}Cl$ can be explained by partial scavenging and fractionation during subsurface gas-liquid interaction. Hence, strong Cl isotope fractionation leading to very high $\delta^{37}Cl$ in Poás' fumaroles indicates that they followed a wet pathway. Highest $\delta^{37}Cl$ values in the lake water were found mostly in periods when it received a significant input from subaqueous fumaroles or when high temperatures and low pH caused HCl evaporation. It is concluded that combined monitoring of $\delta^{37}Cl$ and Br/Cl in Laguna Caliente and adjacent fumaroles provides valuable information on activity in the subsurface hydrothermal system with significant relevance for volcanic surveillance of Poás.

Front picture: fumaroles on the composite pyroclastic cone (CPC) and Laguna Caliente on the background, Poás volcano (Costa Rica). Picture taken on April 23rd, 2012.

5.1. INTRODUCTION

Chlorine and bromine are generally extracted from degassing magma in the form of $HCl_{(g)}$ and $HBr_{(g)}$ (Gerlach, 2004; Aiuppa et al., 2005; Martin et al., 2006). While chlorine is generally the most abundant halogen in volcanic gases (Taran and Zelenski, 2015), bromine is present in amounts that are orders of magnitude lower. Gerlach (2004) reported an average molar Br/Cl ratio of 0.0022±0.0020 for high-temperature gas condensates from arc volcanoes. Upon shallow emplacement of magma, both halogens are expelled during cooling and crystallizing, driven by their relatively high H_2O vapour/melt partition coefficients (Villemant and Boudon, 1999; Balcone-Boissard et al., 2010). In subsurface volcanic hydrothermal systems associated with intrusions, they tend to be concentrated in fluid phases, showing a strongly hydrophilic behaviour. Since shallow hydrothermal processes can fractionate Cl and Br (Berndt and Seyfried, 1990; 1997; Lüders, 2002; Liebscher et al., 2006; Foustoukos and Seyfried, 2007), the proportions of these halogens in volcanic fluids are potential signals of interaction and separation processes in the trajectory between magma and atmosphere, such as boiling, condensation, evaporation, mixing and mineral precipitation (Villemant et al., 2003; 2005; 2014; Wu et al., 2012; Fisher et al., 2015). Likewise, the chlorine isotope compositions of fluids from shallow magma degassing are sensitive to fractionation during interaction between deep gases and shallow water bodies within a volcanic edifice (Sharp et al., 2010; Li et al., 2015). Volcanic fumaroles confirm this since the available data show large $\delta^{37}Cl$ variations compared to other terrestrial materials (Eggenkamp, 1994; Wahrenberger et al., 1997; Musashi and Eggenkamp, 2000; Barnes et al., 2008; Sharp et al., 2010; Rizzo et al., 2013).

This paper explores the extent and causes of Cl-Br and chlorine isotope fractionation using time series data for fluids from the active crater of Poás volcano (Costa Rica). Samples were taken from its hyperacid lake (Laguna Caliente) and from a persistently active fumarole field on the southern shore. The lake data cover a period of almost three decades (1985-2012) when marked changes in activity and physicochemical properties were recorded (Rowe et al., 1992a;b; Martínez et al., 2000; Martínez, 2008; Rouwet et al., 2016; and references therein). The fumarole data represent a two-year interval (2010-2012) in which the temperatures ranged between 763 and 107°C, and showed a declining trend. For a preceding period (2001-2007), Sharp et al. (2010) documented a strong $\delta^{37}Cl$ fractionation in other (low-temperature) fumaroles that were temporarily active within the crater, and attributed this to a distillation-recondensation process within the plumbing system. Fischer et al. (2015) presented data sets on the chemical and isotopic compositions of fumarolic discharges that cover both periods. Our results demonstrate that halogen signatures of Laguna Caliente and associated fumaroles signal active magma-gas-liquid interaction processes in the subsurface volcanic-hydrothermal system of Poás. The observed time series trends, in conjunction with other chemical parameters recorded at this volcano, provide insights into the potential of chlorine and bromine for monitoring purposes as an aid to mitigate hazards from eruptive activity.

5.2. GEOLOGICAL SETTING

Quaternary volcanism in Central America is associated with subduction of the Cocos plate under the Caribbean plate. The convergence offshore from Nicoya Peninsula in Costa Rica occurs at a rate of 74-85 mm/yr at 20-22° azimuth (DeMets et al., 2010). Poás, in the Central Cordillera of Costa Rica (Fig. 5.1), is a complex basaltic andesitic stratovolcano with a maximum elevation of 2708 m amsl. Erupted products mainly consist of calc-alkaline basaltic and andesitic lavas and pyroclastics (Prosser and Carr, 1987; Cigolini et al., 1991; Malavassi, 1991). Its 1.3 km wide active crater hosts an acidic lake known as Laguna Caliente in a 300 m-diameter pit, and a ~30 m high pyroclastic cone, which is a site of persistent fumarolic activity (Fig. 5.2). The structure is often referred as "the dome" but since it is composed of tephra from the 1953-55 eruption (Casertano et al., 1987), we will use the term "composite pyroclastic cone" or "CPC", following Martínez et al. (2000) and Martínez (2008). This 1953-55 eruption was the latest with juvenile materials. Such events are relatively rare at Poás, in contrast to the frequent occurrences of phreatic explosions.

Over the last decades, the water of Laguna Caliente has shown pH values ranging between -0.87 and 1.75, and temperatures from 22 to 94°C (Martínez, 2008). Concentrations of sulphate (3300 – 285,000 mg/kg or 34 - 297 mmol/kg) and chloride (2500 – 15,000 mg/kg or 70 - 3244 mmol/kg) fluctuate but have been always extremely high, which also holds for dissolved rock-forming elements (Rowe and Brantley, 1993; Martínez, 2008). The activity of the crater area is characterized by a long history of intermittent phreatic eruptions and persistent fumarolic emissions. Martínez (2008) subdivided the activity of Poás since the early 1970´s into five stages. During Stage I (1972 - August 1980), fumarolic discharges were strong within the lake and were accompanied with occasional phreatic explosions. Stage II (September 1980 – April 1986) was characterized by a relative quiescence in the lake and absence of phreatic activity despite a strong discharge of high-temperature fumaroles through the CPC. In 1981, preceded by a regional earthquake, an inferred rupture of the carapace of a magma body at depth, possibly accompanied by a localized intrusion of gas-rich magma beneath the CPC, triggered an increase in fumarole temperatures from 92 to 1020°C (Casertano et al., 1987; Rymer et al., 2000), the highest temperatures ever recorded in the fumaroles of Poás volcano. In the following Stage III (May 1986 - August 1995), a vigorous subaqueous fumarolic discharge and intense phreatic activity accompanied a strong volume decrease, ultimately leading to a dry-out of the lake. The gradual drop of the lake level in 1987-89 revealed a muddy floor with numerous boiling mud pools where ~1-3 m high yellow ephemeral cones of sulphur and pyroclastic materials formed, acting as sites of vigorous gas emissions (Oppenheimer and Stevenson, 1989). Stage IV (September 1995 – February 2005) was a calm period, when the lake re-established and subaerial fumaroles and hot springs appeared in the surrounding crater area (Vaselli et al., 2003). Stage IV was followed by an intense fumarolic discharge into the lake during Stage V (March 2005 – present) together with frequent phreatic eruptions since March 2006 and a steady decrease of the lake volume. This episode may have been triggered by a new cycle of enhanced volatile supply due to carapace breaking and/or shallow magma intrusion (Martínez, 2008; Rymer et al., 2009). In recent years, fumarolic activity has

been concentrated at the CPC, which has occasionally shown incandescence when gas temperatures rose above 600°C in 2011, 2012 and 2014. Ongoing strong CPC degassing (at least until 2015), testifies a continuous supply of magmatic volatiles (Fischer et al., 2015; OVSICORI-UNA, http://www.ovsicori.una.ac.cr).

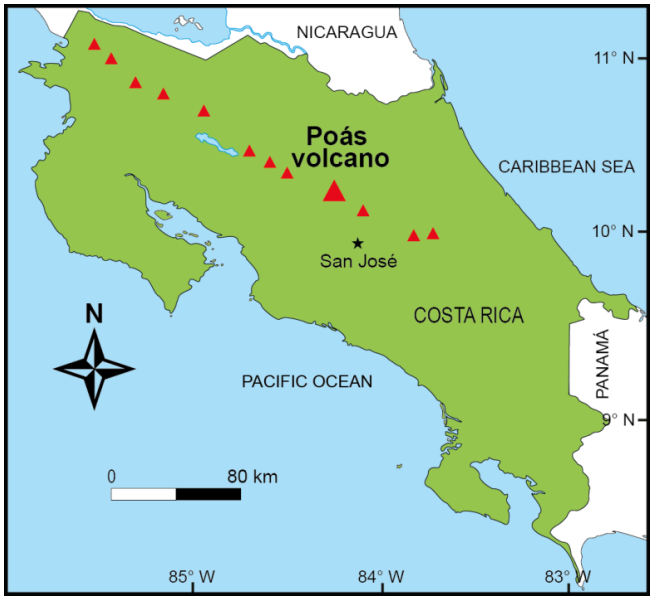

Figure 5.1. Location map of Poás volcano.

Figure 5.2. Poás volcano (May 2012), view from the NE rim of the active crater towards Laguna Caliente and the composite pyroclastic cone (CPC).

5.3. SAMPLING AND ANALYTICAL METHODS

5.3.1. Sampling techniques

Most of the samples from Laguna Caliente and fumarole condensates discussed here were routinely collected by OVSICORI-UNA (Observatorio Sismológico y Vulcanológico de Costa Rica, Universidad Nacional). The samples from Laguna Caliente were usually taken at a relatively easily accessible location on the eastern shore. The temperature and pH of the lake were directly recorded in the field with the aid of a thermocouple and a portable pH electrode, respectively. The water samples had been stored unfiltered and untreated in high density polyethylene (HDPE) bottles at room temperature (20-25°C).

During our field campaign in April – May 2012, fumarole temperatures were measured with a thermocouple, and gas condensate samples were taken at vents were the flow was vigorous and constant. The condensates were collected using a glass condenser connected to a glass Dewar tube, which was in turn coupled to a titanium pipe. The samples were stored in 100 ml HDPE plastic bottles with air tight caps at room temperature. Older fumarole samples analyzed also represent condensates that had been collected by OVSICORI-UNA in a similar way.

5.3.2. Analytical methods

5.3.2.1. Major anions

Because long storage times had occasionally resulted in the formation of precipitates in samples of hyperacid lake waters (mainly gypsum, anhydrite and amorphous silica) and fumarole condensates (elemental sulphur), all of the samples were filtered through a 0.2 μm pore-size cellulose acetate membrane prior to analysis. Measurements of pH, electrical conductivity (C) and redox potential (Eh) at the Department of Earth Sciences of Utrecht University were performed at 19±1°C using a WTW® 3430 portable multimeter. The pH electrode was calibrated with pH 1, 4 and 7 buffers, the conductivity electrode with a 0.01 M KCl standard, and the Eh electrode with a 420 mV buffer solution. The concentration of SO_4^{2-}, Cl^-, F^-, and Br^- were determined by ion chromatography (IC) at the Department of Earth Sciences of Utrecht University, using a Dionex® ICS-3000, equipped with a Dionex®IonPac® AS 19 column. A gradient elution of 10 – 50 mM KOH was utilized. The samples were diluted 10 to 300 times with deionized water (18.2 MΩ/cm) before analysis. Sulphate and Cl^- were determined with a precision of 1%, and F^- and Br^- with a precision of 2 and 5%, respectively. Major cations in crater lake waters (Na, K, Mg and Ca) and total sulphur (S_T) were analysed by inductively coupled plasma optical emission spectrometry (ICP-OES), using a Spectro Ciros® instrument at the Department of Earth Sciences of Utrecht University. The samples were diluted 10 to 100 times and acidified with 2% Suprapur® HNO_3 acid. The analytical precision obtained from control samples was less than 3% for all of these elements.

5.3.2.2. Chlorine isotopes

Samples for $\delta^{37}Cl$ analysis were prepared and analysed following the procedure of Eggenkamp (1994). Ten milligrams of AgCl were precipitated by the addition of 0.2 M $AgNO_3$ to a specific amount of sample, which was determined by its chloride concentration. Before the formation of AgCl precipitate, the ionic strength of the sample was adjusted with 4 ml of 1 M KNO_3, and the pH was fixed to a value of 2.2 through the addition of 2 ml of a Na_2HPO_4-citric acid buffer. Next, the solution was heated to 80°C and 1 ml of 0.2 M $AgNO_3$ was added. Since black precipitates of Ag_2S formed in fumarole condensates and some of the lake water samples due to the presence of $H_2S_{(aq)}$, the procedure was modified in order to completely oxidize the total sulphur to SO_4^{2-}. In these cases, samples were prepared with 4 ml of 1 M KNO_3, 1 ml of H_2O_2 (30 wt.%), and 1 ml of concentrated HNO_3 (65%), and were then heated to 80°C for 30 minutes before the 0.2M $AgNO_3$ was added. The AgCl precipitates were filtered through a Whatman® type GF/F glass fibre filter and dried overnight at 80°C. Subsequently, AgCl was reacted with iodomethane (CH_3I) in order to form chloromethane (CH_3Cl) at 70 - 80°C during 48 hours in vacuum glass ampoules. The chloromethane was separated from excess CH_3I by gas chromatography using a 75 cm long, 6.35 mm OD SS column, filled with Porapak® Q 80-100 mesh at 140°C with helium as carrier gas. The analyses of CH_3Cl were carried out on a VG SIRA 24 EM mass spectrometer at the Department of Earth Sciences of Utrecht University. Chlorine isotope data are reported as a delta notation ($\delta^{37}Cl$), in which the ($^{37}Cl/^{35}Cl$) isotope ratio of a sample is compared to a standard with a known ($^{37}Cl/^{35}Cl$) ratio, commonly taken to be the Standard Mean Ocean Chloride or SMOC (Kaufmann, 1984):

$$\delta^{37}Cl = \frac{(^{37}Cl/^{35}Cl)_{sample} - (^{37}Cl/^{35}Cl)_{SMOC}}{(^{37}Cl/^{35}Cl)_{SMOC}} \times 1000 \qquad (1)$$

Given the constancy of the isotopic composition of ocean water (Kaufmann, 1984; Godon et al., 2004a; Liu et al., 2013) any sample of ocean water can serve as a standard with a $\delta^{37}Cl$ value of 0.00 ‰ versus SMOC. It is here represented by a sample of Atlantic Ocean water collected near Madeira in 1982. The analytical precision was ± 0.16‰ (1 σ), based on long-term analyses of this standard. As a rule, samples were analyzed at least in duplicate. Reproducibility between duplicates was generally better than 0.1‰.

5.4. RESULTS

5.4.1. Cl and Br concentrations in Laguna Caliente and CPC fumaroles

Concentrations of chloride and bromide as well as Br/Cl ratios in Laguna Caliente are shown in Figure 5.3, together with the variations in lake volume, temperature and pH, recorded over almost four decades since the late 1970's. The time series for these parameters are based on the data presented here and the compilation of Martínez (2008). A representative subset is given in Table 5.1. In general, Cl and Br concentrations exhibit roughly similar changes with time. Their abundances were relatively high during Stages III and V when the activity was high. The maximum

concentrations of Br and Cl were measured during Stage III, reaching 1820 mg/kg (23 mmol/kg) and 114,000 mg/kg (32 mmol/kg), respectively. Stage III, when temperatures were highest, was also marked by maximum Br/Cl molar ratios (up to 0.013), whereas they remained virtually constant at ~0.001 throughout Stage V, comparable to values observed in Stage II and at the beginning of Stage III (Fig. 5.3). It should be noted that Laguna Caliente was largely dry during most of Stage III and that samples from this period include those taken from isolated mud pools, which are therefore not necessarily representative for the lake system at large. Conversely, lowest Cl and Br concentrations were found during Substages IVA, IVC and IVE when the activity was weak, the lake water had cooled and pH values were relatively high. Measured concentrations were 4 mg/kg (0.05 mmol/kg) for Br and 10,200 mg/kg (288 mmol/kg) for Cl. This tendency of decreasing concentrations was enhanced by periods of high rainfall in 1995-1997 and 2003-2005 that further contributed to the dilution and volume increase of the lake. Also, Br/Cl ratios decreased considerably after Stage III, reaching minimum values during Substage IVE (Br/Cl molar ratio = 0.0003). During most of Stage IV (mid 1997-mid 2004), when the lake temperature was low (usually <40°C), the Cl concentration in the lake exceeded that of SO_4, which is an uncommon feature for Laguna Caliente (Martínez, 2008).

The data set for Cl, Br and Br/Cl in the CPC fumarole condensates encompasses the period 2010-2012, within Stage V. The results are given in Table 5.2 and are illustrated in Figure 5.5. Despite substantial fluctuations there is a tendency of decreasing Cl and Br concentrations, decreasing temperature and increasing pH with time. Peak concentrations of Cl and Br are 47,000 mg/kg (1326 mmol/kg) and 78 mg/kg (1 mmol/kg), respectively. The molar Br/Cl ratios exhibit some variation, but there is no obvious temporal trend. The majority of data scatter around 0.001, i.e. close to base line values found in the lake.

5.4.2. Cl isotope compositions of Laguna Caliente and CPC fumaroles

The $\delta^{37}Cl$ results for Laguna Caliente and CPC fumaroles (Tables 5.1 and 5.2) are shown in Figures 5.3, 5.4 and 5.5. The values for the lake show minor fluctuations between +0.02±0.06‰ and +0.74±0.03‰. An exceptional value of +1.15±0.09‰ was found in one of the samples (September 1994) taken from pools when the lake had dried out. The $\delta^{37}Cl$ data can be ranked according to the Stages and Substages: III ≈ IVC-IVE > II ≈ V > IVA-IVB-IVD. Thus, the more active periods (II, III, and V) tend to be marked by higher $\delta^{37}Cl$ values than the most quiet one (IV), with the exception of Substages IVC and IVE. Data reported by Sharp et al. (2010) for samples taken in 2005 and 2006 are consistent with the slightly elevated values seen in our data for Stage V. As the time series of Figure 5.3 illustrate, the modest rises in $\delta^{37}Cl$ during the active periods were associated with increased temperatures, halogen concentrations and acidity, relative to stage IV. Conversely, $\delta^{37}Cl$ values were also high during Substages IVC and IVE, when the lake was very quiet, temperatures low (ca. 30°C) and pH relatively high (>1). Figure 5.4 summarizes the relationship between $\delta^{37}Cl$ and temperature of Laguna Caliente and the exceptional conditions during Substages IVC and IVE.

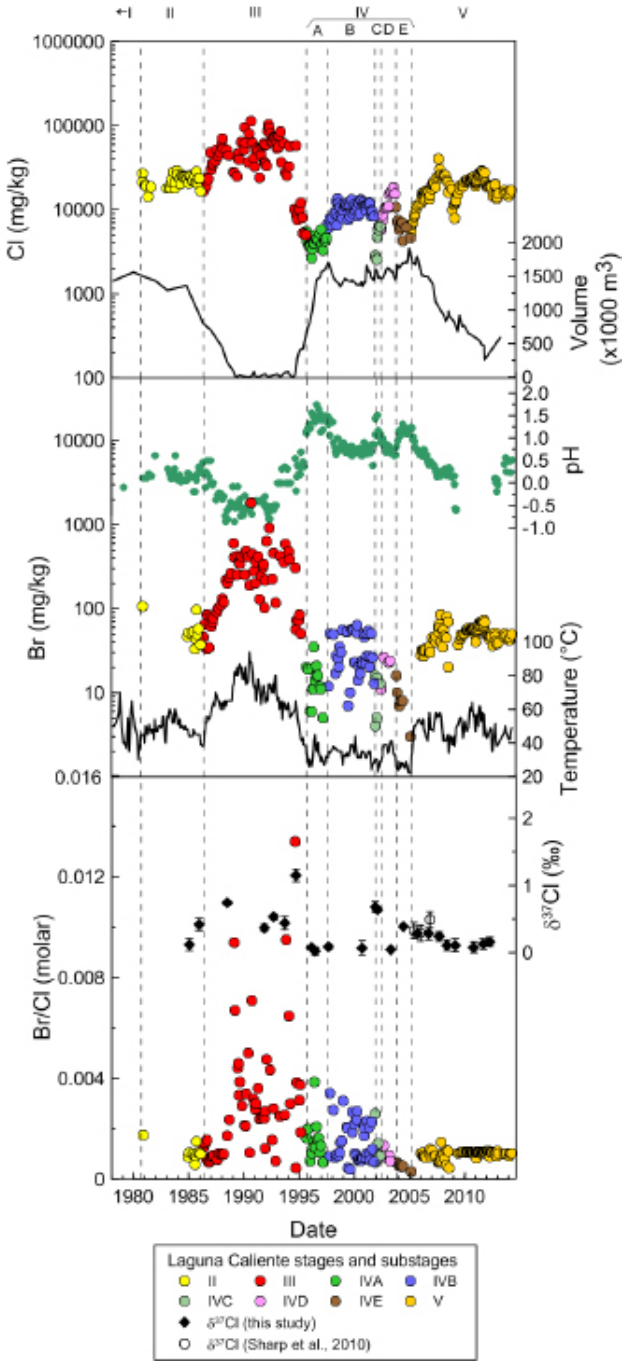

Figure 5.3. Time series of Cl and Br concentrations, Br/Cl ratios, $\delta^{37}Cl$ values, lake volume, pH and temperature for Laguna Caliente. A trend of $\delta^{37}Cl$ composition with temperature is showed in Figure 5.4.

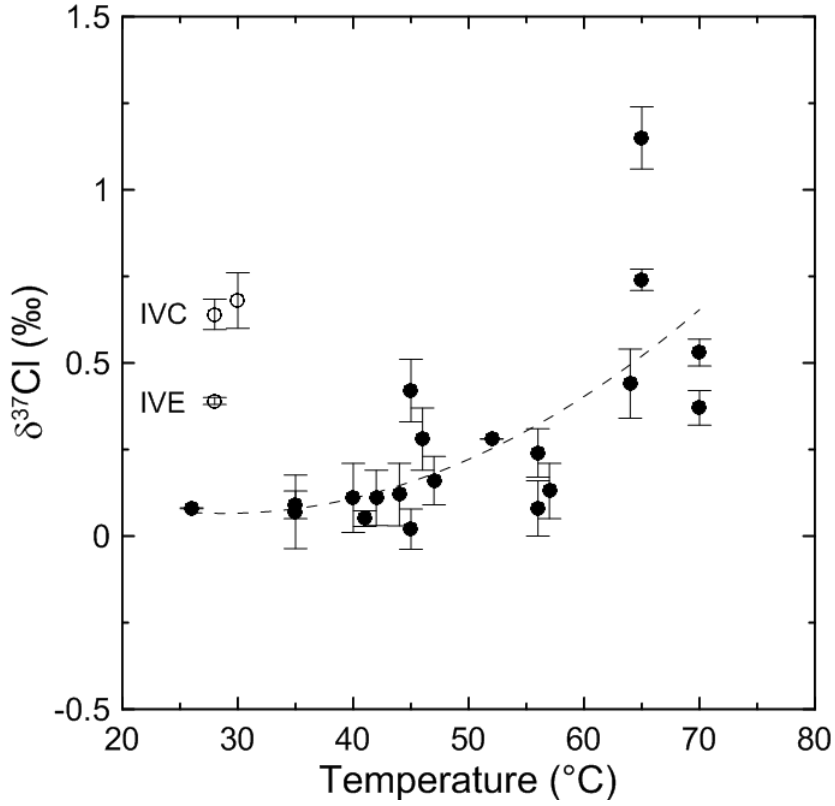

Figure 5.4. Relationship between the $\delta^{37}Cl$ composition of Laguna Caliente water and temperature, illustrating increasing $\delta^{37}Cl$ at higher activity levels of the magmatic hydrothermal system. Note that the $\delta^{37}Cl$ values for low-activity substages IVC and IVE do not follow the trend, presumably because the entrance of brine water was temporarily blocked and volatile supply was restricted to gaseous input (cf. Martínez, 2008).

In contrast to the modest range in the lake water, the CPC fumarole condensates display a large variation in $\delta^{37}Cl$, with a maximum of +14.09±0.08‰ at the lowest gas temperatures (<200°C) and a tendency of decreasing $\delta^{37}Cl$ values towards ca. 0‰ at the highest temperatures (>600°C), although relatively low isotope ratios were also found in some samples when temperatures were around 300°C (Fig. 5.5). Sharp et al. (2010) reported a comparable a large $\delta^{37}Cl$ range (from -1.3‰ to +18.75‰) in condensates and gas samples from low-temperature fumaroles (<160°C) on the eastern terrace of the active crater (Main and Naranja fumaroles), which were collected in 2001 (Stage IV) and 2006-2007 (early Stage V) (Fig. 5.6).

Table 5.1. Chemical composition, physicochemical parameters and $\delta^{37}Cl$ values for selected samples from Laguna Caliente and Río Agrio hot spring, Poás volcano. Concentrations in mg/kg and molar elemental ratios. Conductivity and pH were measured in the laboratory at T=24±2°C.

Date	$T_{sampling}$ (°C)	pH_{lab}	$Cond._{lab}$ (mS/cm)	SO_4	S_T [(a)]	Cl	Br	F	Mg	SO_4/Cl	S_T/Cl	Br/Cl	F/Cl	Mg/Cl	$\delta^{37}Cl$ (‰)	Source
Stage II																
11-Jan-85	44	-0.21	324[b]	52000	16800	20400	51	1120	640	0.94	0.91	0.0011	0.102	0.046	0.12±0.09	(1,2)
29-Nov-85	45	0.30	390	62700	21000	23400	57	1090	650	0.99	0.99	0.0011	0.087	0.040	0.42±0.09	(1,2)
Stage III																
24-Jun-88	65	-0.61	n.d.[c]	175000	25300	51600	200	2970	990	1.25	0.54	0.0017	0.107	0.028	0.74±0.03	(1,2,3)
01-Nov-91	70	-0.50	371	72100	n.d.	61100	330	6790	770	0.44		0.0024	0.207	0.018	0.37±0.05	(1,2,4)
18-Sep-92	70	-0.60	n.d.	93100	30000	73000	460	8390	1210	0.47	0.45	0.0028	0.214	0.024	0.53±0.04	(1,2,5)
09-Sep-93	64	0.35	n.d.	50400	18100	61400	350	5840	1280	0.30	0.33	0.0026	0.177	0.030	0.44±0.10	(1,2,6)
23-Sep-94	65	-0.18	483	27000	21800	57500	56	2660	610	0.17	0.42	0.0004	0.086	0.016	1.15±0.09	(1,2,6)
Substage IVA																
23-Feb-96	26	1.55	n.d.	4480	n.d.	2630	6	140	n.d.	0.63		0.0010	0.100		0.08±0.00	(1,2,6)
14-Jun-96	45	1.35	57	7000	4000	4960	14	330	480	0.52	0.89	0.0013	0.123	0.141	0.02±0.06	(1,2,6)
Substage IVB																
05-Sep-97	35	1.30	n.d.	4060	2790	5960	12	170	480	0.25	0.52	0.0009	0.053	0.117	0.09±0.04	(1,2,6)
12-Sep-00	35	0.60	106	9410	3630	12700	24	620	520	0.27	0.32	0.0008	0.091	0.060	0.07±0.11	(2,7)
Substage IVC																
27-Nov-01	30	1.07	56	3450	1260	2720	16	82	250	0.47	0.51	0.0026	0.056	0.134	0.68±0.08	(2,7)
31-Jan-02	30	1.51	22	3590	1470	2540	5	52	230	0.52	0.64	0.0009	0.038	0.132	0.64±0.04	(2,7)
Substage IVD																
30-Apr-03	41	0.67	134	10500	5100	16100	n.d.	620	430	0.24	0.35		0.072	0.039	0.05±0.02	(2,7)
Substage IVE																
11-Jun-04	28	1.20	39	4540	1980	6480	b.d.l.[d]	65	330	0.26	0.34		0.019	0.074	0.39±0.01	(2,7)

Table 5.1 (continued).

Substage V																
20-Sep-05	52	0.70	123	12800	6560	11100	n.d.	750	360	0.43	0.65		0.126	0.047	0.28±0.00	(2,7)
05-Oct-06	46	0.40	163	28400	9410	16700	n.d.	1140	620	0.63	0.62		0.127	0.054	0.28±0.09	(2,7)
12-Sep-07	56	0.16	371	98300	21700	40300	61	1800	730	0.90	0.60	0.0007	0.083	0.026	0.24±0.07	(2,7)
04-Jun-08	42	0.16	323	75200	18500	31300	80	1450	580	1.23	0.65	0.0011	0.086	0.027	0.11±0.08	(2,8)
25-Feb-09	40				9830	11500			290						0.11±0.10	(2,8)
9-Nov-10	56	0.04[b]	498[b]	81000	27900	23900	57	990	380	1.22	1.29	0.0011	0.077	0.023	0.08±0.08	(1,2)
14-Sep-11	57	-0.06	587[b]	10740	37000	28200	69	1150	410	1.29	1.45	0.0011	0.076	0.021	0.13±0.08	(1,2)
18-Apr-12	47	-0.15	452[b]	92400	27200	21800	43	1020	280	1.76	1.38	0.0009	0.087	0.019	0.16±0.07	(1,2)
Río Agrio																
20-Jul-99	52	1.12		15700	4970	6210	11	150	850	0.93	0.89	0.0008	0.045	0.199	0.33±0.09	(2,9)
14-Jun-00	52	1.45		17100	5660	6280	14	140	920	1.01	1.00	0.0010	0.042	0.213	0.23±0.08	(2,9)
25-Oct-00	53	1.06		16600	5180	6300	14	135	850	0.97	0.91	0.0010	0.040	0.196	0.24±0.02	(2,9)
29-Apr-02	51	1.07		17100	5880	6300	16	170	850	1.00	1.04	0.0011	0.051	0.198	0.23±0.04	(2,9)

Notes: (a) S_t refers to total sulphur, measured by ICP-OES; (b) physicochemical parameters measured at T=19±1°C; (c) n.d. = not determined; (d) b.l.d = below detection limit.

Sources: (1) OVSICORI-UNA; (2) This study; (3) Rowe et al., 1992b; (4) Nicholson et al., 1992; (5) Nicholson et al., 1993; (6) Martínez et al., 2000; (7) Martínez, 2008; (8) Ayres, 2012; (9) Martínez et al., 1999; 2000 and 2002; unpublished data.

Table 5.2. Chemical composition, physicochemical parameters and $\delta^{37}Cl$ values for gas condensate samples from the CPC fumaroles. Conductivity and pH were measured in the laboratory at T=19±1°C.

Date	$T_{sampling}$ (°C)	pH	Cond. (mS/cm)	SO_4	Cl	Br	F	SO_4/Cl	Br/Cl	F/Cl	$\delta^{37}Cl$ (‰)
19-Jan-10	650	0.09	231	1176	21894	50.8	72	0.0198	0.0010	0.0061	0.19±0.03
23-Feb-10	640	0.00	272	914	26549	51.6	104	0.0127	0.0009	0.0073	
07-Apr-10	566	2.02	2.5	2773	5441	6.3	104	0.1881	0.0005	0.0358	
21-May-10	148	0.91	35.4	2397	234	b.d.l.[a]	7.9	3.7803	0.0000	0.0630	
25-Jun-10	763	0.07	241	610	21855	58.7	80	0.0103	0.0012	0.0069	-0.43±0.09
16-Aug-10	650	0.14	212	282	19843	35.5	43	0.0052	0.0008	0.0041	
08-Sep-10	760	0.09	231	654	21366	14.0	14	0.0113	0.0003	0.0012	0.67±0.01
22-Oct-10	590	0.58	73.8	2911	4221	8.0	130	0.2545	0.0008	0.0573	
09-Nov-10	595	0.60	148	3730	10182	24.0	264	0.1352	0.0010	0.0484	1.52±0.09
27-Jan-11	360	0.51	84.0	1259	7649	14.8	192	0.0607	0.0009	0.0468	1.73±0.03
22-Feb-11	480	0.65	63.6	1696	3880	6.4	103	0.1613	0.0007	0.0497	7.37±0.07
18-Mar-11	250	-0.27	465	68	47014	78.4	86	0.0005	0.0007	0.0034	
15-Apr-11	250	0.09	216	860	19594	24.6	19	0.0162	0.0006	0.0018	0.64±0.08
27-May-11	280	0.12	216	614	20103	25.4	5.9	0.0113	0.0006	0.0005	
22-Jul-11	760	0.10	213	1210	20774	17.7	44	0.0215	0.0004	0.0040	-0.25±0.10
13-Oct-11	186	1.05	22.7	988	929	1.8	75	0.3925	0.0009	0.1500	14.09±0.08
27-Oct-11	114	0.84	23.2	3647	104	b.d.l.	31	12.9412		0.5561	
25-Jan-12	508	0.27	150	4273	12284	24.7	n.d.[b]	0.1284	0.0009		
10-Feb-12	107	0.46	103	5480	39	b.d.l.	3.8	51.8549		0.1818	
24-Feb-12	107	1.14	18.1	1226	832	b.d.l.	6.4	0.5438		0.0144	13.48±0.04
22-Mar-12	307	0.42	116	1570	2790	0.7	80	0.2077	0.0001	0.0534	
21-Apr-12	410	0.84	n.d.	1750	2622	4.5	73	0.2463	0.0008	0.0522	4.04±0.05
08-May-12	238	0.63	n.d.	1401	3218	8.1	65	0.1607	0.0011	0.0378	
29-May-12	209	0.65	n.d.	6365	3347	6.8	169	0.7018	0.0009	0.0942	
20-Jul-12	301	0.84	n.d.	4001	103	b.d.l.	30	14.3352		0.5344	

Notes: (a) b.d.l. = below detection limit; (b) n.d. = not determined.

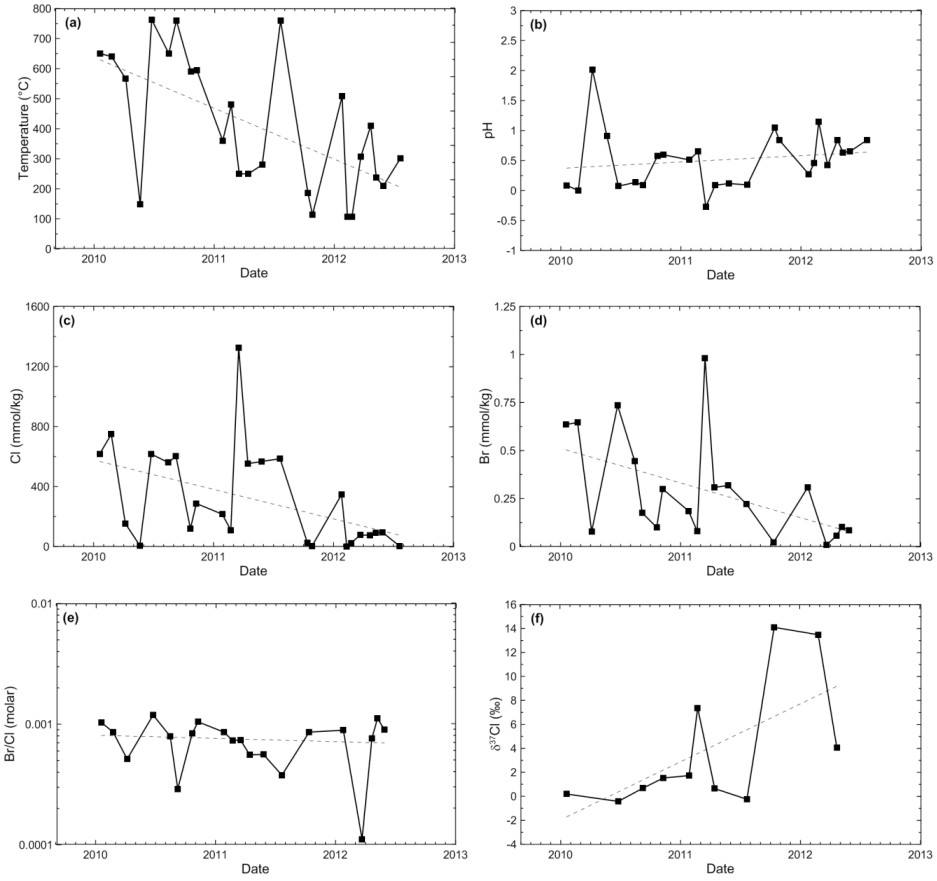

Figure 5.5. Time series of temperature, pH, Cl, Br, Br/Cl ratios and $\delta^{37}Cl$ values for condensates from the CPC fumaroles. Hyphenated lines indicate generalized trends.

5.5. DISCUSSION

Figure 5.7 compares Cl and Br contents of terrestrial reservoirs and bulk igneous rocks with fumarole gases and condensates from Poás and other subduction-related volcanoes. The Br/Cl molar ratios in most of these materials show little variation (mostly between 0.01 and 0.001) and the fractionation of these elements relative to chondritic values is modest. Fumarole condensates from arc volcanoes fall within this range but also include considerably lower values. Some of the variability in Br/Cl ratios among fumarole condensates might be attributable to a mantle source heterogeneity, considering the variation in pre-eruptive magmatic values and the usually conservative behaviour of these halogens during magma differentiation and degassing (Balcone-Boissard et al., 2010). It is conceivable that the mantle source range extends towards the low end of Br/Cl ratios (Fig. 5.7), since values lower than 0.00034 have been reported for condensates from high-temperature (T>500ºC) fumaroles (e.g., Taran et al., 1995). Nevertheless, a shift towards lower values is not necessarily a primary feature but may also be the result of preferential partitioning

among coexisting fluid phases in shallow volcanic environments.

Figure 5.8 shows a compilation of $\delta^{37}Cl$ compositions of terrestrial materials. Values generally scatter around 0‰, indicating that chlorine isotopes do not fractionate significantly relative to Earth's ocean water. The mantle $\delta^{37}Cl$ composition is rather controversial since values from < -3.0 to 0.0‰ have been proposed (Sharp et al., 2007; Bonifacie et al., 2008b; Layne et al., 2009; Sharp et al., 2013). The most significant fractionation occurs at low temperatures, making isotope signatures useful tracers of near-surface processes (Barnes et al., 2009; Sharp et al., 2010; Li et al., 2015). The most negative values have been found in marine pore waters and formation waters (Eggenkamp, 1994; Eastoe et al., 1999). Fumarolic gases and condensates from Poás and other volcanoes represent the opposite side of the range. They exhibit the most positive $\delta^{37}Cl$ values and the largest spread in the entire spectrum of terrestrial materials (Eggenkamp, 1994; Wahrenberger et al., 1997; Musashi and Eggenkamp, 2000; Barnes et al., 2008; Sharp et al., 2010; Rizzo et al., 2013). The following sections will discuss the possible origins of the observed temporal variations in Br/Cl ratios and $\delta^{37}Cl$ values observed in the lake water and fumarole condensates of Poás volcano. For both signatures, we will explore possible fractionation effects from magmatic processes, gas-liquid-solid interactions in shallow subsurface environments and from evaporation of the lake water body at the surface. Finally, we will discuss implications for volcano monitoring and surveillance.

5.5.1. Behaviour of halogens in magmas

Since chlorine and bromine have large ionic radii (Cl^- = 181 pm, Br^- = 196 pm), they cannot be easily accommodated into crystalline structures so that only a few minerals (e.g., sodalite and apatite group) are potential carriers of these elements. Therefore, both halogens tend to behave as incompatible elements in magmatic processes (Schilling et al., 1980; Villemant and Boudon, 1999). Additionally, large Cl and Br fractionations cannot be generated as a consequence of low-pressure fractional crystallization or partial melting (Schilling et al., 1980). Conversely, substantial differences in Cl contents between lava blocks and pumice clasts at Soufrière Hills volcano illustrate that the interaction between groundwater vapours with a lava dome can control Cl and probably Br variations (Harford et al., 2003). Lowenstern et al. (2012) demonstrated that large amounts of halogens can be released during near-surface crystallization of rhyolitic lavas. Fluorine, on the other hand, has a distinct behaviour. Because of its much smaller ionic radius (F^-= 133 pm), F is capable of substituting OH^- groups into major rock forming minerals (Luth, 2003) and therefore is much less efficiently extracted from magmas during degassing processes, compared to Cl and Br (Villemant et al., 2003; Balcone-Boissard et al., 2010). As a result, ratios of F over other halogens in magmatic gases are relatively low and variable, and the F/Cl ratios of a melt tend to increase with halogen degassing (Villemant et al., 2003; Wang et al., 2014). Since chlorine and bromine are extracted with similar efficiency, they do not show a significant fractionation from melts at high pressures by H_2O-rich fluids exsolved from magmas or during slow effusive magma degassing (Balcone-Boissard et al., 2010). In summary, the incompatibility of halogens during magma degassing can be expressed as Cl ≈ Br > F (Pyle and Mather, 2009; Wang et al., 2014).

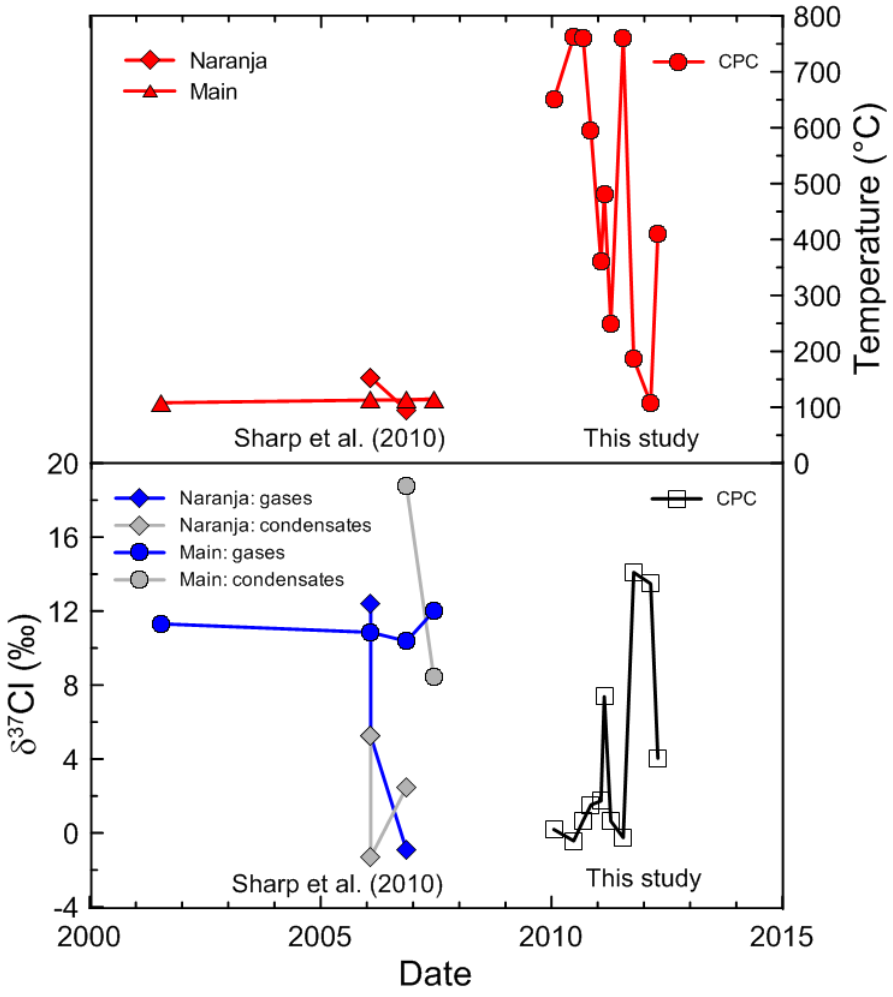

Figure 5.6. Times series of fumarole temperatures and $\delta^{37}Cl$ values of condensates for the CPC fumaroles (this study) in comparison with data for the Naranja and Main fumaroles on the eastern side of the crater (Sharp et al., 2010). The error bars for $\delta^{37}Cl$ do not exceed the size of the symbols.

To the best of our knowledge, there are no Cl and Br data from bulk lavas or melt inclusions from Poás volcano, which implies that there are no constraints regarding original magmatic Br/Cl ratios. Given the restricted range in subduction related calc-alkaline magmas (molar Br/Cl ratios between 0.0007 and 0.004, Balcone-Boissard et al., 2010), it is reasonable to assume a ratio on the order of 0.001. Chlorine and bromine are exsolved from degassing magmas as $HCl_{(g)}$ and $HBr_{(g)}$, respectively (Aiuppa, 2009). The abundances of these compounds in magmatic gases remain virtually intact when the magmatic gases rise to the surface as long as there is no significant interaction with shallow hydrothermal systems or aquifers (Symonds and Reed, 1993). When gases interact with shallow, low temperature aqueous systems, the halogen acids will usually be completely dissolved owing to their high aqueous solubilities (Symonds et al., 2001; Villemant et al., 2005), provided that the gas/wa-

ter ratio is not excessively high and that the system is able to attain equilibrium. For these reasons, our discussion will be oriented to fractionation between Br and Cl in near-surface processes, starting from the assumption that the magmatic Br/Cl signature at Poás falls within the range of subduction-related high-temperature gases and condensates worldwide.

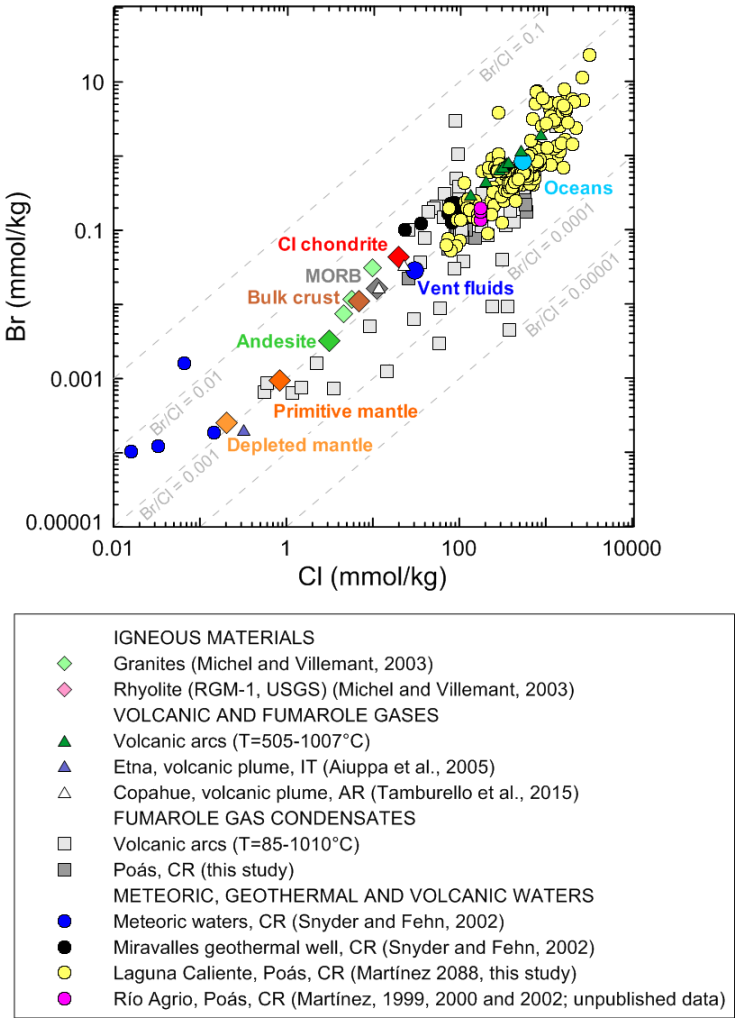

Figure 5.7. Compilation of Cl and Br contents of igneous rocks, volcanic gases and condensates, meteoric, volcanic and geothermal waters, CI chondrite and major terrestrial reservoirs. Data sources: CI chondrite (Palme and Beer, 1993), primitive mantle (Palme and O´Neill, 2007), depleted mantle (Schilling et al., 1980), MORB (Shinonaga et al., 1994), bulk crust (Rudnick and Gao, 2003), andesite (reference material JA-2) (Shinonaga et al., 1994), vent fluids (German and Von Damm, 2003), oceans (Bruland and Lohan, 2003), fumarole gases in volcanic arcs (Menyailov et al., 1986; Giggenbach, 1993, Shinohara et al., 1993; Symonds et al., 1996; Taran et al., 1995; Giggenbach, 1996; Hammouya et al., 1998), fumarole gas condensates in volcanic arcs (Gemmell, 1987; Symonds et al., 1987; Taran et al., 1995; Symonds et al., 1990; Goff and McMurtry, 2000).

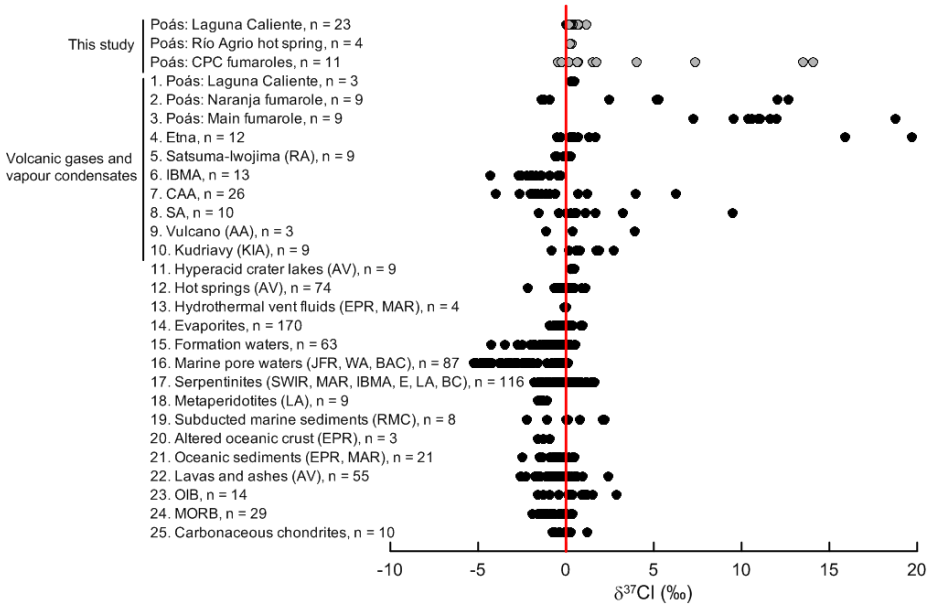

Figure 5.8. Compilation of $\delta^{37}Cl$ data from solid and fluid materials from various geological settings. MORB = mid-ocean ridge basalts, OIB = oceanic island basalts, AV = volcanic arcs, EPR = East Pacific Rise, MAR = Mid-Atlantic Ridge, RMC = Raspas Metamorphic Complex, LA = Ligurian Alps, SWIR = Southwest Indian Ridge, IBMA = Izu-Bonin Mariana Arc, E = Elba island, BC = Beltic Cordillera, JFR = Juan de Fuga Ridge, WA = West Atlantic, BAC = Barbados Accretionary Complex, KIA = Kurile Islands Arc, AA = Aeolian Arc, SA = Sunda Arc, CAA = Central American Arc, RA = Ryukyu Arc. References: (1,2,3) Sharp et al., 2010; (4) Rizzo et al., 2013; (5) Musashi and Eggenkamp, 2000); (6) Barnes and Sharp, 2008; (7) Sharp et al., 2010; (8) Eggenkamp, 1994; 9) Wahrenberger et al., 1997; (10) Wahrenberger et al. , 1997; Sharp et al., 2010; (11) Eggenkamp, 1994; Sharp et al., 2010; Rodríguez, 2014, unpublished data; (12) Eggenkamp, 1994; Musashi et al., 2008; Sharp et al., 2010; Rodríguez, 2014, unpublished data; Li et al., 2015; (13) Bonifacie et al., 2005; (14) Eggenkamp, 1994; Eastoe et al., 1999, 2007; Sharp et al., 2007; (15) Eggenkamp, 1994); Eastoe et al. (1999); (16) Hesse et al., 2000; Godon et al., 2004b; Bonifacie et al., 2007; (17) Barnes and Sharp, 2006; Barnes et al., 2006;2008; Bonifacie et al., 2008b; John et al., 2010; (18) Bonifacie et al., 2008b; (19) John et al., 2010; (20) Bonifacie et al., 2007; (21,22) Barnes et al., 2008; 2009; (23) John et al., 2010; (24) Boniface et al., 2008a; Sharp et al., 2007; (25) Sharp et al., 2013. The error bars for $\delta^{37}Cl$ do not exceed the size of the symbols.

5.5.2. Br-Cl fractionation due to vapour-liquid phase separation

There is an ongoing debate on the fractionation mechanisms that affect Cl and Br during vapour-liquid phase separation. Fluids from submarine hot springs at mid-ocean ridges typically have Cl concentrations and Br/Cl ratios that depart significantly from seawater values. Bruland and Lohan (2003) report, for seawater, Cl = 546 mmol/kg, and Br/Cl = 0.00154 (molar). For instance, hydrothermal fluids from the East Pacific Rise (EPR) at 9- 10°N have chlorine concentrations as low as 32.6 mmol/kg, while the lowest Br/Cl ratios (40% of seawater) were found in the low-salinity fluids (Oosting and Von Damm, 1996). Berndt and Seyfried (1990) suggested a combined effect of phase separation and halite precipitation or dissolution, since their experiments in the system NaCl-NaBr-H_2O could not explain the anomalous Br/Cl ratios values observed at mid-ocean ridges by simple subcritical phase sepa-

ration alone. On the other hand, fluid inclusions in sphalerite with Br/Cl ratios higher than twice that of seawater from the JADE field (Central Okinawa Trough, Japan) indicated a stronger effect of phase separation on Br/Cl ratios than predicted by experimental data. Halite precipitation could also produce high Br/Cl ratios but the observed co-variation with a significant $\delta^{37}Cl$ range argues against this explanation in view of the very little Cl isotopic fractionation between brine and halite (Lüders et al., 2002). Koschinsky et al. (2008) also reported relatively high Br/Cl ratios for hydrothermal vent fluids produced under subcritical or supercritical phase separation conditions at 5°S on the Mid-Atlantic Ridge. Liebscher et al. (2006) found a preferential partitioning of Br into the liquid in their experiments at 380 – 450°C and 229 – 417 bars. In contrast to the closed-system conditions of the experiments mentioned above, Foustoukos and Seyfried (2007) determined values for Br and Cl partitioning between vapour, brine and halite under extreme phase separation conditions using an open-system approach in a flow-through reactor (388 – 550°C, 244 – 351 bars, $pH_{25°C,1\ bar}$ = 3.5 – 6.9). Their results indicated a preferential partitioning of Br into the vapour phase. Considering this available evidence, the fractionation of Br and Cl due to phase separation is inconclusive. A significant difference between the experiments indicating a preferential Br uptake by the vapour (Berndt and Seyfried, 1990; 1997; Foustoukos and Seyfried, 2007) and the ones favouring a stronger partitioning into the liquid (Liebscher et al., 2006) is that the former were carried out in a more complex system than NaCl-NaBr-H_2O, containing additional components such as K, Ca, Li, Sr, Rb, B and Ba. We assume that results from such more complex systems are more applicable to the hyperacid brines of Poás volcano, given their elevated concentrations of dissolved rock-forming elements.

5.5.3. Br-Cl fractionation due to mineral precipitation

Precipitation of halite is a potential mechanism to fractionate halogens, with Br tending to remain in the fluid and Cl fractionating in the solid (Stoessell and Carpenter, 1986; Siemann and Schramm, 2000). However, even during Stage III when Cl and Br concentrations were the highest, they remained well below the saturation levels for halite, consistent with the absence of chloride precipitates in Laguna Caliente. Only potassium-bearing halite $K_{0.2}Na_{0.8}Cl$ has been found as a minor phase in sediments around the lake, presumably an evaporation product of acid brines expulsed from the lake during phreatic explosions. In view of its rarity and the intense rain fall in the summit area of Poás volcano, its existence will be transient and insignificant for any effective Cl-Br fractionation in the lake water. Zhao et al. (2014) found experimentally that jarosite $KFe_3(SO_4)_2(OH)_6$ can incorporate halogens when it precipitates from a Cl- and Br-bearing aqueous solution, and that the remaining solution becomes more depleted in Br due to preferential uptake of this anion by the mineral. Jarosite has been found on rock surfaces in the surroundings of Laguna Caliente as alteration product of basaltic andesites and acid rain or brine spray. Because of its inconspicuous abundance and absence of detectable Cl or Br in EPMA results, we discard a role of jarosite in controlling Cl/Br ratios in the lake water. Among the minerals that will be stable in the deeper and hotter parts of volcanic-hydrothermal system at Poás, alunite $KAl_3(SO_4)_2(OH)_6$ could have an effect on Br/Cl in associated brine water assuming if it would have a similar preference for Br com-

pared to jarosite. Since precipitation and re-dissolution of alunite has an influence on the chemistry of the lake water (Martínez, 2008), a role in the fractionation of Br and Cl is conceivable. In any case, further work is needed to test this hypothesis. Other halogen-bearing minerals that can potentially fractionate Br from Cl during their formation include amphiboles, scapolite and Fe-Mg hydroxyl-chlorides, as has been advocated for oceanic crust environments (Seyfried et al., 1986; Campbell and Edmond, 1989). In the absence of evidence for their presence in the subsurface of Poás, we consider a role of these minerals unlikely. In the following sections, the effect of phase separation and mixing of deep gases with shallow aquifers on Br-Cl fractionation will be discussed.

5.5.4. Br/Cl ratios in Laguna Caliente

Once the magmatic gases $HCl_{(g)}$ and $HBr_{(g)}$ reach a water body (lake or a subsurface aquifer), they dissociate into the correspondent anions Cl^- and Br^- according to the reactions:

$$HCl_{(g)} = HCl_{(aq)} \quad (2)$$

$$HCl_{(aq)} + H_2O = H_3O^+ + Cl^- \quad (3)$$

$$HBr_{(g)} = HBr_{(aq)} \quad (4)$$

$$HBr_{(aq)} + H_2O = H_3O^+ + Br^- \quad (5)$$

Considering the difference in the acid dissociation constants for reactions (3) and (5) at 25°C (log K equals 0.51 and 8.60, respectively; Johnson and Pytkowicz, 1978; Pokrovskii, 1999), $HBr_{(aq)}$ is a stronger acid and dissociates even more readily than $HCl_{(aq)}$ (Myers, 1976) if the system is able to attain equilibrium. In cases of extreme acidy, the equilibrium shift towards the left hand side of the equations will promote the formation of both $HCl_{(g)}$ and $HBr_{(g)}$. Therefore, given this dissociation difference between the acids, $HCl_{(g)}$ could form and escape preferentially from acid brines under circumstances of decreasing pH, leaving a relative Br-enriched solution. Evaporation of HCl fumes from Laguna Caliente occurs during periods of high activity and extremely low pH (Rowe et al., 1992a;b; Martínez, 2008; Rouwet and Ohba, 2015). Rouwet et al. (2016) used a mass balance approach to estimate the Cl concentration in the evaporation plume at 13,300 mg/l for the period 2005-2010, i.e. during the initial years of the active Stage V. This value falls in the range of Cl concentrations measured in the CPC fumarole condensates (Table 5.2). Hence, the increased Br/Cl ratios in the lake during the highly active Stage III could, at least partly, be associated with evaporative loss of $HCl_{(g)}$. It must be noted that many of the high Br/Cl values for Stage III are from samples taken when the lake had dried out, and represent small-volume hot pools that were more susceptible to evaporation effects.

An alternative explanation is that the elevated Br/Cl ratios observed during active periods had a deep origin and were created in a two-phase zone above the chilled margin of the magma body. Commonly, this will be a vapour-dominated zone in the

deeper parts and a liquid-dominated one at shallower depths (Rowe et al., 1992a), but shifts in the gas/liquid proportions in response to changes in the rate of magmatic degassing, temperature or open/closed system conditions are to be expected.

We explore the subsurface behaviour of the halogens using enthalpy vs. Cl and Br diagrams, which predict the concentrations in a deep fluid reservoir and the coexistence of vapour and liquid (Arnórsson, 2000), and calculate Br/Cl ratios for both phases based on vapour-liquid distribution coefficients from Berndt and Seyfried (1990). Reservoir temperatures required to compute the enthalpy and steam fraction are estimated by the Na-K geothermometer from Arnórsson et al. (1998), which is considered more reliable than SiO_2 or Na-K-Ca geothermometers in view of the abundant precipitation of amorphous silica and gypsum in the lake. Even though the temperatures calculated for the deep aquifer fluids (T=225-456°C) should be taken as crude approximations only, since the acid nature of the fluids questions an equilibrium with alkali feldspars on which the calibration of the Na-K geothermometer is based, these inferred temperatures exhibit similar trends compared to the measured surface temperatures of Laguna Caliente waters. The cold end-members of this plot are represented by the meteoric waters of Botos Lake (Snyder and Fehn, 2002) and hot springs on the eastern and north-eastern terraces of Laguna Caliente that were active from 1999 till 2006 (Martínez, 2008). Additionally, samples from Río Agrio hot spring water were included, which is assumed to correspond to the acid brine circulating through deeper parts of Poás volcanic system (Table 5.1).

According to the enthalpy vs. Cl and Br diagrams (Fig. 5.9) most of the water compositions from Stage III and V show an enthalpy excess, which can be explained by the presence of steam-rich fluids. Conversely, dominant processes during Stage II and IV were evaporation or steam loss and mixing with meteoric waters. Based on the concentrations inferred for the deep reservoir (Fig. 5.9), the approximate Br/Cl molar ratio of the magmatic component (i.e., parent fluid before boiling, evaporation and mixing with meteoric waters) is ca. 0.0016, close to the arc-type magmatic signature expected for Poás (see section 5.5.1). Calculated Br/Cl ratios are higher for the steam than for the liquid phase during Stages III and V (Fig. 5.10), when the lake was extremely active. Increased Br/Cl ratios in the lake can thus be anticipated if gaseous input predominates over liquid influx, i.e., at high gas/liquid ratios that will be promoted when the magmatic hydrothermal system is hot. The observed elevated Br/Cl ratios in the lake and pool waters during Stage III are consistent with this scenario. The eventual drying out of the lake is in line with a prevalent supply of volatiles in gaseous form and with an intense evaporation, both leading to increased Br/Cl ratios. Although Stage V samples also exhibit an enthalpy excess, indicating an increased gas/liquid ratio during the renewed phreatic activity, the absence of a rise in Br/Cl suggests that halogen input via liquid water was still sufficiently large to avoid a significant deviation from magmatic values as seen during Stage III. This supposition is supported by the observation that the lake did not disappear during Stage V despite its volume reduction.

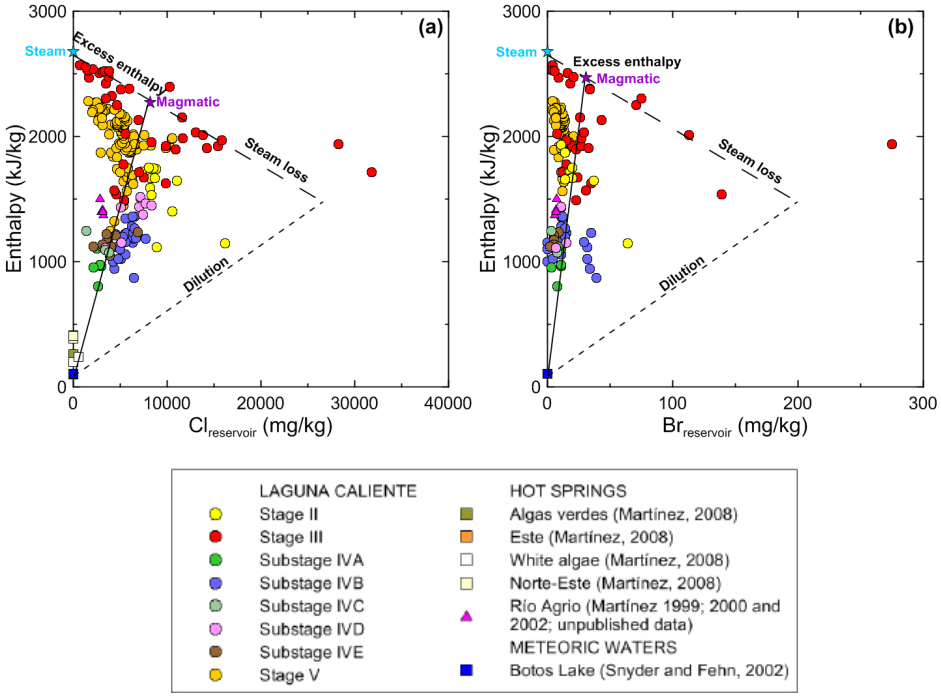

Figure 5.9. Enthalpy vs. Cl and Br diagrams for Laguna Caliente samples, hot springs within and outside (Río Agrio spring) the active crater and meteoric waters represented by Botos Lake.

5.5.5. Br/Cl ratios in the CPC fumaroles

Molar Br/Cl ratios in the CPC fumaroles are considerably more uniform than those of the lake and do not show a systematic change with time (Fig. 5.5). Absence of clear correlations with temperature, pH, $\delta^{37}Cl$ or other chemical parameters suggests that the original Br/Cl ratio of fumarolic gas is largely preserved, despite the tendency for a progressive loss of both halogens through absorption by water. The average molar Br/Cl ratio of 0.0008±0.0003 falls within the range of fumarolic values for arc volcanoes (Fig. 5.7) and compares reasonably well with the value of ca. 0.0016 inferred above for the magmatic component, taking the uncertainties into account. As will be discussed below, the chlorine isotope the data of the condensates show stronger fluctuations and seem more susceptible to gas-water interaction than the Br/Cl ratios.

5.5.6. Chlorine isotopes in magmatic systems

Arc-related magmatism is expected to have slightly negative $\delta^{37}Cl$ values considering the common contribution of subducted components (marine sediments and altered oceanic crust) to sub-arc mantle sources (Straub and Layne, 2003; Sun et al., 2007; Bonifacie et al., 2008a; Pyle and Mather, 2009; John et al., 2010). Nonetheless, there is considerable overlap between $\delta^{37}Cl$ data reported for arc volcanics and MORB. Theoretical calculations and experiments indicate that chlorine isotope fraction-

ation between minerals, melts and fluids at high temperatures (>400°C) is insignificant (Schauble et al., 2003; Liebscher et al., 2006; Czarnacki and Halas, 2012), since chlorine is incompatible and does not experience speciation changes during melting and crystallization processes (Richet et al., 1977; Schilling et al., 1980). Consequently, chlorine isotope fractionation during partial melting, magma degassing, hydrothermal alteration and weathering is minimal so that the isotopic composition of the source material will be largely preserved (Bonifacie et al., 2007; Barnes et al., 2008; Bonifacie et al., 2008a;b; Rizzo et al., 2013), with the possible exception when sorption processes in low-temperature aqueous environments play a role (Musashi et al., 2007).

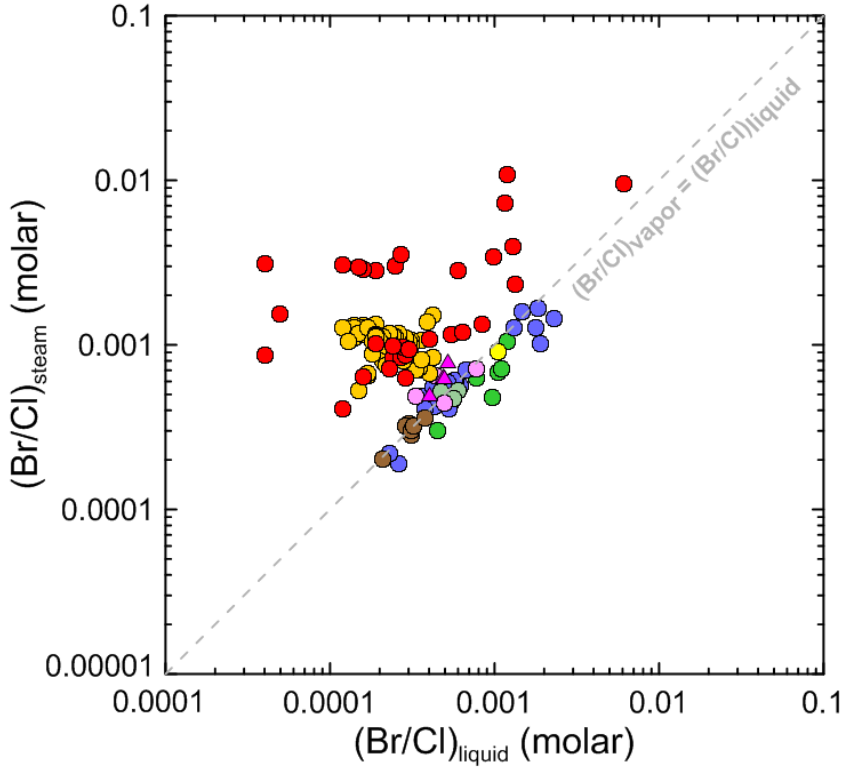

Figure 5.10. Calculated Br/Cl molar ratios for steam and liquid fractions for Laguna Caliente and Río Agrio spring, based on the relationships between enthalpy and halogen contents inferred for the deep reservoir (cf. Fig. 5.9) and the vapour-liquid distribution coefficients of Berndt and Seyfried (1990) operating during phase separation at depth. See texts for further explanation. The legend is the same as in Figure 5.9.

5.5.7. Chlorine isotope fractionation effects in Laguna Caliente.

The overall $\delta^{37}Cl$ signature of the lake water is similar to data from other hyperacid crater lakes (Fig. 5.8). The slightly positive values are equal to those of the high temperature gas condensates of the CPC fumaroles and fall in the range of island-arc volcanics (Figs. 5.4 and 5.8), which suggests that the Cl isotope composition of Poás lake water is close to that of the local magmatic gas. Input into the lake occurs di-

rectly via subaqueous fumaroles or through influx of brine from a subsurface water body that had interacted with high-temperature gases. The $\delta^{37}Cl$ variation in the lake water may either reflect changes in the input signature or be a result of fractionation accompanying loss of Cl from the lake. In experiments with concentrated hydrochloric acid, Sharp et al. (2010) found that evaporation resulted in a $\delta^{37}Cl$ increase in the remaining acid, since the escaping hydrogen chloride was preferentially enriched in ^{35}Cl. Evaporation of $HCl_{(g)}$, which is a relatively common feature for hyperacid lakes (Rouwet and Ohba, 2015; Capaccioni et al., 2016), is thus expected to enrich the Laguna Caliente water in the heavier ^{37}Cl isotope. When ignoring the data for Substages IVC and IVE (see below), $\delta^{37}Cl$ tends to correlate positively with temperature (cf., Fig. 5.4), which would hint at an evaporation effect, since HCl fumes have been noticed during periods when the lake temperature was high, and an evaporative loss of HCl has been predicted from a combined mass and Cl balance for a period overlapping Stage V (Rouwet et al., 2016). Still, evaporation effects on the $\delta^{37}Cl$ composition of the lake water will be minor and difficult to substantiate, given the large size of the dissolved Cl reservoir relative to the presumed evaporated amount, and the continuous supply of fresh brine and gas at the lake bottom. A significant chlorine isotope shift in the lake water due to evaporation may have been restricted to parts of Stage III when data represent isolated hot pools rather than a sizeable lake. Alternatively, the $\delta^{37}Cl$ variability of Laguna Caliente reflects temporal fluctuations in the mode of activity associated with magmatic volatile supply and/or changes in the gas-liquid ratio of the input. Increases in $\delta^{37}Cl$ that coincide with elevated chloride concentrations and temperature indicate that excess input of volatiles and heat into the lake produces a relative increase in heavy ^{37}Cl, presumably induced by the gas phase, in agreement with the frequent occurrence of phreatic eruptions during the active stages III and V. The alleged ^{37}Cl-enrichment is conceivable if pristine magmatic gas experienced scavenging before entering the lake water, and gaseous input was in excess relative to bulk supply through the combined input of gas and brine water.

In contrast, we attribute the relatively elevated $\delta^{37}Cl$ during the quiet Substages IVC and IVE to specific conditions in volatile transport. The low activity, reduced temperature and increased pH suggest that subsurface conduits were largely clogged (Martínez, 2008). Consequently, halogen supply was restricted to input of low-temperature gas and not (or much less) via influx of brine water. The data from the subaerial fumaroles on the CPC and eastern terraces (this work and Sharp et al., 2010) indicate that this low-temperature gas would have a high $\delta^{37}Cl$ signature (Fig. 5.6).

5.5.8. Chlorine isotope fractionation in the CPC fumaroles

A similar large range and strongly positive $\delta^{37}Cl$ values as observed in the CPC fumaroles also marked the Main and Naranja fumaroles on the eastern terrace (Sharp et al., 2010) that were active during Stage IV and the early years of Stage V, indicating that the CPC data are representative for tracing sources and processes governing the behaviour of halogens at Poás (Fig. 5.6). The extreme $\delta^{37}Cl$ values at the high end of the range are uncommon but are not unique to Poás. For instance, strongly elevated $\delta^{37}Cl$ values in gas and condensates up to +9.47±0.37‰, +19.7±0.2‰ and +6.39±0.12‰ have also been found at Lewotolo, Indonesia (Eggenkamp, 1994), Etna, Italy (Rizzo et al., 2013) and Santa Ana, El Salvador (Sharp et al., 2010), respec-

tively (Fig. 5.8).

According to experimental work and theoretical approaches, the equilibrium chlorine isotope fractionation between HCl gas and dissolved Cl^- in an associated aqueous solution is modest, reaching a maximum of ca. 1.5‰ between 50 and 100°C, with the gas phase being preferentially enriched in ^{37}Cl (Schauble et al., 2003; Sharp et al., 2010). The large $\delta^{37}Cl$ range in our fumarole samples and values up to +14.09±0.08‰ are therefore difficult to explain with simple equilibrium fractionation in a gas-liquid system. Furthermore, because the magmatic $\delta^{37}Cl$ signature is expected to be close to zero or slightly negative, mixing with another Cl source can be ruled out to explain the trend, as there are no know terrestrial reservoirs with a sufficiently positive signature to generate $\delta^{37}Cl$ values up to +15‰ or more. Since our data were obtained on condensates and not on samples of the entire fumarolic gas, a sampling bias is conceivable. However, $\delta^{37}Cl$ data on condensate and gas samples, collected from the east flank fumaroles at Poás on the same day (Sharp et al., 2010), provide no evidence for a systematic shift, as the isotopic compositions of condensates were equal, lower or higher than those obtained in the corresponding gases. The behaviour suggests that results from condensates approximate the signatures of bulk fumarolic gas as long as the entire Cl budget is captured during sampling. The $\delta^{37}Cl$ range must therefore be attributed to an alternative fractionation mechanism.

The inverse relationship between $\delta^{37}Cl$ and sampling temperature in the CPC data, together with the temperature decrease from 763 to 107°C between 2010 and 2012, favour a gradual change in the behaviour of the fumarole system over a period of approximately 2.5 years (Fig. 5.5). Also, when combining the CPC data with those of the 2001-2007 fumaroles with relatively low temperatures (95 to 153°C) on the eastern flank (Sharp et al., 2010), it appears that the spread in $\delta^{37}Cl$ increases with decreasing temperature (Fig 5.6). We attribute these tendencies to a transition from freely degassing magma with a near-primary $\delta^{37}Cl$ signature in a relatively dry pathway to a stronger interaction with more abundant water present in the shallow subsurface that created the ^{37}Cl-enrichment. Based on the results of flow-through experiments, Sharp et al. (2010) explained the high $\delta^{37}Cl$ values by a distillation process whereby recondensation of fumarolic gases on the conduit walls preferentially strips ^{35}Cl from the vapour. The authors argue that the liquid water on the wall must be continuously refreshed and dripping back in order to take up the large proportion of Cl required to create the high $\delta^{37}Cl$ in the remaining vapour. The time series for our CPC condensate samples also favours a preferential removal of ^{35}Cl by water but seems difficult to reconcile with a conduit-wall control alone, given the change in the fractionation magnitude with time. Instead, we attribute the temporal $\delta^{37}Cl$ increase in the CPC fumarole to an increase in the water/gas ratio during subsurface interaction with a water-rich body, which was promoted either by a decrease in the rate of magmatic degassing or by a larger supply of cool (meteoric) groundwater to a shallow aquifer. The roughly decreasing Cl and Br concentrations, decreasing temperature and increasing pH (Fig. 5.11), together with the correlations between $\delta^{37}Cl$ and temperature (R^2 =0.57) and 1/Cl (R^2 = 0.92) and 1/Br (R^2 =0.90) are consistent with more scavenging and thus support this scenario.

Musashi and Eggenkamp (2000) observed an opposite trend in fumarolic gases from Satsuma-Iwojima, i.e. an increase in $\delta^{37}Cl$ values with temperature, and suggested a possible influence of marine water in the low temperature samples, whereas the high temperature gas would have better preserved the isotopic composition of the magma source. A marine influence is unlikely for the CPC fumarole signatures, given Poás position in the Central Cordillera, away from any coast.

5.5.9 Halogen ratios and $\delta^{37}Cl$: implications for volcano monitoring at Poás

The temporal evolution of halogen concentrations in hydrothermal springs and fumaroles is a potential indicator of subsurface magmatic activity (Ohba et al., 1994; Villemant et al., 2005; Aiuppa et al., 2009; Villemant et al., 2014). However, concentration changes do not necessarily signal magma degassing, since they can also be controlled by non-magmatic processes such as evaporation, condensation, interaction with halogen-bearing lithologies, minerals or both deep and surface fluids. Chlorine isotopes may be more adequate if the Cl budget in spring water or fluids is a mixture of a magmatic contribution and one or more sources of shallow, non-magmatic origin (e.g., groundwater or seawater), and if their respective $\delta^{37}Cl$ signatures are sufficiently constrained. For example, Li et al. (2015) used a difference between local magmatic fluid (-0.65‰) and meteoric and seawater Cl (ca. 0‰) to test the applicability of $\delta^{37}Cl$ in thermal springs as monitor of the levels of magmatic Cl in the shallow hydrothermal systems of La Soufrière (Guadeloupe) and Montagne Pelée (Martinique). They inferred that magmatic Cl has a relatively short residence time of <30-80 years in arc volcanic springs and that Cl isotopes are particularly useful for monitoring systems that are infrequently active at centennial scale. Villemant et al. (2005) found that the halogen concentrations of the thermal spring waters of La Soufrière provide a record of magmatic degassing pulses that are delayed as a function of distance to the source. They associated intermittent Cl injections with the shallow intrusion of a magma body, invoking decompression-induced degassing during magma emplacement and a subsequent step degassing regime controlled by magma cooling and crystallization that lasted ca. 15 years since the seismo-volcanic crisis of 1976–1977. Renewed seismic activity in 1992, marking the onset of increasing gas flux and possibly recording the emplacement of fresh magma, ultimately resulted in increase in Cl in only one of the springs ca. a decade later (Villemant et al., 2014).

Our findings at Poás volcano further demonstrate that active processes in a vapour liquid system between intruded magma and the surface can be monitored if the compositions of lake water and fumaroles (Cl, Br concentrations, Br/Cl ratios and $\delta^{37}Cl$) are recorded over longer periods of time. Rises in Cl and Br contents in Laguna Caliente usually signal an increased supply of these volatiles from the magma source, either due to a new intrusion or by opening up new pathways, for example when volatiles pass freshly formed cracks in a solidified envelope of an earlier emplaced magma batch. Elevated Cl and Br contents in Laguna Caliente during Stage III and V indicate that this has repeatedly happened in the last decades. In both cases, an initial rise in Cl and Br concentrations (Fig. 5.3), as well as in F, SO_4 and polythionates (Martínez, 2008), accompanied by an increasing temperature and decreasing pH, preceded the onset of a period of phreatic eruptions of the

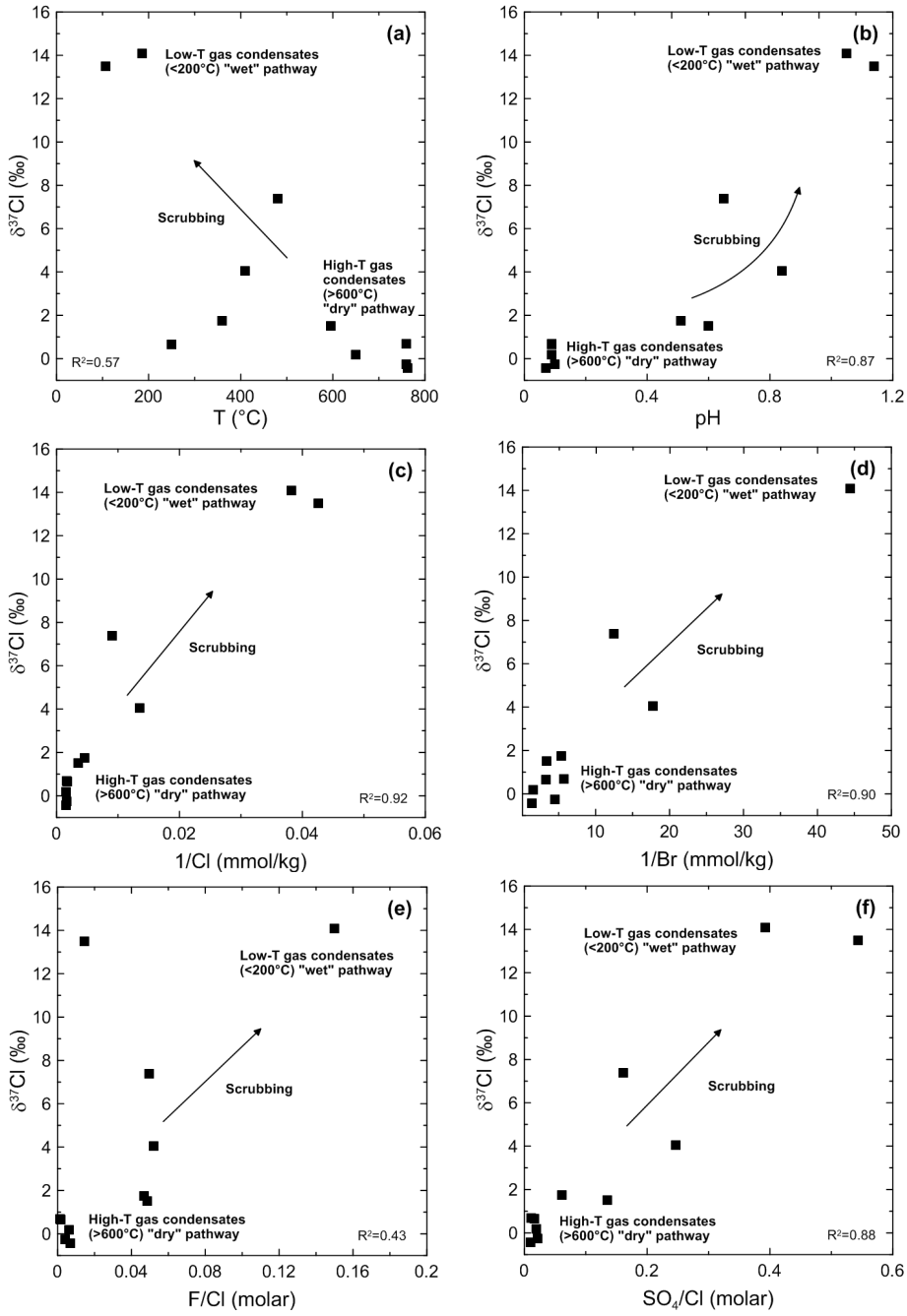

Figure 5.11. Relationships between $\delta^{37}Cl$ and temperature, pH, 1/Cl, 1/Br, F/Cl and SO_4/Cl for CPC fumarole condensates, showing the effects of scrubbing. Increasing water/gas ratios during subsurface interaction correspond to a shift from a "dry" to a "wet" pathway. The $\delta^{37}Cl$ error bars do not exceed the size of the symbols.

lake. The Br/Cl ratios in Laguna Caliente may largely reflect the proportion of gaseous versus liquid-water input derived from the two-phase subsurface system. The relatively low Br/Cl ratios during Stage V are close to magmatic values, which points to bulk volatile supply from both gas and liquid without significant fractionation. The contrasting high Br/Cl ratios of Stage III are mainly from isolated pool waters sampled when the lake had dried out, and may therefore not be representative for the system at large. However, in the first years when the lake was still intact and its volume decreased, a gradual increase in Br/Cl accompanied the concentration increase of both halogens (Fig. 5.3). We attribute this apparent Br excess to a predominance of gaseous over liquid input into the lake, whereby vapour was derived from boiling (phase separation) at depth. Interestingly, the Cl concentrations in the lake water started to decline earlier than Br (Fig. 5.3), marking the onset of HCl evaporation when the pH had reached sufficiently low values (see section 5.5.4). Monitoring the $\delta^{37}Cl$ values in the lake provides information on the mode of volatile supply (gas versus liquid input) and on the relative proportions of interacting gas and water in the hydrothermal system where the magmatic volatiles are processed.

Sensible interpretations of the Cl isotope signals can only be achieved in combination with other monitored parameters. Base line values will be low (close to 0‰), which will be the case when the original magmatic signature is entirely transferred to the lake through the combined supply of gas and liquid from the hydrothermal system. A rise in the lake's $\delta^{37}Cl$ values is likely to record an excess input of gas that is previously enriched in ^{37}Cl during interaction with water within the edifice. This may occur during periods of high activity as well as during extremely quiet intervals. In the first case, the $\delta^{37}Cl$ rise will be accompanied with increasing temperature, Cl and Br concentrations, together with decreasing pH and lake volume, following the arrival of new magma or a prominent change in subsurface conditions that enhanced the transport of heat and volatiles such as rock fracturing or rupturing of the solidified shell of an older, cooling intrusion. Alternatively, when the $\delta^{37}Cl$ rise is associated with decreasing temperature, Cl and Br concentrations and increasing pH and lake volume, the internal porosity and permeability is reduced to such an extent that brine input is prevented and volatile supply is restricted to gas input only.

Geochemical modelling has shown that scrubbing of magmatic gas by subsurface water has a strong influence on the rate and composition of fumarolic gas emissions of "wet" volcanoes (Symonds et al., 2001; Marini and Gambardella, 2005). Interaction with a water body will affect primary magmatic gas components to a different extent, depending on their respective solubilities in aqueous systems and on the gas/water ratio. Hence, the presence of water within the edifice of Poás poses limitations to the monitoring of fumarolic gas species with the purpose of detecting the intrusion of magma at an early stage. Instead, our findings indicate that monitoring the $\delta^{37}Cl$ signals as well as Cl and Br contents together with F/Cl and SO_4/Cl ratios in condensates from the CPC fumarole provides information on the status of the subsurface two-phase system, in particular the extent of interaction with liquid water that magma-derived gas experiences en route to the surface. A "dry" pathway is indicated by the combination of low $\delta^{37}Cl$, high temperature, high Cl and Br concentrations, and low F/Cl and SO_4/Cl ratios (Fig. 5.11). Conversely, high $\delta^{37}Cl$ values,

accompanied with low temperatures and Cl and Br concentrations, as well as high F/Cl and SO_4/Cl ratios, point towards extensive interaction with liquid water before the fumarolic gas reaches the surface, indicating a "wet" pathway. The positive correlations between $\delta^{37}Cl$, F/Cl, SO_4/Cl and pH, and inverse correlations with Cl and Br concentrations and temperature (Fig. 5.11) are consistent with a scrubbing control, in agreement with thermochemical modelling results (Symonds et al., 2001) and the predicted fractionation behaviour of the Cl isotopes (Sharp et al., 2010). Therefore, the time series for the 2.5 years period covered by our data suggests a gradual wetting of the system (Fig. 5.5). Following these systematics, the opposite sequence (decreasing $\delta^{37}Cl$, SO_4/Cl and F/Cl, increasing temperature, Cl and Br concentrations) would be a signal of system dry-out, which may precede a magmatic eruption. We infer that a predominant influx of brine water during repose intervals produces $\delta^{37}Cl$ and Br/Cl ratios that largely coincide with magmatic values, which can be explained by complete condensation of the deep gases coming from a degassing magma body without any significant phase separation.

The input sources and processes that regulate the shallow lake-hydrothermal system at Poás volcano can be deduced when combining $\delta^{37}Cl$ signatures of Laguna Caliente and CPC fumaroles with S_T/Cl (lake water) or SO_4/Cl (gas condensates) ratios, taking temperature and status of activity into account (Fig. 5.12). The primary magmatic source is represented by the composite high-T (>600°C) Poás gas end-member, having a S_T/Cl ratio defined by an average of CPC high-T gas, and a $\delta^{37}Cl$ value corresponding to the average for condensate samples. Compared to this magmatic gas composition, the CPC high-T condensate has a significantly lower SO_4/Cl ratio due to loss of sulphur, which precipitates when the gas cools down and interacts with water. The low-T (<200°C) CPC condensates with high $\delta^{37}Cl$ values represent scrubbed gas that already interacted with a shallow water body before reaching the surface. The acid hot spring water of Río Agrio is taken as analogue of brine water from within the volcanic edifice that also feeds the lake. In this simplified scheme, the lake water composition can be created by input from a combination of these end-members. During most of the time covered by our data set, the lake composition was close to brine water, suggesting that this is a dominant input source. Strongest deviations are seen during Stage III and Substage IVC when increased $\delta^{37}Cl$ suggest a prevailing input of ^{37}Cl-enriched gas that had experienced subsurface scrubbing. During the active Stage III, excess gas input is consistent with the occurrence of phreatic eruptions. Evaporation of HCl, driven by the lowered pH and temperature rise due to the large input of volatiles and heat, also contributed to ^{37}Cl-enrichment in the lake water. For the quiet Substage IVC, when the system was cool and conduits were largely clogged, the $\delta^{37}Cl$ increase can be attributed to a reduced supply of brine water, and input being restricted to low-T gas. The samples from Stage V with the highest S_T/Cl ratios point to an input of high-T gas in addition to brine, in agreement with the high activity and frequent occurrence of phreatic eruptions during this period.

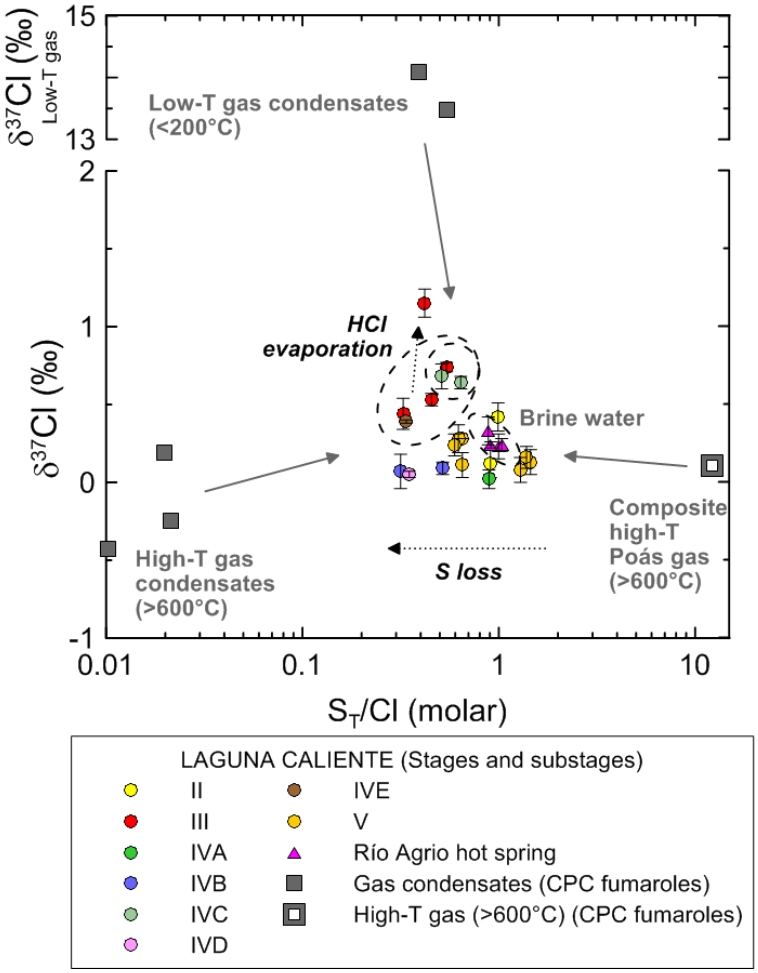

Figure 5.12. Input sources and processes responsible for the composition of Laguna Caliente, inferred from relationships between $\delta^{37}Cl$ values and molar S_T/Cl ratios. The lake compositions can be made up via input of (1) brine water, represented by the water from Río Agrio hot spring, (2) high-T magmatic gas, (3) high-T gas condensates and (4) low-T gas condensates, which are all represented by data from the CPC fumaroles. The composite high-T gas (>600°C) is an average of chemical compositions from OVSICORI (unpublished data) and $\delta^{37}Cl$ values from this study. The gas condensates have experienced loss of sulphur relative to the composite high-T gas, which resulted in lower S_T/Cl ratios (here as measured SO_4/Cl ratios). Note that variations in lake compositions can be explained by shifts in the proportions of the input sources that correspond to the activity sub(stages) defined by Martínez (2008), see text for details. The $\delta^{37}Cl$ error bars in gases and gas condensates do not exceed the size of the symbols.

5.6. CONCLUSIONS

Temporal changes in $\delta^{37}Cl$, Cl-Br concentrations and Br/Cl ratios in the hyperacid water of Laguna Caliente (1985-2012) and subaerial fumaroles (2010-2012) reflect variations in the mode and magnitude of volatile supply. Most of the variations can be attributed to the interaction between magma-derived gas and liquid water in the

volcanic-hydrothermal system below the crater.

The $\delta^{37}Cl$ variations in the lake water are moderate (between 0.02±0.06‰ and 1.15±0.09‰) and are associated with changes in the input and output of Cl-bearing fluid phases. The lowest values, which likely approximate magmatic signatures, result from Cl supply through brine influx or high-temperature (>600°C) subaqueous fumarolic activity. High values correspond to periods either when water temperatures were high (>60°C) and the budget of dissolved Cl was influenced by $HCl_{(g)}$ evaporation, or when input was probably restricted to low-temperature (<200°C) gas condensates. A relatively strong Br/Cl diversity is recorded in the lake water. Lowest Br/Cl ratios are presumably close to values of primary gaseous emissions from cooling magma, whereas elevated ratios are either due to preferential input of Br-enriched steam originating from phase separation/boiling at depth, and/or to loss of Cl through evaporation of $HCl_{(g)}$ from the lake surface.

Changes in $\delta^{37}Cl$ and halogen contents of fumarole condensates can be explained as a result of subsurface interaction between deeply derived gas and shallow liquid water. A large range in $\delta^{37}Cl$ (from -0.43±0.09‰ to +14.09±0.08‰) is attributable to partial scavenging and fractionation, with highest values, together with lowest temperatures and Br-Cl concentrations, being generated when the gas/water ratio is low and scavenging is most effective. Our data thus corroborate the earlier result of Sharp et al. (2010) that the absence of an aqueous phase in the system is often expressed by low $\delta^{37}Cl$ in high-temperature fumaroles.

Our findings at Poás volcano demonstrate that combined monitoring of $\delta^{37}Cl$ and Br-Cl signatures of fluids over longer periods of time provides insights into active processes in the vapour-liquid system between intruded magma and the surface as well as into the input-output controls that regulate the behaviour of the lake.

ACKNOWLEDGEMENTS

We are grateful to OVSICORI-UNA colleagues, especially Erick Fernández, Jorge Barquero, Geoffroy Avard and Jorge Brenes for providing most of the samples and invaluable help during field work. Our thanks go also to Arnold van Dijk for measuring the samples in the gas mass spectrometer at Utrecht University. The manuscript benefited from careful reviews by Maarten de Moor and an anonymous reviewer. Funding for this work was provided by NWO (Netherlands Organization for Scientific Research), project ALW-GO-PL/10-03.

CHAPTER

6

Experimental evaporation of hyperacid brines

ABSTRACT

The hyperacid brines from active volcanic lakes are one of the most chemically complex aqueous solutions on Earth and represent valuable samples in order to assess the elemental transfer processes from a magma body to the surface. Additionally, hyperacid brines have been a mayor alteration path on Mars. This paper describes the changes in chemical and $\delta^{37}Cl$ compositions observed in an evaporation experiment that lasted 1750 hours, using hyperacid brines from the active lake of Kawah Ijen volcano, Indonesia. Anions such as HSO_4^-, Cl^- and F^- are commonly forming complexes with cations such as Na^+, K^+, Ca^{2+}, Fe^{2+}, Mg^{2+}, Al^{3+} and Fe^{3+}; therefore increasing the solubility of these metals. A direct consequence of this effect is that the precipitation of sulphates and halides is probably inhibited for longer times during an evaporative process. The secondary phases formed during the experiment were anatase ($a_{H2O} \leq 0.95$), anhydrite ($a_{H2O} \leq 0.86$) and hydrogen chloride ($a_{H2O} \leq 0.86$). Nevertheless, evaporation simulations predict the formation of elemental sulphur at lower water activities ($a_{H2O} \leq 0.58$) as well the elemental fractionation between Br-Cl and S_T-Cl. Additionally, the presence of similar hyperacid brines on Mars´ surface could extend the liquid water stability down to 183 K (-90.15°C). Chlorine isotope fractionation of hyperacid brines follows the Rayleigh distillation process. The calculated fractionation factors between $HCl_{(g)}$ and dissolved Cl after 499 hours (1000 ln $\alpha_{HCl(g)\text{-}Cl_{diss.}}$= -5.67±0.17‰ to -3.97±0.08‰) are in agreement with the values reported in literature. However, before 499 hours, the evaporating $HCl_{(g)}$ is isotopically heavier than the dissolved Cl in the brine (1000 ln $\alpha_{HCl(g)\text{-}Cl_{diss.}}$ = +1.55±0.49‰ to +3.37±1.10‰). If hyperacid brines with similar chemical composition with respect to the ones from this study exist on Mars, evaporation processes up to the extent reported here (a_{H2O} = 0.85), would give a positive $\delta^{37}Cl$ signature to them (+0.68±0.05‰).

Front picture: Kawah Ijen crater lake, Java (Indonesia). A permanent solfatara is present on the south-eastern border or this hyperacid lake. Photo taken by M.J. van Bergen.

6.1. INTRODUCTION

The former presence of SO_4-Cl hyperacid brines on Mars has been considered as a major requirement for the formation of sulphate- and chloride-rich mineral assemblages currently found on its surface (Brass, 1980; Clark and Van Hart, 1981; Clark et al., 2005; Tosca and McLennan, 2006; Osterloo et al., 2008; 2010). Brines are particularly relevant because large amounts of dissolved components could strongly increase the stability of liquid H_2O on Mars by depressing the freezing point and extending its P-T field. Furthermore, minerals formed as result of evaporation or freezing processes might be an important H_2O-sink on Mars´ surface and could have played a major role in controlling acidity and salinity of Martian paleofluids and hence the habitability on the planet . Investigating changes, in chemical and isotopic compositions of hyperacid brines induced by evaporation could provide useful information to infer conditions under which sulphate- and chloride-bearing minerals could have formed in the presence of these fluids on Mars.

Evaporation is a major process in active volcanic lakes where it contributes to an increase in the concentration of total dissolved solids and decreases the abundances of volatile species. Many crater lakes hosted by active volcanoes are hyperacid brines, which are complex aqueous solutions from a chemical point of view. Because the composition of volcanic lake water is influenced by multiple processes, it is difficult to single out the effect of evaporation from studies in natural settings. For this purpose, laboratory experiments under controlled conditions are preferred. This chapter describes the effects of evaporation on the chemical and Cl-isotopic composition of a hyperacid sulphate-chloride brine at 60°C.

The brine water used in the experiment comes from the hyperacid lake of Kawah Ijen, an active andesitic volcano located at the rim of Ijen caldera, the easternmost volcanic complex on Java, Indonesia. The Kawah Ijen crater lake is one of the world's largest bodies of natural hyperacid brine, and is characterized by a high load of dissolved elements (often >100 g/l), very low pH (<1) and high concentrations of chlorine (often >2000 ppm), sulphate (often >60,000 ppm) and rock-forming elements (Delmelle and Bernard, 1994; Delmelle et al., 2000; Van Hinsberg et al., 2010).

6.2. METHODS

6.2.1. Evaporation experiment

The brine solution used in this experiment comes from a batch of approximately 15 litres of Kawah Ijen lake water, collected on October 30th, 2002. Upon storage for many years, amorphous silica and gypsum had precipitated at the bottom of the bottles. For this reason, the total amount used for the evaporation experiment (1.4 l) was filtered through a 0.2 μm pore size cellulose acetate membrane. A total of 26 plastic Greiner® tubes were filled with approximately 50 ml of this filtered crater-lake water, and were collectively placed on a plastic rack that was partially

submerged in a water bath at 60°C. The initial weight of all samples was recorded before the evaporation experiment started. The experiment lasted 1750 hours (73 days) during which duplicate samples were removed from the water bath at certain time intervals. Directly after removal, the final weight, pH and electrical conductivity, measured at room temperature (20±1°C), were determined for each sample. Next, six aliquots of approximately 1.6, 0.6 and 0.2 grams were diluted 10, 25 and 100 times with deionised water for IC (ion-chromatography) analysis; and 10, 25 and 100 times with 2% Suprapur® HNO_3 solution for ICP-OES (inductively coupled plasma optical emission spectrometry) analysis. Towards the end of the evaporation experiment, some samples had to be further diluted up to 650 times for IC analysis. Four control samples of deionised water (blanks) were used to check for vapour contamination coming from the lake-water samples. The pH and conductivity measurements were performed with a WTW® 3430 portable multimeter at room temperature (20°C). The pH electrode was calibrated with pH 1, 4 and 7 buffers. The conductivity electrode was calibrated with a 0.01 M KCl standard. Both electrodes were calibrated before every measurement.

6.2.2. Analytical methods

6.2.2.1. Major elements

The fluoride concentrations were determined by ion chromatography (IC), using a Dionex® ICS-3000, equipped with a Dionex®IonPac® AS 19 column. A gradient elution of 10 – 50 mM KOH was utilized. Total sulphur, Cl, Al, B, Br, Ca, Fe, K, Mg, Mn, Na, P, Si, Sr, Ti, V and Zn were analysed by inductively coupled plasma optical emission spectrometry (ICP-OES) with a Spectro® Ciros® instrument. All the aforementioned analyses where carried out at the Department of Earth Sciences, Utrecht University.

6.2.2.2. Chlorine isotopes

Samples for $\delta^{37}Cl$ analysis were prepared following a variation of the method described by Eggenkamp (1994). Based on the Cl concentrations determined by ICP-OES, an aliquot of an undiluted sample from the evaporation experiment was treated with 4 ml of 1 M KNO_3, 1 ml of H_2O_2 (30 wt.%) and 1 ml of concentrated HNO_3 (65%). Then it was heated to 80°C for 30 minutes before 1 ml of 0.2 M $AgNO_3$ was added. In this way, approximately 10 mg of AgCl precipitated from each sample, which was collected after filtering through a Whatman® type GF/F glass fibre and dried overnight at 80°C. Subsequently, the AgCl was reacted with iodomethane (CH_3I) in order to form chloromethane (CH_3Cl) at 70 - 80°C during 48 hours in vacuum glass ampoules. The chloromethane was separated from the excess CH_3I by gas chromatography using a 75 cm long, 6.35 mm OD SS column, filled with Porapak® Q 80-100 mesh at 140°C with helium as carrier gas. The analyses of CH_3Cl were carried out on a VG SIRA 24 EM mass spectrometer at the Department of Earth Sciences of Utrecht University.

Chlorine isotope data are reported as a delta notation ($\delta^{37}Cl$) using a reference sample of sea water from the Atlantic Ocean collected near Madeira in 1982. This sample is known as the Standard Mean Ocean Chloride or SMOC (Kaufmann, 1984). The analytical precision was ±0.16‰ (1σ) based on long-term analyses of this standard.

$$\delta^{37}Cl = \frac{\left(^{37}Cl/^{35}Cl\right)_{sample} - \left(^{37}Cl/^{35}Cl\right)_{SMOC}}{\left(^{37}Cl/^{35}Cl\right)_{SMOC}} \times 1000 \qquad (1)$$

6.2.3. Geochemical modelling

The geochemical modelling software PHREEQC, version 3.1 (Parkhurst and Appelo, 1999), was used to calculate aqueous species distributions and mineral saturation states. The Lawrence Livermore National Laboratories thermodynamic database (llnl.dat) was used. Additionally, ion interaction parameters from many ion pairs were included (Pitzer and Mayorga, 1973). The pH values at 60°C were recalculated by charge balance with PHREEQC, this approach has been recommended for extremely acid waters (Nordstrom et al., 2000).

6.3. RESULTS

6.3.1. Evaporation rates

The total duration of the evaporation experiment was 1750 hours (~73 days). The weight loss of the brine virtually stopped after 1340 hours (samples 12 and 13) when a maximum of 58% was reached. Weight loss measurements on the blank, consisting of deionised water, did not cover the entire experiment because of the strong evaporation. The last sample was taken just after 594 hours (82% of weight loss) (Fig. 6.1; Table 6.1). Evaporation rates were calculated taking the transversal area of the Greiner® tubes (0.0601 dm^2) into account. Both brine and blank exhibited a decrease in evaporation rates throughout the experiment. In particular at 400 hours, the brine showed a marked decrease (from 1.01 to 0.83 $g/h/dm^2$), after which there was a smooth decline until the end of the experiment.

6.3.2. Chemical composition, mineral saturation states and speciation in the brines

The brine water of Kawah Ijen has a hyperacid SO_4-Cl composition as a result of the condensation of magmatic SO_2 and HCl gases in water of largely meteoric origin. The acidity comes mainly from HSO_4^- dissociation, together with contributions of $HCl_{(aq)}$, $HF_{(aq)}$ and $HBr_{(aq)}$. Because of the strong acidity, the fluid contains high concentrations of rock-forming elements such as Ca, Al, Fe, Mg, Na, K and Si derived from dissolution of volcanic rocks. At the start of the experiments, the initial concentrations of total sulphur (S_T), Cl, F, Br, Al, Fe, K, Na, Ca, and Mg in the brine were 21,800; 22,100;1410; 56; 5730; 1970; 1230; 1110; 690 and 690 mg/kg, respectively.

Total dissolved solids (TDS) were 96 g/kg and pH 0.10 (20±1°). At the end of the experiment, upon 58 wt.% of evaporation, the final concentrations were (in the same order): 52,400; 45,900; 3110; 124; 13,800; 4920; 2920; 2610; 700 and 1630 mg/kg. The total dissolved solids increased up to 234 g/kg, and pH decreased down to -0.41 (20±1°) (Table 6.2).

In order to explore elemental losses by mineral precipitation or evaporation of volatile phases, measured concentrations were plotted against calculated concentrations assuming evaporative loss of pure water only. A significant departure from the equivalent line (expressing a 1:1 ratio for measured and calculated concentrations) would indicate if an element is conservative or non-conservative during the evaporation process. If an element plots above the equivalent line, it has become depleted in the solution through mineral precipitation or volatilization.

Measured Cl concentrations are lower than predicted from H_2O loss, with a tendency of increasing departure with time (Fig. 6.2), which points to escape of $HCl_{(g)}$ from the evaporating brine, even though $\log f_{HCl}$ values only approached equilibrium after more than 800 hours (Fig. 6.4a). Acicular crystals were observed from sample 10 (762 hours) onward until the end of the experiment. There was not enough sample for XRD determinations, but the observed decrease in calcium together with the extremely high total sulphur concentrations, indicate that the mineral was Ca-sulphate, presumably anhydrite $CaSO_4$ because of the 60°C temperature at which the experiment was performed (Fig. 6.3f). Although the models suggest undersaturation of anhydrite throughout the experiment (Fig. 6.4b), the initial rise of the saturation index, followed by a flattening of the trend (or minor decrease), suggests that saturation was reached at some point between samples 9 and 10 (594 - 732 hours).

The behaviour of strontium supports the formation of anhydrite. Lower measured concentrations than predicted (Fig. 6.3n) can be attributed to substitution of celestine $SrSO_4$ in anhydrite, since Ca-sulphate can take up large amounts of Sr (e.g., Grahmann, 1920; Steward, 1968). The deviation for silicon (Fig. 6.3m) is probably due to precipitation of amorphous silica. Although this phase theoretically reamained undersaturated (Fig. 6.4b), the saturation index shows an increase until approximately 600 hours, followed by a decrease. Calculations using the solubilities reported by Gunnarsson and Arnórsson (2000) confirm that this phase remained undersaturated during the experiment. It should be noted that Ijen crater-lake water is commonly saturated in amorphous silica (Delmelle and Bernard, 1994; Delmelle et al., 2000). The initial silica-undersaturation in the experiments can be explained by precipitation of silica during long-term storage of the sample at room temperature, i.e. much lower than the experimental temperature of 60°C.

The saturation states of mineral and gaseous phases of interest can be described as follows. The fugacity of $SiF_{4(g)}$ augmented steeply and then flattened off, without approaching saturation levels (Fig. 6.4a). Likewise, the fugacity of $HBr_{(g)}$ increased

steadily during the experiment but always remained far from saturation (Fig. 6.4a).

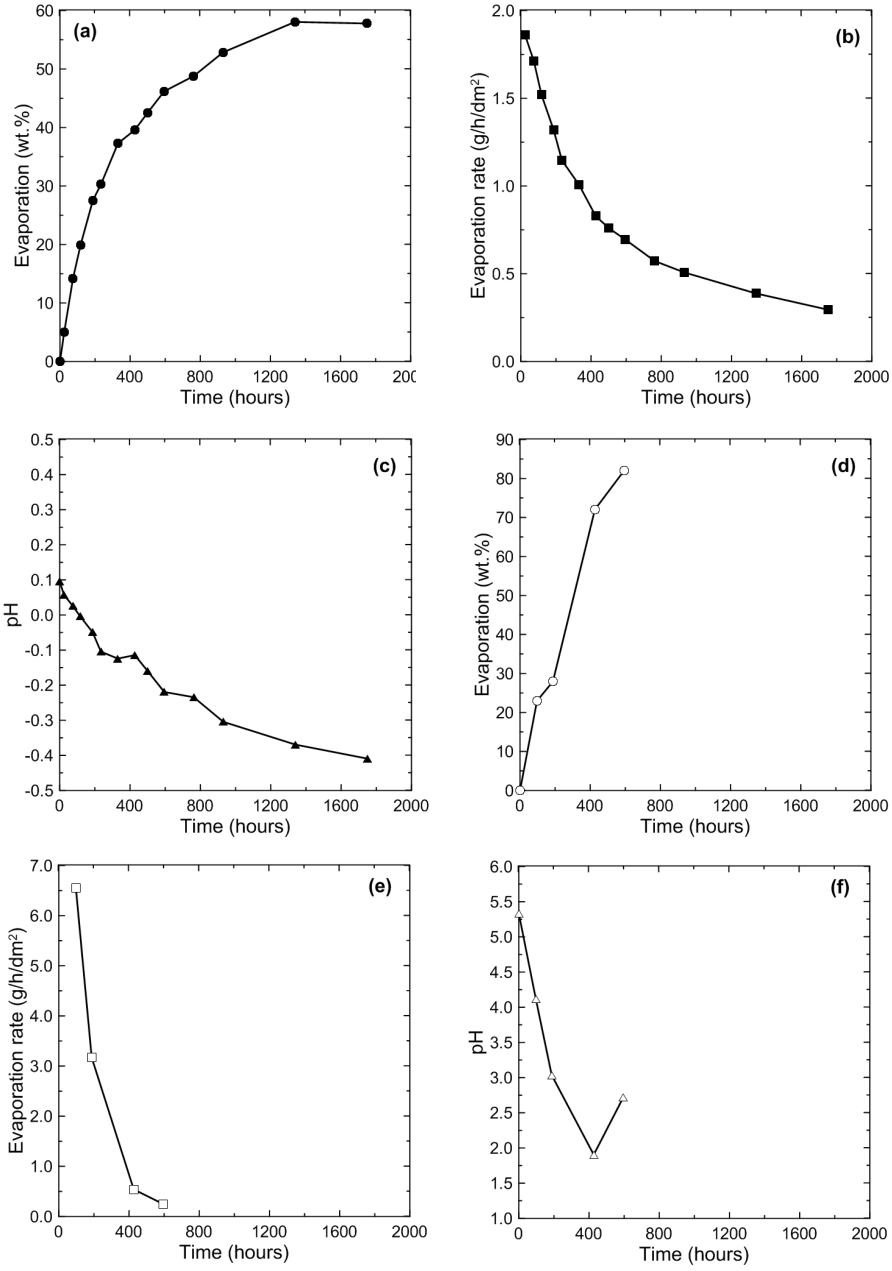

Figure 6.1. Evaporation losses (wt.%), rates (g/h/dm^2) and pH in the course of experimental evaporation of the Kawah Ijen hyperacid brine. Results for experiments on deionized water, used as blank, are shown as well (open symbols).

Table 6.1. Results of the evaporation experiment on the hyperacid Kawah Ijen brine.

Sample	Time (h)	pH (20±1°C)	EC (mS/cm) (20±1°C)	$W_{initial}$ (g)	W_{final} (g)	W_{loss} (g)	Evaporation (wt.%)	Evaporation rate (g/h/dm²)
0	0	0.10	283	n.d.	n.d.	n.d.	n.d.	n.d.
1	24	0.06	288	53.7677	51.0734	2.6944	5.01	1.86
2	74	0.03	308	53.7424	46.1068	7.6356	14.21	1.71
3	117	-0.01	322	53.8037	43.0863	10.7175	19.92	1.52
4	187	-0.05	342	53.7731	44.5965	9.1765	27.52	1.32
5	234	-0.11	351	53.1711	37.0523	16.1189	30.31	1.15
6	331	-0.13	367	53.7166	33.6840	20.0326	37.29	1.01
7	427	-0.12	376	53.6621	32.4211	21.2410	39.58	0.83
8	499	-0.16	383	53.7552	30.9041	22.8511	42.51	0.76
9	594	-0.22	229	53.7663	28.9339	24.8324	46.19	0.70
10	762	-0.24	395	53.7697	27.5417	26.2281	48.78	0.57
11	930	-0.31	401	53.7009	25.3190	28.3819	52.85	0.51
12	1340	-0.37	397	53.7580	22.5509	31.2071	58.05	0.39
13	1750	-0.41	392	53.6935	22.6709	31.0226	57.78	0.29
Blank	**Time (h)**	**pH (20±1°C)**	**EC (mS/cm) (20±1°C)**	**$W_{initial}$ (g)**	**W_{final} (g)**	**W_{loss} (g)**	**Evaporation (wt.%)**	**Evaporation rate (g/h/dm²)**
B0	0	5.3	n.d.	n.d.	n.d.	n.d.	n.d.	0.00
B1	97	4.1	n.d.	49.5385	38.1527	11.3858	22.98	1.96
B2	187	3.0	n.d.	49.4904	35.6654	13.8250	27.93	1.23
B3	427	1.9	n.d.	49.5252	13.8458	35.6794	72.04	1.39
B4	594	2.7	n.d.	49.5354	8.8718	40.6636	82.09	1.14

Table 6.2. Changes in the chemical composition of the hyperacid Kawah Ijen brine and the blanks during the evaporation experiment. Concentrations in mg/kg.

Sample	Time (h)	pH (20±1°C)	S_T[a]	Cl	F	Al	B	Br	Ca	Fe	K	Mg	Mn	Na	P	Si	Sr	Ti	V	Zn	TDS[b]
0[c]	0	0.10	21800	22100	1410	5730	49	56	690	1970	1230	690	41	1110	48	32	15	7.1	9.4	4.4	96
1	24	0.06	22600	22900	1500	5920	51	60	730	2080	1270	710	42	1150	50	33	15	7.4	9.8	4.5	100
2	74	0.03	24500	24500	1570	6400	55	60	790	2250	1370	770	46	1240	54	35	17	8.2	10.6	5.0	111
3	117	-0.01	26500	26300	1710	6970	61	62	860	2450	1490	830	50	1340	59	38	18	9.0	11.6	5.3	119
4	187	-0.05	29700	29700	1900	7790	68	68	960	2750	1660	920	56	1510	65	42	20	10.3	13.0	6.0	137
5	234	-0.11	30900	30400	1880	8010	70	71	990	2830	1710	950	58	1540	68	43	21	10.6	13.5	6.2	142
6	331	-0.13	34800	33900	2240	8970	79	80	1110	3160	1910	1070	65	1730	76	48	23	12.1	15.2	7.0	160
7	427	-0.12	36200	35100	2260	9340	81	83	1150	3300	1990	1120	68	1800	79	50	24	12.7	15.9	7.2	166
8	499	-0.16	38000	36900	2400	9820	87	88	1220	3470	2100	1180	72	1890	83	53	25	13.4	16.7	7.7	174
9	594	-0.22	40500	39000	2440	10500	91	95	1300	3720	2240	1260	76	2000	88	56	27	14.4	17.9	8.2	185
10	762	-0.24	42700	40700	2640	11200	97	104	1230	3940	2360	1330	81	2110	93	60	27	15.2	18.9	8.9	195
11	930	-0.31	47400	44900	2980	12500	106	106	1000	4380	2620	1470	89	2330	102	66	28	17.0	21.0	9.8	214
12	1340	-0.37	53200	47700	3340	14000	118	125	790	4930	2960	1650	100	2630	117	70	31	19.1	23.7	10.8	239
13	1750	-0.41	52400	45900	3110	13800	116	124	700	4920	2920	1630	97	2610	115	55	29	19.0	23.6	10.7	234
B0	0	5.33	n.d	n.d.	n.d.	n.d.	n.d.	n.d.	n.d.	n.d.	n.d.	n.d.	n.d.	n.d.	n.d.	n.d.	n.d.	n.d.	n.d.	n.d.	n.d.
B1	97	4.12	2.4	17.8	0.04	b.d.l.	b.d.l.	b.d.l.	0.3	b.d.l.	b.d.l.	b.d.l.	b.d.l.	0.6	0.0	0.0	b.d.l.	b.d.l.	b.d.l.	b.d.l.	n.d.
B2	187	3.04	2.4	19.1	0.05	b.d.l.	b.d.l.	b.d.l.	0.5	b.d.l.	b.d.l.	b.d.l.	b.d.l.	0.7	0.0	0.2	b.d.l.	b.d.l.	b.d.l.	b.d.l.	n.d.
B3	427	1.90	2.2	27.3	0.13	b.d.l.	b.d.l.	b.d.l.	0.4	b.d.l.	b.d.l.	b.d.l.	b.d.l.	0.5	0.0	0.1	b.d.l.	b.d.l.	b.d.l.	b.d.l.	n.d.
B4	594	2.72	2.2	27.3	0.15	b.d.l.	b.d.l.	b.d.l.	0.4	b.d.l.	b.d.l.	b.d.l.	b.d.l.	0.5	0.1	0.1	b.d.l.	b.d.l.	b.d.l.	b.d.l.	n.d.

Notes: (a) total sulphur, measured by ICP-OES; (b) calculated total dissolved solids (g/kg); (c) the chemical composition of the sample 0 (t=0 hours) was extrapolated based on the analyses of the consecutive sample; n.d. = not determined; b.d.l. = below detection limit.

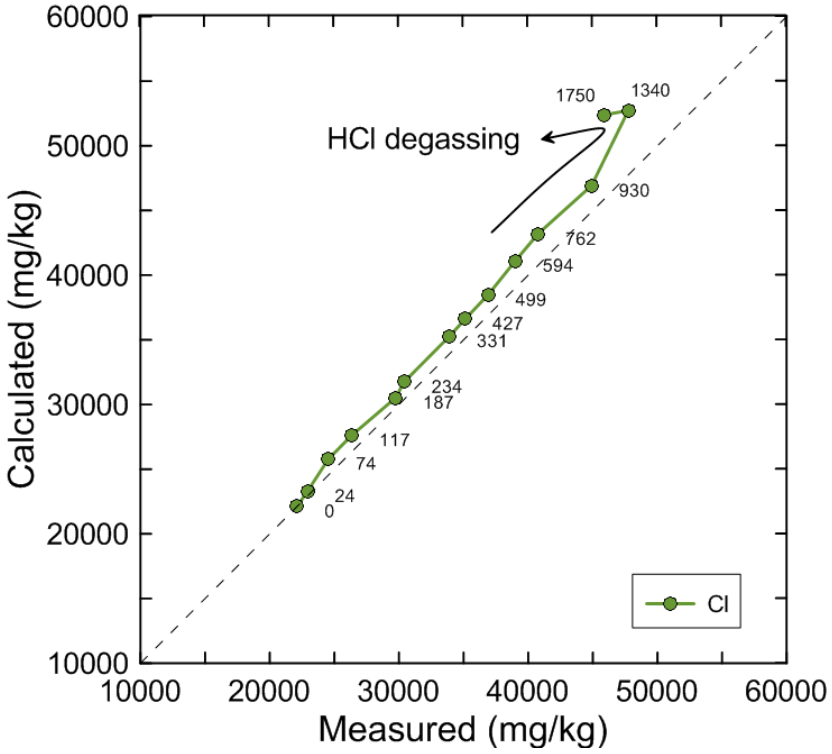

Figure 6.2. Calculated vs. measured Cl concentrations during the evaporation experiment. Departure of measured values from equivalent concentrations (dashed line) is interpreted to indicate HCl degassing. The small numbers next to the points correspont to the time (hours) at which sample was taken.

For this reason, the up to ca. 10% lower measured concentrations of Br relative to the calculated ones (Fig. 6.3e) are probably not due to escaping $HBr_{(g)}$ from the solutions but reflect a minor analytical bias.

Anatase TiO_2 is a common phase in Kawah Ijen´s lake water (Delmelle and Bernard, 1994; Delmelle et al., 2000) and was always oversaturated in the brine during the experiment (Fig. 6.4b). The deviation of Ti concentrations from the equivalent line (Fig. 6.3o) is inconsistent with precipitating anatase, since measured concentrations in the solution are somewhat higher than expected. Presumably, this tendency is due to imprecise calibration for the ICP-OES measurement of this element. Fluorite CaF_2, cryolite AlF_3 and halite NaCl remained always well undersaturated, showing an initial increase in SI values followed by a levelling off (Fig. 6.4c).

Iron and magnesium sulphates remained undersaturated throughout the experiment. The saturation indices of the iron sulphates szolmolnokite $FeSO_4 \cdot H_2O$, rozenite

$FeSO_4 \cdot 4H_2O$, siderotile $FeSO_4 \cdot 5H_2O$, ferrohexahydrite $FeSO_4 \cdot 6H_2O$ and melanterite $FeSO_4 \cdot 7H_2O$ show an initial increase, then a decline and finally an increase again towards the end of the experiment (Fig. 6.4d). The SI values of the magnesium sulphates kieserite $MgSO_4 \cdot H_2O$, starkeyite $MgSO_4 \cdot 4H_2O$, pentahydrite $MgSO_4 \cdot 5H_2O$, hexahydrite $MgSO_4 \cdot 6H_2O$ and epsomite $MgSO_4 \cdot 7H_2O$ increased steadily with time (Fig. 6.4e). In summary, the only phases that apparently reached oversaturation during the evaporation experiments were anhydrite, hydrogen chloride and anatase.

Total dissolved chlorine ($Cl_{diss.}$) is present in the form of undissociated hydrogen chloride (HCl^0) and Cl^-, with the activity of the latter species being dominant (Fig. 6.5a). When evaporation proceeded, the activity of HCl^0 increased strongly, reflecting displacement of the equilibrium of reaction (2) to the left hand side due to the increase of H^+. The same mechanism favoured the formation of $H_2SO_4^0$ and HBr^0, but activities of these species were several orders of magnitude lower than that of HCl^0 (reactions 3 and 4) (Fig. 6.5a).

Aluminium has a strong tendency to form complexes with F^-, since most of this element is present in the following species: AlF_2^+, AlF^{2+} and AlF_3 (Fig. 6.5b). On the other hand, Fe^{2+} and Fe^{3+} are predominantly complexed with Cl^-, forming $FeCl^+$ and $FeCl^{2+}$, respectively (Figs. 6.5c and 6.5d). It should be mentioned that, due to the extreme acidity of the Kawah Ijen lake water, iron is predominantly in its lower oxidation state (Fe^{2+}). Magnesium and calcium are present as Mg^{2+} and Ca^{2+}, respectively, but also form complexes with SO_4^{2-} and Cl^- such as $MgCl^+$, $MgSO_4^0$, $CaCl^+$ and $CaSO_4^0$, where the sulphur-bearing species always have higher activities than their chlorine-bearing counterparts (Figs. 6.5e and 6.5f). Finally, potassium and sodium tend to remain largely as K^+ and Na^+, with the most significant complexes being $KHSO_4^0$ and $NaCl^0$, respectively (Figs. 6.5g and 6.5h). The consequence of the formation of all these complexes is that the solubilities of Al, Fe, Mg, Ca, K and Na are strongly increased in the hyperacid brine, which is probably a limiting factor for the precipitation of sulphates and chlorides.

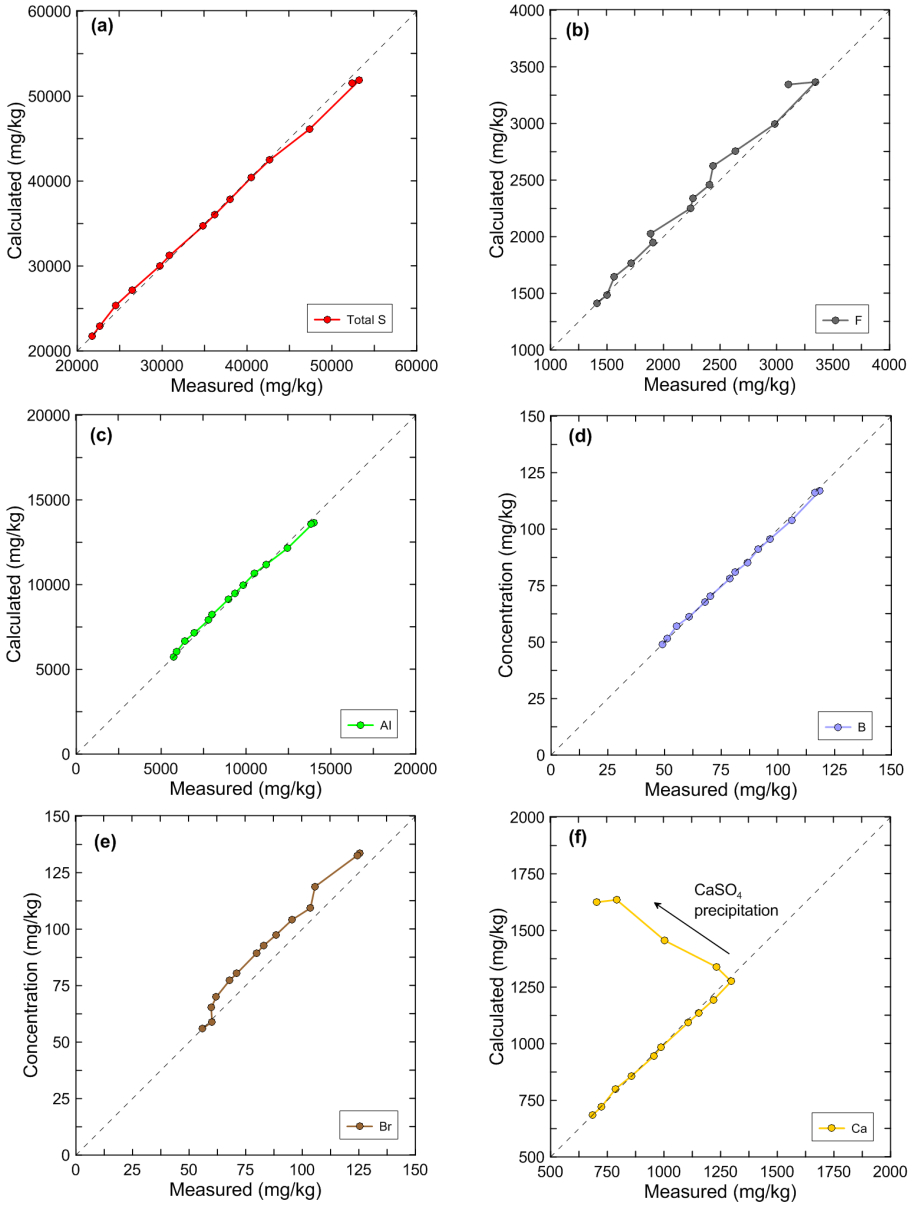

Figure 6.3. Evaporation experiment. Calculated vs. measured concentrations of: (a) total sulphur; (b) fluoride; (c) aluminium; (d) boron; (e) bromide and (f) calcium. Note that in the case of calcium, the deviation of the points from the equivalent concentration trend (dashed line) indicates anhydrite ($CaSO_4$) precipitation.

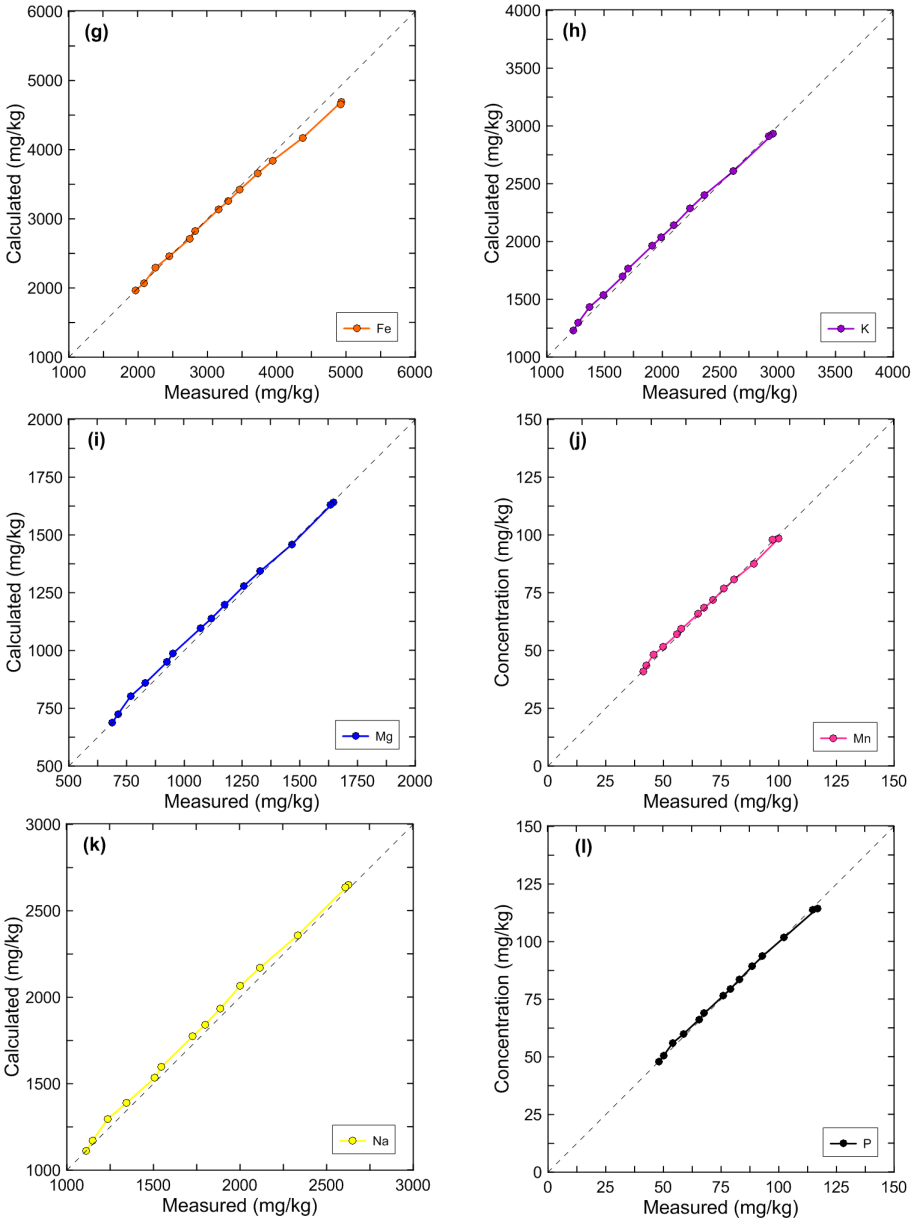

Figure 6.3 (continued). Evaporation experiment. Calculated vs. measured concentrations of: (g) total iron; (h) potassium; (i) magnesium; (j) manganese; (k) sodium; and (l) phosphorous.

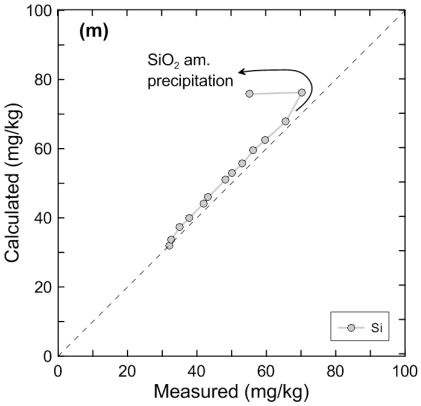

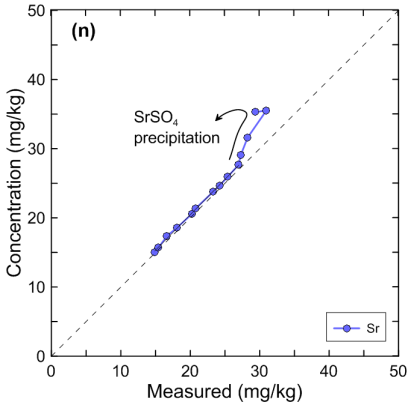

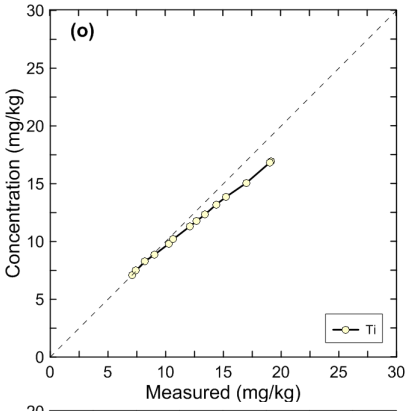

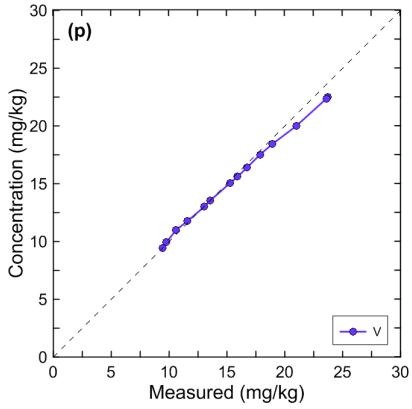

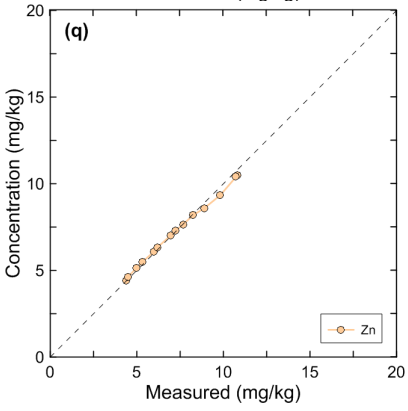

Figure 6.3 (continued). Evaporation experiment. Calculated vs. measured concentrations of: (m) silicon; (n) strontium; (o) titanium; (p) vanadium; and (q) zinc. Note that in the case of silicon and strontium, the deviation of the points from the equivalent concentration trend (dashed line) probably indicates amorphous silica SiO_2 am. and celestine $SrSO_4$ precipitation, respectively.

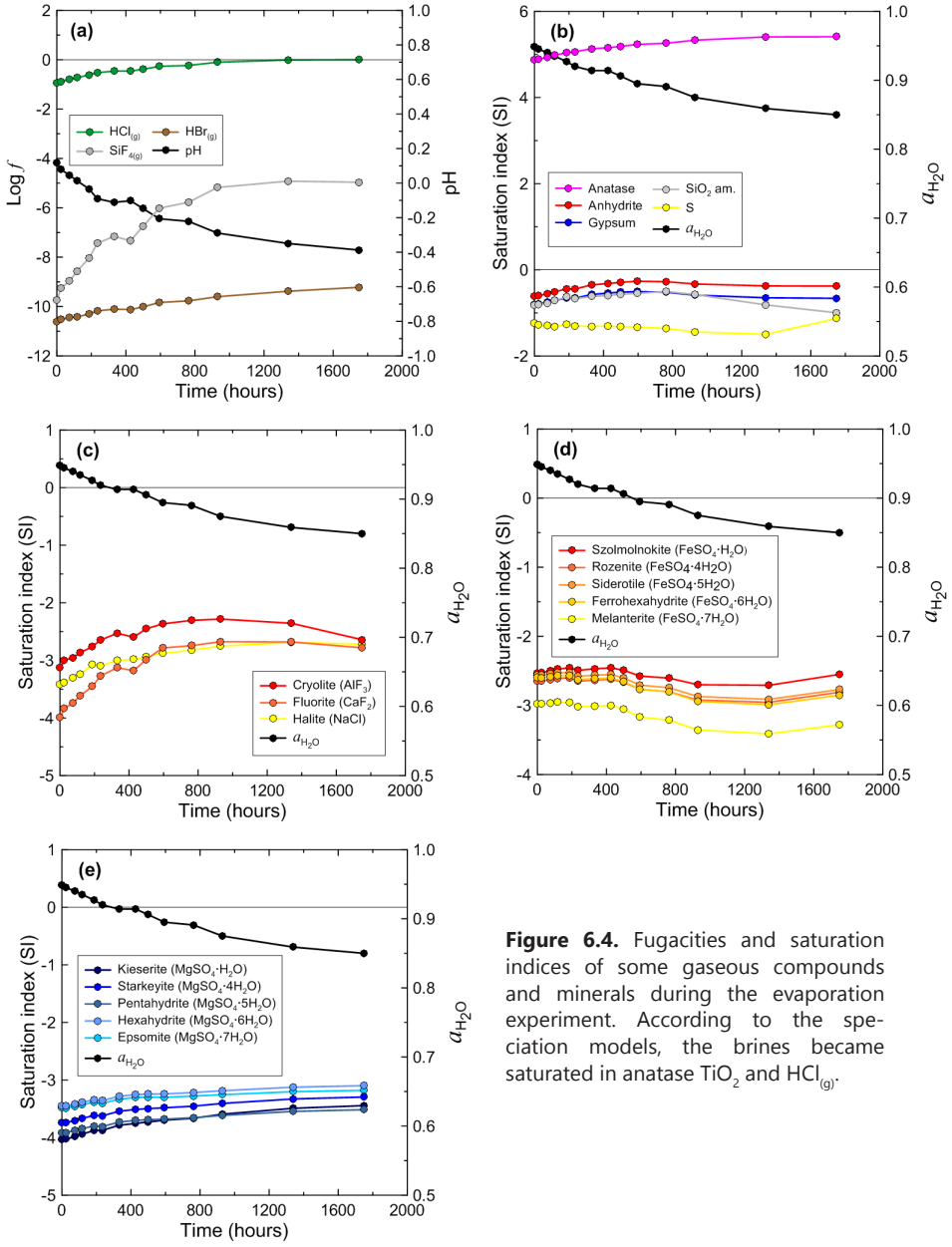

Figure 6.4. Fugacities and saturation indices of some gaseous compounds and minerals during the evaporation experiment. According to the speciation models, the brines became saturated in anatase TiO_2 and $HCl_{(g)}$.

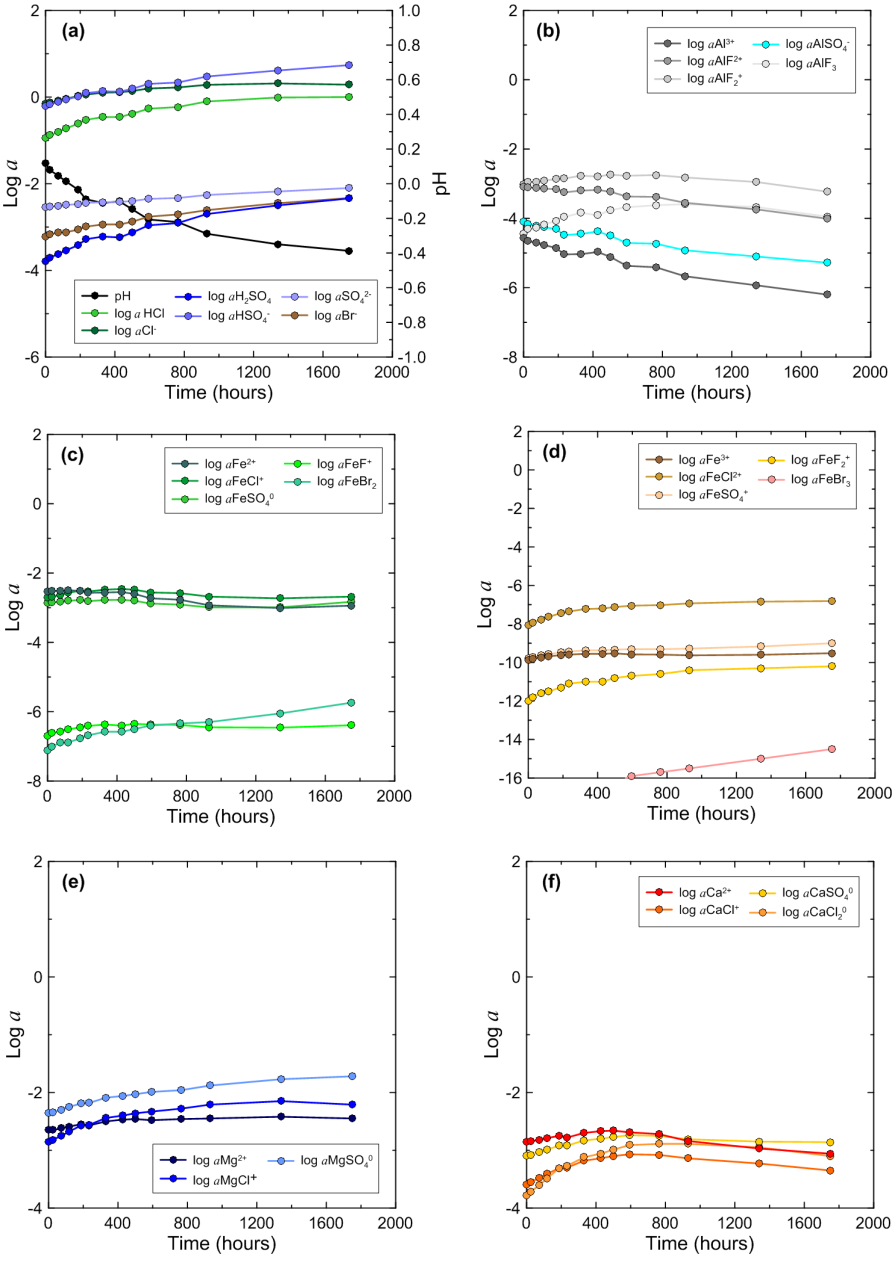

Figure 6.5. Activities of the main species of (a) S(VI), Cl and Br, (b) Al, (c) Fe(II), (d) Fe(III), (e) Mg, and (f) Ca.

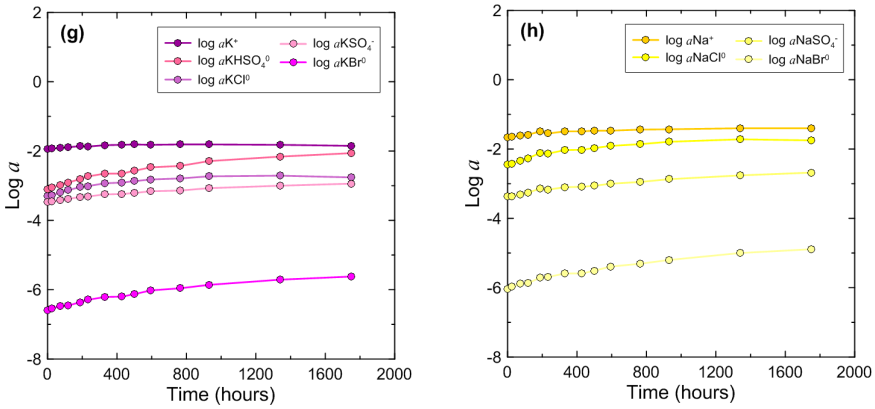

Figure 6.5 (continued). Activities of the main species of: (g) K and (h) Na.

6.3.3. Chlorine isotope composition and Cl losses

From the initial δ^{37}Cl composition of the hyperacid brine (+0.36±0.05‰) until sample 9 (499 hours), a slight decrease down to +0.22±0.04‰ was observed. This trend was followed by a significant increase up to +0.68±0.05‰ in the last sample (Table 6.3, Fig. 6.6). These changes in isotope composition are accompanied by chlorine losses through escaping $HCl_{(g)}$, given the absence of solid precipitating Cl-bearing phases during the experiment. The significant increase in $\log f_{HCl}$ values after 499 hours (Fig. 6.4a) suggests that extra $HCl_{(g)}$ may have been escaping from that moment on (Figs. 6.2 and 6.4a).

Chlorine losses by degassing $HCl_{(g)}$ were calculated from the differences between measured and calculated Cl concentrations (Table 6.3). The concentration differences were transformed in mass losses (mg) for each sample, based on the remaining liquid mass (Table 6.1). Fractionation between $HCl_{(g)}$ and total dissolved Cl ($Cl_{diss.}$) during the evaporation experiment can be calculated using the Rayleigh fractionation model:

$$\delta_f - \delta_i = (1000 + \delta_i)(F^{(\alpha-1)} - 1) \quad (5)$$

Where δ_i and δ_f are the δ^{37}Cl composition for the initial Kawah Ijen hyperacid brine (+0.36±0.05‰; sample t=0) and the subsequent δ^{37}Cl compositions during the evaporation experiment, respectively. F is the total chlorine remaining in the liquid, defined by:

$$F = \frac{Cl_{final}(mg)}{Cl_{initial}(mg)}$$

Expressing equation (5) in a linear form gives:

$$\ln\left(\frac{\delta_f + 1000}{\delta_i + 1000}\right) = (\alpha - 1)F \qquad)$$

Where α can be obtained from the slope of the line. The experiments yielded two distinctive trends for different time intervals (Table 6.3, Fig. 6.7a). The corresponding $\alpha_{HCl_{(g)}\text{-}Cl_{diss.}}$ values are 1.00300±0.00002 (t=0-499 hours) and 0.99448±0.00000 (t=499-1750 hours). The fractionation factors (1000 ln $\alpha_{HCl_{(g)}\text{-}Cl_{diss.}}$) before and after 499 hours, are +2.96±0.01‰ and -5.53±0.00‰, respectively. This implies that the $HCl_{(g)}$ produced during the first 499 hours of the experiment was enriched in ^{37}Cl compared to the $Cl_{diss.}$ in the hyperacid brine, whereas after 499 hours it was depleted in ^{37}Cl (Figure 6.8a).

An alternative approach to calculate these fractionation factors is by using *F* values derived from the ratio between Cl and a conservative element such as boron. For each experimental solution, the Cl/B ratio was determined and normalized to the ratio in the initial brine (sample t=0). In this case:

$$Cl_{final}(mg) = Cl_{initial}(mg)\left(\frac{Cl_{final}/B_{final}}{Cl_{initial}/B_{initial}}\right) \qquad)$$

and then,

$$Cl_{initial}(mg) - Cl_{final}(mg) = Cl_{loss} = HCl_{(g)} \qquad 9)$$

The resulting *F* values and fractionation factors were again obtained from equations (6) and (7) by linear regression, assuming Rayleigh fractionation (Table 6.4; Figs. 6.7b and 6.8b). In a similar way, *F* values and fractionation factors were also calculated for Fe and Mg as conservative elements (Tables 6.5 and 6.6; Figs. 6.7c, 6.7d, 6.8c and 6.8d). A summary of all these results is presented in Table 6.7.

6.4. DISCUSSION

6.4.1. Chemical composition, mineral saturation states and speciation in the brine

Hyperacid brines such as that of Kawah Ijen anions like HSO_4^-, Cl^- and F^- commonly form complexes with cations (Na^+, K^+, Ca^{2+}, Fe^{2+}, Mg^{2+}, Al^{3+} and Fe^{3+}). Consequently, the solubility of these metals will be significantly higher than without these complexes. A direct effect is that precipitation of sulphates and halides is probably delayed or completely inhibited during progressive evaporation. Relatively common minerals observed in acidic brine waters are calcium sulphates (anhydrite and/or gypsum) and amorphous silica. Anhydrite and was inferred to have formed in the course of the experiment, despite the fact that the SI values of this mineral remained slightly below equilibrium saturation. Using solubility data from Gunnarsson and Arnórsson

(2000), amorphous silica solubility at T=60°C is $3.59x10^{-3}$ moles/kg H_2O. Since the maximum concentrations reached during the experiment were $1.23x10^{-3}$ moles/kg (almost 3 times lower), it can be seen that amorphous silica remained undersaturated throughout the experiment. Similar calculations done at T=20°C confirmed that the initial solution was amorphous silica-undersaturated. Therefore, the long-term storage of the Kawah Ijen crater late water at room temperature precipitated enough amorphous silica in order to drive this phase to undersaturation conditions.

According to experiments and models reported in literature, calcium sulphates are often the first phases to precipitate upon evaporation of saline brine waters, followed by magnesium sulphates (Tosca and McLennan, 2006; Gamazo et al., 2011; Elsenousy et al., 2015; Toner et al., 2015). Gamazo et al. (2011) modelled the evaporation of Mg-Na-Cl-SO_4 brine water from Quero lake (Spain), and inferred the appearance of an anhydrite-gypsum paragenesis at a_{H_2O}= 0.78, followed by epsomite-hexahydrite and hexahydrite-kieserite paragenesis at a_{H_2O} values of 0.57 and 0.50, respectively. Similarly, based on the Na-K-Ca-Mg-Cl-SO_4-ClO_4 brines that could have produced the salt assemblages at the Phoenix landing site on Mars, evaporation models of Toner et al. (2015) indicate the appearance of anhydrite-gypsum, epsomite-hexahydrite and hexahydrite-kieserite paragenesis at a_{H_2O} values of 0.68, 0.56 and 0.52, respectively. The water activity towards the end of our experiments when anhydrite precipitated (a_{H_2O} = 0.85) was higher than in those cases, apparently reflecting the different chemistries.

Table 6.3. Results of evaporation experiments (mass loss of the solution, $\delta^{37}Cl$ of dissolved Cl and inferred $HCl_{(g)}$ loss) performed on the hyperacid brine water of Kawah Ijen. Calculations of *F* values (fractions of Cl remaining in solution) based on differences between measured and calculated Cl concentrations, as well as water-vapour losses (see Table 6.1). $\delta^{37}Cl_{HCl(g)}$ values obtained from calculated fractionation factors, assuming Rayleigh fractionation (see Figs. 6.7 and 6.8). 1000 ln $\alpha_{HCl(g)\text{-}Cl_{diss.}}$ (‰) values are the same from 0 to 499 hours and from 499 to 1750 hours.

Sample	Time (h)	Evaporation (wt.%)	pH (20±1°C)	$\delta^{37}Cl_{diss.}$ (‰)	$Cl_{measured}$ (mg/kg)	$Cl_{calculated}$ (mg/kg)	Cl_{loss} (mg/kg)	Cl_{loss} (mg)	$Cl_{initial}$ (mg)	*F*	ln *F*	ln [illegible]	1000 ln $\alpha_{HCl(g)\text{-}Cl_{diss.}}$ (‰)	$\delta^{37}Cl_{HCl(g)}$ (‰)
0	0	0.00	0.10	+0.36±0.05	22100	22100	0	0		1	0	0	+2.96±0.01	+3.33±0.01
1	24	5.01	0.06	+0.26±0.01	22900	23300	370	20	1190	0.98	-0.0162	-9.8719E-05		+3.23±0.01
2	74	14.21	0.03	+0.24±0.02	24500	25800	1250	60	1190					
3	117	19.92	-0.01	+0.22±0.06	26300	27600	1270	50	1190					
4	187	27.52	-0.05	+0.31±0.04	29700	30500	780	30	1190	0.97	-0.0259	-4.6734E-05		+3.28±0.01
5	234	30.31	-0.11	+0.22±0.04	30400	31700	1350	50	1180	0.96	-0.0434	-1.4371E-04		+3.18±0.01
6	331	37.29	-0.13	+0.28±0.16	33900	35300	1370	50	1190	0.96	-0.0396	-7.9604E-05		+3.25±0.01
7	427	39.58	-0.12	+0.19±0.01	35100	36600	1490	50	1190	0.96	-0.0415	-1.6770E-04		+3.16±0.01
8	499	42.51	-0.16	+0.22±0.03	36900	38500	1590	50	1190	0.96	-0.0421	-1.4321E-04	-5.53±0.00	-5.30±0.00
9	594	46.19	-0.22	+0.22±0.04	39000	41100	2100	60	1190	0.95	-0.0525	-1.3871E-04		-5.30±0.00
10	762	48.78	-0.24	+0.26±0.18	40700	43200	2440	70	1190	0.94	-0.0580	-9.9598E-05		-5.26±0.00
11	930	52.85	-0.31	+0.32±0.04	44900	46900	2020	50	1190					
12	1340	58.05	-0.37	+0.53±0.05	47700	52700	4990	110	1190	0.91	-0.0993	1.7017E-04		-4.99±0.00
13	1750	57.78	-0.41	+0.68±0.05	45900	52400	6510	150	1190	0.88	-0.1326	3.1908E-04		-4.84±0.00

Table 6.4. Same as Table 6.3 but *F* values were calculated from Cl/B ratios assuming that B is perfectly conservative. 1000 ln $\alpha_{HCl_{(g)}\text{-}Cl_{diss.}}$ (‰) values are the same from 0 to 499 hours and from 499 to 1750 hours.

Sample	Time (h)	Evaporation (wt.%)	pH (20±1°C)	$\delta^{37}Cl_{diss.}$ (‰)	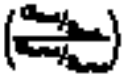	$Cl_{initial}$ (mg)	Cl_{final} (mg)	Cl_{loss} (mg)	*F*	ln *F*	ln 	1000 ln $\alpha_{HCl_{(g)}\text{-}Cl_{diss.}}$ (‰)	$\delta^{37}Cl_{HCl_{(g)}}$ (‰)
0	0	0.00	0.10	+0.36±0.05	1.00				1	0	0	+1.55±0.49	+1.91±0.49
1	24	5.01	0.06	+0.26±0.01	0.99	1190	1180	10	0.99	-0.0099	-9.8719E-05		+1.81±0.49
2	74	14.21	0.03	+0.24±0.02	0.98	1190	1170	20	0.98	-0.0177	-1.1721E-04		+1.79±0.49
3	117	19.92	-0.01	+0.22±0.06	0.96	1190	1140	50					
4	187	27.52	-0.05	+0.31±0.04	0.97	1190	1160	30	0.97	-0.0280	-4.6734E-05		+1.87±0.49
5	234	30.31	-0.11	+0.22±0.04	0.96	1180	1130	50	0.96	-0.0417	-1.4371E-04		+1.77±0.49
6	331	37.29	-0.13	+0.28±0.16	0.95	1190	1130	60	0.95	-0.0487	-7.9604E-05		+1.83±0.49
7	427	39.58	-0.12	+0.19±0.01	0.96	1190	1140	50					
8	499	42.51	-0.16	+0.22±0.03	0.94	1190	1120	70	0.94	-0.0571	-1.4321E-04		+1.77±0.49
9	594	46.19	-0.22	+0.22±0.04	0.95	1190	1120	60	0.95	-0.0557	-1.3871E-04	-5.64±0.17	-5.40±0.17
10	762	48.78	-0.24	+0.26±0.18	0.93	1190	1110	80	0.93	-0.0674	-9.9598E-05		-5.36±0.17
11	930	52.85	-0.31	+0.32±0.04	0.94	1190	1110	70	0.94	-0.0642	-3.6238E-05		-5.30±0.17
12	1340	58.05	-0.37	+0.53±0.05	0.89	1190	1060	130	0.89	-0.1118	1.7017E-04		-5.09±0.17
13	1750	57.78	-0.41	+0.68±0.05	0.87	1190	1040	150	0.87	-0.1338	3.1908E-04		-4.94±0.17

Table 6.5. Same as Table 6.3 but *F* values were calculated from Cl/Fe ratios assuming that Fe is perfectly conservative. 1000 ln $\alpha_{HCl_{(g)}\text{-}Cl_{diss.}}$ (‰) values are the same from 0 to 499 hours and from 499 to 1750 hours.

Sample	Time (h)	Evaporation (wt.%)	pH (20±1°C)	$\delta^{37}Cl_{diss.}$ (‰)		$Cl_{initial}$ (mg)	Cl_{final} (mg)	Cl_{loss} (mg)	*F*	ln *F*	ln 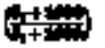	1000 ln $\alpha_{HCl_{(g)}\text{-}Cl_{diss.}}$ (‰)	$\delta^{37}Cl_{HCl_{(g)}}$ (‰)
0	0	0.00	0.10	+0.36±0.05	1.00				1	0	0	+2.31±0.33	+2.67±0.33
1	24	5.01	0.06	+0.26±0.01	0.98	1190	1160	30	0.98	-0.0222	-9.8719E-05		+2.57±0.33
2	74	14.21	0.03	+0.24±0.02	0.97	1190	1150	40	0.97	-0.0303	-1.1721E-04		+2.55±0.33
3	117	19.92	-0.01	+0.22±0.06	0.96	1190	1140	50					
4	187	27.52	-0.05	+0.31±0.04	0.96	1190	1150	40	0.96	-0.0383	-4.6734E-05		+2.62±0.33
5	234	30.31	-0.11	+0.22±0.04	0.96	1180	1120	50	0.96	-0.0447	-1.4371E-04		+2.53±0.33
6	331	37.29	-0.13	+0.28±0.16	0.95	1190	1130	50	0.95	-0.0467	-7.9604E-05		+2.59±0.33
7	427	39.58	-0.12	+0.19±0.01	0.95	1190	1120	60	0.95	-0.0545	-1.6770E-04		+2.50±0.33
8	499	42.51	-0.16	+0.22±0.03	0.95	1190	1120	60	0.95	-0.0562	-1.4321E-04		+2.53±0.33
9	594	46.19	-0.22	+0.22±0.04	0.93	1190	1110	80	0.93	-0.0710	-1.3871E-04	-3.97±0.08	-3.74±0.08
10	762	48.78	-0.24	+0.26±0.18	0.92	1190	1090	100	0.92	-0.0836	-9.9598E-05		-3.70±0.08
11	930	52.85	-0.31	+0.32±0.04	0.91	1190	1080	100	0.91	-0.0917	-3.6238E-05		-3.64±0.08
12	1340	58.05	-0.37	+0.53±0.05	0.86	1190	1020	170	0.86	-0.1497	1.7017E-04		-3.43±0.08
13	1750	57.78	-0.41	+0.68±0.05	0.83	1190	980	200	0.83	-0.1873	3.1908E-04		-3.28±0.08

Table 6.6. Same as Table 6.3 but *F* values were calculated from Cl/Mg ratios assuming that Mg is perfectly conservative. In $\alpha_{HCl_{(g)}\text{-}Cl_{diss.}}$ (‰) values are the same from 0 to 499 hours and from 499 to 1750 hours.

Sample	Time (h)	Evaporation (wt.%)	pH (20±1°C)	$\delta^{37}Cl_{diss.}$ (‰)	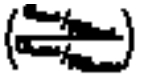	$Cl_{initial}$ (mg)	Cl_{final} (mg)	Cl_{loss} (mg)	*F*	ln *F*	ln 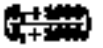	1000 ln $\alpha_{HCl_{(g)}\text{-}Cl_{diss.}}$ (‰)	$\delta^{37}Cl_{HCl_{(g)}}$ (‰)
0	0	0.00	0.10	+0.36±0.05	1.00				1	0	0	+3.37±1.11	+3.73±1.11
1	24	5.01	0.06	+0.26±0.01	1.00	1190	1190	0	1	0.0002	-9.8719E-05		+3.63±1.11
2	74	14.21	0.03	+0.24±0.02	0.99	1190	1180	10	0.99	-0.0054	-1.1721E-04		+3.61±1.11
3	117	19.92	-0.01	+0.22±0.06	0.99	1190	1170	20	0.99	-0.0142	-1.3421E-04		+3.60±1.11
4	187	27.52	-0.05	+0.31±0.04	1.00	1190	1190						
5	234	30.31	-0.11	+0.22±0.04	0.99	1180	1170	10	0.99	-0.0060	-1.4371E-04		+3.59±1.11
6	331	37.29	-0.13	+0.28±0.16	0.98	1190	1170	20	0.98	-0.0157	-7.9604E-05		+3.65±1.11
7	427	39.58	-0.12	+0.19±0.01	0.98	1190	1160	30	0.98	-0.0229	-1.6770E-04		+3.56±1.11
8	499	42.51	-0.16	+0.22±0.03	0.98	1190	1160	30	0.98	-0.0240	-1.4321E-04		+3.59±1.11
9	594	46.19	-0.22	+0.22±0.04	0.97	1190	1150	40	0.97	-0.0356	-1.3871E-04	-4.54±0.04	-4.31±1.11
10	762	48.78	-0.24	+0.26±0.18	0.95	1190	1130	60	0.95	-0.0474	-9.9598E-05		-4.27±0.04
11	930	52.85	-0.31	+0.32±0.04	0.95	1190	1130	60	0.95	-0.0485	-3.6238E-05		-4.20±0.04
12	1340	58.05	-0.37	+0.53±0.05	0.90	1190	1070	120	0.90	-0.1028	1.7017E-04		-4.00±0.04
13	1750	57.78	-0.41	+0.68±0.05	0.87	1190	1040	150	0.87	-0.1346	3.1908E-04		-3.85±0.04

Table 6.7. Summary of chlorine isotope fractionation factors obtained from the evaporation experiments at T=60°C, based on Rayleigh fractionation and different approaches for calculating *F* factors (see Figs. 6.7 and 6.8).

Method	t = 0 - 499 h		t = 499 - 1750 h	
	$\alpha_{HCl_{(g)}\text{-}Cl_{diss.}}$	1000 ln $\alpha_{HCl_{(g)}\text{-}Cl_{diss.}}$ (‰)	$\alpha_{HCl_{(g)}\text{-}Cl_{diss.}}$	1000 ln $\alpha_{HCl_{(g)}\text{-}Cl_{diss.}}$ (‰)
Cl independent mass loss	1.00300±0.000002	+2.96±0.0	0.99448±0.00000	-5.53±0.00
Cl/B	1.00155±0.00049	+1.55±0.49	0.99438±0.00017	-5.64±0.17
Cl/Fe	1.00211±0.00033	+2.31±0.33	0.99603±0.00008	-3.97±0.08
Cl/Mg	1.00337±0.00111	+3.37±1.11	0.99547±0.00004	-4.54±0.04

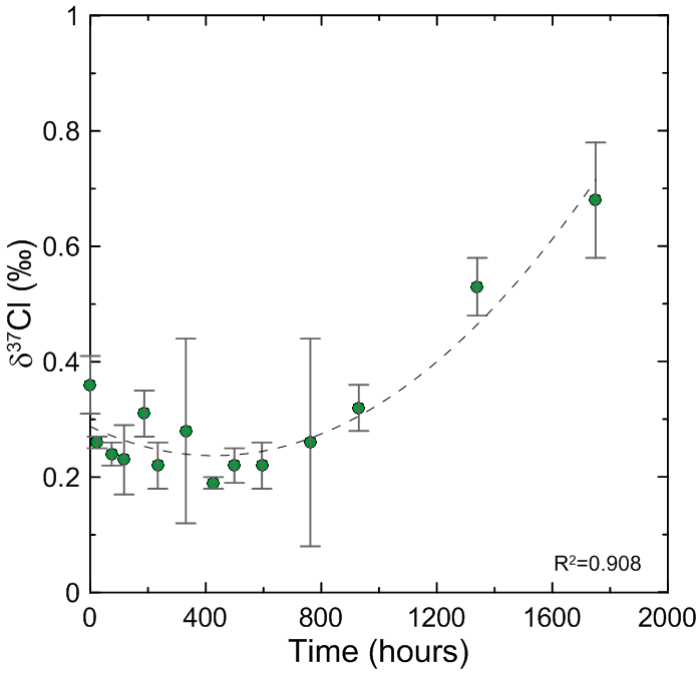

Figure 6.6. $\delta^{37}Cl$ compositions of the hyperacid brine during the evaporation experiment (T=60°C).

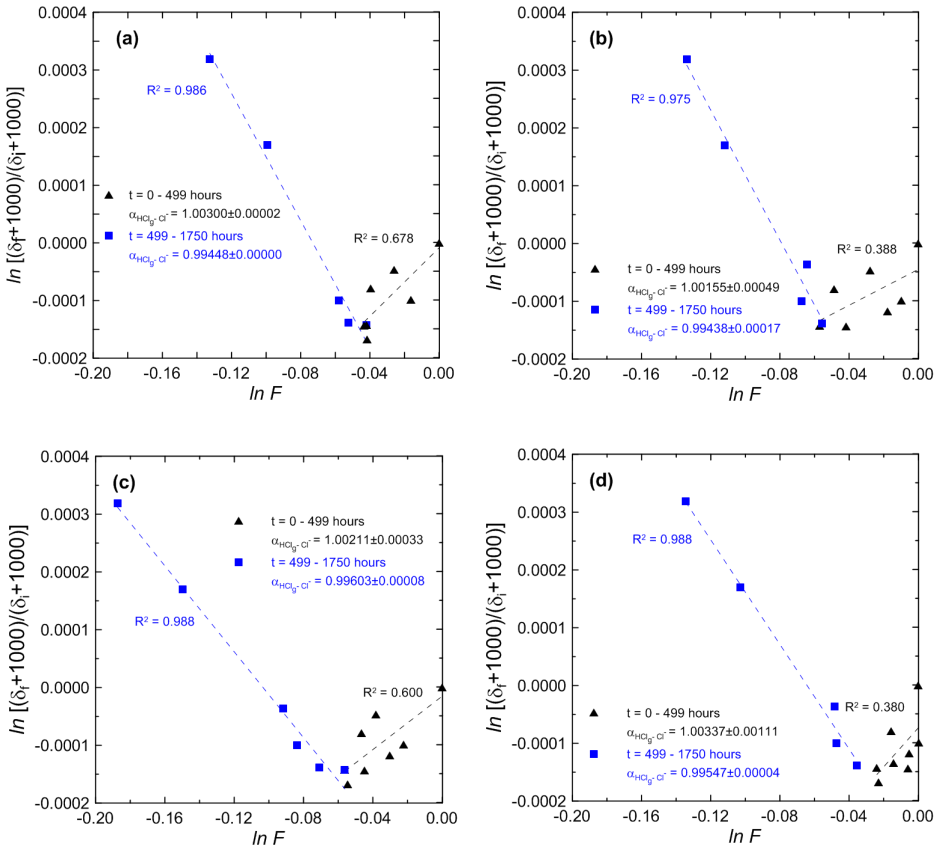

Figure 6.7. Effect of Rayleigh distillation on the fractionation factor between $HCl_{(g)}$ and $Cl_{diss.}$ ($\alpha_{HCl(g)\text{-}Cl_{diss.}}$). Mass-losses of Cl (*F* values) based on (a) Cl concentrations and water loss, (b) Cl/B, (c) Cl/Fe and (d) Cl/Mg ratios. Note the significant change in α values after approximately 499 hours of evaporation.

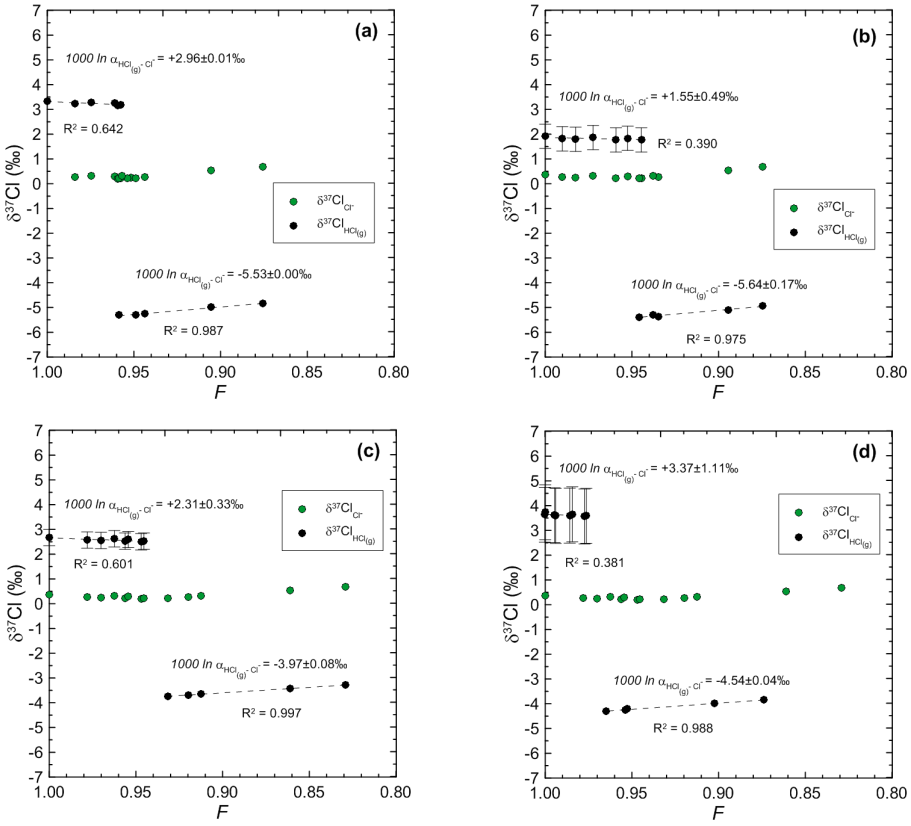

Figure 6.8. Measured $\delta^{37}Cl$ values for dissolved Cl (Cl_{diss}) and calculated $\delta^{37}Cl$ values for $HCl_{(g)}$ in the course of the evaporation experiment. Calculations based on (a) Cl independent mass loss, (b) Cl/B, (c) Cl/Fe and (d) Cl/Mg ratios. Note the significant change in $\delta^{37}Cl$ after approximately 499 hours of evaporation.

In order to investigate further changes in the hyperacid Kawah Ijen brine, below the lowest water activity reached during the evaporation experiments (a_{H_2O} = 0.85), an evaporation process was simulated in PHREEQC, whereby one litre of brine with the same composition as the initial experimental sample was evaporated by removing 904 g of water in 1000 steps at 60°C. The run did not converge after the 993th step, when 97% of the initial water content was removed and the ionic strength of the brine reached 182.3 molal. The water activity values (a_{H_2O}) dropped from 0.95 to 0.26. The only phases that reached saturation were anatase, anhydrite, hydrogen chloride and elemental sulphur (Fig. 6.9). Among iron and magnesium sulphates, ferrohexahydrite $FeSO_4 \cdot 6H_2O$ and szolmolnokite $FeSO_4 \cdot H_2O$ together with epsomite $MgSO_4 \cdot 7H_2O$ and hexahydrite $MgSO_4 \cdot 6H_2O$ approached saturation levels closest. Nevertheless, none of these salts was predicted to precipitate, even at the lowest

a_{H_2O} values of the simulation (Fig. 6.10). The elevated concentrations of Cl and S_T (total sulphur) reached upon evaporation resulted in complexation with Mg and Fe, mainly as $FeCl^+$, $FeCl^{2+}$, $FeSO_4^0$, $MgCl^+$ and $MgSO_4^0$, which increased the solubilities of these cations considerably and prevented them from precipitating as salts (Fig. 6.11).

A further important implication of the evaporation model relates to the depression of the freezing temperature of the aqueous solution. The simulation results were used to calculate the theoretical freezing temperature of the residual liquid after evaporation (Chevrier and Altheide, 2008; Elsenousy et al., 2015):

$$T_E = \frac{1}{\frac{1}{T_0} - \frac{R \ln a_{H_2O}}{\Delta H_f}} \quad 10)$$

$$\Delta H_f = 3.34768 + \frac{1.85714}{1 + \exp\left(\frac{a_{H_2O} - 0.53822}{0.05031}\right)} + 1.8555921 \cdot a_{H_2O} \quad 1)$$

Where T_E is the freezing temperature, R is the ideal gas constant, a_{H_2O} is the activity of water, T_0 = 273.15 K, and ΔH_f is the enthalpy of fusion.

If on Mars a similar hyperacid brine as that of the evaporation experiment would have been created (e.g., as a result of interaction of magmatic volatiles and ice, combined with an intense water-rock interaction), its minimum freezing temperature would be 183 K (-90.15°C) (Fig. 6.12). This value is close to the freezing point for the acids of Cl^- and SO_4^{2-} (Clark and Van Hart, 1981), which are among the strongest freezing point depressors. Other salts that significantly lower freezing points in aqueous solutions are $Mg(ClO_4)_2 \cdot 6H_2O$ (184.15 K) and $Mg(ClO_3)_2 \cdot 6H_2O$ (177.15 K) (Elsenousy et al., 2015). Taking the yearly average temperature of 240 K (-33.15°C) on Mars´ surface into account (Mellon et al., 2004), the presence of brines would thus greatly extend the stability of liquid water on this planet.

Even though mineral saturation states accurately predicted the solid phases observed during the evaporation experiment, there was a disagreement for $HCl_{(g)}$, since the values predicted that this gas only reached saturation at ca. 1000 hours (Fig. 6.4a), whereas the mass measurements indicated that $HCl_{(g)}$ started to escape much earlier. Also, it is known that $HCl_{(g)}$ readily evaporates from warm, hyperacid volcanic lakes (Taburello et al., 2015; Capaccioni et al., 2016; Rouwet et al., 2016). The log K_{HCl} used in the models was 0.51 (Johnson and Pytckowicz, 1978), but it should be pointed out that equilibrium constants for HCl vary by more than four orders of magnitude between different authors (Pokrovskii, 1999). Calculations in PHREEQC indicate that chlorine species in the Kawah Ijen brine include Cl^-, HCl^0 and

complexed Cl (mainly $FeCl^+$, $FeCl^{2+}$, $MgCl^+$, $CaCl^+$, $NaCl^0$ and KCl^0). For instance, Cl^- accounted for 80.5% of the total chlorine molality at the beginning of the experiment (t=0 hours), whereas HCl^0 and complexed Cl represented only 16.2% and 3.3%, respectively. As water was removed and pH decreased, the molalities of both HCl^0 and complexed Cl increased progressively. After 499 hours, Cl^- was not any longer the most abundant Cl species but HCl^0 instead. At the end of the experiment (t=1750 hours) the percentages of Cl^-, HCl^0 and complexed Cl were 14.8, 60.5 and 24.7%, respectively (Figure 6.13).

The evaporation experiment and modelling results also highlight that $HCl_{(g)}$ volatilization can be an efficient mechanism to fractionate Cl from Br, two elements that commonly show a similar hydrophilic behaviour in most terrestrial environments (Aiuppa et al., 2009). For example, the molar Br/Cl ratio at the beginning of the evaporation simulation was 0.001 and went up to 0.036 in response to $HCl_{(g)}$ volatilization. The ratio of total sulphur against chlorine also showed a marked increase (Figure 6.14). The Laguna Caliente hyperacid brine (Poás volcano) is a natural example where bromine-chlorine fractionation through $HCl_{(g)}$ evaporation has been documented (Rodríguez et al., 2016; see Chapter 4).

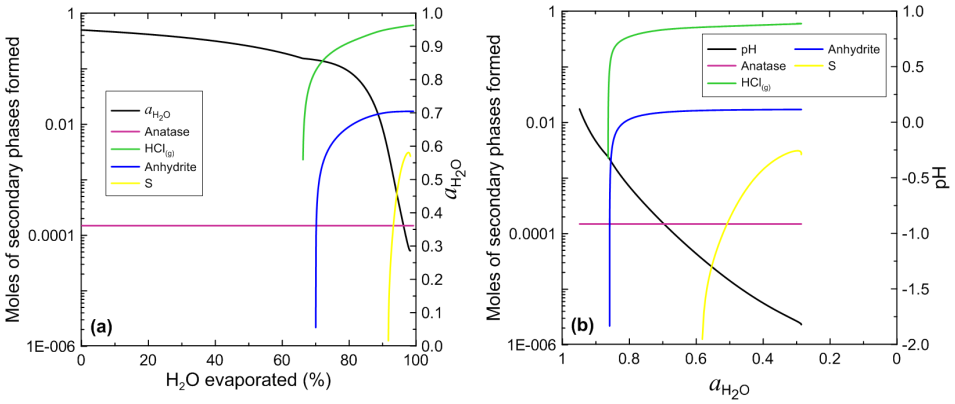

Figure 6.9. Secondary phases formed during evaporation based on PHREEQC simulation (T=60°C) as a function of (a) H_2O evaporated (wt.%) and (b) water activity (a_{H2O}).

6.4.2. Chlorine isotope fractionation – changing mechanism during evaporation

Theoretical equilibrium values at 60°C reported by Czarnacki and Halas (2012) are +1.55‰ and +1.69‰, based on data from Urey and Greiff (1935) and Schauble et al. (2003), respectively. Experimental results of Sharp et al. (2010) for equilibrium Cl isotope fractionation between $HCl_{(g)}$ and hydrochloric acid were +1.4 to +1.8‰ between 50 and 79°C. These authors attributed the preference of the heavy Cl isotope for the gas phase to the difference bond type, because the bond between Cl and H in the $HCl_{(g)}$ molecule will be stronger than that of a solvated Cl^- ion in an aqueous

solution.

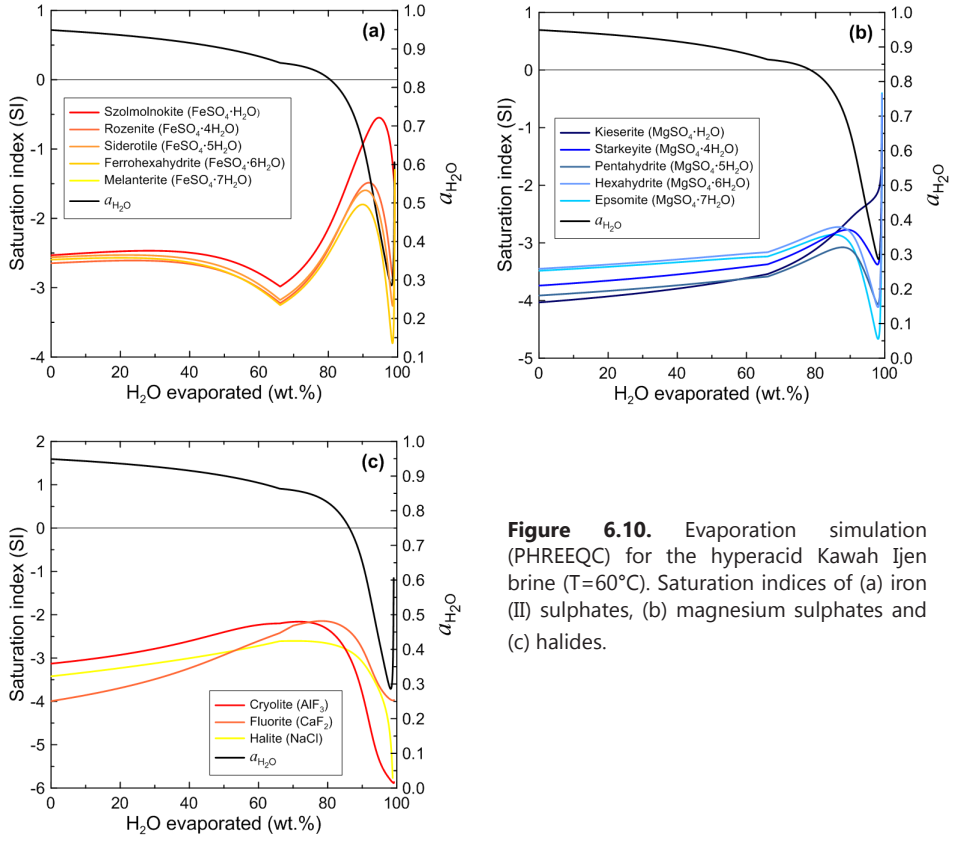

Figure 6.10. Evaporation simulation (PHREEQC) for the hyperacid Kawah Ijen brine (T=60°C). Saturation indices of (a) iron (II) sulphates, (b) magnesium sulphates and (c) halides.

The experimental results of this study before 499 hours are consistent with the tendency that ^{37}Cl preferentially escapes in evaporating $HCl_{(g)}$. However, the magnitude of fractionation is higher (average of four estimates is +2.5‰, Table 6.7), although for one approach (Cl mass losses based on B/Cl ratios) the result of +1.55±0.49‰ is close to the theoretical values of Czarnacki and Halas (2012). This enhanced isotopic fractionation effect can be explained by the experimental conditions of open-system evaporation, instead of the closed-system equilibrium cases on which the previous theoretical and experimental results were based. In contrast, the experimental results after 499 hours point to fractionation in opposite direction, i.e. with a strong preference of light ^{35}Cl for the gas phase (average of four estimates is -4.9‰, Table 6.7). Sharp et al. (2010) found a similar partitioning behaviour in a kinetic evaporation experiment with a 1 M HCl solution at room temperature, which yielded a 1000 ln $\alpha_{HCl(g)\text{-}Cl_{diss.}}$ value of -4.0‰. They ascribed this to a kinetic effect associated with the higher translational velocity of $H^{35}Cl$, which will thus escape more readily from the solution.

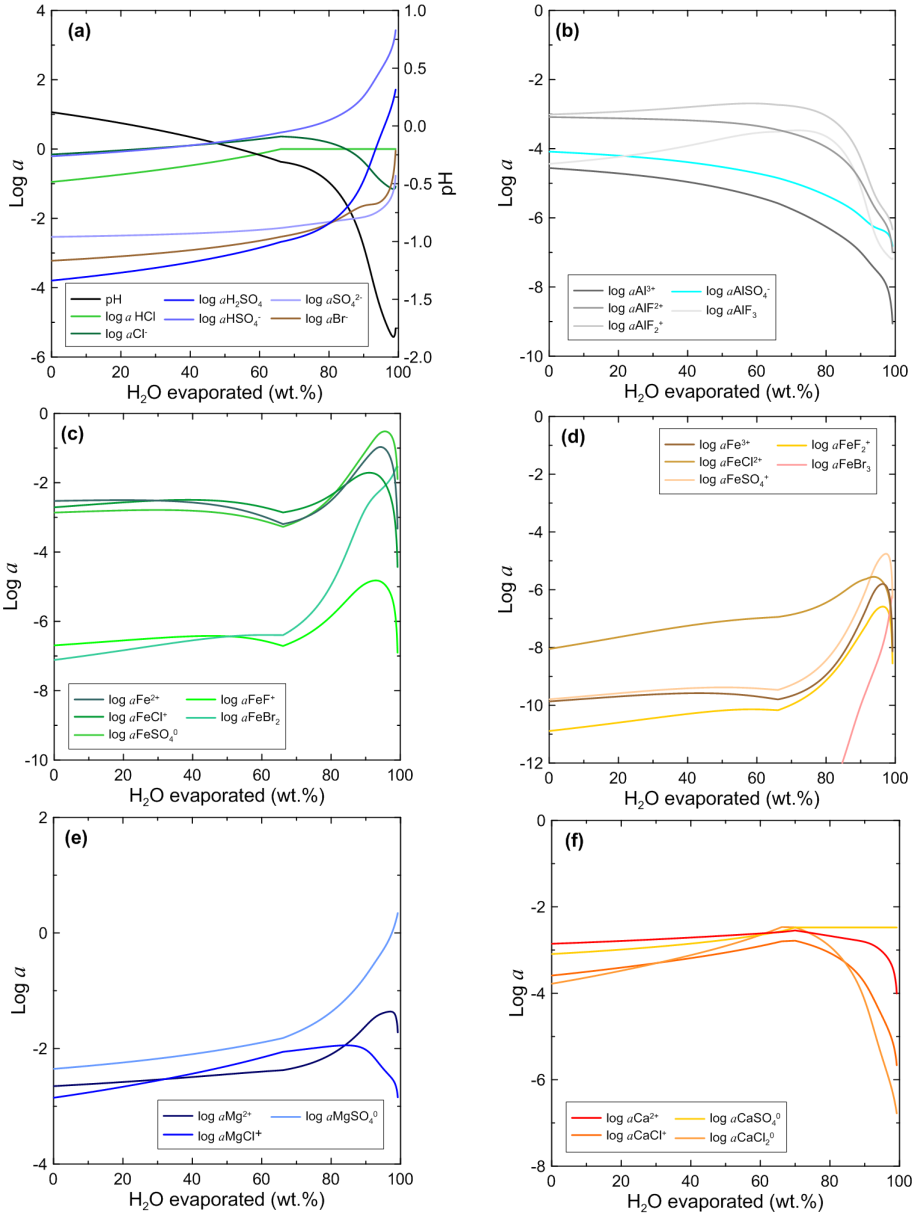

Figure 6.11. Evaporation simulation (PHREEQC) for the hyperacid Kawah Ijen brine (T=60°C). Activities of the main species of (a) S(VI), Cl and Br, (b) Al, (c) Fe(II), (d) Fe(III), (e) Mg, and (f) Ca. Note that the Y-axis scale is variable.

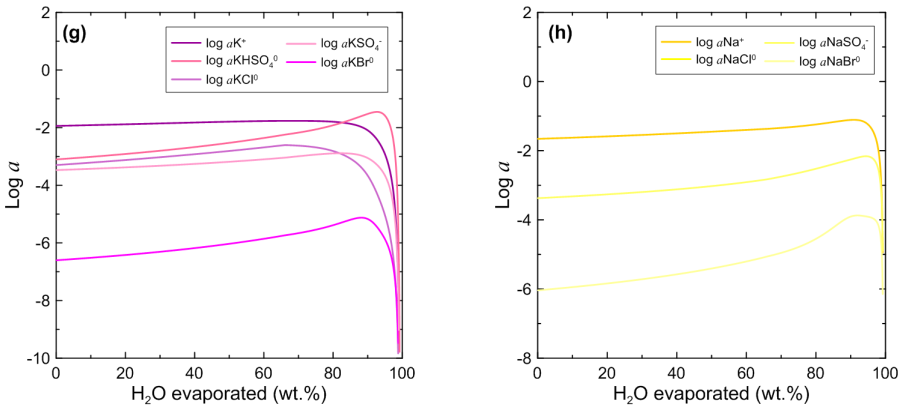

Figure 6.11 (continued). Evaporation simulation (PHREEQC) for the hyperacid Kawah Ijen brine (T=60°C). Activities of the main species of (g) K and (h) Na. Note that the Y-axis scale is variable.

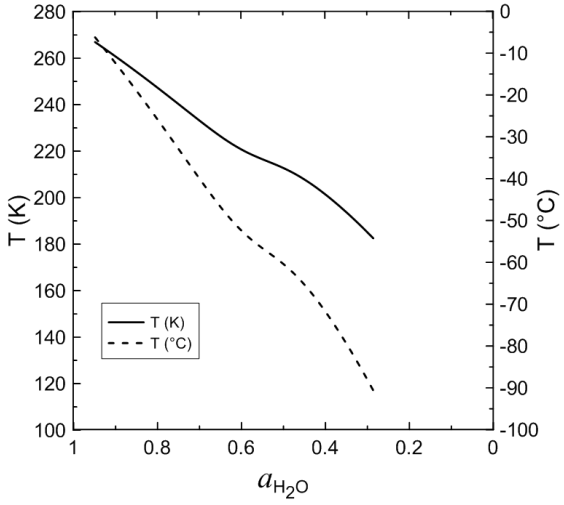

Figure 6.12. Calculated freezing temperatures for remaining liquid during evaporation of the hyperacid Kawah Ijen brine. Input data were obtained from the PHREEQC simulation of the evaporation experiment at T=60°C.

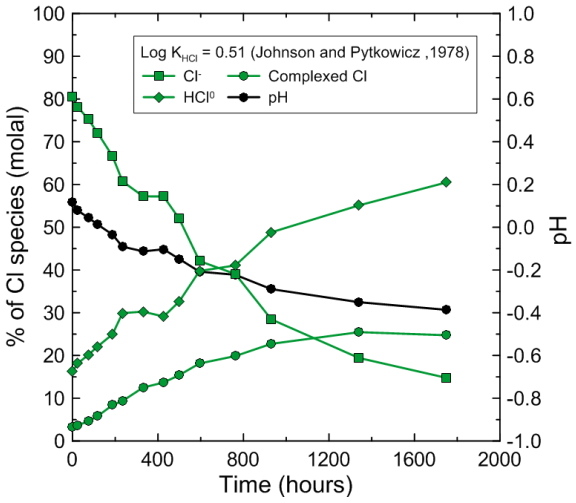

Figure 6.13. Distribution of dissolved Cl species during the evaporation experiment on the hyperacid Kawah Ijen brine, expressed as percentage of the total Cl molality. Note that after 499 hours HCl^0 is more abundant than Cl^-.

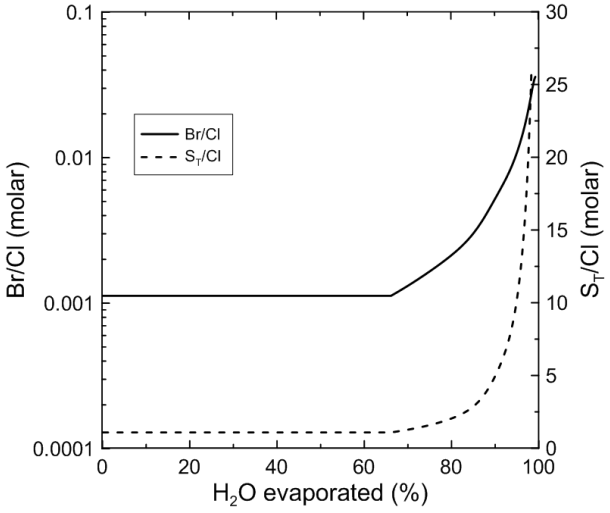

Figure 6.14. Br/Cl and S_T/Cl molar ratios obtained from simulated evaporation of the hyperacid Kawah Ijen brine at T=60°C. The increase in both ratios with time is consistent with loss of gaseous $HCl_{(g)}$ from the brine (see Fig. 6.9).

The change in overall fractionation behaviour in the course of the evaporation experiment can be explained by individual fractionation steps during the two successive reactions needed to form gaseous $HCl_{(g)}$ from the solution:

$$Cl^- + H^+ \Leftrightarrow HCl^0 \quad (12)$$

$$HCl^0 \Leftrightarrow HCl_{(g)} \quad 13)$$

The formation of aqueous HCl^0 (reaction 12) is associated with a positive fractionation factor, and the evaporation step (reaction 13) with a negative one. Competition between these opposing effects thus determines the sign and magnitude of the overall isotopic fraction between gaseous $HCl_{(g)}$ and total dissolved Cl.

According to the speciation calculations, Cl^- was the dominant Cl species in solution before 499 hours, which suggests that reaction (12) was the rate limiting step in the formation of $HCl_{(g)}$. Apparently, the effect of the associated isotopic fractionation overwhelmed that of the subsequent evaporation step, so that the first escaping hydrogen chloride consisted mainly of $H^{37}Cl_{(g)}$. After 499 hours, HCl^0 became the dominant species, which turned kinetic fractionation accompanying reaction (13) into the determining factor. Hence, as soon as much of the chlorine in the solution was converted into HCl^0, the bonding effect became less important in fractionating the isotopes during $HCl_{(g)}$ evaporation in comparison to the kinetic effect associated with translational velocity differences between $H^{35}Cl^0$ and $H^{37}Cl^0$. Consequently, from then on hydrogen chloride preferentially escaped as $H^{35}Cl_{(g)}$.

In a concentrated (12.1 M) hydrochloric acid solution at 25°C, HCl^0 accounts for the 63.1% of the total chlorine concentration, while 36.9% for Cl^-; meaning that the kinetic evaporation experiments of Sharp et al. (2010) mainly measured the fractionation between HCl^0 and $HCl_{(g)}$ as a product of reaction (13), similar to the conditions after 499 hours. Following this reasoning, the sign and magnitude of apparent fractionation between gaseous HCl and total Cl in an aqueous solution depend on the speciation of dissolved Cl, i.e. on the proportions of Cl^- and HCl^0. As the PHREEQC calculations demonstrate, the experimental brine may also contain substantial amounts of various complexed Cl species. Because fractionation factors among all these dissolved species are unknown, a rigorous quantitative approach is not feasible, so that the inferred magnitudes for the initial and final part of the experiment should be taken as approximations for the two different fractionation regimes. Further experimental and theoretical work is needed to substantiate these findings and to clarify the underlying controls.

At this point, it could be possible to infer that if a brine with a similar chemical composition to the Kawah Ijen ones exist on Mars surface and, if they have experienced

some degree of water-loss either by evaporation or freezing (up to a_{H_2O} = 0.85), they would probably carry a slightly positive $\delta^{37}Cl$ signature (+0.68±0.05‰). Nevertheless, it has to be bear in mind that salts in which Cl is present in higher oxidation states, such as chlorates and perchlorates, will also be preferentially enriched in the heaviest ^{37}Cl isotope, consequently exhibiting high $\delta^{37}Cl$ abundances (Schauble et al., 2003). Moreover, salts formed from these brines also could show variations in both Br/Cl and S_T/Cl ratios in response to HCl evaporation due to extremely low pH conditions. This question will be solved until the availability of return samples from Mars.

6.5. CONCLUSIONS

From the results of experimental evaporation on hyperacid brine water from Kawah Ijen crater lake, in combination with geochemical modelling, the following conclusions can be drawn:

1. The solubilities of metals (Al, Fe, Mg, Ca, Na and K) are strongly enhanced by the high contents of HSO_4^-, Cl^- and F^- in these acid waters, because of the formation of a range of complexes that increase in concentration with increasing water loss. The only phases inferred to have formed during the experiment were anatase ($a_{H_2O} \leq$ 0.95), anhydrite ($a_{H_2O} \leq 0.86$) and $HCl_{(g)}$ ($a_{H_2O} \leq 0.86$). Theoretical simulations also predict the formation of elemental sulphur at lower water activities ($a_{H_2O} \leq 0.58$).

2. Escape of gaseous hydrogen chloride occurred throughout a large part of the experiment ($a_{H_2O} \leq 0.86$). This demonstrates that evaporative loss of $HCl_{(g)}$ can be an effective mechanism to fractionate Cl from Br and S_T in acidic sulphate-chloride solutions.

3. The sign and magnitude of chlorine isotope fractionation during evaporation of $HCl_{(g)}$ changed in the course of the experiment, which is inferred to be related to the speciation of Cl in the solution. Before 499 hours, the evaporating $HCl_{(g)}$ was isotopically heavier than the total Cl in solution. The calculated fractionation factor (1000 ln $\alpha_{HCl_{(g)}\text{-}Cl_{diss.}}$) for Rayleigh-type fractionation is +1.55±0.49‰ to +3.7±0.19‰, depending on the approach to determine the Cl losses from the brine compositions. In contrast, the evaporating $HCl_{(g)}$ was isotopically lighter after 499 hours, with a corresponding fractionation factor between -5.54±0.17‰ and -3.97±0.08‰. This change in behaviour coincides with a transition between Cl^- and HCl^0 as dominant Cl species in the solution. This finding indicates that sign and magnitude of Cl isotope fractionation during evaporation of acid brines depends on mechanisms associated with the distribution of dissolved Cl species.

4. The results of this work have several implications for former conditions on Mars: (a) If hyperacid chloride-sulphate brines with a similar chemical composition as many terrestrial volcanic fluids existed, they would have extended the stability of liquid water on the planet's surface down to 183 K (-90.15°C); (b) Solid residues of

evaporation (e.g., salts) may show variations in Cl/Br or Cl/S ratios due to fractionation induced by preferential loss of gaseous HCl. (c) Chlorine isotopic compositions of Cl-bearing solid phases, formed from acidic solutions, may show variations depending on pH and evaporation history.

ACKNOWLEDGEMENTS

We are grateful to Arnold van Dijk for carrying out the mass spectrometer measurements at Utrecht University. The help of Helen de Waard, Ton Zalm and Dineke van de Meent with experiments, ICP-OES and IC analyses was highly appreciated. Funding for this work was provided by NWO (Netherlands Organization for Scientific Research), project ALW-GO-PL/10-03.

CHAPTER

7

Synthesis

7.1. CONCEPTS AND FINDINGS

The principal question addressed in this thesis concerns the applicability of fluid-rock interaction processes, operating at or near the surface of volcanoes with active magmatic-hydrothermal systems, as model to explain the origin of sulphate-rich terrains containing a diversity of associated secondary minerals in the ancient history of Mars. The hypothesis was tested in field studies of stratovolcanoes where intruded magma produces sulphur- and halogen-rich gases that either escape to the atmosphere or are intercepted by water bodies, creating hyperacid lakes, springs and streams. Continuous interaction between the aggressive acidic fluids and local volcanic materials enriches the waters in all common rock-forming elements. A large variety of secondary minerals was encountered in areas exposed at the surface, either as a residue of primary fluid-rock interaction, or as products of further evolution of the aqueous solution in subsurface reservoirs, confined basins or watersheds. The mineral assemblages record the processes and conditions under which they formed. Dynamic changes in subsurface volcanic-hydrothermal activity or atmospheric conditions explain why alteration minerals in these settings are highly diverse and often transient in nature.

These volcanic-hydrothermal systems are marked by strong gradients in temperature, fluid chemistry and redox conditions (**Chapter 2**), which further promote heterogeneity of alteration minerals at relatively small spatial scales. Due to the properties of magma-derived gases, the primary hydrous solutions are commonly of an acid-sulphate-chloride type. Consequently, the nature and formation mechanisms of secondary minerals will differ from to those associated with acid-sulphate aqueous systems originating from hydrous oxidation of sulphides. Nonetheless, volcanic areas often issue acid-sulphate and (near-) neutral thermal waters as well, usually more in the periphery of the complexes.

The formation of secondary minerals as residue of acid leaching below or at the surface is governed by relatively low pH, higher-than-ambient temperature and anoxic redox conditions, apart from the composition of the host rock. Once issued at the surface, concentrated water/brine produces secondary minerals in springs, lakes and streams, largely driven by cooling, increasing pH in response to mixing with neutral waters or progressive interaction with fresh rock, oxidation and evaporation. The water/rock ratio is a critical parameter in all cases.

The active volcanoes studied cover a wide range of sub-environments where numerous different sulphates and other secondary minerals form under a variety of conditions. At Copahue (Argentina), they are aligned along a ca. 40 km long stretch of an

Front picture: Pehuén (*Araucaria araucana*) forest on the outskirts of Copahue volcano (Argentina).

acidic river (Río Agrio) that has its source in the summit area, passes a glacial lake, and receives input from neutral tributaries. The sub-environments at Poás (Costa Rica) include a hyperacid crater lake (Laguna Caliente), hot springs, fumarole vents and areas exposed to acid rain/spray.

The alteration mineralogy displayed by these surface expressions of volcanic-hydrothermal systems is largely similar. Minerals observed in the Copahue watershed (**Chapter 3**) include mono- and polyhydrated ferrous sulphates, mono- and polyhydrated Mg-sulphates, jarosite-alunite group minerals, hydrated ferric and aluminium sulphates, hematite and other oxides, schwertmannite, gypsum/anhydrite, amorphous silica, sulphides, clay minerals and halides. Downstream changes in pH and concentrations of dissolved elements accompany geographic variations in the appearance of these minerals. Thermodynamic calculations illustrate this, showing that goethite, hematite, ferrihydrite are close to or above saturation along the entire river, whereas for jarosite and Mg-nontronite this holds only in the upstream part (pH between 1 and 3.5), and for gibbsite, kaolinite, Mg-montmorillonite, stilbite and leonhardite only in the downstream part (pH ca. 8). Conditions for the saturation of schwertmannite were only reached after substantial dilution (pH around 3), where its formation was probably mediated by Fe-oxidizing acidophilic bacteria and photochemical processes. Geochemical modelling with spring-water compositions predicts that evaporation can induce precipitation of amorphous silica, gypsum, iron (III) fluoride, barite and anatase. In water-rock interaction models, simulating the reaction between andesite rock and water from the hot spring, amorphous silica and anatase were saturated from the start, and were followed, with increasing reaction progress, first by gypsum, jarosite and jurbanite, then by goethite, alunite and kaolinite, and finally by montmorillonite and magnetite. Models for the formation of Mg-sulphates were only successful in a complex scenario involving interaction between relatively small volumes of acid fluid and Mg-rich solid (olivine) in combination with evaporation.

Field evidence and geochemical modelling demonstrate that acid fluids of Poás volcano (pH<2 for the Laguna Caliente lake, and 1-2.5 for hot springs) are capable of producing mineral assemblages, including Ca-, Al-, Fe- and Mg-sulphates, with similar complexity as observed at Copahue, albeit in a more confined area of the active summit crater (**Chapter 4**). Amorphous silica is here a predominant secondary phase, formed either as residue of solid volcanic materials affected by acid leaching or from precipitation out of saturated lake water. In lake sediments, silica is associated with gypsum, native sulphur and minor barite, anatase and pyrite. Various sub-environments in the crater area enabled testing the importance of water/rock ratios in acid alteration processes. In general, the Fe- and Mg-sulphates require the lowest water/rock ratios to form, with the presence of olivine as an indispensable ingredient. These restrictions explain why these sulphates were only found on surfaces of olivine-bearing rocks affected by acid rain or spray from the lake. Conversely, Al-sulphates are present where brine water is more abundant, and pH and/or

temperature are higher than the ambient conditions.

Reaction path models for water-rock interaction predict the stability of secondary minerals over a range of pH, which is a rough indicator of the reaction progress. In lake water models, minerals that appeared to be sensitive to pH are (in order of increasing pH, starting at ca.1): H- and K-jarosite, Na- and K-alunite, $Al(OH)SO_4$, kaolinite, fluorite, pyrite and illite. Comparable trends are valid for fluid-rock interactions involving hot spring waters or gas condensates.

Special attention has been paid to the behaviour of halogens because of (1) their potential as guide to identify processes acting in sulphate-producing volcanic environments, (2) their association with sulphates in volcanic areas on Mars with evidence for acid alteration, and (3) the observed elemental fractionation among halogens (Br and Cl) in Martian surface samples. Time-series results obtained for lake water (27 years) and fumarole condensates (2 years) show significant elemental Br/Cl and stable isotopes of chlorine isotopic fractionation, which reflects interactions between liquid water and vapour (**Chapter 5**). The variability in halogen concentrations, ratios and Cl isotopes observed in the acidic surface waters and fumarolic gases is largely attributable to subsurface processes, comprising phase separation within the magmatic-hydrothermal system at depth and interaction between volcanic gases and shallow groundwaters. Evaporation of $HCl_{(g)}$ from the lake surface produces additional Cl isotopic fractionation effects.

Further insights into the consequences of evaporation acid sulphate-chloride solutions were obtained in experiments with natural crater-lake water of Kawah Ijen, Indonesia (**Chapter 6**). The results demonstrate that the elevated contents of chloride and sulphate in these waters promote the formation of complexes with cations to the extent that the saturation of major solid phases under ambient conditions is limited to amorphous silica, gypsum/anhydrite and anatase. Important findings concern the effects of HCl evaporation and associated chlorine isotopic fractionation. Monitoring the composition of the residual liquid during progressive evaporation shows a marked transition in the isotopic fractionation behaviour between dissolved and gaseous chlorine. Both sign and magnitude of apparent fractionation changed in the course of the experiment, which can be explained by a dependence of the fractionation mechanism on the species distribution of dissolved chlorine as a function of pH.

7.2. COROLLARIES FOR MARS

The results provide a framework for complementary models that can explain the origin of sulphate-bearing settings on the Martian surface, specifically at locations with signs of hydrothermally driven acid alteration. The geological record of Mars provides compelling evidence for hydrothermal environments, which were created either by magmatic activity or by impacts. They were probably more abundant and widespread during the early history of the planet, when liquid water was abundant,

although some hydrothermal activity might still persist today. Locations with a high hydrothermal potential are marked by indications for (1) the presence of liquid water, (2) volcanic constructions and/or lava flows, (3) a centre of magmatic-driven tectonics, (4) topographic depressions and/or valleys that could have been the result of structurally controlled collapse and/or rifting, respectively, (5) impact craters in ice-rich regions, (6) presence of minerals or volatile enrichments that are commonly associated with hydrothermal activity, and (7) geological similarity to hydrothermal environments on Earth (Schulze-Makuch et al., 2007; El Maarry et al., 2013).

Thermal energy and water mobility, the key ingredients of hydrothermal activity, can be delivered via volcanic as well as impact-induced processes. An acid sulphate-chloride character of hydrothermal fluids seems difficult to reconcile with impact-driven activity if water is largely derived from groundwater, melting of ground ice or glaciers or from decomposition of hydrated minerals such as phyllosilicates. Supply of sulphur and halogens, together with heat from magma intrusions and accompanying interaction with water bodies is a more coherent scenario, similar to what commonly sustains acid volcanic lakes on Earth. Still, from observations at terrestrial impact craters, it cannot be excluded that impact-driven hydrothermal activity also created acid-alteration type mineral assemblages, for example when target rocks contain sulphates and halides, or when alteration, weathering, and/or remobilization of primary hydrothermal minerals produce Fe-sulphates and Fe-oxy(hydroxides) such as jarosite, schwertmannite and ferrihydrite (cf. Osinski et al., 2013).

Candidate targets for hydrothermal activity on the Martian surface are open- or closed-basin lakes with secondary mineral assemblages that spectrally deviate from those in nearby watersheds. However, detailed mapping focusing on localized features such as former conduits for escape of steam or waters is required to distinguish settings with endogenic sources from those controlled by impact. A recently described example is Cross Crater (Terra Sirenum), west of the Tharsis rise volcanic edifice, where small outcrops of alunite deposits, intermixed with kaolinite group minerals and silica (or montmorillonite), have been interpreted as products of cooling and oxidation of sulphurous magmatic hydrothermal fluids that rose through fractures and leached local rocks (Ehlman et al., 2016). In nearby Columbus Crater, interpreted as a groundwater-fed paleolake (Wray et al., 2011), various associations of kaolinite-group minerals, opaline silica, gypsum and other polyhydrated sulphates, ferric oxides/hydroxides, jarosite and possible alunite are also consistent with an aqueous system acidified by magmatic volatiles. Chloride salts have not been detected in this crater, which has been attributed to limitations in infrared spectral analysis, burial by younger sediments and lavas, and/or dissolution during later aqueous or diagenetic events (Wray et al., 2011). The common absence/scarcity of chlorides in acid volcanic lake settings such as Poás as well as in the evaporation experiments **(Chapter 6)** indicate that chloride salts do not normally form in acid sulphate-chloride fluids of volcanic origin.

There are many other locations on Mars where secondary mineralogy could have resulted from interaction with, or precipitation from fluids that were acidified by magmatic volatiles. For example, the mineralogy, geochemistry, variability and geologic setting of the Paso Robles class soils in Gusev Crater suggest that their formation was associated with hydrothermal and fumarolic condensates derived from magma degassing and/or oxidative alteration of crustal iron sulphide deposits (Yen et al. 2008). Several different explanations have been given for the formation of sulphur-rich sedimentary rocks of the Burns Formation at Meridiani Planum, but the mineral assemblage (amorphous silica, Mg- and Ca-sulphates, jarosite, hematite and possibly chlorides), pointing to low-pH aqueous conditions, seems also consistent with a reaction between rocks and condensed sulphur dioxide- and water-bearing vapours emitted from fumaroles (McCollom and Hynek, 2005), and thus with a role of volcanic-derived fluids. Voluminous volcanism in Valles Marineris in the early history of Mars when water was still abundant (McEwen et al., 1999) may have created local conditions favourable for interactions between magmatic fluids, rocks and water bodies as well.

The findings at Poás (**Chapter 4**) provide direct field support for Martian chemical weathering regimes where not only low-pH sulphuric acid-rich conditions prevailed but water-rock ratios were also a significant factor in the formation of secondary minerals (Hurowitz and McLennan, 2007). The occurrence of Mg- and Fe-sulphates in areas affected by acid rain or spray confirms the requirement of incipient alteration under water-limited conditions so that only olivine is dissolved. On the other hand, Al mobility needed for the formation of Al-sulphates is promoted by high water/rock ratios and more advanced rock dissolution involving plagioclase, as is substantiated by the high Al contents of Laguna Caliente water and the presence of alunite and other Al-bearing sulphates in the lake environment and ejected lithics.

The abundance of amorphous silica in the crater of Poás has also a bearing on the question of water availability for alteration processes on Mars. For example, the presence of outcrops and soil rich in opaline silica in Gusev Crater has been taken as evidence for hydrothermal activity but there is uncertainty as to whether the silica was produced by leaching from fumarole condensates or precipitated as sinter in a hot spring environment (Yen et al., 2008; Ruff et al., 2011). The latter option, supported by the stratiform distribution of the silica-rich outcrops and their porous and brecciated microtextures, would imply a long-term supply of enough hydrothermal water to allow the growth of sizeable sinter layers. The observations at Poás (and other acid crater-lake hosting volcanoes) demonstrate that silica with different origins can intimately coexist in confined areas affected by hydrothermal activity. Silica-rich lithologies in the crater area are not only present as end-products of acid leaching of local volcanic rocks or pyroclastics, but also as layers in lake sediments formed by precipitation out of saturated hyperacid water. Hence, an alternative option to be considered is that the layered silica deposits of Gusev Crater accumulated at the bottom of a lake that was (partly) fed by hydrothermal input, in

view of the evidence that lake systems in Martian craters may have intermittently existed (Grotzinger et al., 2015). Although the complex hydrothermal history in Gusev Crater, with alterations having occurred at various temperatures and water/rock ratios under different geological conditions (Filiberto and Schwenzer, 2013), does not necessarily require a volcanic source throughout its evolution, many aspects are consistent with a volcanic lake setting, at least locally and with a transient character. The same considerations also apply to other locations where silica deposits are associated with sulphates, such as Cross Crater in Terra Sirenum (Ehlmann et al., 2006) and Ophir Chasma (Wendt et al., 2011), Juventae Chasma (Bishop et al., 2009) and Melas Chasma (Metz et al., 2009) in Valles Marineris.

Recently, chlorine isotope data have been obtained on a suite of Martian meteorites (Sharp et al., 2016; Williams et al., 2016) and sediments in Gale Crater (Farley et al., 2016). Bulk and in-situ apatite analysis of Martian meteorites, which represent a wide diversity of environments, processes and ages, yielded a $\delta^{37}Cl$ range from -3.8 to +8.6‰, much larger than all values reported for terrestrial basalts and ultramafic samples (Sharp et al., 2016 and references therein). The data range could be the result of mechanical mixing between a mantle end-member (-2 to -4‰) and crust/surface material, thought to have been heterogeneously enriched in ^{37}Cl through impact, fluid interaction, and assimilation-fractional crystallization (Williams et al., 2016).

High $\delta^{37}Cl$ values mark all Martian samples with evidence of crustal contamination, with near-surface infiltration of evaporitic waters and magma contamination by evaporites as plausible mechanisms. Although the high $\delta^{37}Cl$ values of crustal materials have been attributed to loss of light ^{35}Cl to space, they may well have been the result of fractionation when rising volcanic gases percolated through groundwater, as discussed in **Chapter 5** (see also Sharp et al., 2010). Furthermore, the experimental results (**Chapter 6**) demonstrate that progressive evaporation of an acid sulphate-chloride solution produces residual brines with variable $\delta^{37}Cl$ due to the escape of gaseous HCl and inconstancy of the isotopic fractionation mechanism. The likelihood that volcanic-hydrothermal systems are locally important for the supply of chlorine and for its surficial cycle on Mars is further supported by the observation that highest concentrations occur in a region with a long history of volcanic activity, where they are presumably related to exhalations and/or chemical alteration through hydrothermal activity (Keller et al., 2006). Uniquely light (down to ca. –50‰) and highly variable $\delta^{37}Cl$ values, measured in Gale Crater by the Sample Analysis at Mars (SAM) instrument on the Curiosity Rover, are far outside the known range for terrestrial volcanic surface environments. They signal a possible role of perchlorates produced from volcanic gas emissions by atmospheric chemical reactions (Farley et al., 2016).

Despite indications that the bulk Br/Cl ratio of Mars is close to chondritic values (Taylor et al., 2010), surface rocks and soils, particularly at Gusev Crater and Merid-

iani Planum, are not only marked by overall halogen enrichment, but also by excess Br and variable Br/Cl ratios (Brückner et al., 2008). This variability in Br/Cl is poorly understood and has been attributed to multiple causes including aqueous alteration, evaporative processes, post-depositional fluid migration, partitioning during uptake in halite and other Cl minerals, possibly controlled by repeated dissolution/precipitation, and photochemical influences on volatilization at the surface (e.g., Clark et al., 2005; Karunatillake et al., 2013; Marion et al., 2009; Rao et al., 2009; Yen et al., 2005 and references therein). As discussed in **Chapter 5**, phase separation in a volcanic-hydrothermal system associated with a degassing magma batch may also be accompanied by Cl-Br fractionation, creating variations in Br/Cl ratios in fluids already before they reach the surface, depending on whether they are gaseous or liquid brine. It is conceivable that such a process caused Br/Cl diversity in Martian soils in cases where hydrothermal supply was linked to acidic fluids of magmatic origin. Another potential fractionation mechanism is preferential evaporation of HCl relative to HBr from hyperacid surface water as inferred for Laguna Caliente and theoretically predicted to occur during advanced stages of brine evaporation (**Chapter 6**). According to the evaporation models presented in that chapter, $HCl_{(g)}$ loss at extremely low pH can cause a significant Br-Cl fractionation, comparable to that observed in soils at Meridiani Planum and Gusev Crater (Brückner et al., 2008).

An important implication of the existence of concentrated acid brines with a sulphate-chloride character is their ability to travel over long distances and precipitate minerals far away from the location where most of the water-rock interaction processes took place, as demonstrated along the trajectory of the acid stream of Río Agrio in the Copahue area (**Chapter 3**; see also Varekamp et al., 2009). The observations testify that the dynamic nature of volcanic-hydrothermal outflow settings is favourable for strong gradients and transient environmental conditions, which promote diversity of secondary minerals on relatively small spatial scales and temporal fluctuations in their stability. The Copahue example illustrates the variety of controls that can play a role, including changes in acid supply depending on volcanic activity, mixing with waters from other sources, and seasonally controlled dilution with melt water from ice and snow. The existence and mobility of liquid hyperacid Cl-SO_4 brines issued on the Martian surface may suffer little from ambient atmospheric conditions given the strong reduction of evaporation rates (Chevrier and Altheide, 2008) and because their concentrated nature and any further effect of evaporation will lead to a significant lowering of the freezing temperature of liquid water, extending its presence on Martian surface or subsurface environments.

7.3. CONCLUDING REMARKS

Sulphate deposits on Mars, categorized into Hesperian layered sulphates, Interior Layered Deposits (ILD), polar deposits, intracrater sediments, as constituent of the global dust and regolith, and as secondary vein minerals, have multiple origins (Gaillard et al., 2013). The results from field observations at Poás and Copahue volcanoes,

experiments and thermodynamic simulations presented in this thesis indicate that active volcanic-hydrothermal processes should be considered as a concrete option in the spectrum of mechanisms proposed for the formation of sulphate-bearing mineral assemblages on the Martian surface. The many candidate paleolakes (Goudge et al. 2015) and volcanic calderas (Robbins et al., 2011) identified on Mars call for detailed investigations to further test this inferred analogy with terrestrial volcanic settings. Surface expressions of terrestrial volcanic hosted hydrothermal systems with their large diversity in alteration products of acid fluid-rock interactions (cf. Hynek et al., 2013) provide direct insights into processes and local variables that controlled the formation of similar secondary mineral assemblages under Martian conditions, despite differences between the two planets in global chemical weathering paths and in the predominance rock types involved (mostly andesitic on Earth, mostly basaltic on Mars). The volcanic settings studied not only provide a conceptual framework for the origin and diversity of acid fluids enriched in sulphur and chlorine, but also illustrate formation environments for a variety of sulphate-bearing mineral assemblages, which emulate surface conditions inferred for major parts of the Martian history.

References

Abramov, O. and Kring, D.A., 2005. Impact-induced hydrothermal activity on early Mars. J. Geophys. Res. 110, E12S09, doi: 10.1029/2005JE002453.

Acero P., Ayora C., Torrento C., Nieto J.M., 2006. The behaviour of trace elements during schwertmannite precipitation and subsequent transformation into goethite and jarosite. Geochim Cosmochim Acta 70, 4130–4139.

Africano F. and Bernard A., 2000. Acid alteration of the fumarolic environment of Usu volcano, Hokkaido, Japan. J. Volcanol. Geotherm. Res. 97, 475-495.

Agusto M.R, Varekamp J.C., 2015. The Copahue volcanic-hydrothermal system and applications for volcanic surveillance. In: Tassi F., Vaselli O. and Caselli, A. (eds.). Copahue volcano. Springer-Verlag Berlin Heidelberd, pp. 199-238, doi: 10.1007/978-3-662-48005-2.

Aiuppa A., 2009. Degassing of halogens from basaltic volcanism: Insights from volcanic gas observations. Chem. Geol. 263, 99-109.

Aiuppa A., Baker D.R. and Webster J.D., 2009. Halogens in volcanic systems. Chem. Geol. 263: 1-18.

Aiuppa A., Federico C., Franco A., Giudice G., Gurrieri S., Inguaggiato S., Liuzzo M., McGonigle A.J.S. and Valenza M., 2005. Emission of bromine and iodine from Mount Etna volcano. Geochem. Geophys. Geosyst. 6, 1-8.

Alexander E.W., 2014. Aqueous geochemistry of an active magmato-hydrothermal system: Copahue Volcano, Río Agrio, and Lake Caviahue, Neuquén, Argentina. Undergraduate thesis, Wesleyan University, Middle-town CT, USA, pp. 1 – 100.

Allison J.D., Brown D.S., Novo-Gradak K.J., 1991. MINTEQA2/PRODEAFA2, a geochemical assessment model for environmental systems. U.S. Environmental Protection Agency, Washington DC, EPA/600/3-91/021.

Altheide T., Chevrier V., Nicholson C. and Denson J., 2009. Experimental investigation of the stability and evaporation of sulfate and chloride brines on Mars. EPSL 282, 69-78.

Alvarado G.E., 2009. Los volcanes de Costa Rica: geología, historia, riqueza natural y su gente. Third edition. EUNED, San José, Costa Rica, 355 p.

Andrews-Hanna J.C, Zuber M.T., Arvidson R.E., Wiseman S.M., 2010. Early Mars hydrology: Meridiani playa deposits and the sedimentary record of Arabia Terra. J. Geophys. Res. 115, E06002.

Arnórsson S., 2000. Assessment of reservoir fluid composition from wet steam well data. In: Arnórsson S. (ed.), Isotopic and chemical techniques in geothermal exploration, development and use. International Atomic Energy Agency (IAEA), Vienna, pp. 212-228.

Arnórsson S., Andrésdóttir A., Gunnarsson I. and Stefánsson A., 1998. New calibration for the quartz and Na/K geothermometers, valid in the range 0-350°C. Proc. Geoscience Society of Iceland Annual Meeting (in Icelandic), Iceland, pp. 42-43.

Arnórsson S., Stefánsson A. and Bjarnason J.Ö., 2007. Fluid-fluid interactions in geothermal systems. In: Liebscher A. and Heinrich C. (eds): Reviews in Mineralogy and Geochemistry, volume 65. Min. Soc. Am. (Virginia, USA), pp. 259-312.

Arvidson R.E., Anderson R.C., Bartlett P., Bell J.F., Christensen P.R., Chu P., Davis K., Ehlmann B.L., Golombek M.P., Gorevan S., Guinness E.A., Haldemann A.F.C., Herkenhoff K.E., Landis G., Li R., Lindemann R., Ming D.W., Myrick T., Parker T., Richter L., Seelos F.P., Soderblom L.A., Squyres S.W., Sullivan R.J. and Wilson J., 2004. Localization and physical property experiments conducted by opportunity at Meridiani Planum. Science 306, 1730-1733.

Arvidson R.E., Poulet F., Morris R.V., Bibring J.P., Bell J.F., Squyres S.W., Christensen P.R., Bellucci G., Gondet B., Ehlmann B.L., Farrand W.H., Fergason R.L., Golombek M., Griffes J.L., Grotzinger J., Guinness E.A., Herkenhoff K.E., Johnson J.R., Klingelhöfer G., Langevin Y., Ming D., Seelos K., Sullivan R.J., Ward J.G., Wiseman S.M. and Wolff M., 2006. Nature and origin of the hematite-bearing plains of Terra Meridiani based on analyses of orbital and Mars Exploration rover data sets. J. Geophys. Res., 111, E12S08, doi:10.1029/2006JE002728.

Baffico GD, Díaz M.M., Wenzel M.T., Koschorreck M., Schimmele, M., Neu T.R. and Pedrozo F., 2004. Community structure and photosynthetic activity of epilithon from a highly acidic (pH 2) mountain stream in Patagonia, Argentina. Extremophiles 8, 463–473.

Baird A., Toulmin P., Clark B., Rose H., Keil K., Christian R. and Gooding J., 1976. Mineralogic and Petrologic Implications of Viking Geochemical Results from Mars. Interim-Report. Science 194, 1288-1293.

Baker V., Strom R., Gulick V., Kargel J., Komatsu G. and Kale V., 1991. Ancient oceans, ice sheets and the hydrological cycle on Mars. Nature 352: 589-594.

Balcone-Boissard H., Villemant B. and Boudon G., 2010. Behavior of halogens during the degassing of felsic magmas. Geochem. Geophys. Geosyst. 11(9), Q09005, doi: 10.1029/2010GC003028.

Baldridge A.M., Hook S.J., Crowley J.K., Marion G.M., Kargel J.S., Michalski J.L., Thomson B.J., de Souza Filho C.R., Bridges N.T. and Brown A.J., 2009. Contemporaneous deposition of phyllosilicates and sulfates: Using Australian acidic saline lake deposits to describe geochemical variability on Mars. Geophys. Res. Lett. 36, L19201.

Ballirano P., 2006. Crystal chemistry of the halotrichite group $XAl_2(SO_4)_4 \cdot 22H_2O$: the X = Fe- Mg-Mn-Zn compositional tetrahedron. Eur. J. Mineral. 18, 463-469.

Bandfield J.L., 2008. High-silica deposits of an aqueous origin in western Hellas Basin, Mars. Gephys. Res. Lett., L12205, doi: 10.1029/2008GL033807.

Bandfield J.L. and Rogers A.D., 2008. Olivine dissolution by acidic fluids in Argyre Planitia, Mars: Evidence for a widespread process? Geology 36, 579-582, doi:10.1130/G24724A.1.

Bandfield J.L., Hamilton V.E. and Christensen P.R., 2000. A global view of Martian surface compositions from MGS-TES: Science 287, 1626–1630, doi: 10.1126/science. 287.5458.1626.

Banin A., Clark B.C. and Wänke H., 1992. Surface chemistry and mineralogy. In: H.H. Kieffer, B.M. Jakosky, C.W. Snyder and M.S. Matthews (eds.), Mars. Univ. Arizona Press, USA, pp. 594-625.

Baratoux D., Pinet P., Toplis M.J., Mangold N., Greeley R. and Baptista A.R., 2009. Shape, rheology and emplacement times of small Martian shield volcanoes. J. Volcanol. Geotherm. Res. 185, 47-68.

Barnes J.D. and Sharp Z.D., 2006. A chlorine isotope study of DSDP/ODP serpentinized ultramafic rocks: insights into the serpentinization process. Chem. Geol. 228, 246-265.

Barnes J.D., Sharp Z.D. and Fischer T.P., 2008. Chlorine isotope variations across the Izu-Bonin-Mariana Arc. Geology 36, 883-886.

Barnes J.D., Sharp Z.D., Fischer T.P., Hilton D.R. and Carr M.J., 2009. Chlorine isotope variations along the Central American volcanic front and back arc. Geochem. Geophys. Geosyst. 10(11), Q11S17, doi: 10.1029/2009GC002587.

Barnhart C.J., Nimmo F. and Travis B.J., 2010. Martian post-impact hydrothermal systems incorporating freezing. Icarus 208, 101-117.

Bayliss P. and Atencio D., 1985. X-ray power diffraction data and cell parameters for copiapite-group minerals. Can. Mineral. 23, 53-56.

Bell J., McSween H., Crisp J., Morris R., Murchie S., Bridges N., Johnson J., Britt D., Golombek M., Moore H., Ghosh A., Bishop J., Anderson R., Bruckner J., Economou T., Greenwood J., Gunnlaugsson H., Hargraves R., Hviid S., Knudsen J., Madsen M., Reid R., Rieder R. and Soderblom L., 2000. Mineralogic and compositional properties of Martian soil and dust: results from Mars Pathfinder. J. Geophys. Res. 105, 1721-1755.

Benison K., 2006. A Martian analogue in Kansas: Comparing Martian strata with Permian acid saline lake deposits. Geology 34, 385-388.

Benison K. and Bowen B., 2006. Acid saline lake systems give clues about past environments and the search for life on Mars. Icarus 183, 225-229.

Benison K. and Goldstein R., 2001. Evaporites and siliciclastics of the Permian Nippewalla Group of Kansas, USA: a case for non-marine deposition in saline lakes and saline pans. Sedimentology 48, 165-188.

Benison K.C., and LaClair, D.A., 2003. Modern and ancient extremely acid saline deposits: Terrestrial analogs for Martian environments? Astrobiology 3, 609–618, doi:10.1089/153110703322610690.

Benison K.C., Bowen B.B., Oboh-Ikuenobe F.E., Jagniecki E.A., LaClair D.A., Story S.L., Mormile M.R. and Hong B., 2007. Sedimentology of acid saline lakes in southern Western Australia: Newly described processes and products of an extreme environment. J. Sed. Res. 77, 366-388.

Benner S.A., Devine K.G., Matveeva L.N. and Powell, D.H., 2000. The missing organic molecules on Mars. Proceedings of the National Academy of Sciences 97(6), 2425-2430.

Bermúdez A. and Delpino D., 1995. Mapa de los peligros potenciales en el área del Volcán Copahue – sector Argentino. Volcanic Hazard Map. The Geological Survey of the Province of Neuquén, Argentina.

Bernard A., Escobar C.E., Mazot A. and Gutiérrez R.E., 2004. The acid volcanic lake of Santa Ana volcano, El Salvador. In: Rose W.I., Bommer J.J., López D.L., Carr M.J. and Major J.J. (eds.), Natural Hazards in El Salvador, GSA Special Paper 375, Boulder, CO, pp. 121-133.

Berndt M.E. and Seyfried Jr. W.E, 1990. Boron, bromine, and other trace elements as clues to the fate of chlorine in mid-ocean ridge vent fluids. Geochim. Cosmochim. Acta 54, 2235-2245.

Berndt M.E. and Seyfried Jr., W.E., 1997. Calibration of BrCl fractionation during subcritical phase separation of seawater: Possible halite at 9 to 10°N East Pacific Rise. Geochim. Cosmochim. Acta 61, 2849-2854.

Bibring J., Langevin Y., Gendrin A., Gondet B., Poulet F., Berthe M., Soufflot A., Arvidson R., Mangold N., Mustard J., Drossart P., and OMEGA Team, 2005. Mars surface diversity as revealed by the OMEGA/Mars Express observations. Science 307, 1576-1581.

Bibring J., Langevin Y., Mustard J., Poulet F., Arvidson R., Gendrin A., Gondet B., Mangold N., Pinet P., Forget F. and OMEGA team, 2006. Global mineralogical and aqueous Mars history derived from OMEGA/Mars express data. Science 312, 400-404.

Bigham J. and Nordstrom D.K., 2000. Iron and aluminum hydroxysulfates from acid sulfate waters. In: Alpers C.N., Jambor J.L. & Nordstrom D.K. (eds.) Sulfate Minerals, Crystallography, Geochemistry and Environmental Significance. Reviews in Mineralogy and Geochemistry, volume 40. Min. Soc. Am. (Virginia, USA), 351-403.

Bigham J.M., Schwertmann U., and Pfab G., 1996. Influence of pH on mineral speciation in a bioreactor simulating acid mine drainage. App. Geochem. 11, 845–849.

Bigham J.M., Schwertmann U., Carlson L. and Murad E., 1990. A poorly crystallized oxyhydoxysulphate of iron formed by bacterial oxidation of Fe (II) in acid mine waters, Geochim. Cosmochim. Acta 54, 2743–2758.

Bigham J.M., Schwertmann, U., Traina S.J., Winland RL and Wolf M., 1996. Schwertmannite and the chemical modeling of iron in acid sulphate waters, Geochim. Cosmochim. Acta 60, 2111–2121.

Bishop J.L., and Murad E. 1996, Schwertmannite on Mars? Spectroscopic analyses of schwertmannite, its relationship to other ferric minerals, and its possible presence in the surface material of Mars, in: Mineral Spectroscopy: A Tribute to Roger. G. Burns (eds. M. D. Dyar, C. McCanmon and M. W. Schaefer), Geochemical Society Sp. Pub. 5, 337-358.

Bishop J.L., Dyar M.D., Lane M.D. and Bandfield J.F., 2005. Spectral identification of hydrated sulfates on Mars and comparison with acidic environments on Earth. Int. J. Astrobiol. 3, 275-285.

Bishop J.L., Parente M., Weitz C.M., Dobre, E.Z.N., Roach L.H., Murchie S.L., McGuire P.C., McKeown N.K., Rossi C.M., Brown A.J., Calvin W.M., Milliken R. and Mustard J.F., 2009. Mineralogy of Juventae Chasma: Sulfates in the light-toned mounds, mafic minerals in the bedrock, and hydrated silica and hydroxylated ferric sulfate on the plateau. J. Geophys. Res. 114, E00D09, doi: 10.1029/2009JE003352.

Blodau C., and Knorr K.H., 2006. Experimental inflow of groundwater induces a "biogeochemical regime shift" in iron-rich and acidic sediments, J. Geophys. Res. 111, G02026.

Bonifacie M., Busigny V., Mével C., Philippot P., Agrinier P., Jendrzejewski N., Scambelluri M. and Javoy M., 2008a. Chlorine isotopic composition in seafloor serpentinites and high-pressure metaperidotites. Insights into oceanic serpentinization and subduction processes. Geochim. Cosmochim. Acta 72, 126-139.

Bonifacie M., Jendrzejewski N., Agrinier P., Humler E., Coleman M. and Javoy M., 2008b. The chlorine isotope composition of Earth's mantle. Science 319, 1518-1520.

Bonifacie M., Monnin C., Jendrzejewski N., Agrinier P. and Javoy M., 2007. Chlorine stable isotopic composition of basement fluids of the eastern flank of the Juan de Fuca Ridge (ODP Leg 168). Earth Planet. Sci. Lett. 260, 10-22.

Borowska Z., Mauzerall D., 1986. Formation of hydrogen on irradiation of aqueous ferrous iron by UV-light at neutral pH. Orig. Life Evol. Biosph. 16(3-4), 194-195.

Brady K.S., Bigham J.M., Jaynes W.F. and Logan, T.J. 1986. Influence of sulphate on Fe-oxide formation: Compositions with a stream receiving acid mine drainage. Clays and Clay Minerals 34, 266–274.

Braitsch O., 1971. Salt deposits, their origin and composition. Springer-Verlag, New York, 297 p.

Brass G.W., 1980. Stability of brines on Mars. Icarus 42, 20-28.

Braterman P., Cairns-Smith A.G., Sloper R.W., 1983. Photo-oxidation of hydrated Fe^{2+}-significance for banded iron formations. Nature 303(5913), 163-164.

Bridges J., Catling D., Saxton J., Swindle T., Lyon I. and Grady M., 2001. Alteration assemblages in Martian meteorites: implications for near-surface processes. Space Science Reviews 96, 365-392.

Broz P. and Hauber E., 2012. A unique volcanic field in Tharsis, Mars: Pyroclastic cones as evidence for explosive eruptions. Icarus 218, 88-99.

Broz P. and Hauber E., 2013. Hydrovolcanic tuff rings and cones as indicators for phreatomagmatic explosive eruptions on Mars. J. Geophys. Res. 118, 1656-1675.

Brückner J., Dreibus G., Gellert R., Squyres S., Wanke H., Yen A. and Zipfel J., 2008. Mars Exploration Rovers: Chemical composition by the APXS. In: Bell J. (ed.): The Martian Surface: Composition, Mineralogy, and Physical Properties. Cambridge Univ. Press, Cambridge, U.K., pp. 58-101.

Bruland K.W. and Lohan M.C., 2003. 6.02 - Controls of Trace Metals in Seawater. In: Turekian, H.D.H.K. (ed.), Treatise on Geochemistry. Pergamon, Oxford. pp. 23-47.

Burgess R., Cartwright J.A. and Filiberto J., 2013. Halogen abundances of the Martian mantle. Goldschmidt 2013 (abstract). Mineralogical Magazine, 77(5), p. 793.

Burns R.G., 1993. Rates and mechanisms of chemical weathering of ferromagnesian silicate minerals on Mars. Geochim. Cosmochim. Acta 57, 4555-4574.

Burns R. and Fisher D., 1990. Evolution of sulphide mineralization on Mars. J. Geophys. Res. 95, 14169-14173.

Burns R. and Fisher D., 1993. Rates of oxidative weathering on the surface of Mars. J. Geophys. Res.98, 3365-3372.

Cairns-Smith A.G., 1978. Precambrian solution photochemistry, inverse segregation, and banded iron formations. Nature 276 (5690), 807-808.

Campbell A.C. and Edmond J.M., 1989. Halide systematics of submarine hydrothermal vents. Nature 342, 168-170.

Campos L.A., Castro L., Gazel E., Montes N., Murillo S., Ramírez S., Ruiz P. and Sequiera M., 2004. Geología, geomorfología, amenazas naturales del Cantón de Poás, Alajuela. Informe de Campaña Geológica, Universidad de Costa Rica, 60 p.

Capaccioni B., Rouwet D. and Tassi F., 2016. HCl degassing from extremely acidic crater lakes: preliminary results from experimental determinations and implications for geochemical monitoring. In: Ohba, T., Capaccioni, B. and Caudron, C. (eds.), Geochemistry and Geophysics of Active Volcanic Lakes. Special Publications 437, The Geological Society, London, doi: org/10.1144/SP437.12.

Carr M.H. and Head J.W., 2010. Geologic history of Mars. EPSL 294, 185-203.

Carr M.J., Saginor I., Alvarado G.E., Bolge L.L., Lindsay F.N., Milidakis K., Turrin B.D., Feigenson M.D. and Swisher C.C. III, 2007. Element fluxes from the volcanic front of Nicaragua and Costa Rica. Geochem. Geophys. Geosyst. 8, Q06001, doi: 10.1029/2006GC001396.

Carter J. and Poulet F., 2012. Orbital identification of clays and carbonates in Gusev crater. Icarus 219, 250-253.

Casertano L., Borgia A., Cigolini C., Morales L.D., Montero W., Gómez M. and Fernández J.F., 1987. An integrated dynamic model for the volcanic activity at Poás volcano, Costa Rica. Bull. Volc. 49, 588-598.

Catling D.C. and Moore J.M., 2003. The nature of coarse-grained crystalline hematite and its implications for the early environment of Mars. Icarus 165, 277-300.

Chapman M.G., 2002. Layered, massive and thin sediments on Mars: possible Late Noachian to Late Amazonian tephra? In: Smellie, J.L., Chapman, M.G. (eds.), Volcano/Ice Interactions on Earth and Mars, Special Publication 202, The Geological Society, London, pp. 273–293.

Chapman M.G. and Tanaka K.L., 2001. Interior trough deposits on Mars: Sub ice volcanoes? J. Geophys. Res. 106, 10087-10100.

Chevrier V.F. and Altheide T.S., 2008. Low temperature aqueous ferric sulfate solutions on the surface of Mars. Geophys. Res. Lett. 35, L22101.

Chevrier V. and Mathé P.E., 2007. Mineralogy and evolution of the surface of Mars: a review. Planet. Space Sci. 55, 289-314.

Chevrier V., Rochette P., Mathé P. and Grauby O., 2004. Weathering of iron-rich phases in simulated Martian atmospheres. Geology 32, 1033-1036.

Chevrier V., Mathé P.E., Rochette P., Grauby O., Bourrie G. and Trolard F., 2006. Iron weathering products in a CO_2+(H_2O or H_2O_2) atmosphere: implications for weathering processes on the surface of Mars. Geochim. Cosmochim. Acta 70, 4295-4317.

Christensen P.R., Bandfield J.L., Clark R.N., Edgett K.S., Hamilton V.E., Hoefen T., Kieffer H.H., Kuzmin R.O., Lane M.D., Malin M.C., Morris R.V., Pearl J.C., Pearson R., Roush T.L., Ruff S.W. and Smith M.D., 2000. Detection of crystalline hematite mineralization on Mars by the Thermal Emission Spectrometer: Evidence for near-surface water. J. Geophys. Res. 105, 9623-9642.

Christensen P., Bandfield J., Hamilton V., Ruff S., Kieffer H., Titus T., Malin M., Morris R., Lane M., Clark R., Jakosky B., Mellon M., Pearl J., Conrath B., Smith M., Clancy R., Kuzmin R., Roush T., Mehall G., Gorelick N., Bender K., Murray K., Dason S., Greene E., Silverman S. and Greenfield M., 2001. Mars Global Surveyor Thermal Emission Spectrometer experiment: investigation description and surface science results. J. Geophys. Res. 106, 23823-23871.

Christensen P.R., Wyatt M.B., Glotch T.D., Rogers A.D., Anwar S., Arvidson R.E., Bandfield J.L., Blaney D.L., Budney C., Calvin W.M., Faracaro A., Fergason R.L., Gorelick N., Graff T.G., Hamilton V.E., Hayes A.G., Johnson J.R., Knudson A.T., McSween H.Y., Mehall G.L., Mehall L.K., Moersch J.E., Morris R.V., Smith M.D., Squyres S.W., Ruff S.W. and Wolff M.J., 2004. Mineralogy at Meridiani Planum from the Mini-TES experiment on the Opportunity Rover. Science 306, 1733-1739.

Christenson B. and Wood C., 1993. Evolution of a vent-hosted hydrothermal system beneath Ruapehu crater lake, New Zealand. Bull. Volc. 55, 547-565.

Christenson B., Németh K., Rouwet D., Tassi F., Vandemeulebrouck J. and Varekamp J.C., 2015. Volcanic Lakes. In: Rouwet D., Christenson B. Tassi, F. and Vandemeulebrouck J. (eds.) Volcanic Lakes Springer, Heidelberg. pp. 1-21.

Cigolini C., Kudo A.M., Brookins D.G. and Ward D., 1991. The petrology of Poás volcano lavas: basalt-andesite relationship and their petrogenesis within the magmatic arc of Costa Rica. J. Volcanol. Geotherm. Res. 48, 367-384.

Clark B.C. and Van Hart D.C., 1981. The salts of Mars. Icarus 45, 370-378.

Clark B.C., Baird A.K., Rose H.J., Toulmin P., Keil K., Castro A.J., Kelliher W.C., Rowe C.D. and Evans P.H., 1976. Inorganic analyses of Martian surface samples at the Viking landing sites. Science 194, 1283-1288.

Clark B.C., Baird A.K., Weldon R.J., Tsusaki D.M., Schnabel L. and Candelaria M.P., 1982. Chemical composition of Martian fines. J. Geophys. Res. 87, 10059-10067.

Clark B.C., Morris R.V., McLennan S.M., Gellert R., Jolliff B., Knoll A.H., Squyres S.W., Lowenstein, T.K., Ming D.W., Tosca N.J., Yen A., Christensen P.R., Gorevan S., Bruckner J., Calvin W., Dreibus G., Farrand W., Klingelhöfer G., Waenke H., Zipfel J., Bell J.F., Grotzinger J., McSween H.Y. and Rieder R., 2005. Chemistry and mineralogy of outcrops at Meridiani Planum. EPSL 240, 73-94.

Clark R.N, Swayze G.A, Wise R.A, Eric Livo K., Hoe-fen T.M., Kokaly R.F. and Sutley S.J., 2007. USGS digital spectral library splib06a. U.S. Geological Survey, Digital Data Series 231.

Collienne R.H., 1983. Photo-reduction of iron in the epilimnion of acidic lakes. Limnol. Oceanogr. 28(1), 83-100.

Cousins C.R., Crawford I.A., Carrivick J.L., Gunn M., Harris J., Kee T.P., Karlsson M., Carmody L., Cockell C., Herschy B., Joy K.H., 2013. Glaciovolcanic hydrothermal environments in Iceland and implications for their detection on Mars. J. Volc. Geotherm. Res. 256, 61–77.

Czarnacki M. and Halas S., 2012. Isotope fractionation in aqua-gas systems: Cl_2-HCl-Cl^-, Br_2-HBr-Br^- and H_2S-S^{2-}. Isot. Environ. Health Stud. 48, 55-64.

David F., David P.G., 1976. Photoredox chemistry of iron (III) chloride and iron (III) perchlorate in aqueous media. A comparative study. J. Phys. Chem. 80, 579-583.

Dehouck E., Chevrier V., Gaudin A., Mangold N., Mathé P. and Rochette P., 2012. Evaluating the role of sulfide-weathering in the formation of sulfates or carbonates on Mars. Geochim. Cosmochim. Acta 90, 47-63.

Delmelle P. and Bernard A., 1994. Geochemistry, mineralogy and chemical modelling of the acid crater lake of Kawah-Ijen Volcano, Indonesia. Geochim. Cosmochim. Acta 58, 2445-2460.

Delmelle P. and Bernard A., 2000, Downstream composition changes of acidic volcanic waters discharged into the Banyupahit stream, Ijen caldera, Indonesia. J. Volcanol. Geotherm. Res. 97, 55–75.

Delmelle P., Bernard A., Kusakabe M., Fischer T.P. and Takano B., 2000. Geochemistry of the magmatic-hydrothermal system of Kawah Ijen volcano, East Java, Indonesia. J. Volcanol. Geotherm. Res. 97, 31-53.

DeMets C., Gordon R.G. and Argus D.F., 2010. Geologically current plate motions. Geophys. J. Int. 181, 1-80.

Dohm J.M., Williams J., Anderson R.C., Ruiz J., McGuire P.C., Komatsu G., Davila A.F., Ferris J.C., Schulze-Makuch D., Baker V.R., Boynton W.V., Fairen A.G., Hare T.M., Miyamoto H., Tanaka K.L. and Wheelock S.J., 2009. New evidence for a magmatic influence on the origin of Valles Marineris, Mars. J. Volcanol. Geotherm. Res. 185, 12-27.

Dreibus G. and Wänke H., 1987. Volatiles on Earth and Mars: A comparison. Icarus 71, 225-240.

Eastoe C.J., Long A. and Knauth L., 1999. Stable chlorine isotopes in the Palo Duro Basin, Texas: Evidence for preservation of Permian evaporite brines. Geochim. Cosmochim. Acta 63, 1375-1382.

Eastoe C.J., Peryt T.M., Petrychenko O.Y. and Geisler-Cussey D., 2007. Stable chlorine isotopes in Phanerozoic evaporites. Appl. Geochem. 22, 575-588.

Economou T., 2001. Chemical analyses of Martian soil and rocks obtained by the Pathfinder Alpha Proton X-ray spectrometer. Radiat. Phys. Chem. 61, 191-197.

Eggenkamp H.G.M., 1994. The Geochemistry of chlorine isotopes. Ph.D. thesis, Utrecht University, 150 p.

Ehlmann B.L. and Edwards C.S., 2014. Mineralogy of the Martian surface. Ann. Rev. EPSL 42, 291-315.

Ehlmann B.L., Mustard J.F., Murchie S.L., Bibring J., Meunier A., Fraeman A.A. and Langevin Y., 2011. Subsurface water and clay mineral formation during the early history of Mars. Nature 479, 53-60.

Ehlmann B.L., Swayze G.A., Milliken R.E., Mustard J.F., Clark R.N., Murchie S.L., Breit G.N., Wray J.J., Gondet B., Poulet F., Carter J., Calvin W.M., Benzel W.M. and Seelos K.D., 2016. Discovery of alunite in Cross crater, Terra Sirenum, Mars: Evidence for acidic, sulfurous waters. Am. Mineral. 101, 1527-1542.

Einaudi M.T., Hedenquist J.W. and Inan E.E., 2003. Sulfidation State of Fluids in Active and Extinct Hydrothermal Systems: Transitions from Porphyry to Epithermal Environments. In: Simmons, S.F. and Graham I. (eds.): Volcanic, Geothermal, and Ore-Forming Fluids: Rulers and Witnesses of Processes within the Earth. Society of Economic Geologists, Special Publication No. 10. Littleton, Colorado (USA), 285-314.

El Maarry M.R., Dohm J.M., Marzo G.A., Fergason R., Goetz W., Heggy E., Pack A. and Markiewicz W.J., 2012. Searching for evidence of hydrothermal activity at Apollinaris Mons, Mars. Icarus 217, 297-314.

Elsenousy A., Hanley J. and Chevrier V.F., 2015. Effect of evaporation and freezing on the salt paragenesis and habitability of brines at the Phoenix landing site. EPSL 421, 39-46.

Elwood-Madden M., Bodnar R. and Rimstidt J., 2004. Jarosite as an indicator of water-limited chemical weathering on Mars. Nature 431, 821-823.

Elwood-Madden M.E., Madden A.S. and Rimstidt J., 2009. How long was Meridiani Planum wet? Applying a jarosite stopwatch to determine the duration of aqueous diagenesis. Geology 37, 635-638.

Emmenegger L., Schönenberger R., Sigg L., Sulzberger B., 2001. Light-induced redox cycling of iron in circumneutral lakes. Limnol. Oceanogr. 46, 49-61.

Fairén A., Fernández-Remolar D., Dohm J., Baker V. and Amils R., 2004. Inhibition of carbonate synthesis in acidic oceans on early Mars. Nature 431, 423-426.

Farley K. A., Martin P., Archer Jr. P.D., Atreya S.K., Conrad P.G., Eigenbrode J.L., Fairén A.G., Franz H.B., Freissinet C., Glavin D.P., Mahaffy P.R., Malespín C., Ming D.W., Navarro-González R. and Sutter B., 2016. Light and variable $^{37}Cl/^{35}Cl$ ratios in rocks from Gale Crater, Mars: Possible signature of perchlorate. EPSL 438, 14-24.

Farrand W.H., Glotch, T.D., Rice Jr. J.W., Hurowitz J.A. and Swayze G.A., 2009. Discovery of jarosite within the Mawrth Vallis region of Mars: Implications for the geologic history of the region, Icarus 204, 478-488.

Faure G., 1998. Principles and applications of geochemistry. Prentice Hall (New Jersey, USA): 600 pp.

Fernández-Remolar D. and Knoll A.H., 2008. Fossilization potential of iron-bearing minerals in acidic environments of Río Tinto, Spain: implications for Mars exploration. Icarus 194, 72-85.

Fernández-Remolar D., Gómez-Elvira J., Gómez F., Sebastián E., Martin J., Manfredi J., Torres J., Kesler C. and Amils R., 2004. The Tinto River, an extreme acidic environment under control of iron, as an analog of the Terra Meridiani hematite site of Mars. *Planet.* Space Sci. 52, 239-248.

Fernández-Remolar D., Morris R., Gruener J., Amils R. and Knoll A., 2005. The Rio Tinto basin, Spain: Mineralogy, sedimentary geobiology, and implications for interpretation of outcrop rocks at Meridiani Planum, Mars. EPSL 240, 149-167.

Fernández-Remolar D., Prieto-Ballesteros O., Gómez-Ortiz D., Fernández-Sanpedro M., Sarrazin P., Gailhanou M. and Amils R., 2011. Río Tinto sedimentary mineral assemblages: A terrestrial perspective that suggests some formation pathways of phyllosilicates on Mars. Icarus 211, 114-138.

Filiberto J. and Schwenzer S.P., 2013. Alteration mineralogy of the Home Plate and Columbia Hills – Formation conditions in context to impact, volcanism, and fluvial activity. Meteor. Planet. Sci. 48, 1937–1957, doi: 10.1111/maps.12207.

Filiberto J. and Treiman A.H., 2009. Martian magmas contained abundant chlorine, but little water. Geology 37, 1087-1090.

Filiberto J., Chin E., Day J.M.D., Franchi I.A., Greenwood R.C., Gross J., Pennisto-Dorland S.C., Schwenzer S.P. and Treiman A.H., 2012. Geochemistry of intermediate olivine-phyric shergottite Northwest Africa 6234, with similarities to basaltic shergottite Northwest Africa 480 and olivine-phyric shergottite Northwest Africa 2990. Meteor. Planet. Sci.47, 1256-1273.

Fischer T.P., Ramírez C., Mora-Amador R.A., Hilton D.R., Barnes J.D., Sharp Z.D., Le Brun M., de Moor J.M., Barry P.H., Fueri E. and Shaw A.M., 2015. Temporal variations in fumarole gas chemistry at Poás volcano, Costa Rica. J. Volcanol. Geotherm. Res. 294, 56-70.

Fishbaugh K.E., Poulet F., Chevrier V., Langevin Y. and Bibring J., 2007. On the origin of gypsum in the Mars north polar region. J. Geophys. Res. 112, E07002, doi: 10.1029/2006JE002862.

Flahaut J., Quantin C., Allemand P., Thomas P. and Le Deit L., 2010. Identification, distribution and possible origins of sulfates in Capri Chasma (Mars), inferred from CRISM data. J. Geophys. Res. 115, E11007, doi: 10.1029/2009JE003566.

Flahaut J., Quantin C., Clenet H., Allemand P., Mustard J.F. and Thomas P., 2012. Pristine Noachian crust and key geologic transitions in the lower walls of Valles Marineris: Insights into early igneous processes on Mars. Icarus 221, 420-435.

Foley C., Economou T. and Clayton R., 2003. Final chemical results from the Mars Pathfinder alpha proton X-ray spectrometer. J. Geophys. Res. 108 (E12), 8096, doi: 10.1029/2002JE002019.

Fournier R.O. and Rowe J.J., 1966. Estimation of underground temperatures from the silica content of water from hot springs and wet-steam wells. Am. J. Sci. 264, 685-697.

Foustoukos D.I. and Seyfried Jr., W.E., 2007. Trace element partitioning between vapour, brine and halite under extreme phase separation conditions. Geochim. Cosmochim. Acta 71, 2056-2071.

Fueten F. Flahaut J., Stesky R., Hauber E. and Rossi A.P., 2014. Stratigraphy and mineralogy of Candor Mensa, West Candor Chasma, Mars: Insights into the geologic history of Valles Marineris. J. Geophys. Res. 119, 331–354, doi: 10.1002/2013JE004557.

Gagliano W.B., Brill, M.R., Bigham J.M., Jones F.S. and Traina S.J., 2004. Chemistry and mineralogy of ochreous sediments in a constructed mine drainage wetland. Geochim. Cosmochim. Acta 68, 2119–2128.

Gaillard F., Michalski J., Berger G., McLennan S.M. and Scaillet B., 2013. Geochemical reservoirs and timing of sulfur cycling on Mars. Space Sci. Rev. 174, 251-300.

Gamazo P., Bea S.A., Saaltink M.W., Carrera J. and Ayora C., 2011. Modeling the interaction between evaporation and chemical composition in a natural saline system. J. Hydrol. 401, 154-164.

Gammons C.H., Nimick D.A., Parker S.R., Cleasby, T.E., McClesky R.B., 2005b. Diel behavior of iron and other heavy metals in a mountain stream with acidic to neutral pH: Fisher Creek, MT, USA. Geochim. Cosmochim. Acta. 69, 2505-2516.

Gammons C.H., Wood S.A., Pedrozo F., Varekamp J.C., Nelson B., Shope C.L., and Baffico G., 2005a. Hydrogeochemistry and rare earth element behavior in a volcanically acidified watershed in Patagonia, Argentina. Chem. Geol. 222, 249-267.

Gazel E. and Ruiz P., 2005. Los conos piroclásticos de Sabana Redonda: componente magmático enriquecido del volcán Poás. Rev. Geol. Amér. Cent. 33, 45-60.

Gellert R., Rieder R., Anderson R., Bruckner J., Clark B., Dreibus G., Economou T., Klingelhöfer G., Lugmair G., Ming D., Squyres S., d'Uston C., Wanke H., Yen A. and Zipfel J., 2004. Chemistry of rocks and soils in Gusev crater from the alpha particle X-ray spectrometer. Science 305, 829-832.

Gellert R., Rieder R., Bruckner J., Clark B., Dreibus G., Klingelhöfer G., Lugmair G., Ming D., Wanke H., Yen A., Zipfel J. and Squyres S., 2006. Alpha particle X-ray spectrometer (APXS): Results from Gusev crater and calibration report. J. Geophys. Res. 111, E02S05, doi: 10.1029/2005JE002555.

Gemmell J.B., 1987. Geochemistry of metallic trace elements in fumarolic condensates from Nicaraguan and Costa Rican volcanoes. J. Volcanol. Geotherm. Res. 33, 161-181.

Gendrin A., Mangold N., Bibring J., Langevin Y., Gondet B., Poulet F., Bonello G., Quantin C., Mustard J., Arvidson R. and LeMouelic S., 2005. Sulfates in Martian layered terrains: the OMEGA/Mars Express view. Science 307, 1587-1591.

Gerlach T., 2004. Volcanic sources of tropospheric ozone-depleting trace gases. Geochem. Geophys. Geosyst. 5, Q09007, doi:10.1029/2004GC000747.

German C.R. and Von Damm K.L., 2003. 6.07 - Hydrothermal Processes. In: Turekian, H.D.H.K. (ed.), Treatise on Geochemistry. Pergamon, Oxford, pp. 181-222.

Giggenbach W.F., 1991. Chemical techniques in geothermal exploration. In: D´Amore F. (ed.). Application of Geochemistry in Geothermal Reservoir Development. UNITAR/UNDP Centre on Small Energy Resources, pp. 119-144.

Giggenbach W.F., 1996. Chemical composition of volcanic gases. In: Scarpa, R. and Tilling, R.I. (eds.), Monitoring and Mitigation of Volcanic Hazards. Springer Verlag, Heidelberg. pp. 221-256.

Giggenbach W.F. and Corrales R., 1992. Isotopic and Chemical-Composition of Water and Steam Discharges from Volcanic Magmatic Hydrothermal Systems of the Guanacaste Geothermal Province, Costa-Rica. Appl. Geochem. 7, 309-332.

Giggenbach W.F., Minissale A.A. and Scandiffio G., 1988. Isotopic and chemical assessment of geothermal potential of the Colli Albani Are, Latium region, Italy. Appl. Geochem. 3, 475-486.

Gíslasson S.R. and Arnórsson S., 1993. Dissolution of primary basaltic minerals in natural waters - saturation state and kinetics. Chem. Geol. 105, 117-135.

Glotch T.D. and Bandfield J.L., 2006. Determination and interpretation of surface and atmospheric Miniature Thermal Emission Spectrometer spectral end-members at the Meridiani Planum landing site. J. Geophys. Res. 111, E12S06, doi: 10.1029/2005JE002671.

Glotch T.D., Bandfield J.L., Christensen P.R., Calvin W.M., McLennan S.M., Clark B.C., Rogers A.D. and Squyres S.W., 2006. Mineralogy of the light-toned outcrop at Meridiani Planum as seen by the Miniature Thermal Emission Spectrometer and implications for its formation. J. Geophys. Res. 111, E12S03, doi: 10.1029/2005JE002672.

Godon A., Jendrzejewski N., Castrec-Rouelle M., Dia A., Pineau F., Boulègue J. and Javoy M., 2004b. Origin and evolution of fluids from mud volcanoes in the Barbados accretionary complex. Geochim. Cosmochim. Acta 68, 2153-2165.

Godon A., Jendrzejewski N., Eggenkamp H.G.M., Banks D.A., Ader M., Coleman M.L. and Pineau F., 2004a. A cross-calibration of chlorine isotopic measurements and suitability of seawater as the international reference material. Chem. Geol. 207, 1-12.

Goff F. and McMurtry G.M., 2000. Tritium and stable isotopes of magmatic waters. J. Volcanol. Geotherm. Res. 97, 347-396.

Golden D., Ming D., Morris R. and Mertzman S., 2005. Laboratory-simulated acid-sulfate weathering of basaltic materials: implications for formation of sulfates at Meridiani Planum and Gusev crater, Mars. J. Geophys. Res. 110, E12S07, doi: 10.1029/2005JE002451.

Goudge T.A., Aureli K.L., Head J.W., Fassett C.I. and Mustard J.F., 2015. Classification and analysis of candidate impact crater-hosted closed-basin lakes on Mars. Icarus 260, 346-367.

Grahmann W., 1920. Uber barytocolestin und das verhaltnis von anhydrit zu colestin und baryt. Neues Jahrb Mineral 1, 1-23.

Greenwood J.P., 2005. Chlorine-rich apatites in SNC´s: evidence for magma-brine interactions on Mars? 68th Annual Meteoritical Society Meeting. Abstract 349: 285-293.

Greenwood J.P. and Blake R.E., 2006. Evidence for an acidic ocean on Mars from phosphorus geochemistry of Martian soils and rocks. Geology 34, 953-956.

Grindrod P.M. and Balme M.R., 2010. Groundwater processes in Hebes Chasma, Mars. Gephys. Res. Lett. 37, L13202, doi: 10.1029/2010GL044122.

Gross J., Filiberto J. and Bell A.S., 2013. Water in the Martian interior: evidence for terrestrial MORB mantle-like volatile contents from hydroxyl-rich apatite in olivine–phyric shergottite NWA 6234. EPSL 369–370, 120-128.

Grott M., Baratoux D., Hauber E., Sautter V., Mustard J., Gasnault O., Ruff S.W., Karato S., Debaille V., Knapmeyer M., Sohl F., van Hoolst T., Breuer D., Morschhauser A. and Toplis M.J., 2013. Long-term evolution of the Martian crust-mantle system. Space Sci, Rev. 174, 49-111.

Grotzinger J., Arvidson R., Bell J., Calvin W., Clark B., Fike D., Golombek M., Greeley R., Haldemann A., Herkenhoff K., Jolliff B., Knoll A., Malin M., McLennan S., Parker T., Soderblom L., Sohl-Dickstein J., Squyres S., Tosca N. and Watters W., 2005. Stratigraphy and sedimentology of a dry to wet aeolian depositional system, Burns formation, Meridiani Planum, Mars. EPSL 240, 11-72.

Grotzinger J.P., Gupta S., Malin M.C., Rubin D.M., Schieber J., Siebach K., Sumner D.Y., Stack K.M., Vasavada A.R., Arvidson R.E., Calef F., Edgar L., Fischer W.F., Grant J.A., Griffes J., Kah L.C., Lamb M.P., Lewis K.W., Mangold N., Minitti M.E., Palucis M., Rice M., Williams R.M.E., Yingst R.A., Blake D., Blaney D., Conrad P., Crisp J., Dietrich W.E., Dromart G., Edgett K.S., Ewing R.C., Gellert R., Hurowitz J.A., Kocurek G., Mahaffy P., McBride M.J., McLennan S.M., Mischna M., Ming D., Milliken R., Newsom H., Oehler D., Parker T.J., Vaniman D., Wiens R.C. and Wilson S.A., 2015. Deposition, exhumation, and paleoclimate of an ancient lake deposit, Gale crater, Mars. Science 350, aac7575, doi:10.11 26/science.aac 7575.

Gunnarsson I. and Arnórsson S., 2000. Amorphous silica solubility and the thermodynamic properties of $H_4SiO^0_4$ in the range of 0° to 350°C at P_{sat}. Geochim. Cosmochim. Acta 64, 2295-2307.

Hammarstrom J.M., Seal R.R.I., Meier A.L. and Kornfeld J.M., 2005. Secondary sulfate minerals associated with acid drainage in the eastern US: recycling of metals and acidity in surficial environments. Chemical Geology 215, 407-431.

Hammouya G., Allard P., Jean-Baptiste P., Parello F., Semet M.P. and Young S.R., 1998. Pre- and syn-eruptive geochemistry of volcanic gases from Soufrière Hills of Montserrat, West Indies. Geophys. Res. Lett. 25, 3685-3688.

Hanley J., Chevrier V.F., Berget D.J. and Adams R.D., 2012. Chlorate salts and solutions on Mars. Geophys. Res. Lett. 39, L08201, doi: 10.1029/2012GL051239.

Harford C., Sparks R. and Fallick A., 2003. Degassing at the Soufrière Hills Volcano, Montserrat, recorded in matrix glass compositions. J. Petrol. 44, 1503-1523.

Hartmann W.K. and Neukum G., 2001. Crater chronology and the evolution of Mars. Space Sci. Rev. 96, 165-194.

Haskin L., Wang A., Jolliff B., McSween H., Clark B., Des Marais D., McLennan S., Tosca N., Hurowitz J., Farmer J., Yen A., Squyres S., Arvidson R., Klingelhöfer G., Schroder C., de Souza P., Ming D., Gellert R., Zipfel J., Bruckner J., Bell J., Herkenhoff K., Christensen P., Ruff S., Blaney D., Gorevan S., Cabrol N., Crumpler L., Grant J. and Soderblom L., 2005. Water alteration of rocks and soils on Mars at the Spirit rover site in Gusev crater. Nature 436, 66-69.

Hauber E., Broz P., Jagert F., Jodlowski P. and Platz T., 2011. Very recent and wide-spread basaltic volcanism on Mars. Geophys. Res. Lett. 38, L10201, doi: 10.1029/2011GL047310.

Hausrath E.M., Golden D.C., Morris R.V., Agresti D.G. and Ming D.W., 2013. Acid sulfate alteration of fluorapatite, basaltic glass and olivine by hydrothermal vapours and fluids: implications for fumarolic activity and secondary phosphate phases in sulfate-rich Paso Robles soil at Gusev crater, Mars. J. Geophys. Res. 118, 1-13, doi: 10.1029/2012JE004246.

Hausrath E.M., Navarre-Sitchler A.K., Sak P.B., Steefel C.I. and Brantley S.L., 2008. Basalt weathering rates on Earth and the duration of liquid water on the plains of Gusev Crater, Mars. Geology 36, 67-70.

Heald P., Foley N.K. and Hayba D.O., 1987. Comparative anatomy of volcanic-hosted epithermal deposits: acid-sulfate and adularia-sericite. Econom. Geol. 82: 1-26.

Henley R.W. and Ellis A.J., 1983. Geothermal systems ancient and modern, a geochemical review. Earth Sci. Rev. 19, 1-50.

Hesse R., Frape S.K., Egeberg P.K. and Matsumoto R., 2000. Stable isotope studies (Cl, O, and H) of interstitial waters from Site 997, Blake Ridge gas hydrate field, West Atlantic. Proceedings of the Ocean Drilling Program: Scientific Results 164, 129-137.

Hodges C. and Moore H., 1994. Atlas of Volcanic Landforms on Mars. US Geological Survey (Washington): 194 pp.

Horgan B.H., Bell J.F. III, Dobrea E.Z.N., Cloutis E.A., Bailey D.T., Craig M.A., Roach L.H. and Mustard J.F., 2009. Distribution of hydrated minerals in the north polar region of Mars. J. Geophys. Res. 114, E01005, doi:10.1029/2008JE003187.

Howarth G.H., Pernet-Fisher J.F., Bodnar R.J. and Taylor L.A., 2015. Evidence for the exsolution of Cl-rich fluids in martian magmas: Apatite petrogenesis in the enriched lherzolitic shergottite Northwest Africa 7755. Geochim. Cosmochim. Acta 166, 234-248.

Hubbard C.G., Black S. and Coleman M.L., 2009. Aqueous geochemistry and oxygen isotope compositions of acid mine drainage from the Rio Tinto, SW Spain, highlight inconsistencies in current models. Chem. Geol. 265, 321-334.

Hurowitz J.A. and Fischer W.W., 2014. Contrasting styles of water–rock interaction at the Mars Exploration Rover landing Sites, Geochim. Cosmochim. Acta, 127, 25-38.

Hurowitz J.A. and McLennan S.M., 2007. A similar to 3.5 Ga record of water-limited, acidic weathering conditions on Mars. EPSL 260, 432-443.

Hurowitz J.A., Fischer W.W.,Tosca N.J., and Milliken R.E., 2010. Origin of acidic surface waters and the evolution of atmospheric chemistry on early Mars. Nature Geoscience 3, 323-326.

Hynek B.M., McCollom T.M., Marcucci E.C., Brugman K. and Rogers K.L., 2013. Assessment of environmental controls on acid-sulfate alteration at active volcanoes in Nicaragua: applications to relic hydrothermal systems on Mars. J. Geophys. Res. 118, 2083-2104.

Hynek B.M., Phillips R.J. and Arvidson R.E., 2003. Explosive volcanism in the Tharsis region: global evidence in the Martian record. J. Geophys. Res. 108, 5111, doi: 10.1029/2003JE002062.

Jambor J.L., Nordstrom D.K. and Alpers C.N., 2000. Metal-sulfate salts from sulfide mineral oxidation. In: Alpers C.N., Jambor J.L. and Nordstrom D.K. (eds.), Sulfate minerals, crystallography, geochemistry and environmental significance. Rev. Min. Geochem. 40, pp. 305-350.

John T., Layne G.D., Haase K.M. and Barnes J. D., 2010. Chlorine isotope evidence for crustal recycling into the Earth's mantle. Earth Planet. Sci. Lett. 298, 175-182.

Johnson J.R., Bell J.F. III, Cloutis E., Staid M., Farrand W.H., McCoy T., Rice M., Wang A. and Yen A., 2007. Mineralogical constraints on sulfur-rich soils from Pancam spectra at Gusev crater, Mars. Geophys. Res. Lett. 34, L13202, doi: 10.1029/2007GL029894.

Jonsson J., Persson P., Sjoberg S and Lovgren L., 2005. Schwertmannite precipitated from acid mine drainage: phase transformation, sulphate release and surface properties, Appl. Geochem. 20, 179–191.

Johnson K.S. and Pytkowicz R.M., 1978. Ion association of the Cl^- with H^+, Na^+, K^+, Ca^{2+} and Mg^{2+} in aqueous solutions at 25°C. Am. J. Sci. 278, 1428-1447.

Kading T.J., 2010. Natural pollutant attenuation by schwertmannite at Copahue Volcano, Argentina. M.Sc. thesis, Wesleyan University, 247pp.

Kading T. and Varekamp J.C., 2009. Lake Caviahue (Argentina) as a source-sink for volcanic arsenic and phosphorus. Geo. Soc. Am. Abstr. Programs 41, p. 645.

Kading T. and Varekamp J.C., 2011. Schwertmannite precipitation in glacial Lake Caviahue, Neuquén, Argentina. Geo. Soc. Am. Abstr. Programs 43, p. 77.

Karunatillake S., Zhao Y. S., McLennan S. M., Skok J. R. and Button N. E. (2013) Does martian soil release reactive halogens to the atmosphere? Icarus 226, 1438-1446.

Kaufmann R.S., 1984. Chlorine in groundwater: stable isotope distribution. Ph.D. thesis, University of Arizona, 137 p.

Keller J.M., Boynton W.V., Karunatillake S., Baker V.R., Dohm J.M., Evans L.G., Finch M.J., Hahn B.C., Hamara D.K., Janes D.M., Kerry K.E., Newsom H.E., Reedy R.C., Sprague A.L., Squyres S.W., Starr R.D., Taylor G.J. and Williams R.M.S., 2006. Equatorial and midlatitude distribution of chlorine measured by Mars Odyssey GRS. J. Geophys. Res. 111, E03S08.

Kempter K.A. and Rowe G.L., 2000. Leakage of active crater lake brine through the north flank at Rincón de la Vieja volcano, northwest Costa Rica, and implications for crater collapse. J. Volcanol. Geotherm. Res. 97, 143-159.

Kim J.D., Yee N., Nanda V. and Falkowski P.G., 2013. Anoxic photochemical oxidation of siderite generates molecular hydrogen and iron oxides. Proc. Natl. Acad. Sci. 110, 10073-10077.

Kimball B.A., McKnight D.M., Wetherbee G.A., and Harnish, R.A., 1992. Mechanisms of iron photo-reduction in a metal-rich, acidic stream (St. Kevin Gulch, Colorado, USA). Chem. Geol. 96, 227-239.

King H.E., Plümper O., Geisler T. and Putnis A., 2011. Experimental investigations into the silicification of olivine: Implications for the reaction mechanism and acid neutralization. Am. Mineral. 96, 1503-1511.

King P.L. and McLennan S. M., 2010. Sulfur on Mars. Elements 6, 107-112.

Kite E.S., Lucas A. and Fassett C.I., 2013. Pacing early Mars river activity: embedded craters in the Aeolis Dorsa region imply river activity spanned greater than or similar to (1-20) Myr. Icarus 225, 850-855.

Klingelhöfer G., Morris R., Bernhardt B., Schroder C., Rodionov D., de Souza P., Yen A., Gellert R., Evlanov E., Zubkov B., Foh J., Bonnes U., Kankeleit E., Gutlich P., Ming D., Renz F., Wdowiak T., Squyres S. and Arvidson R., 2004. Jarosite and hematite at Meridiani Planum from Opportunity's Mossbauer spectrometer. Science 306, 1740-1745.

Knauth L., Burt D. and Wohletz K., 2005. Impact origin of sediments at the Opportunity landing site on Mars. Nature 438, 1123-1128.

Komatsu G., Geissler P.E., Strom R.G. and Singer R.B., 1993. Stratigraphy and erosional landforms of layered deposits in Valles Marineris, Mars. J. Geophys. Res. 98, 11105-11121.

Komatsu G., Ori G.G., Ciarcelluti P. and Litasov Y.D., 2004. Interior layered deposits of Valles Marineris, Mars: analogous sub ice volcanism related to Baikal rifting, southern Siberia. Planet. Space Sci. 52, 167-187.

Koschinsky A., Garbe-Schoenberg D., Sander S., Schmidt K., Gennerich H. and Strauss H., 2008. Hydrothermal venting at pressure-temperature conditions above the critical point of seawater, 5 degrees S on the Mid-Atlantic Ridge. Geology 36, 615-618.

Kounaves S.P., Carrier B.L., O'Neil G.D., Stroble S.T. and Claire M.W., 2014. Evidence of martian perchlorate, chlorate, and nitrate in Mars meteorite EETA79001: Implications for oxidants and organics. Icarus 229, 206-213.

Kumpulainen S., Carlson L. and Raisanen M.L., 2007. Seasonal variations of ochreous precipitates in mine effluents in Finland. Appl. Geochem. 22, 760–777.

Kusakabe M. and Komoda Y., 1992. Sulfur isotopic effects in the disproportionated reaction of sulfur dioxide at hydrothermal temperatures. Rep. Geol. Surv. Jpn. 279, 93-96.

Kusakabe M., Komoda Y., Takano B. and Abiko T., 2000. Sulfur isotopic effects in the disproportionation reaction of sulfur dioxide in hydrothermal fluids: implications for the delta S-34 variations of dissolved bisulfate and elemental sulfur from active crater lakes. J. Volcanol. Geotherm. Res. 97, 287-307.

Kussmaul S., 1988. Comparación petrológica entre el piso del Valle Central y la Cordillera Central de Costa Rica. Ciencia y Tecnología 12, 109-116.

Langevin Y., Poulet F., Bibring J. and Gondet B., 2005. Sulfates in the north polar region of Mars detected by OMEGA/Mars express. Science 307, 1584-1586.

Layne G.D., Kent A.J.R. and Bach W., 2009. Delta Cl-37 systematics of a back-arc spreading system: The Lau Basin. Geology 37, 427-430.

Lees H., Kwok S.C., Suzuki I., 1969. The thermodynamics of iron oxidation by the Ferrobacilli. Can. J. Microbiol. 15, 43-46.

Lewis K.W., Aharonson O., Grotzinger J.P., Squyres S.W., Bell J.F. III, Crumpler L.S. and Schmidt M.E., 2008. Structure and stratigraphy of Home Plate from the Spirit Mars Exploration Rover. J. Geophys. Res. 113, E12S36, doi: 10.1029/2007JE003025.

Li L., Bonifacie M., Aubaud C., Crispi O., Dessert C. and Agrinier P., 2015. Chlorine isotopes of thermal springs in arc volcanoes for tracing shallow magmatic activity. EPSL 413, 101-110.

Liebscher A., Lüders V., Heinrich W. and Schettler G., 2006. Br/Cl signature of hydrothermal fluids: liquid-vapour fractionation of bromine revisited. Geofluids 6, 113-121.

Liu Y., Zhou A., Gan Y., Liu C., Yu T., and Li X., 2013. An online method to determine chlorine stable isotope composition by continuous flow isotope ratio mass spectrometry (CF-IRMS) coupled with a Gasbench II. J. Central South University 20, 193-198.

Lodders K., 1998. A survey of shergottite, nakhlite and chassigny meteorites whole-rock compositions. Meteor. Planet. Sci. 33, A183-A190.

Lodders K. and Fegley B., 1997. An oxygen isotope model for the composition of Mars. Icarus 126, 373-394.

Lorand J., Chevrier V. and Sautter V., 2005. Sulfide mineralogy and redox conditions in some shergottites. Meteor. Planet. Sci. 40, 1257-1272.

Lowenstern J.B., Bleick H., Vázquez J.A., Castro J.M. and Larson P.B., 2012. Degassing of Cl, F, Li, and Be during extrusion and crystallization of the rhyolite dome at Volcán Chaitén, Chile, during 2008 and 2009. Bull. Volcanol. 74, 2303-2319.

Lucchitta B.K., 1987. Valles Marineris, Mars, wet debris flows and ground ice. Icarus 72, 411-429.

Lucchitta B.K., 1990. Young volcanic deposits in the Valles Marineris, Mars? Icarus 86, 476-509.

Lucchitta B.K., Isbell N.K. and Howington-Kraus A., 1994. Topography of Valles Marineris: implications for erosional and structural history. J. Geophys. Res. 99, 3783-3798.

Lüders V., Banks D. and Halbach P., 2002. Extreme Cl/Br and delta Cl-37 isotope fractionation in fluids of modern submarine hydrothermal systems. Miner. Deposita 37, 765-771.

Lundgreen B., Jensen H.G., Knudsen J.M., Olsen M., and Vistisen L., 1989. Photostimulated oxidation of $Fe^{2+}_{(aq)}$: a Mars simulation experiment studied by Mössbauer spectroscopy. Physica Scripta, 39(5), 670.

Luth R.W., 2003. Mantle volatiles, distribution and consequences. In: Turekian, H.D.H.K. (ed.), Treatise on Geochemistry. Pergamon, Oxford, U.K., pp. 319-361.

Malavassi E., 1991. Magma sources and crustal processes at the terminous of the Central American Volcanic Front. PhD Thesis, University of California, Santa Cruz, USA, 435 p.

Mangold N., Gendrin A., Gondet B., LeMouelic S., Quantin C., Ansan V., Bibring J., Langevin Y., Masson P. and Neukum G., 2008. Spectral and geological study of the sulfate-rich region of West Candor Chasma, Mars. Icarus 194, 519-543.

Marcucci E.C. and Hynek B.M., 2014. Laboratory simulations of acid-sulfate weathering under volcanic hydrothermal conditions: implications for early Mars. J. Geophys. Res. 119, 679-703.

Marcucci E.C., Hynek B.M., Kierein-Young K.S. and Rogers K.L., 2013. Visible-near-infrared reflectance spectroscopy of volcanic acid-sulfate alteration in Nicaragua: Analogues for early Mars. J. Geophys. Res. 118, 2213-2233.

Marini L. and Gambardella B., 2005. Geochemical modeling of magmatic gas scrubbing. Annals of Geophysics 48, 739-753.

Marini L., Vetuschi-Zuccolini M. and Saldi G., 2003. The bimodal pH distribution of volcanic lake waters. J. Volcanol. Geotherm. Res. 121, 83-98.

Marion G.M., Catling D.C. and Kargel J.S., 2009. Br/Cl partitioning in chloride minerals in the Burns formation on Mars. Icarus 200, 436-445.

Marion G.M., Catling D.C., Zahnle K.J. and Claire M.W., 2010. Modeling aqueous perchlorate chemistries with applications to Mars. Icarus 207, 675-685.

Martin R.S., Mather T.A. and Pyle D.M., 2006. High-temperature mixtures of magmatic and atmospheric gases. Geochem. Geophys. Geosyst. 7, Q04006, doi:10.1029/2005GC001186.

Martin R., Rodgers K.A. and Browne P.R.L., 1999. The nature and significance of sulphate-rich, aluminous efflorescences from the Te Kopia geothermal field, Taupo Volcanic Zone, New Zealand. Mineral. Magazine 63, 413-419.

Martínez M., 2008. Geochemical evolution of the acid crater lake of Poás volcano (Costa Rica): Insights into volcanic-hydrothermal processes. Ph.D. thesis, Utrecht University, 162 pp.

Martínez M., Fernández E., Valdés J., Barboza V., van der Laat R., Duarte E., Malavassi E., Sandoval L., Barquero J. and Marino T., 2000. Chemical evolution and volcanic activity of the active crater lake of Poás volcano, Costa Rica, 1993-1997. J. Volcanol. Geotherm. Res. 97, 127-141.

Massé M., Bourgeois O., Le Mouélic S., Verpoorter C., Le Deit L. and Bibring J.P., 2010. Martian polar and circum-polar sulfate-bearing deposits: sublimation tills derived from the North Polar Cap. Icarus 209, 434-451.

McCanta M.C., Dyar M.D. and Treiman A.H., 2014. Alteration of Hawaiian basalts under sulfur-rich conditions: Applications to understanding surface-atmosphere interactions on Mars and Venus. Am. Mineral. 99, 291-302.

McCauley, J.F., 1978. Geological map of the Coprates quadrangle of Mars. US Geol. Surv. Misc. Invest. Ser. Map, I-897, scale 1:5,000,000.

McCollom T. and Hynek B., 2005. A volcanic environment for bedrock diagenesis at Meridiani Planum on Mars. Nature 438, 1129-1131.

McCollom T.M., Hynek B.M., Rogers K., Moskowitz B. and Berquo T.S., 2013. Chemical and mineralogical trends during acid-sulfate alteration of pyroclastic basalt at Cerro Negro volcano and implications for early Mars. J. Geophys. Res. 118, 1719-1751.

McEwen A.S., Malin M.C., Carr M.H. and Hartmann W.K., 1999. Voluminous volcanism on Early Mars revealed in Valles Marineris. Nature 397, 584-586, doi:10.1038/17539.

McHenry L.J., Vhevrier V. and Schröder C., 2011. Jarosite in a Pleistocene East African saline-alkaline paleolacustrine deposit: Implications for Mars aqueous geochemistry, J. Geophys. Res. 116, E04002.

McKnight D. and Bencala K.E., 1988. Diel variations in iron chemistry in an acidic stream in the Colorado Rocky Mountains, USA. Arctic and Alpine Res., 20(4), 492-500.

McKnight D.M. and Duren S.M., 2004. Biogeochemical processes controlling midday ferrous iron maxima in stream waters affected by acid rock drainage. Appl. Geochem. 19, 1075-1084.

McKnight D.M., Kimball B.A., Bencala K.E., 1988. Iron photo-reduction and oxidation in an acidic mountain stream, Science, 240, 637-640.

McKnight D.M., Kimball B.A., Runkel R.L., 2001. The pH dependence of iron photo-reduction in a rocky mountain stream affected by acid mine drainage. Hydrol. Proc. 15, 1979-1992.

McLennan S.M., Anderson R.B., Bell J.F. III, Bridges J.C., Calef F. III, Campbell J.L., Clark B.C., Clegg S., Conrad P., Cousin A., Des Marais D.J., Dromart G., Dyar M.D., Edgar L.A., Ehlmann B.L., Fabre C., Forni O., Gasnault O., Gellert R., Gordon S., Grant J.A., Grotzinger J.P., Gupta S., Herkenhoff K.E., Hurowitz J.A., King P.L., Le Mouelic S., Leshin L.A., Leveille R., Lewis K.W., Mangold N., Maurice S., Ming D.W., Morris R.V., Nachon M., Newsom H.E., Ollila A.M., Perrett G.M., Rice M.S., Schmidt M.E., Schwenzer S.P., Stack K., Stolper E.M., Sumner D.Y., Treiman A.H., VanBommel S., Vaniman D.T., Vasavada A., Wiens R.C., Yingst R.A. and MSL Sci Team, 2014. Elemental Geochemistry of Sedimentary Rocks at Yellowknife Bay, Gale Crater, Mars. Science 343, 1244734.

McLennan S.M., Bell J.F., Calvin W.M., Christensen P.R., Clark B C., de Souza P.A., Farmer J., Farrand W.H., Fike D.A., Gellert R., Ghosh A., Glotch T.D., Grotzinger J.P., Hahn B., Herkenhoff K.E., Hurowitz J.A., Johnson J.R., Johnson S.S., Jolliff B., Klingelhofer G., Knoll A.H., Learner Z., Malin M.C., McSween H.Y., Pocock J., Ruff S.W., Soderblom L.A., Squyres S.W., Tosca N.J., Watters W.A., Wyatt M.B. and Yen A., 2005. Provenance and diagenesis of the evaporite-bearing Burns formation, Meridiani Planum, Mars. EPSL 240, 95-121.

McSween H.Y. Jr., 1999. Meteorites and Their Parent Planets, Revised 2nd Edition, Cambridge University Press, New York, 310 p.

McSween H.Y. Jr, Taylor G.J. and Wyatt M.B., 2009. Elemental Composition of the Martian Crust, Science 324, 736-739, doi: 10.1126/science.1165871.

McSween H.Y., Ruff S.W., Morris R.V., Gellert R., Klingelhöfer G., Christensen P.R., McCoy T.J., Ghosh A., Moersch J.M., Cohen B.A., Rogers A.D., Schroeder C., Squyres S.W., Crisp J. and Yen A., 2008. Mineralogy of volcanic rocks in Gusev Crater, Mars: reconciling Mossbauer, Alpha Particle X-ray Spectrometer, and Miniature Thermal Emission Spectrometer spectra. J. Geophys. Res. 113, E06S04, doi: 10.1029/2007JE002970.

McSween H., Wyatt M., Gellert R., Bell J., Morris R., Herkenhoff K., Crumpler L., Milam K., Stockstill K., Tornabene L., Arvidson R., Bartlett P., Blaney D., Cabrol N., Christensen P., Clark B., Crisp J., Des Marais D., Economou T., Farmer J., Farrand W., Ghosh A., Golombek M., Gorevan S., Greeley R., Hamilton V., Johnson J., Joliff B., Klingelhöfer G., Knudson A., McLennan S., Ming D., Moersch J., Rieder R., Ruff S., Schroder C., de Souza P., Squyres S., Wanke H., Wang A., Yen A. and Zipfel J., 2006. Characterization and petrologic interpretation of olivine-rich basalts at Gusev Crater, Mars. J. Geophys. Res. 111, E02S10, doi: 10.1029/2005JE002477.

Mellon M.T., Feldman W.C. and Prettyman T.H., 2004. The presence and stability of ground ice in the southern hemisphere of Mars. Icarus 169, 324-340.

Menyailov I.A., Nikitina L.P., Shapar V.N. and Pilipenko V.P., 1986. Temperature increase and chemical change of fumarolic gases at Momotombo Volcano, Nicaragua, in 1982–1985: Are these indicators of a possible eruption? J. Geophys. Res. 91, 12199-12214.

Metz J.M., Grotzinger J.P., Mohrig D., Milliken R., Prather B., Pirmez C., McEwen A.S. and Weitz C.M., 2009. Sublacustrine depositional fans in southwest Melas Chasma. J. Geophys. Res. 114, E10002.

Miller J.L., Elwood-Madden A.S., Phillips-Lander C.M., Pritchett B.N. and Elwood-Madden M.E., 2016. Alunite dissolution rates: Dissolution mechanisms and implications for Mars. Geochim. Cosmochim. Acta 172, 93-106.

Milliken R.E., Grotzinger J.P. and Thomson B.J., 2010. Paleoclimate of Mars as captured by the stratigraphic record in Gale Crater. Gephys. Res. Lett. 37, L04201.

Milliken R.E., Swayze G.A., Arvidson R.E., Bishop J.L., Clark R.N., Ehlmann B.L., Green R.O., Grotzinger J.P., Morris R.V., Murchie S.L., Mustard J.F. and Weitz C., 2008. Opaline silica in young deposits on Mars. Geology 36, 847-850.

Ming D.W., Morris R.V. and Clark B.C., 2008. Aqueous alteration on Mars. In: Bell J. (ed.): The Martian surface: composition, mineralogy and physical properties. Cambridge University Press (Cambridge), pp. 519-540.

Ming D.W., Archer P.D. Jr., Glavin D.P., Eigenbrode J.L., Franz H.B., Sutter B., Brunner A E., Stern J.C., Freissinet C., McAdam A.C., Mahaffy P.R., Cabane M., Coll P., Campbell J.L., Atreya S.K., Niles P.B., Bell J.F. III, Bish D.L., Brinckerhoff W.B., Buch A., Conrad P.G., Des Marais D.J., Ehlmann B.L., Fairen A.G., Farley K., Flesch G.J., Francois P., Gellert R., Grant J.A., Grotzinger J.P., Gupta S., Herkenhoff K.E., Hurowitz J.A., Leshin L.A., Lewis K.W., McLennan S.M., Miller K.E., Moersch J., Morris R.V., Navarro-González R., Pavlov A.A., Perrett G.M., Pradler I., Squyres S.W., Summons R.E., Steele A., Stolper E.M., Sumner D.Y., Szopa C., Teinturier S., Trainer M.G., Treiman A.H., Vaniman D.T., Vasavada A.R., Webster C.R., Wray J.J., Yingst R. A. and MSL Sci Team, 2014. Volatile and Organic Compositions of Sedimentary Rocks in Yellowknife Bay, Gale Crater, Mars. Science 343, 6169, doi: 10.1126/science.1245267.

Ming D., Mittlefehldt D., Morris R., Golden D., Gellert R., Yen A., Clark B., Squyres S., Farrand W., Ruff S., Arvidson R., Klingelhöfer G., McSween H., Rodionov D., Schroder C., de Souza P. and Wang A., 2006. Geochemical and mineralogical indicators for aqueous processes in the Columbia Hills of Gusev crater, Mars. J. Geophys. Res. 111, E02S12, doi: 10.1029/2005JE002560.

Mizutani Y. and Sugiura T., 1996. The chemical equilibrium of the $SO_2+2H_2S\leftrightarrow 3S+2H_2O$ reaction in solfataras of the Nasudake Volcano. Bull. Chem. Soc. Jpn. 39, 2411-2414.

Morris R.V., Ming, D.W., Golden, D.C., and Bell III, J.F., 1996. An occurrence of jarosite tephra on Mauna Kea, Hawaii: Implications for the ferric mineralogy of the Martian surface. In: M.D. Dyar, C. McCammon and M.W. Schaefer (eds.), Mineral Spectroscopy: A tribute to Roger G. Burns. The Geochemical Society Special Publication 5, 327-336.

Morris R., Klingelhöfer G., Bernhardt B., Schroder C., Rodionov D., de Souza P., Yen A., Gellert R., Evlanov E., Foh J., Kankeleit E., Gutlich P., Ming D., Renz F., Wdowiak T., Squyres S. and Arvidson R., 2004. Mineralogy at Gusev crater from the Mossbauer spectrometer on the Spirit rover. Science 305, 833-836.

Morris R., Klingelhöfer G., Schroder C., Rodionov D., Yen A., Ming D., de Souza P., Fleischer I., Wdowiak T., Gellert R., Bernhardt B., Evlanov E., Zubkov B., Foh J., Bonnes U., Kankeleit E., Gutlich P., Renz F., Squyres S. and Arvidson R., 2006. Mössbauer mineralogy of rock, soil, and dust at Gusev crater, Mars: Spirit's journey through weakly altered olivine basalt on the plains and pervasively altered basalt in the Columbia Hills. J. Geophys. Res. 111, E02S13, doi: 10.1029/2005JE002584.

Murchie S.L., Mustard J.F., Ehlmann B.L., Milliken R.E., Bishop J.L., McKeown N.K., Dobrea E.Z.N., Seelos F.P., Buczkowski D.L., Wiseman S.M., Arvidson R.E., Wray J.J., Swayze G., Clark R.N., Marais D.J.D., McEwen A.S. and Bibring J., 2009. A synthesis of Martian aqueous mineralogy after 1 Mars year of observations from the Mars Reconnaissance Orbiter. J. Geophys. Res. 114, E00D06, doi: 10.1029/2009JE003342.

Musashi M. and Eggenkamp H.G.M., 2000. Cl isotope compositions of fumarolic gas from a Japanese volcanic island. 10th Annual Goldschmidt Conference 5(2), p. 733. Oxford, U.K.

Musashi M., Oi T., Eggenkamp H.G.M. and Matsuo M., 2008. Chlorine isotope fractionation associated with volcanic activity at the Kusatsu-Bandaiko hot spring in Japan. Isot. Environ. Health Stud. 44, 305-313.

Musashi M., Oi T., Eggenkamp H.G.M., Yato Y. and Matsuo M., 2007. Anion-exchange chromatographic study of the chlorine isotope effect accompanying hydration. J. Chromatography A1140, 121-125.

Musselwhite D.S., Dalton H.A., Kiefer W.S. and Treiman A.H., 2006. Experimental petrology of the basaltic shergottite Yamato-980459: implications for the thermal structure of the Martian mantle. Meteor. Planet. Sci. 41, 1271-1290.

Mustard J.F., Murchie S.L., Pelkey S.M., Ehlmann B.L., Milliken R.E., Grant J.A., Bibring J., Poulet F., Bishop J., Dobrea E N., Roach L., Seelos F., Arvidson R.E., Wiseman S., Green R., Hash C., Humm D., Malaret E., McGovern J.A., Seelos K., Clancy T., Clark R., Des Marais D., Izenberg N., Knudson A., Langevin Y., Martin T., McGuire P., Morris R., Robinson M., Roush T., Smith M., Swayze G., Taylor H., Titus T. and Wolff M., 2008. Hydrated silicate minerals on mars observed by the Mars Reconnaissance Orbiter CRISM instrument. Nature 454, 305-309.

Mustard J., Poulet F., Gendrin A., Bibring J., Langevin Y., Gondet B., Mangold N., Bellucci G. and Altieri F., 2005. Olivine and pyroxene, diversity in the crust of Mars. Science 307, 1594-1597.

Myers R.T., 1976. The strength of the hydroalic acids. J. Chem. Educ. 53, 17-19.

Nedell S.S., Squyres S.W. and Andersen D.W., 1987. Origin and evolution of the layered deposits in the Valles Marineris, Mars. Icarus 70, 409-441.

Nesbitt H.W. and Wilson R.E., 1992. Recent chemical weathering of basalts. Am. J. Sci. 292, 740-777.

Nesbitt H.W. and Young G.M., 1984. Prediction of some weathering trends of plutonic and volcanic-rocks based on thermodynamic and kinetic considerations. Geochim. Cosmochim. Acta 48, 1523-1534.

Neukum G., Jaumann R., Hoffmann H., Hauber E., Head J., Basilevsky A., Ivanov B., Werner S., van Gasselt S., Murray J., McCord T. and HRSC Co-investigator Team, 2004. Recent and episodic volcanic and glacial activity on Mars revealed by the High Resolution Stereo Camera. Nature 432, 971-979.

Newsom H., Hagerty J. and Goff F., 1999. Mixed hydrothermal fluids and the origin of the Martian soil. J. Geophys. Res. 104, 8717-8728.

Nicholson R.A., Howells M.F., Baxter P.J., Clegg S.L. and Barquero J., 1993. Gas geochemistry studies at Poás Volcano, Costa Rica. March 1992 - January 1993. Overseas Geology Series. Technical Report WC/93/21, 40 pp.

Nicholson R.A., Howells M.F., Roberts P.D. and Baxter P.J., 1992. Gas geochemistry studies at Poás Volcano, Costa Rica. November 1991. Overseas Geology Series. Technical Report WC/92/10, 34 pp.

Niles P.B. and Michalski J., 2009. Meridiani Planum sediments on Mars formed through weathering in massive ice deposits. Nat. Geosci. 2, 215-220.

Nimick D.A., Gammons C.H. and Parker S.R., 2011. Diel biogeochemical processes and their effect on the aqueous chemistry of streams: A review. Chem. Geol. 283, 3-17.

Nordstrom D.K., 1982. The effect of sulfate on aluminium concentrations in natural waters: some stability relations in the system Al_2O_3-SO_3-H_2O at 298 K. Geochim. Cosmochim. Acta 46, 681-692.

Nordstrom D. and Alpers C., 1999. Negative pH, efflorescent mineralogy, and consequences for environmental restoration at the Iron Mountain Superfund site, California. Proc. Natl. Acad. Sci. U.S.A. 96, 3455-3462.

Nordstrom D., Alpers C., Ptacek C. and Blowes D., 2000. Negative pH and extremely acidic mine waters from Iron Mountain, California. Environ. Sci. Technol. 34, 254-258.

Oelkers E.H., 2001. General kinetic description of multioxide silicate mineral and glass dissolution. Geochim. Cosmochim. Acta 65, 3703-3719.

Ohba T., Hirabayashi J. and Nogami K., 1994. Water, heat and chloride budgets of the crater lake, Yugama at Kusatsu-Shirane volcano, Japan. Geochem. J. 28, 217-231.

Oosting S.E. and Von Damm K.L., 1996. Bromide/chloride fractionation in seafloor hydrothermal fluids from 9–10°N East Pacific Rise. Earth Planet. Sci. Lett. 144, 133-145.

Oppenheimer C. and Stevenson D., 1989. Liquid sulfur lakes at Poás volcano. Nature 342, 790-793.

Osinski G.R., Tornabene L.L., Banerjee N.R., Cockell C.S., Flemming R., Izawa M.R.M., McCutcheon J., Parnell J., Preston L.J., Pickersgill A.E., Pontefract A., Sapers H.M. and Southam G., 2013. Impact-generated hydrothermal systems on Earth and Mars. Icarus 224, 347-363.

Osterloo M.M., Anderson F.S., Hamilton V.E. and Hynek B.M., 2010. Geologic context of proposed chloride-bearing materials on Mars. J. Geophys. Res. 115, E10012, doi:10.1029/2010JE00361329.

Osterloo M.M., Hamilton V.E., Bandfield J.L., Glotch T.D., Baldridge A.M., Christensen P.R., Tornabene L.L. and Anderson F.S., 2008. Chloride-bearing materials in the southern highlands of Mars. Science 319, 1651-1654.

Ouimette A.P., 2000. Hydrothermal processes at an active volcano, Copahue, Argentina. M.Sc. thesis, Wesleyan University, 219 pp.

Owen T., 1992. The composition and early history of the atmosphere of Mars. In: Kieffer, H.H., Jakosky, B.M., Snyder, C.W. and Matthews, M.S. (eds.), Mars. University of Arizona Press, Tucson, pp. 818-834.

Palme H. and Beer H., 1993. Landolt-Borstein Group VI: astronomy and astrophysics: instruments; methods; Solar System. In: Voigt, H.H. (ed.), Abundances of the elements in the solar system. Springer, Berlin. pp. 196-221.

Palme H. and O'Neill H.S.C., 2007. 2.01 - Cosmochemical Estimates of Mantle Composition. In: Turekian, H.D.H.K. (ed.), Treatise on Geochemistry. Pergamon, Oxford. pp. 1-38.

Papike J.J., Karner J.M., and Shearer C.K., 2006. Comparative planetary mineralogy: Implications of Martian and terrestrial jarosite: A crystal chemical perspective. Geochim. Cosmochim. Acta 70, 1309–1321, doi:10.1016/j.gca.2005.11.004.

Papike J.J., Karner J.M., Spilde M.N. and Shearer C.K., 2006. Terrestrial analogues of Martian sulfates: major and minor element systematics of alunite-jarosite from Goldfield, Nevada. Am. Mineral. 91, 1197-1200.

Parkhurst D.L. and Appelo C.A.J., 1999. User's guide to PHREEQC (Version 2), a computer program for speciation, batch-reaction, one-dimensional transport, and inverse geochemical calculations. USGS Report 99-4259 (Denver), 312 pp.

Pasternack G.B. and Varekamp J.C., 1997. Volcanic lake systematics 1. Physical constraints. Bull. Volc. 58, 528-538.

Pedrozo F., Kelly L., Díaz M., Temporetti P., Baffico G., Kringel R., Friese K., Mages M., Geller W. and Woelfl S., 2001. Water chemistry, plankton and trophic status of an Andean acidic lake of volcanic origin in Patagonia, Hydrobiologia 452, 129–137.

Peterson C., 1981. A secondary origin for the central plateau of Hebes Chasma. Proc. 11th Lunar Planet. Sci., 1459–1471.

Pitzer K.S. and Mayorga G., 1973. Thermodynamics of electrolytes II. Activity and osmotic coefficients for strong electrolytes with one or both ions univalent. J. Phys. Chem. 77, 2300-2308.

Pokrovskii V.A., 1999. Calculation of the standard partial molal thermodynamic properties and dissociation constants of aqueous HCl^0 and HBr^0 at temperatures to 1000°C and pressures to 5 kbar. Geochim. Cosmochim. Acta 63, 1107-1115.

Poppe L.J., Paskevich V.F., Hathaway J.C. and Blackwood D.S., 2002. A Laboratory Manual for X-Ray Powder Diffraction. USGS Report 01-041 http://pubs.usgs.gov/of/2001/of01-041/index.htm

Poulet F, Bibring J.P., Mustard J.F., Gendrin A., Mangold N., Langevin Y., Arvidson R.E., Gondet B, Gómez C., Berthé M., Erard S., Forni O., Manaud N., Poulleau G., Soufflot A., Combes M., Drossart P., Encrenaz T., Fouchet T., Melchiorri R., Bellucci G., Altieri F., Formisano V., Fonti S., Capaccioni F., Cerroni P., Coradini A., Korablev O., Kottsov V., Ignatiev N., Titov D., Zasova L., Pinet P., Schmitt B., Sotin C., Hauber E., Hoffmann H., Jaumann R., Keller U., Forget F. and Omega Team, 2005. Phyllosilicates on Mars and implications for early Martian climate. Nature 438, 623-627.

Prosser J.T., 1983. The Geology of Poás Volcano, Costa Rica. MSc. thesis, Dartmouth College, Virginia, USA, 165 p.

Prosser J.T. and Carr M.J., 1987. Poás volcano, Costa Rica: Geology of the summit region and spatial and temporal variations among the most recent lavas. J. Volcanol. Geotherm. Res. 33, 131-146.

Pyle D.M. and Mather T.A., 2009. Halogens in igneous processes and their fluxes to the atmosphere and oceans from volcanic activity: a review. Chem. Geol. 263, 110-121.

Rao M.N., Bogard D.D., Nyquist L.E., McKay D.S. and Masarik J., 2002. Neutron capture isotopes in the martian regolith and implications for martian atmospheric noble gases. Icarus 156, 352-372.

Rao M.N., Nyquist L.E., Sutton S.R., Dreibus G., Garrison D.H. and Herrin J., 2009. Fluid-evaporation records preserved in salt assemblages in Meridiani rocks. EPSL 286, 396-403.

Reed M.H., 1982. Calculation of Multicomponent Chemical-Equilibria and Reaction Processes in Systems Involving Minerals, Gases and an Aqueous Phase. Geochim. Cosmochim. Acta 46, 513-528.

Regenspurg S. and Peiffer S., 2005. Arsenate and chromate incorporation in schwertmannite Appl. Geochem. 20, 1226– 1239

Richet P., Bottinga Y. and Javoy M., 1977. Review of hydrogen, carbon, nitrogen, oxygen, sulfur, and chlorine stable isotope fractionation among gaseous molecules. Annu. Rev. Earth Planet. Sci. 5, 65-110.

Rieder R., Gellert R., Anderson R., Bruckner J., Clark B., Dreibus G., Economou T., Klingelhöfer G., Lugmair G., Ming D., Squyres S., d'Uston C., Wanke H., Yen A. and Zipfel J., 2004. Chemistry of rocks and soils at Meridiani Planum from the alpha particle X-ray spectrometer. Science 306, 1746-1749.

Rieder R., Wanke H., Economou T. and Turkevich A., 1997. Determination of the chemical composition of Martian soil and rocks: The alpha proton X-ray spectrometer. J. Geophys. Res. 102, 4027-4044.

Rizzo A.L., Caracausi A., Liotta M., Paonita A., Barnes J.D., Corsaro R.A. and Martelli M., 2013. Chlorine isotope composition of volcanic gases and rocks at Mount Etna (Italy) and inferences on the local mantle source. Earth Planet. Sci. Lett. 371, 134-142.

Roach L.H., Mustard J.F., Murchie S.L., Bibring J.P., Forget F., Lewis, K.W., Aharonson O., Vincendon M., Bishop J.L., 2009. Testing evidence of recent hydration state change in sulphates on Mars. J. Geophys. Res. 114, E00D02, doi:10.1029/2008JE003245.

Robbins S.J., Achille G.D. and Hynek B.M., 2011. The volcanic history of Mars: High-resolution crater-based studies of the calderas of 20 volcanoes. Icarus 211, 1179-1203.

Robinson C., 1999. The role of jarosite and copiapite in the chemical evolution of acid drainage waters, Richmond mine, Iron Mountain, California. Queen´s University, Ontario, Canada, 205 p.

Rodríguez A. and van Bergen M.J., 2015. Volcanic hydrothermal systems as potential analogues of Martian sulphate-rich terrains. Nederlands Journal of Geosciences, doi: http://dx.doi.org/10.1017/njg.2015.12.

Rossi A.P., Neukum G., Pondrelli M., van Gasselt S., Zegers T., Hauber E., Chicarro A. and Foing B. (2008) Large-scale spring deposits on Mars? J. Geophys. Res. 113, E08016, doi: 10.1029/2007JE003062.

Rouwet D. and Ohba T. 2015. Isotope fractionation and HCl partitioning during evaporative degassing from active crater lakes. In: Rouwet, D., Tassi, F., Christenson, B. and Vandemeulebrouck, J. (eds.). Volcanic Lakes, Advances in Volcanology. Springer-Verlag, Berlin Heidelberg. pp. 179-200.

Rouwet D., Mora-Amador R., Ramírez-Umaña C.J., González G. and Inguaggiato S., 2016. Dynamic fluid recycling at Laguna Caliente (Poás, Costa Rica) before and during the 2006–ongoing phreatic eruption cycle (2005–10). In: T. Ohba, B. Capaccioni and C. Caudron (eds.), Geochemistry and Geophysics of Active Volcanic Lakes. Geological Society of London, Special Publications, 437, http:doi.org/10.1144/SP437.11.

Rowe G.L. and Brantley S.L., 1993. Estimation of the dissolution rates of andesitic glass, plagioclase and pyroxene in a flank aquifer of Poás Volcano, Costa Rica. Chem. Geol. 105, 71-87.

Rowe G.L., Brantley S.L., Fernández M., Fernández J.F., Borgia A. and Barquero J., 1992a. Fluid-volcano interaction in an active stratovolcano: the crater lake system of Poás volcano, Costa Rica. J. Volcanol. Geotherm. Res. 49, 23-51.

Rowe G.L., Ohsawa S., Takano B., Brantley S.L., Fernández J.F. and Barquero J., 1992b. Using crater lake chemistry to predict volcanic activity at Poás Volcano, Costa Rica. Bull. Volcanol. 54, 494-503.

Rudnick R.L. and Gao S., 2003. 3.01 - Composition of the Continental Crust. In: Turekian, H.D.H.K. (ed.), Treatise on Geochemistry. Pergamon, Oxford. pp. 1-64.

Ruff S.W., Niles P.B., Alfano F. and Clarke A.B., 2014. Evidence for a Noachian-aged ephemeral lake in Gusev crater, Mars. Geology 42: 359-362.

Ruff S.W., Farmer J.D., Calvin W.M., Herkenhoff K.E., Johnson J.R., Morris R.V., Rice M.S., Arvidson R.E., Bell J.F. III, Christensen P.R. and Squyres S.W., 2011. Characteristics, distribution, origin, and significance of opaline silica observed by the Spirit rover in Gusev crater, Mars. J. Geophys. Res. 116, E00F23, doi:10.1029/2010JE003767.

Ruiz P., Gazel E., Alvarado G.E., Carr M.J. and Soto G.J., 2010. Geochemical and petrographical characterization of the geological units of Poás volcano massif, Costa Rica (in Spanish). In: Mora R. and Alvarado R. (eds.) Volumen especial: Volcán Poás. Rev. Geol. Amér. Cent. 43, 37-66.

Rymer H., Cassidy J., Locke C., Barboza M., Barquero J., Brenes J. and Van der Laat R., 2000. Geophysical studies of the recent 15-year eruptive cycle at Poás Volcano, Costa Rica. J. Volcanol. Geotherm. Res. 97, 425-442.

Rymer H., Locke C.A., Borgia A., Martínez M., Brenes J., Van der Laat R. and Williams-Jones G., 2009. Long-term fluctuations in volcanic activity: implications for future environmental impact. Terra Nova 21, 304–309.

Sanford W.E., Konikow L.F., Rowe G.L. Jr. and Brantley S.L., 1995. Groundwater transport of crater-lake brine at Poás Volcano, Costa Rica. J. Volcanol. Geotherm. Res. 64, 269-293.

Schauble E.A., Rossman G.R. and Taylor Jr, H.P., 2003. Theoretical estimates of equilibrium chlorine-isotope fractionations. Geochim. Cosmochim. Acta 67, 3267-3281.

Scher S., Williams-Jones A.E. and Williams-Jones G., 2013. Fumarolic Activity, Acid-Sulfate Alteration, and High Sulfidation Epithermal Precious Metal Mineralization in the Crater of Kawah Ijen Volcano, Java, Indonesia. Economic Geology 108, 1099–1118.

Schilling J., Bergeron M. and Evans R., 1980. Halogens in the mantle beneath the North-Atlantic. Phil. Trans. R. Soc. Lond. A 297, 147-178, doi: 10.1098/rsta.1980.0208.

Schmidt M.E., Farrand W.H., Johnson J.R., Schroeder C., Hurowitz J.A., McCoy T.J., Ruff S.W., Arvidson R.E., Marais D.J.D., Lewis K.W., Ming D.W., Squyres S.W. and de Souza P.A.Jr., 2009. Spectral, mineralogical, and geochemical variations across Home Plate, Gusev Crater, Mars indicate high and low temperature alteration. EPSL 281, 258-266.

Schmidt M.E., Ruff S.W., McCoy T.J., Farrand W.H., Johnson J.R., Gellert R., Ming D.W., Morris R.V., Cabrol N., Lewis K.W. and Schroeder C., 2008. Hydrothermal origin of halogens at Home Plate, Gusev Crater. J. Geophys. Res. 113, E06S12.

Schroth A.W.; Parnell R.A. 2005. Trace metal retention through the schwertmannite to goethite transformation as observed in a field setting, Alta Mine, MT Appl. Geochem, 20, 907– 917.

Schulze-Makuch D., Dohm J.M., Fan C., Fairén A.G., Rodriguez J.A.P., Baker V.R. and Fink W., 2007. Exploration of hydrothermal targets on Mars. Icarus 189, 308-324.

Schwenzer S.P., Abramov O., Allen C.C., Bridges J.C., Clifford S.M., Filiberto J., Kring D.A., Lasue J., McGovern P.J., Newsom H.E., Treiman A.H., Vaniman D.T., Wiens R.C. and Wittmann A., 2012. Gale Crater: Formation and post-impact hydrous environments. Planet. Space Sci.70, 84-95.

Schwertmann U. and Cornell R.M., 2000. Iron Oxides in the Laboratory. Preparation and Characterisation, Wiley-VCH, Weinheim, 138 pp.

Sefton-Nash E. and Catling D.C., 2008. Hematitic concretions at Meridiani Planum, Mars: Their growth timescale and possible relationship with iron sulfates. EPSL 269, 365-375.

Sefton-Nash E., Catling D.C., Wood S.E., Grindrod P.M. and Teanby N.A., 2012. Topographic, spectral and thermal inertia analysis of interior layered deposits in Iani Chaos, Mars. Icarus 221, 20-42.

Seyfried Jr. W.E., Berndt M.E. and Janecky D.R., 1986. Chloride depletions and enrichments in seafloor hydrothermal fluids: constraints from experimental basalt alteration studies. Geochim. Cosmochim. Acta 50, 469-475.

Sharp Z.D., Barnes J.D., Brearley A. J., Chaussidon M., Fischer T.P. and Kamenetsky V.S., 2007. Chlorine isotope homogeneity of the mantle, crust and carbonaceous chondrites. Nature 446, 1062-1065.

Sharp Z. D., Barnes J. D., Fischer T. P. and Halick M., 2010. An experimental determination of chlorine isotope fractionation in acid systems and applications to volcanic fumaroles. Geochim. Cosmochim. Acta 74, 264-273.

Sharp Z.D., Mercer J.A., Jones R.H., Brearley A.J., Selverstone J., Bekker A. and Stachel T., 2013. The chlorine isotope composition of chondrites and Earth. Geochim. Cosmochim. Acta 107, 189-204.

Sharp Z., Williams J., Shearer C., Agee C. and McKeegan K., 2016. The chlorine isotope composition of Martian meteorites 2. Implications for the early solar system and the formation of Mars. Meteoritics & Planetary Science, doi: 10.1111/maps.12591.

Sherman D.M., 2005. Electronic structures of iron (III) and manganese (IV) (hydr)oxide minerals: Thermodynamics of photochemical reductive dissolution in aquatic environments. Geochim. Cosmochim. Acta 69, 3249-3255.

Shinohara H., Giggenbach W.F., Kazahaya K. and Hedenquist J.W., 1993. Geochemistry of volcanic gases and hot springs from Satsuma-Iwojima, Japan. Geochem. J. 27, 271-285.

Shinonaga T., Ebihara M., Nakahara H., Tomura K. and Heumann K., 1994. Cl, Br and I in Igneous Standard Rocks. Chem. Geol. 115, 213-225.

Siemann M.G. and Schram M., 2000. Thermodynamic modelling of the Br partition between aqueous solutions and halite. Geochim. Cosmochim. Acta 64, 1681-1693.

Singer P.C., and Stumm W., 1970. Acidic mine drainage: The rate-determining step. Science 167, 1121-1123.

Skok J.R., Mustard J.F., Ehlmann B.L., Milliken R.E. and Murchie S.L., 2010. Silica deposits in the Nili Patera caldera on the Syrtis Major volcanic complex on Mars. Nat. Geosci. 3, 838-841.

Snyder G. and Fehn U., 2002. Origin of iodine in volcanic fluids: I-129 results from the Central American Volcanic Arc. Geochim. Cosmochim. Acta 66, 3827-3838.

Squyres S.W. and Knoll A.H., 2005. Sedimentary rocks at Meridiani Planum: origin, diagenesis, and implications for life on Mars. EPSL 240, 1-10.

Squyres S.W., Aharonson O., Clark B.C., Cohen B.A., Crumpler L., de Souza P.A., Farrand W.H., Gellert R., Grant J., Grotzinger J.P., Haldemann A.F.C., Johnson J.R., Klingelhöfer G., Lewis K.W., Li R., McCoy T., McEwen A.S., McSween H.Y., Ming D.W., Moore J.M., Morris R.V., Parker T.J., Rice J.W. Jr, Ruff S., Schmidt M., Schroeder C., Soderblom L.A. and Yen A., 2007. Pyroclastic activity at home plate in Gusev Crater, Mars. Science 316, 738-742.

Squyres S., Arvidson R., Bell J., Bruckner J., Cabrol N., Calvin W., Carr M., Christensen P., Clark B., Crumpter L., Des Marais D., d'Uston C., Economou T., Farmer J., Farrand W., Folkner W., Golombek M., Gorevan S., Grant J., Greeley R., Grotzinger J., Haskin L., Herkenhoff K., Hviid S., Johnson J., Klingelhöfer G., Knoll A., Landis G., Lemmon M., Li R., Madsen M., Malin M., McLennan S., McSween H., Ming D., Moersch J., Morris R., Parker T., Rice J., Richter L., Rieder R., Sims M., Smith M., Smith P., Soderblom L., Sutlivan R., Wanke H., Wdowiak T., Wolff M. and Yen A., 2004a. The Opportunity Rover's Athena science investigation at Meridiani Planum, Mars. Science 306, 1698-1703.

Squyres S.W., Arvidson R.E., Ruff S., Gellert R., Morris R.V., Ming D.W., Crumpler L., Farmer J.D., Des Marais D.J., Yen A., McLennan S.M., Calvin W., Bell, J.F. III, Clark B.C., Wang A., McCoy T.J., Schmidt M.E. and de Souza P.A. Jr., 2008. Detection of silica-rich deposits on Mars. Science 320, 1063-1067.

Squyres S.W., Grotzinger J.P., Arvidson R.E., Bell J.F., Calvin W., Christensen P.R., Clark B.C., Crisp J.A., Farrand W.H., Herkenhoff K.E., Johnson J.R., Klingelhöfer G., Knoll A.H., McLennan S.M., McSween H.Y., Morris R.V., Rice J.W., Rieder R. and Soderblom L.A., 2004b. *In situ* evidence for an ancient aqueous environment at Meridiani Planum, Mars. Science 306, 1709-1714.

Stefánsson A., Gíslason S.R. and Arnórsson S., 2001. Dissolution of primary minerals in natural waters - II. Mineral saturation state. Chemical Geology 172, 251-276.

Steiner A., 1977. The Wairakei geothermal area, North Island, New Zealand. New Zealand Geological Survey Bulletin 90, 136 pp.

Steward F. H., 1968. Geochemistry of marine evaporite deposits. GSA 88, 539-540.

Stoessell R.K. and Carpenter A.B., 1986. Stoichiometric saturation tests of $NaCl_{1-x}Br_x$ and $KCl_{1-x}Br_x$. Geochim. Cosmochim. Acta 50, 1465-1474.

Stoffregen R.E., 1993. Stability relations of jarosite and natrojarosite at 150 - 250°C. Geochim. Cosmochim. Acta 57, 2417-2429.

Stoffregen R.E., Alpers C.N. and Jambor J.L., 2000. Alunite-jarosite crystallography, thermodynamics, and geochronology. In: Alpers C.N., Jambor J.L. and Nordstrom D.K. (eds.), Sulfate minerals, crystallography, geochemistry and environmental significance. Rev. Min. Geochem. 40, pp. 453-479.

Story S., Bowen B.B., Benison K.C. and Schulze D.G., 2010. Authigenic phyllosilicates in modern acid saline lake sediments and implications for Mars. J. Geophys. Res. 115, E12012.

Straub S. and Layne G., 2003. The systematics of chlorine, fluorine, and water in Izu arc front volcanic rocks: implications for volatile recycling in subduction zones. Geochim. Cosmochim. Acta 67, 4179-4203.

Stumm W. and Morgan J.J., 1996. Aquatic chemistry: chemical equilibria and rates in natural waters, 3rd ed. John Wiley & Sons, Inc., USA, 1042 p.

Sullivan A.B., Drever J.I. and McKnight D.M., 1998. Diel variation in element concentrations, Peru Creek, Summit County, Colorado. J. Geochem. Explor. 64, 141-145.

Sun W.D., Binns R.A., Fan A.C., Kamenetsky V.S., Wysoczanski R., Wei G.J., Hu Y.H. and Arculus R.J., 2007. Chlorine in submarine volcanic glasses from the eastern Manus basin. Geochim. Cosmochim. Acta 71, 1542-1552.

Sutton S.R., Rao M.N., Dreibus G., McKay D.S., Wänke H., Wentworth S., Newville M., Trainor T. and Flynn G.J., 2001. Chlorine/bromine ratios in fracture-filling aqueous alteration products in Nakhla olivine. 33th Lunar Planet. Sci. Conf., 1278.

Symonds R.B., 1990. Applications of multicomponent chemical equilibria to volcanic gases at Augustine volcano, volcanic halogen emissions, and volcanological studies of gas-phase transport. Ph.D. thesis, Michigan Technological University, USA, 512 p.

Symonds R.B. and Reed M.H., 1993. Calculation of multicomponent chemical equilibria in gas-solid-liquid systems: calculation methods, thermochemical data and applications to studies of high-temperature volcanic gases with examples from Mount St. Helens. Am. J. Sci. 293, 758-864.

Symonds R.B., Gerlach T.M. and Reed M.H., 2001. Magmatic gas scrubbing: implications for volcano monitoring. J. Volcanol. Geotherm. Res. 108, 303-341.

Symonds R.B, Mizutani Y. and Briggs P., 1996. Long-term geochemical surveillance of fumaroles at Showa-Shinzan dome, Usu volcano, Japan. J. Volcanol. Geotherm. Res. 73, 177-211.

Symonds R.B., Reed M.H. and Rose W.I., 1992. Origin, speciation, and fluxes of trace-element gases at Augustine volcano, Alaska: Insights into magma degassing and fumarolic processes. Geochim. Cosmochim. Acta 56, 633-657.

Symonds R.B., Rose W.I., Gerlach T.M., Briggs P.H. and Harmon R.S., 1990. Evaluation of gases, condensates, and SO_2 emissions from Augustine Volcano, Alaska, the degassing of a Cl-rich volcanic system. Bull. Volcanol, 52, 355-374.

Symonds R.B., Rose W.I., Reed M.H., Lichte F.E. and Finnegan D.L., 1987. Volatilization, transport and sublimation of metallic and non-metallic elements in high temperature gases at Merapi Volcano, Indonesia. Geochim. Cosmochim. Acta 51, 2083-2101.

Takano B., Saitoh H. and Takano E., 1994. Geochemical implications of subaqueous molten sulfur at Yugama crater lake, Kusatsu-Shirane volcano, Japan. Geochem. J. 28, 199-216.

Tamburello G., Agusto M., Caselli A., Tassi F., Vaselli O., Calabrese S., Rouwet D., Capaccioni B., Di Napoli R., Cardellini C., Chiodini G., Bitetto M., Brusca L., Bellomo S. and Aiuppa A., 2015. Intense magmatic degassing through the lake of Copahue volcano, 2013–2014. J. Geophys. Res. 120, 6071-6084.

Tanaka K.L., Scott D.H. and Greeley R., 1992. Global Stratigraphy. In: Kieffer H.H., Jakosky B.M., Synder C.W. and Matthews M.S. (eds). University of Arizona Press (Tucson), pp. 345-382.

Tanaka K.L., Robbins S.J., Fortezzo C.M., Skinner Jr. J.A. and Hare T.M., 2014. The digital global geologic map of Mars: chronostratigraphic ages, topographic and crater morphologic characteristics, and updated resurfacing history. Planet. Space Sci. 95, 11-24.

Tanaka KL., Skinner J.A., Jr., Dohm J.M., Irwin R.P. III, Kolb, E.J., Fortezzo C.M., Platz T., Michael, G.G., and Hare T.M., 2014. Geologic map of Mars: U.S. Geological Survey Scientific Investigations Map 3292, scale 1:20,000,000, pamphlet p. 43, http://dx.doi.org/10.3133/sim3292.

Taran Y. and Zelenski M., 2015. Systematics of water isotopic composition and chlorine content in arc-volcanic gases. Geol. Soc. Lond., Special Publications 410, 237-262.

Taran Y.A., Hedenquist J.W., Korzhinsky M.A., Tkachenko S.I. and Shmulovich K.I., 1995. Geochemistry of magmatic gases from Kudryavy volcano, Iturup, Kuril Islands. Geochim. Cosmochim. Acta 59, 1749-1761.

Tassi F., Vaselli O., Capaccioni B., Giolito C., Duarte E., Fernández E., Minissale A. and Magro G., 2005. The hydrothermal-volcanic system of Rincón de la Vieja volcano (Costa Rica): a combined (inorganic and organic) geochemical approach to understanding the origin of the fluid discharges and its possible application to volcanic surveillance. J. Volcanol. Geotherm. Res. 148, 315-333.

Taylor G.J., Boynton W.V., McLennan S.M. and Martel L.M.V., 2010. K and Cl concentrations on the Martian surface determined by the Mars Odyssey Gamma Ray Spectrometer: implications for bulk halogen abundances in Mars. Gephys. Res. Lett. 37, L12204.

Thollot P., Mangold N., Ansan V., Le Mouelic S., Milliken R.E., Bishop J.L., Weitz C.M., Roach L.H., Mustard J.F. and Murchie S.L., 2012. Most Mars minerals in a nutshell: various alteration phases formed in a single environment in Noctis Labyrinthus. J. Geophys. Res. 117, E00J06.

Thomson B.J., Bridges N.T., Milliken R., Baldridge A., Hook S.J., Crowley J.K., Marion G.M., de Souza Filho C.R., Brown A.J. and Weitz C.M., 2011. Constraints on the origin and evolution of the layered mound in Gale Crater, Mars using Mars Reconnaissance Orbiter data. Icarus 214, 413-432.

Toner J.D., Catling D.C. and Light B., 2015. Modeling salt precipitation from brines on Mars: Evaporation versus freezing origin for soil salts. Icarus 250, 451-461.

Tosca N.J. and McLennan S.M., 2006. Chemical divides and evaporite assemblages on Mars. EPSL 241, 21-31.

Tosca N.J., McLennan S.M., Clark B.C., Grotzinger J.P., Hurowitz J.A., Knoll A.H., Schroder C. and Squyres S.W., 2005. Geochemical modeling of evaporation processes on Mars: insight from the sedimentary record at Meridiani Planum. EPSL 240, 122-148.

Tosca N.J., McLennan S.M., Lindsley D.H. and Schoonen M.A.A., 2004. Acid-sulfate weathering of synthetic Martian basalt: the acid fog model revisited. J. Geophys. Res. 109, E05003, doi: 10.1029/2003JE002218.

Toulmin P., Clark B., Baird A., Keil K. and Rose H., 1976. Preliminary results from Viking X-ray fluorescence experiment, 1st sample from Chryse-Planitia, Mars. Science 194, 81-84.

Truesdell A., 1991. Origins of acid fluids in geothermal reservoirs. Geothermal Research Council Trans. 15, 289-296.

Urey H.C. and Greiff L.J., 1935. Isotopic exchange equilibria. J. Amer. Chem. Soc. 54, 3211-327.

Van Hinsberg V., Berlo K., Van Bergen M. and Williams-Jones A., 2010. Extreme alteration by hyperacidic brines at Kawah Ijen volcano, East Java, Indonesia: I. Textural and mineralogical imprint. J. Volcanol. Geotherm. Res. 198, 253-263.

Vaniman D., Bish D., Chipera S., Fialips C., Carey J. and Feldman W., 2004. Magnesium sulphate salts and the history of water on Mars. Nature 431, 663-665.

Varekamp J.C., 2004. Copahue Volcano: a modern terrestrial analogue for the Opportunity landing site? EOS 85, 401-407, doi: 10.1029/2004EO410002.

Varekamp J.C, 2008. The acidification of glacial Lake Caviahue, Province of Neuquén, Argentina. J. Volcanol. Geotherm. Res., special issue "Volcanic Lakes and Environmental Impacts of Volcanic Fluids" 178, pp. 184-196.

Varekamp J.C., Ouimette, A. and Kreulen, R., 2004. The magmato-hydrothermal system of Copahue volcano, Argentina: Proc. 11th Intl Conf. on Water-Rock Interaction, WRI-11, vol. 1, p. 215-218.

Varekamp J.C., Pasternack G.B. and Rowe G.L., 2000. Volcanic lake systematics II. Chemical constraints. J. Volc. Geotherm. Res. 97, 161-179.

Varekamp J.C., de Moor M.J. Merrill M., Colvin A., Goss A., Vroon P. And Hilton D., 2006. The geochemistry and isotopic characteristics of the Caviahue Copahue volcanic complex, Province of Neuquén, Argentina. Geol. Soc. Am. Special Paper 407, pp. 317–342.

Varekamp J.C., Ouimette A., Herman S., Bermúdez A. and Delpino D., 2001. Hydrothermal element fluxes from Copahue, Argentina: A "beehive" volcano in turmoil. Geology 29, 1059-1062.

Varekamp J.C, Ouimette A.P, Herman S.W., Flynn K.S., Bermúdez A. and Delpino D., 2009. Naturally acid waters from Copahue volcano, Argentina. Appl. Geochem. 24, 1354-1354.

Varekamp J.C., Zareski J., Camfield L., and Todd E., 2015. Copahue volcano and its regional magmatic setting. this volume In: Tassi F., Vaselli O. and Caselli, A. (eds.), Copahue volcano, pp. 81-118. Springer-Verlag Berlin Heidelberg, doi: 10.1007/978-3-662-48005-2.

Vaselli O., Tassi F., Minissale A., Montegrossi G., Duarte E., Fernández E. and Bergamaschi F., 2003. Fumarole migration and fluid geochemistry at Poás volcano (Costa Rica) from 1998 to 2001. In: Oppenheimer C., Pyle D.M. and Barkley J. (eds), Volcanic Degassing. The Geological Society, London. pp. 247-262.

Vaucher J., Baratoux D., Mangold N., Pinet P., Kurita K. and Gregoire M., 2009. The volcanic history of central Elysium Planitia: implications for Martian magmatism. Icarus 204, 418-442.

Villemant B. and Boudon G., 1999. H_2O and halogen (F, Cl, Br) behaviour during shallow magma degassing processes. EPSL 168, 271-286.

Villemant B., Boudon G., Nougrigat S., Poteaux S. and Michel A., 2003. Water and halogens in volcanic clasts: tracers of degassing processes during Plinian and dome-building eruptions. Special Publications 213, The Geological Society, London, pp. 63-79.

Villemant B., Hammouya G., Michel A., Semet M., Komorowski J., Boudon G. and Cheminee J., 2005. The memory of volcanic waters: shallow magma degassing revealed by halogen monitoring in thermal springs of La Soufrière volcano (Guadeloupe, Lesser Antilles). Earth EPSL 237, 710-728.

Villemant B., Komorowski J.C., Dessert C., Michel A., Crispi O., Hammouya G., Beauducel F. and De Chabalier J.B., 2014. Evidence for a new shallow magma intrusion at La Soufrière of Guadeloupe (Lesser Antilles), insights from long-term geochemical monitoring of halogen-rich hydrothermal fluids. J. Volcanol. Geotherm. Res. 285, 247-277.

Voelker B., Morel F.M.M., and Sulzberger B., 1997. Iron redox cycling in surface waters: Effects of humic substances and light. Environ. Sci. Technol. 30, 1106-1114.

Wahrenberger C., Eastoe C.J., Seward T.M. and Dietrich V., 1997. Stable chlorine isotope composition of volcanic gas condensates. 7th Annual Goldschmidt Conference, Tucson, Arizona.

Wang A., Bell J.F., Li R., Johnson J.R., Farrand W.H., Cloutis E.A., Arvidson R. E., Crumpler L., Squyres S.W., McLennan S.M., Herkenhoff K.E., Ruff S.W., Knudson A.T., Chen W. and Greenberger R., 2008. Light-toned salty soils and coexisting Si-rich species discovered by the Mars Exploration Rover Spirit in Columbia Hills. J. Geophys. Res. 113, E12S40, doi: 10.1029/2008JE003126.

Wang A., Haskin L., Squyres S., Jolliff B., Crumpler L., Gellert R., Schroder C., Herkenhoff K., Hurowitz J., Tosca N., Farrand W., Anderson R. and Knudson A., 2006. Sulfate deposition in subsurface regolith in Gusev crater, Mars. J. Geophys. Res. 111, E02S17.

Wang L., Marks M.A.W., Keller J. and Markl G., 2014. Halogen variations in alkaline rocks from the Upper Rhine Graben (SW Germany): Insights into F, Cl and Br behaviour during magmatic processes. Chem. Geol. 380, 133-144.

Webster J.G., Swedlund P.J. and Webster K.S., 1998. Trace metal adsorption onto an acid mine drainage iron (III) oxyhydroxysulphate. Environ. Sci. Technol. 32, 1361–1368.

Weitz C.M., and J.L. Bishop, 2016. Stratigraphy and formation of clays, sulfates, and hydrated silica within a depression in Coprates Catena, Mars, J. Geophys. Res. 121, 805–835, doi:10.1002/2015JE004954.

Weitz C.M., Bishop J.L., Thollot P., Mangold N. and Roach L.H., 2011. Diverse mineralogies in two troughs of Noctis Labyrinthus, Mars. Geology 39, 899-902.

Weitz C.M., Milliken R.E., Grant J.A., McEwen A.S., Williams R.M.E., Bishop J.L. and Thomson B.J., 2010. Mars Reconnaissance Orbiter observations of light-toned layered deposits and associated fluvial landforms on the plateaus adjacent to Valles Marineris. Icarus 205, 73-102.

Wendt L., Gross C., Kneissl T., Sowe M., Combe J., LeDeit L., McGuire P.C. and Neukum G., 2011. Sulfates and iron oxides in Ophir Chasma, Mars, based on OMEGA and CRISM observations. Icarus 213, 86-103.

Werner S.C., 2009. The global Martian volcanic evolutionary history. Icarus 201, 44-68.

Williams D.A., Greeley R., Fergason R.L., Kuzmin R., McCord T.B., Combe J., Head J.W. III, Xiao L., Manfredi L., Poulet F., Pinet P., Baratoux D., Plaut J. J., Raitala J., Neukum G. and HRSC Co-Investigator Team, 2009. The Circum-Hellas Volcanic Province, Mars: Overview. Planet. Space Sci. 57, 895-916.

Williams J.T., Shearer C.K., Sharp Z.D., Burger P.V., McCubbin F.M., Santos A.R., Agee C.B. and McKeegan K.D., 2016. The chlorine isotopic composition of Martian meteorites 1: Chlorine isotope composition of Martian mantle and crustal reservoirs and their interactions. Meteoritics & Planetary Science, doi: 10.1111/maps.12647.

Wilson L. and Head J.W., 1994. Mars, review and analysis of volcanic-eruption theory and relationships to observed landforms. Rev. Geophys. 32, 221-263.

Wilson L., Scott E.D. and Head J.W., 2001. Evidence for episodicity in the magma supply to the large Tharsis volcanoes. J. Geophys. Res. 106, 1423-1433.

Wolff-Boenish D., Gíslason S.R. and Oelkers E.H., 2006. The effect of crystallinity on dissolution rates and CO_2 consumption capacity of silicates. Geochim, Cosmochim. Acta Acta 70, 858-870.

Wolff-Boenisch D., Gíslason S.R., Oelkers E.H. and Putnis C.V., 2004. The dissolution rates of natural glasses as a function of their composition at pH 4 and 10.6, and temperatures from 25 to 74°C. Geochim. Cosmochim. Acta 63, 4843–4858.

Wray J.J., 2013. Gale crater: The Mars Science Laboratory/Curiosity Rover Landing Site. Int. J. Astrobiol. 12, 25-38.

Wray J.J., Milliken R.E., Dundas C.M., Swayze G.A., Andrews-Hanna J.C., Baldridge A.M., Chojnacki M., Bishop J.L., Ehlmann B.L., Murchie S.L., Clark R.N., Seelos F.P., Tornabene L.L. and Squyres S.W., 2011. Columbus crater and other possible groundwater-fed paleolakes of Terra Sirenum, Mars. J. Geophys. Res. 116, E01001, doi:10.1029/2010JE003694.

Wu S., You C., Valsami-Jones E., Baltatzis E. and Shen M., 2012. Br/Cl and I/Cl systematics in the shallow-water hydrothermal system at Milos Island, Hellenic Arc. Mar. Chem. 140–141, 33-43.

Wyatt M.B., McSween H.Y., Tanaka K.L., and Head J.W., 2004. Global geologic context for rock types and surface alteration on Mars, Geology, 32, 645-648.

Xiao L., Huang J., Christensen P.R., Greeley R., Williams D.A., Zhao J. and He Q., 2012. Ancient volcanism and its implication for thermal evolution of Mars. EPSL 323, 9-18.

Yen A., Gellert R., Schroder C., Morris R., Bell J., Knudson A., Clark B., Ming D., Crisp J., Arvidson R., Blaney D., Bruckner J., Christensen P., DesMarais D., de Souza P., Economou T., Ghosh A., Hahn B., Herkenhoff K., Haskin L., Hurowitz J., Joliff B., Johnson J., Klingelhofer G., Madsen M., McLennan S., McSween H., Richter L., Rieder R., Rodionov D., Soderblom L., Squyres S., Tosca N., Wang A., Wyatt M. and Zipfel J., 2005. An integrated view of the chemistry and mineralogy of martian soils. Nature 436, 49-54.

Yen A.S., Morris R.V., Clark B.C., Gellert R., Knudson A.T., Squyres S., Mittlefehldt D.W., Ming D.W., Arvidson R., McCoy T., Schmidt M., Hurowitz J., Li R. and Johnson J.R., 2008. Hydrothermal processes at Gusev Crater: An evaluation of Paso Robles class soils. J. Geophys. Res. 113, E06S10, doi: 10.1029/2007JE002978.

Yu J.Y., Heo B., Choi I.K., Cho J.P. and Chang H.W., 1999, Apparent solubilities of schwertmannite and ferrihydrite in natural stream water polluted by mine drainage. Geochim. Cosmochim. Acta 63, 3407–3416.

Zhao Y.S., McLennan S.M. and Schoonen M.A.A., 2014. Behavior of bromide, chloride, and phosphate during low-temperature aqueous Fe(II) oxidation processes on Mars. J. Geophys. Res. 119, 998–1012, doi:10.1002/2013JE004417.

Zhou Y. and Wang A., 2013. A comparison of dehydration processes of Al-, Fe^{2+}- and Mg-sulfates under Mars relevant pressures and three temperatures. 44th Lunar Planet. Sci. Conf., 1797.

Zimbelman D.R., Rye R.O. and Breit G.N., 2005. Origin of secondary sulfate minerals on active andesitic stratovolcanoes. Chem. Geol. 215, 37– 60.

Zolotov M.Y. and Mironenko M.V., 2007. Timing of acid weathering on Mars: a kinetic-thermodynamic assessment. J. Geophys. Res.112, E07006.

Zolotov M. and Shock E., 2005. Formation of jarosite-bearing deposits through aqueous oxidation of pyrite at Meridiani Planum, Mars. Geophys. Res. Lett. 32, L21203, doi: 10.1029/2005GL024253.

Summary

SUMMARY

Remote-sensing observations and rover missions have documented the abundant presence of sulphate-rich mineral associations on the surface of Mars. Mineralogical evidence indicates that the assemblages do not represent present-day conditions. A notable quantity can only have formed in hydrous, acidic and oxidizing environments, which must have been relatively common in Mars´ distant past. Together with widespread occurrences of silica and frequent enrichments of chlorine and bromine in soils and rocks, the sulphate associations are fingerprints of acidic fluids involved in interaction processes with rocks at or near the planet's surface.

The formation of sulphates is often attributed either to alteration of sulphide-rich rocks followed by leaching, transport and evaporation of the fluid, or to *in situ* alteration in the presence of sulphur derived from acid fluid or fog, with a strong control of the local rock composition. However, these explanations are not always convincing, especially in cases where sulphates are spatially associated with silica and enrichment of halogens.

This thesis addresses the question if active volcanic-hydrothermal systems on Earth are plausible analogues of geological settings where sulphates formed in the ancient history of Mars. The hypothesis was tested in field studies of stratovolcanoes in Central and South America where recently intruded magma produces sulphur- and halogen-rich gases that either escape to the atmosphere or are intercepted by water bodies, creating hyperacid lakes, springs and streams.

Field evidence and geochemical modeling have been used to demonstrate how such acid volcanic fluids can produce mineral assemblages with a range of Ca-, Al-, Fe- and Mg-sulphates through temperature changes, interactions with rocks and minerals or evaporation. Mars-like secondary mineral associations were discovered in a wide variety of sub-environments. At Copahue volcano (Argentina), they are distributed along a ca. 40 km long stretch of an acidic stream that has its source in the summit area, passes a glacial lake, and receives input from neutral tributaries. At Poás volcano (Costa Rica), the sub-environments include a hyperacid crater lake, hot springs, fumarole vents and areas exposed to acid rain or spray.

Minerals detected in both settings that also occur on Mars include mono- and polyhydrated ferrous and magnesium sulphates, jarosite-alunite group minerals, hydrated ferric and aluminium sulphates, hematite and other oxides, schwertmannite, gypsum/anhydrite, silica, sulphides, clay minerals and halides. Alunite is uncommon but is an important mineral in the hydrothermal reservoirs below the surface. The relative proportions of rock and acidic fluid during interaction play an essential role in the formation of the sulphates. High rock/water ratios and the presence of olivine are key factors for the formation of Mg- and Fe-sulphates. Modeling results indicate that evolution of acidic fluid in a cyclical sequence of interaction with olivine and evaporation in an open system is required to stabilize Mg-rich sulphates.

Temporal changes in $\delta^{37}Cl$, Cl-Br concentrations and Br/Cl ratios in the hyperacid lake water and subaerial fumaroles of Poás were studied to assess the mode and magnitude of halogen supply from the magma source. The observed variations reflect interactions between magma-derived gas and liquid water in the volcanic-hydrothermal system below the crater, and provide insight into the status of activity of the volcanic-hydrothermal system at depth.

Experiments on hyperacid brine water from Kawah Ijen crater lake (Indonesia), in combination with geochemical modeling, were carried out to investigate the consequences of evaporation of acid sulphate-chloride waters for the solution chemistry, mineral precipitation and escape of gaseous compounds. The results demonstrate that rising chloride and sulphate concentrations promote the formation of complexes with cations, which inhibits the saturation of major solid phases with the only exception of silica, gypsum/anhydrite, anatase and hydrogen chloride. The effects of HCl evaporation and associated chlorine isotopic fractionation were studied by monitoring temporal changes in the composition of the residual liquid. A marked change in sign and magnitude of fractionation between dissolved and gaseous chloride (HCl) in the course of the experiment was detected, which can be explained by a dependence of the fractionation mechanism on the species distribution of dissolved chloride as a function of pH.

From the field observations, experiments and thermodynamic simulations presented in this thesis it is concluded that volcanic-hydrothermal activity has extensively contributed to the formation of sulphate-bearing mineral assemblages on the Martian surface. Surface expressions of terrestrial volcanic-hosted hydrothermal systems provide direct insights into underlying processes that operated early in the Martian history, despite differences in chemical weathering and prevailing rock types between the two planets. The volcanic settings studied offer a conceptual framework for the origin and diversity of sulphur- and chlorine-rich acid fluids, and emulate surface environments for a variety of Mars-type sulphate-bearing mineral assemblages.

Samenvatting

SAMENVATTING

Waarnemingen uit satellieten en op de grond hebben de aanwezigheid aangetoond van aanzienlijke hoeveelheden sulfaatrijke mineraalassociaties op het oppervlak van Mars. De mineraalcombinaties zijn niet representatief voor de huidige omstandigheden. Een aanzienlijk deel kan alleen zijn gevormd in waterhoudende, zure en oxiderende milieus die relatief wijdverbreid moeten zijn geweest in het verre verleden van Mars. Samen met verspreide voorkomens van silica en aanrijkingen van chloor en broom zijn deze sulfaatassociaties indicatief voor interactieprocessen tussen zure vloeistoffen en gesteenten op of dicht onder het oppervlak van deze planeet.

De vorming van sulfaten wordt doorgaans toegeschreven aan omzetting van sulfiderijke gesteenten, gevolgd door uitloging, transport en verdamping van de vloeistof, dan wel aan omzetting in situ in aanwezigheid van zwavel afkomstig van een zure vloeistof of mist, met een sterke invloed van het aanwezige gesteente en verdamping. Deze verklaringen zijn echter niet altijd overtuigend, vooral niet in gevallen waar sulfaten geassocieerd zijn met silica en aanrijking van halogenen.

Dit proefschrift behandelt de vraag of actieve vulkanisch-hydrothermale systemen op Aarde een aannemelijke analogie zijn van geologische settings waar sulfaten werden gevormd in de vroege geschiedenis van Mars. Deze hypothese werd getest in veldstudies van stratovulkanen in Midden- en Zuid-Amerika waar recentelijk geïntrudeerd magma zwavel- en halogeenrijke gassen produceert, die ontnappen naar de atmosfeer of ingevangen worden door volumina water waardoor extreem zure meren, bronnen en stromen ontstaan.

Aan de hand van veldgegevens en geochemische modellen wordt aangetoond hoe via zulke zure vulkanische vloeistoffen mineraalcombinaties met een verscheidenheid aan Ca-, Al-, Fe- en Mg-sulfaten kunnen ontstaan door middel van temperatuurveranderingen, interacties met gesteenten en mineralen of verdamping. Mars-type associaties van secundaire mineralen werden gevonden in verschillende sub-milieus. Bij de Copahue-vulkaan (Argentinië) liggen ze verspreid langs een ca. 40 kilometer lang interval van een zure stroom die ontspringt bij de top, door een gletsjermeer loopt en toevoer ontvangt van neutraal water uit zijbeken. Bij de Poás-vulkaan (Costa Rica) zijn de sub-milieus een extreem zuur kratermeer, warme bronnen, fumarolen en omliggend terrein dat blootgesteld is aan zure regen of spatwater.

Mineralen die in beide settings aangetroffen werden en ook op Mars voorkomen zijn o.m. enkel- en meervoudig gehydrateerde ferro- en magnesiumsulfaten, mineralen van de jarosiet-alunietgroep, gehydrateerde ferri- en aluminiumsulfaten, hematiet en andere oxides, schwertmannite, gips/anhydriet, silica, sulfides, kleimineralen en haliden. Aluniet is zeldzaam maar is een belangrijk mineraal in de ondergrondse hydrothermale reservoirs. De verhouding van de hoeveelheid gesteente en zure vloeistof tijdens de interactie speelt een bepalende rol bij de vorming van de sulfat-

en. Hoge gesteente/water ratio's en de aanwezigheid van olivijn zijn sleutelfactoren voor de vorming van Mg,Fe-sulfaten. Modelleerresultaten laten zien dat Mg-sulfaten alleen kunnen stabiliseren als de zure vloeistof chemisch verandert in een cyclische opeenvolging van interactie met olivijn en verdamping in een open systeem.

Veranderingen van de $\delta^{37}Cl$, Cl-Br concentraties en Br/Cl verhoudingen in het hyperzure meerwater en fumarolen van Poás in de tijd werden bestudeerd om het transportmechanisme en de flux van halogenen uit de magmabron te bepalen. De waargenomen variaties weerspiegelen interacties tussen magmatisch gas en vloeibaar water in het hydrothermale systeem onder de krater. Ze verschaffen inzicht in de staat van activiteit van het systeem op grotere diepte.

Om de gevolgen van verdamping van zure sulfaat-chloridewaters voor hun chemie, mineraalneerslag en de ontsnapping van gasvormige verbindingen te onderzoeken werden experimenten uitgevoerd aan extreem zuur kratermeerwater van de Ijen-vulkaan (Indonesië), in combinatie met geochemische modellering. De resultaten tonen aan dat toenemende concentraties sulfaat en chloride de vorming van complexen met kationen bevorderen, wat de verzadiging van vaste stoffen belemmert met uitzondering van silica, gips/anhydriet en anataas. De effecten van HCl-verdamping en daarmee samenhangende fractionatie van chloorisotopen werden bestudeerd door het monitoren van tijdsafhankelijke veranderingen in de samenstelling van de overblijvende vloeistof. Er werd een opmerkelijke verandering waargenomen in het teken en de grootte van de fractionatie tussen opgeloste en gasvormige chloor in de loop van het experiment. Dit kan verklaard worden wanneer het fractionatiemechanisme afhankelijk is van de verhoudingen waarin verschillende chloorspecies in de oplossing aanwezig zijn als functie van de pH.

De veldgegevens, experimenten en thermodynamische simulaties die dit proefschrift behandelt laten zien dat vulkanisch-hydrothermale activiteit een belangrijk aandeel moet hebben gehad in het ontstaan van sulfaathoudende mineraalassemblages op het oppervlak van Mars. De oppervlakteverschijnselen van zulke hydrothermale systemen op Aarde verschaffen nieuwe inzichten in onderliggende processen die actief waren in de vroege geschiedenis van Mars, ondanks verschillen in chemische verwering en overheersende gesteentesoorten tussen de beide planeten. De bestudeerde vulkanische gebieden leveren een conceptueel raamwerk voor het ontstaan en de diversiteit van zwavel- en chloorrijke vloestoffen, en zijn een aannemelijke analogie van oppervlaktemilieus waar sulfaathoudende mineralen ooit zijn gevormd op Mars.

Resumen

RESUMEN

Sensores remotos y misiones de vehículos no tripulados han documentado la presencia de asociaciones mineralógicas ricas en sulfatos en Marte. La evidencia indica que dichas paragénesis no representan condiciones ambientales actuales. Tales minerales solamente pudieron haber sido formados en ambientes acuosos, ácidos y oxidantes; los cuales fueron relativamente comunes en el pasado de Marte. En conjunto con la presencia de sílice, cloro y bromo en suelos y rocas, los sulfatos son indicadores de que fluidos ácidos interactuaron con rocas en ambientes someros y superficiales.

La formación de sulfatos es normalmente atribuida a la alteración de rocas ricas en sulfuros seguida de lixiviación, transporte y evaporación del fluido resultante; o a la alteración *in situ* en presencia de azufre derivado de vapores ácidos o lluvia ácida; controlada por la composición de las rocas locales. Sin embargo, tales explicaciones no son siempre convincentes, especialmente cuando los sulfatos se encuentran espacialmente asociados a sílice, cloro y bromo.

Esta tesis aborda la interrogante de si los sistemas volcánicos e hidrotermales terrestres son análogos plausibles a las condiciones geológicas en las cuales se formaron los sulfatos en la historia antigua de Marte. Esta hipótesis fue probada en estudios de campo en estratovolcanes de Centro y Suramérica, en donde magma recién intruído produce gases ricos en azufre y halógenos los cuales escapan directamente a la atmósfera o son interceptados por cuerpos de agua someros, creando así lagos hiperácidos, fuentes termales y ríos.

La evidencia de campo, junto con el modelaje geoquímico, han sido utilizados para demostrar como tales fluidos volcánicos ácidos pueden producir paragénesis de sulfatos de Ca, Al, Fe y Mg mediante cambios de temperatura, interacción con rocas y minerales y evaporación. Asociaciones mineralógicas como las de Marte fueron descubiertas en una gran variedad de subambientes. En el volcán Copahue (Argentina), éstos se encuentran distribuidos a lo largo de aproximadamente 40 km de un río ácido cuyo origen se encuentra en la cúspide, trascurre por un lago glacial y recibe varios tributarios de aguas neutras. En el volcán Poás (Costa Rica) los subambientes incluyen un lago cratérico hiperácido, fuentes termales, fumarolas y áreas expuestas a la lluvia ácida o rocío ácido.

Los minerales detectados en ambas localidades incluyen sulfatos ferrosos y magnésicos poli y monohidratados, minerales de los grupos de la jarosita y alunita, sulfatos férricos y de aluminio polihidratados, hematita y otros óxidos, schwertmannita, yeso/anhidrita, sílice, sulfuros, arcillas y halogenuros. Aunque poco común en superficie, la alunita es un importante mineral en el reservorio hidrotermal, bajo la superficie. Las proporciones relativas de roca y fluido ácido durante la interacción agua-roca juegan un papel esencial en la formación de sulfatos. Altas proporciones roca/agua en presencia de olivino son factores clave en la formación de sulfatos de

Fe y Mg. Los resultados del modelaje geoquímico indican que la evolución de un fluido ácido bajo una secuencia de ciclos de evaporación y reacción con olivino en un ambiente abierto, se requiere para estabilizar los sulfatos de Mg.

Los cambios temporales en $\delta^{37}Cl$, concentraciones de Cl, Br y proporciones Br/Cl en el agua del lago hiperácido y en las fumarolas del Poás, fueron estudiados para evaluar el modo y la magnitud del suministro de halógenos desde el magma. Las fluctuaciones observadas reflejan interacciones entre gases magmáticos y agua el sistema volcánico e hidrotermal bajo el cráter y brindan información acerca de la actividad de éste en profundidad.

Experimentos con salmueras hiperácidas del cráter del volcán Kawah Ijen (Indonesia), en combinación con modelos geoquímicos fueron llevados a cabo para investigar las consecuencias de la evaporación de aguas sulfatado-cloruradas sobre su composición química, precipitación de minerales y escape de compuestos volátiles. Los resultados demuestran que un incremento en la concentración de cloruro y sulfato promueve la formación de complejos con cationes que inhibe la saturación de la mayoría de las fases sólidas, con excepción de sílice, yeso/anhidrita, anatasa y cloruro de hidrógeno. La evaporación de HCl y el fraccionamiento isotópico del cloro fueron también evaluadas mediante cambios temporales en la composición del líquido residual. Un marcado cambio en el signo y la magnitud del fraccionamiento isotópico entre el cloruro disuelto y el gaseoso (HCl) en el curso del experimento fue detectado; el cual puede ser explicado por la dependencia del mecanismo del fraccionamiento isotópico en la especiación del cloro en función del pH.

Con base en las observaciones de campo, experimentos y modelos termodinámicos presentados en esta tesis, se concluye que la actividad volcánica e hidrotermal ha contribuido extensamente a la formación de asociaciones minerales ricas en sulfatos sobre la superficie de Marte. Las expresiones superficiales de los sistemas hidrotermales en volcanes terrestres revelan procesos que operaron durante la historia temprana de Marte, a pesar de las diferencias en la meteorización química y los tipos de rocas predominantes entre ambos planetas. Los ambientes volcánicos estudiados ofrecen un marco conceptual para el origen y la diversidad de los fluidos ácidos ricos en azufre y cloro; además emulan los ambientes para varias asociaciones minerales ricas en sulfatos.

Acknowledgements

This PhD project started as an adventure in August 2011 and it has been a rich journey, both from a personal perspective and from a scientific one. During all these years I have met many people from which I learned many valuable things. First of all, I want to thank my parents from whom I got the curiosity to go beyond the things I can perceive, with the necessity of asking questions and never take anything for granted. My sister, nieces, aunt and grandmother have been great examples and inspirations in my life as well.

I also want to thank my supervisor, Manfred van Bergen, for the valuable scientific discussions we have had during all these years. He always encouraged me to go beyond observation and description, and search for the geological processes that could explain the numbers and plots obtained from sample analysis. I am grateful to professor Van Cappellen for his willingness to be my promotor, even long after he left Utrecht and joined the University of Waterloo in Canada. I want to thank Paul Mason also; with his sharp and to-the-point questions during our group meetings he made me rethink how to interpret results. In addition, his support during the last months enabled me to successfully finish this thesis.

Although my colleagues in the Petrology group carry out research in completely different areas, their suggestions, comments and questions during group meetings, lunch, coffee breaks and drinks were helpful to me, thanks to Sonja Geilert, Desiree Roerdink, Igor Nikogosian, Melike Balk, Inge Loes ten Kate, Helen King, Vincent Kofman, Dewany Monsels and Annika Huizinga. Annika, we were the only ones studying volcanic lakes, seduced by the beauty of their hyperacid yellowish waters; thanks for your friendship and your particular sense of humour.

A considerable amount of the results presented in this thesis was possible due to the laboratory assistance of Helen de Waard, Ton Zalm, Dineke van de Meent, Piet Peereboom, Thom Claessen, Arnold van Dijk and Anita van Leeuwen; thanks for your patience in dealing with my extremely acid, saline and hygroscopic samples. Hans Eggenkamp deserves a special mention in this section, since he patiently taught me the sample preparation techniques for chlorine isotope analysis. In addition, the scientific discussions with him were of great value to me. The aid I received from Tilly Bouten and Serguei Matveev in EPM and SEM analysis was highly appreciated.

Thanks to my OVISCORI-UNA colleagues María Martínez, Jorge Brenes, Erick Fernández and Geoffroy Avard, and to those from the Red Sismológica Nacional UCR-ICE Raúl Mora, Gino González and Yemerith Alpízar for your assistance in the field that made the fieldtrip to Costa Rica in 2012 a success. María Martínez kindly prepared and sent me many samples from Poás volcano, making an important contribution to this work. The fieldtrip to Argentina in 2013 was only possible with the support of Joop Varekamp, from whom I learned a lot thanks to his vast scientific experience and advices. Franco Tassi, Orlando Vaselli and Giovanni Chiodini advised me how to take good gas samples. Additionally, Franco kindly received me during a week in Fi-

renze for the gas analysis. My gratitude goes to Paul Oonk, Ellen Alexander and Lauren Camfield for sharing many good moments at Copahue. Paul, thank you for the help and company during this fieldwork, and for joining me afterwards to Neuquén for some days.

I had the pleasure to share, apart from the best office in the building, many good experiences with Paul Oonk, Claudia Giese, Aleksandra Galić and Özlem Ersoy. Claudia, thanks for your friendship, you are an excellent travel mate. I enjoyed the touristic and gastronomic (meat, sausages, beer and wine) incursions into Germany. Many good memories come to my mind from the EUGEN trip to Poland; except for the days we were sick at the campsite, it was great to explore Krakow and its surroundings with you.

I am grateful to Candela García, Alfredo Fernández, Alba de la Vara, Sergio Martínez, Chloé Morales, Dirk Simon and George Marketos. Being expats in The Netherlands were shared a particular perspective of life here, like our conversation topics during lunch breaks which were 90% of the time about food. Special thanks to Alfredo Fernández who helped me a lot with GIS in order to make beautiful maps. Marijke de Visser, thanks for all the years we ran together with Phoenix in Utrecht. There was nothing better after a long day in the laboratory or office than to spend some hours on the track being coached by Henny or Joost. I also enjoyed very much our Dutch-Spanish coffee conversations and the trip to Zeeland in the summer of 2015. Martin Wunderink, thanks for being a great running mate and for enjoying a good dinner together afterwards, with a movie as a reward. Jelle Klaas Beekhuizen, you have been beside me for a considerable amount of time along this process and know how difficult and frustrating thing can be sometimes. Thanks to be so patience with me.

About the author

ABOUT THE AUTHOR

Alejandro Rodríguez was born in 1977 in San José, Costa Rica. In 2002 he finished his Geology degree at the University of Costa Rica. His thesis was entitled: *Natural hazards and geomorphology for land management of the Jabonal river basin, Esparza, Costa Rica*. From 2002 till 2009 he carried out studies for exploration, development and exploitation phases of geothermal resources for the Costa Rican Electricity Institute. In 2009, sponsored by the United Nations University Geothermal Programme (UNU-GTP) and the government of Iceland, he studied at the University of Iceland and received a MSc. degree in Geology in 2011. His work was focused on the geochemistry of geothermal fluids and his thesis was entitled: *Water-rock interaction of silicic rocks: an experimental and geochemical modelling study*. In 2011, he moved to The Netherlands and started his PhD at Utrecht University, where he received his doctoral degree in 2016 with the thesis: V*olcanic lake systems as terrestrial analogue for sulphate rich-terrains on Mars*. During his PhD he published articles on this topic. His scientific areas of interest are volcanic and geothermal systems, exploration geochemistry applied to geothermal resources and water-rock interaction.

LIST OF PUBLICATIONS

Published:

Rodríguez A., Eggenkamp H.G.M., Martínez M. and van Bergen M.J., 2016. Chlorine isotope and Cl-Br fractionation in crater fluids of Poás volcano (Costa Rica): insight into an active volcanic-hydrothermal system. Journal of Volcanology and Geothermal Research 325, 70-85, doi:10.1016/j.jvolgeores.2016.05.020.

Rodríguez A., Varekamp J.C., van Bergen M.J., Kading T.J., Oonk P.B.H., Gammons C.H. and Gilmore M., 2015. Acid rivers and lakes at Caviahue-Copahue volcano as potential terrestrial analogues for aqueous paleo-environments on Mars. In: Tassi F., Vaselli O. and Caselli, A. (eds.), Copahue volcano, pp. 141-172, doi:10.1007/978-3-662-48005-2.

Rodríguez A. and van Bergen M.J., 2015: Volcanic hydrothermal systems as potential analogues of Martian sulphate-rich terrains. Netherlands Journal of Geosciences, 1-17, doi:10.1017/njg.2015.12.

In preparation:

Rodríguez A., Eggenkamp H.G.M., and van Bergen M.J., 2016. Experimental evaporation of hyperacid brines: effects on chemical composition and chlorine isotope fractionation.

Rodríguez A. and van Bergen M.J., 2016. Surface alteration mineralogy in active volcanic systems: an example of Poás volcano, Costa Rica.